The 11th International Symposium on Water Environment Systems

---with Perspective of Global Safety

16th ~ 17th November, 2023

TOHOKU UNIVERSITY

Department of Civil and Environmental Engineering
Graduate School of Engineering
Tohoku University

GP-RSS
International Joint Graduate Program in Resilience and Safety Studies

SyDE
WISE Program for Sustainability in the Dynamic Earth
変動地球共生学卓越大学院プログラム

SPONSORS

International Joint Graduate Program in Resilience and Safety Studies of Tohoku University

http://gp-rss.tohoku.ac.jp/

WISE Program for Sustainability in the Dynamic Earth of Tohoku University
https://syde.tohoku.ac.jp/

Department of Civil and Environmental Engineering, Graduate School of Engineering, Tohoku University

http://www.eng.tohoku.ac.jp/

ORGANIZERS

Dr. So KAZAMA	Professor, Tohoku Univ
Dr. Yu-You LI	Professor, Tohoku Univ
Dr. Daisuke SANO	Professor, Tohoku Univ
Dr. Keiko UDO	Professor, Tohoku Univ
Dr. Kengo KUBOTA	Associate Professor, Tohoku Univ
Dr. Rajapaksha Mudiyansekage Janaka Bamunawala	Assistant Prof., Tohoku Univ

SECRETARIATS

Dr. Yusuke HIRAGA	Assistant Professor, Tohoku Univ
Dr. Yu QIN	Assistant Professor, Tohoku Univ
Mr. Tao YAMAMOTO	DC Student, Tohoku Univ
Mr. Qingkang ZENG	MC Student, Tohoku Univ
Miss Xu WANG	DC Student, Tohoku Univ
Mr. Zehua MA	DC Student, Tohoku Univ

PARTICIPANTS

Suzhou University of Science and Technology
Dapeng Li   Dean, Professor
Zhe Kong   Associate Professor

National Yang Ming Chiao Tung University
Tsun-Hua Josh Yang   Associate Professor
Hsiang-Hsuan LI   Student

University of Macau
Tianwei Hao   Assistant Professor
Zifan Wu   Student
Xingyu Wang   Student

University of Moratuwa
SP Chaminda   Senior Lecturer

The University of Tokyo
Jiayuan Ji   Lecturer
Vu Trung Dung   Project Researcher

Tohoku Institute of Technology
Keisuke Ono   Lecturer
Mio Ishikawa   Student
Keitaro Susukida   Student

China Agricultural University
Jiahao Zhang   Student
Yapang Song   Student

Kyoto University
Eilif Kurnia Deda Djamres   Student

Nanjing Forestry University
Mengni Tao   Student

National Kaohsiung University of Science and Technology

Dun-Sheng Yang	Student

Shanghai University

Yuanyuan Shi	Student
Ruolan Wen	Student

Tokyo Institute of Technology

Hira Satter	Student

Tohoku University

Mohammad Naser Sediqi	Post-Doc researcher
Chise Nisiwaki	Technical Staff
Amalia Nafisah Rahmani Irawan	Student
Araujo Fortes Andre	Student
Atsuya Ikemoto	Student
Ayaka Okamoto	Student
Daisuke Nakahara	Student
Hayata Yanagihara	Student
Juntong Ha	Student
Kazuya Ito	Student
Kumudu Madhawa Kurugama	Student
Munipurage Wasitha Randeepa Ranga Dilshan	Student
Muthiah Sadidah	Student
Qingkang Zeng	Student
Ryotaro Tahara	Student
Sakina Ahmed	Student
Sartsin Phakdimek	Student
Sawitree Rojpratak	Student
Shun Takayama	Student
Sota Tadaki	Student
Tao Yamamoto	Student
Weizhe Xia	Student
Yizhu Sun	Student
Yuki Inoshita	Student

FIELDWORK

16 Nov (Thu)

Fieldwork I: Arahama Elementary School and Natori-Denshokan

・**Arahama Elementary School**

This facility preserves and maintains the school building of the Arahama Elementary School in Sendai, which was damaged by the Great East Japan Earthquake on March 11, 2011, as a relic of the disaster, with the aim of raising awareness of disaster prevention and disaster mitigation among many people. The school building, which still retains clear traces of the disaster, is open to the public and exhibits images and videos of the immediate aftermath of the disaster so that visitors can experience the power and threat of the tsunami.

・**Natori-Denshokan**

The museum aims to pass on the memories and lessons of the Great East Japan Earthquake to the rest of the world and to future generations, to keep the disaster from fading away, and to foster awareness of disaster prevention. We are grateful for all the support we have received and will continue to work together with storytellers and local residents involved in disaster prevention activities to help realize a society that is resilient to natural disasters.

Fieldwork II: Sen-en purification center and JNEX bioplant

・Sen-en purification center

　Sen-en purification center, receiving 120,000 m^3/day of wastewater, is the second largest wastewater treatment plant in Miyagi-ken. The A/O and A/A/O methods are used to treat the wastewater and the sewage sludge is effectively digested for biogas, which is further converted to low-carbon electricity in the plant.

・Jnex bioplant

　　Jnex has been the largest biogas plant in Japan. This plant receives organic solid wastes from local areas and produces biogas, electricity and fertilizers. Jnex is making contributions to sustainable society in Sendai by reducing solid wastes, recycling bio-energy and reusing organic matters and nutrients.

SCHEDULE

17 Nov (Fri)   (GMT +9)

8:50 - 9:00 Opening Speech and Group Photo

9:00-12:09 Oral Session I : *Wastewater, Water and Waste*

9:00 - 9:15	Organic matter recovery from domestic wastewater depending on sludge-based cationic aggregates **Dapeng Li**, *Suzhou University of Science and Technology*
9:15 - 9:30	Carbon-neutral potential in anaerobic treatment of high-strength industrial organic wastewater **Zhe Kong**, *Suzhou University of Science and Technology*
9:30 - 9:35	*Coffee break*
9:35 - 9:47	Occurrence of Viable but Non-Culturable (VBNC) state Escherichia coli in anaerobic digestion of high solid pig manure **Jiahao Zhang**, *China Agricultural University*
9:47 - 9:59	Quantitative microbial risk assessment for the infection of antibiotic resistant pathogenic bacteria contaminating hydroponic vegetables **Shun Takayama**, *Tohoku University*
9:59 -10:11	Using smoke condensed liquids during smoldering wasted fruit-tree branches for mosquito larva control **Dun-Sheng Yang**, *National Kaohsiung University of Science and Technology*
10:11-10:23	Recycling of wetland plants in a novel constructed wetland – microbial fuel cell (CMFC) packed with suspended filler for enhanced denitrification **Mengni Tao**, *Nanjing Forestry University*
10:23-10:28	*Coffee break*
10:28-10:40	Environmental impact of anaerobic digestion on sludge disposal **Yizhu Sun**, *Tohoku University*
10:40-10:52	The effect of recirculation on two-phase anaerobic fermentation system of food waste and paper waste **Qingkang Zeng**, *Tohoku University*
10:52-11:04	Biomethanation of H_2 and CO_2 in an anaerobic membrane reactor **Juntong Ha**, *Tohoku University*
11:04-11:16	Utilizing thermodynamics to analyze methane production AnMBR system for sulfate-laden wastewater treatment **Zifan Wu**, *University of Macau*

11:16-11:21	*Coffee break*
11:21-11:33	Enhanced methanogenesis for dry anaerobic digestion of chicken manure with in-situ ammonia stripping **Yapeng Song**, *China Agricultural University*
11:33-11:45	Ozone pretreatment combined with partial denitrification-anammox process for efficient nitrogen removal from nanofiltration concentrate of landfill leachate **Yuanyuan Shi**, *Shanghai University*
11:45-11:57	Towards sustainable wastewater treatment by chemically enhanced primary treatment and mainstream anammox: Challenges and solutions forward **Ruolan Wen**, *Shanghai University*
11:57-12:09	Optimizing Organic Loads in High-Rate Activated Sludge for Partial Nitritation/ Anammox Integration in a Novel Municipal Treatment Process **Weizhe Xia**, *Tohoku University*

12:10-13:00 *Lunch Break*

13:00-14:30 Poster Session

Classification of Deep-Seated and Shallow Landslides Using Spectral Indices and Amplitude Change Ratio in Response to Rainfall and Earthquake Events
- **Sartsin Phakdimek**, *Tohoku University*

Sensitivity Analysis of Extreme Precipitation Over Western Tohoku Using TIGGE Ensembles
- **Sawitree Rojpratak**, *Tohoku University*

Land Subsidence in Bangkok Vicinity: Causes and Long-term Trend Analysis Using InSAR and Random Forest
- **Sakina Ahmed**, *Tohoku University*

Modeling the Interaction of Flood Hazard and Society in Citarum Watershed, Indonesia: A Socio-Hydrological Perspective
- **Muthiah Sadidah**, *Tohoku University*

Effects of Gravel Mining and Dam Sediment Trapping on Long-Term Sediment Dynamics in Yoshino River, Japan
- **Daisuke Nakahara**, *Tohoku University*

Designing a prototype for disaster education using 3D city models and video games
- **Keitaro Susukida**, *Tohoku Institute of Technology*

An initial assessment of mobile LiDAR scanning for river topographic survey
- **Mio Ishikawa**, *Tohoku Institute of Technology*

Peak flow reduction by the upstream inundation and afforestation in small rivers
- **Yuki Inoshita**, *Tohoku University*

Estimation and analysis of population in river spaces using mobile spatial statistics data
- **Kazuya Ito**, *Tohoku University*

Evaluation of the Amount of Hydraulic Energy in Irrigation Reservoirs Based on Structural Characteristics in Western Japan
- **Atsuya Ikemoto**, *Tohoku University*

Potential of machine learning technique for prediction of 1-dimensional riverbed deformation along the Mogami river
- **Tao Yamamoto**, *Tohoku University*

The Impact of the 2018 Ranch Fire on Extreme Runoff Scenarios and Downstream Flood Risk in the Lake County of North-Central California
- **Munipurage Wasitha Randeepa Ranga Dilshan**, *Tohoku University*

Factor analysis of people migration to flood damage using municipality data
- **Ayaka Okamoto**, *Tohoku University*

Simulation of the training-rainband in the western Tohoku region in 2022
- **Ryotaro Tahara**, *Tohoku University*

Assessment of model transferability and explainability of boosting algorithms in flood susceptibility mapping
- **Kumudu Madhawa Kurugama**, *Tohoku University*

Initial analysis on the characteristics of Atmospheric Rivers inducing heavy precipitaton in Japan
- **Sota Tadaki**, *Tohoku University*

History of Tsunami Prevention Policies in Miyagi Prefecture
- **Chise Nishiwaki**, *Tohoku University*

14:30-17:55 Oral Session II : *Hydrology & Hydro-ecology*

14:30-14:50	Development of an edge computing-based sensory network to mitigate the impact of natural disasters in pond aquaculture **Hsiang-Hsuan LI, Tsun-HuaYANG**, *National Yang Ming Chiao Tung University*
14:50-15:10	A novel approach for monitoring open cast mine restoration process using UAV-based geomatic technology **SP Chaminda**, *University of Moratuwa*
15:10-15:30	Calibrating hydrology models in poorly gaged and heavily regulated basin with satelite data **Vu Trung Dung**, *The University of Tokyo*
15:30-15:50	Optimal Selection and Bias Correction of Satellite Precipitation Datasets in the Data-Scarce Upper Indus Basin **Hira Satter**, *Tokyo Institute of Technology*
15:50-16:10	Analyzing Climatic Variations and Their Implications for Cereal Cultivation Potential in Afghanistan **Mohammad Naser Sediqi**, *Tohoku University*
16:10-16:30	***Coffee break***
16:30-16:50	Land-Use Change Effects on Rainfall Partitioning, Evapotranspiration, and Water Balance in a Humid Tropical Hillslope **Eilif Kurnia Deda Djamres**, *Kyoto University*
16:50-17:05	Agricultural drought assessment in the tropical humid region: A case study of Indonesia **Amalia Nafisah Rahmani Irawan**, *Tohoku University*
17:05-17:20	Remote sensed vegetation parameters in flood modeling **Araujo Fortes Andre**, *Tohoku University*
17:20-17:35	Where should riparian vegetation be cut from for effective flood damage reduction? **Hayata Yanagihara**, *Tohoku University*
17:35-17:55	Maximizing Atmospheric River-induced precipitation in the Maipo River Basin in Chile **Yusuke Hiraga**, *Tohoku University*

17:55 - 18:00 Closing Remarks

18:00 - 20:00 Networking Dinner

The 11th International Symposium on Water Environment Systems
----- with Perspective of Global Safety   (Nov. 16th ~ 17th, 2023)

GP-RSS & SyDE
Tohoku University

Organic matter recovery from domestic wastewater depending on sludge-based cationic aggregates

DAPENG LI[1, 2*]

[1] School of Environmental Science and Engineering, Suzhou University of Science and Technology,
Suzhou, 215009, China
[2] National & Local Joint Engineering Laboratory for Municipal Sewage Resource Utilization Technology,
Suzhou University of Science and Technology, Suzhou, 215009, China
*E-mail: ustsldp@163.com.

Abstract

Capturing the abundant organic matter residing in wastewater can not only reduce the emission of CO_2 from the source, but the enriched organics can also be reused to generate and offset energy consumption in wastewater treatment processes. The key is to find or develop low-cost materials that can capture organic matter. Herein, sewage sludge-derived cationic aggregates (SBC-g-DMC) were successfully prepared via a hydrothermal carbonization (HTC) process coupled with a graft copolymerization reaction for recovering organic matter from wastewater. Preliminary screening indicated that both HTC (e.g., modifiers) and grafting conditions (e.g., monomers, duration) displayed significant impacts on the capture performance of final products, by adjusting the generated phenolic hydroxyl content of SBC precursor or grafting efficiency of aggregates. The optimal condition to prepare cationic aggregates is 0.10 g-HCl/g-dry sludge, 4 h for SBC; 60 mg of initiator, 2.5:1 of DMC-to-SBC mass ratio, 70°C, and 2 h for grafting. Characterization and wastewater treatment experiments showed that the obtained aggregates have a positively charged surface over a wide pH range of 3-11 and a hierarchical micro-/nano-structure, endowing it with an excellent organic matter recovery efficiency (97.2% of pCOD, 68.8% of cCOD, and 71.2% of tCOD). Meanwhile, it exhibits inappreciable trapping ability for the dissolved COD, NH_3-N, and PO_4^{3-}, guaranteeing the regular running of subsequent biological treatment units. This development is expected to provide a theoretical reference for sewage sludge disposal, carbon reduction, and energy recovery during municipal wastewater treatment.

Keywords: Sewage sludge; Hydrothermal carbonization; Graft copolymerization; Cationic aggregates; Organic matter recovery.

1 Introduction

As an energy-extensive industry, the wastewater treatment process can not only consume a large amount of electricity, fuel, and chemicals but also emit vast quantities of CO_2, CH_4, and other greenhouse gases during different treatment units, posing a significant threat to global warming. Reducing energy consumption and related greenhouse gas emissions during wastewater treatment is of great importance to achieving carbon emission peaking. Moreover, wastewater is also a huge "energy sink" containing a great wealth of organic matter (its amount can be simply expressed by COD). Statistically, the resided organic matter can provide about five times more energy than the electrical energy consumed, if some COD chemical energy can be captured and converted into electricity [1]. Thus, energy self-sufficiency or even an oversupply of wastewater treatment plants can be achieved.

Capturing and enriching high-level organic matter from wastewater is the first important tache for the recovery and utilization of COD. Till now, many methods like membrane separation, bio-flocculation, and coagulation with abiotic aggregates have been developed and employed to collect enriched organic matter from influents. Thereinto, the use of aggregates like sorbents, microbubbles, and coagulants shows apparent advantages of low energy consumption and organic matter loss [2]. Coagulants were most commonly used in chemically enhanced primary treatment (CEPT) processes.

Recently, the use of sewage sludge to produce hydrochar products via HTC processes for environmental remediation has attracted wide attention. It can not only achieve the reasonable disposal of sludge, abundant functional groups on the formed hydrochar surface can also serve as active sites to introduce cationic polymers for organic matter recovery. However, how to achieve the optimized synthesis of sludge-based cationic aggregates remains unclear. Whether the HTC and grafting conditions (e.g., methacryloyloxyethyl trimethyl ammonium chloride (DMC) monomer level) influence the performance of final products also needs to be uncovered.

Therefore, this work aims to explore the optimized synthesis of cationic aggregates via the HTC process coupled with graft copolymerization using sewage sludge as a raw material and investigate the feasibility of aggregates for organic matter recovery from wastewater.

2 Materials and methods

2.1 Preparation of SBC precursor and its derived cationic aggregates

A facile HTC method was used to prepare SBC precursors. Initially, a certain amount of dewatered sludge was mixed with different modifiers (e.g., HCl, HNO_3, KOH, etc.) at predetermined levels, and then transferred to a stirred hydrothermal reactor and heated at 170°C, 200 rpm for several hours. Afterward, the reactor was cooled down to room temperature, and the synthesized dark-brown products were separated via vacuum filtration, dried at 75°C overnight, and finally ground into fine powders for further use.

The derived SBC-g-DMC aggregates were prepared using a graft copolymerization reaction. First, certain amounts of SBC precursor and DI water were added to a four-necked flask, and mixed thoroughly; then, the temperature of the reaction system was raised to 50°C with the presence of N_2; subsequently, specified amounts of KPS was introduced, and reacted for 10 min to inhibit the production of homopolymers

The 11th International Symposium on Water Environment Systems
----- with Perspective of Global Safety   (Nov. 16th ~ 17th , 2023)

GP-RSS & SyDE
Tohoku University

on SBC surface; afterward, DMC monomer was dropwise added to the system, and the temperature was elevated to a preset value and maintained for several hours. After reaction, collected final products by centrifugation, dried, and ground.

2.2 Organic matter recovery experiments

Flocculation experiments were used to enrich and recover organic matter from real municipal wastewater. Specifically, a specified volume of SBC-g-DMC stock suspension was first added to the raw municipal wastewater, then the formed mixture was stirred at 120 rpm for 1 min, at 80 rpm for 4 min, and at 30 rpm for 15 min. Afterward, the mixture was settled for 30 min, and the supernatant at 2 cm below the liquid level was extracted to determine the remaining organic matter and nutrients level. The dosage of aggregates was 5~70 mg/L, and the municipal wastewater used in the tests was taken from a wastewater treatment plant in Suzhou.

3 Results and discussion

3.1. Optimized preparation of cationic aggregates

Both HTC and grafting conditions were optimized to obtain aggregates with the best flocculation performance. Results showed that HCl outperformed many modifiers like KOH to produce SBC precursor with a high content of R-OH groups, which facilitates the subsequent grafting process. Initiator and DMC levels, reaction temperature, and duration had a great impact on the grafting efficiency and cationic degree of final products, then affecting their flocculation performance.

3.2. Characterization of obtained aggregates

Zeta potential, SEM, FTIR, and XPS spectra were employed to characterize the synthesized aggregates, and the results are displayed in Fig. 2. As illustrated, SBC-g-DMC$_{2.5}$ displays positive zeta potential values over a wide pH range (3-11), indicating that DMC have been successfully grafted to SBC, and the obtained products have cationic properties. SEM analysis showed that the synthesized aggregates are irregularly shaped agglomerates with hierarchical micro-/nanostructures on their surface. The appearance of C=O and -CH$_2$-N$^+$(CH$_3$)$_3$ stretching vibration at 1728 and 1480 cm^{-1} in the FTIR spectra and -(CH$_2$)$_2$-N$^+$-(CH$_3$)$_2$ group at 403.1 eV in the XPS N 1s spectra also confirmed the successful preparation of cationic aggregates by graft copolymerization.
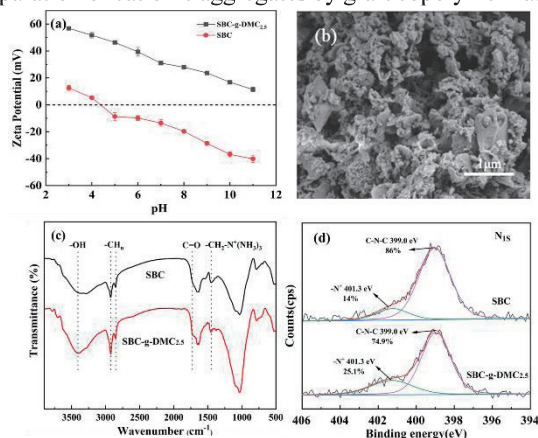

Fig. 2. Characterization of SBC-g-DMC$_{2.5}$: (a) zeta potential; (b) SEM; (c) FTIR; and (d) XPS N 1s spectra.

3.3. Recovery of organic matter from raw wastewater

As-prepared SBC-g-DMC$_{2.5}$ aggregates showed excellent capture performance toward organic matter and turbidity. Fig.

3 presents the effect of SBC-g-DMC$_{2.5}$ dosage on the capture of COD, turbidity, and nutrients from municipal wastewater. Results showed that removal efficiencies of COD and turbidity increased initially, then slowly decreased, and stabilized along with the dosage increase. A maximum COD capture rate of 71.2% and turbidity removal rate of 86.7% can be obtained when 20 mg/L of aggregate was used, prevailing many previously reported natural polymeric coagulants, demonstrating great application potential for sewage sludge disposal and organic matter recovery.
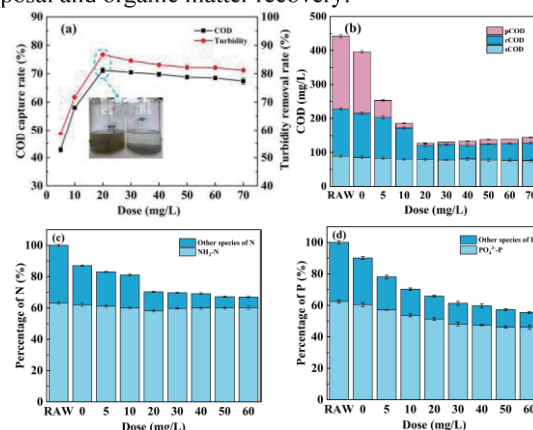

Fig. 3. (a) Capture of COD and turbidity; (b) variation of COD species after SBC-g-DMC$_{2.5}$ treatment; (c) retention of N, and (d) P with different species during coagulation.

In the COD captured by aggregates, particulate (pCOD, 97.2%) and colloidal (cCOD, 68.8%) species occupied very high proportions. Such an excellent trapping ability of SBC-g-DMC$_{2.5}$ could be ascribed as (1) there are vast cationic functional groups in aggregates surface, which facilitates the attraction of negatively-charged colloidal particles to form large flocs by contact and collision for sedimentation and capture; (2) many microporous structures in aggregates could intercept some pCOD and cCOD, ensuring a high COD capture efficiency. Meanwhile, the capture of TN and TP by SBC-g-DMC$_{2.5}$ is relatively poorer than that of COD, only 29.7% of TN and 30.5% of TP were removed by 20 mg/L of aggregates. Moreover, most of nutrients (N, P) captured are particulate forms instead of mobile NH$_4^+$-N and PO$_4^{3-}$ species, thus the follow-up biological treatment processes will not be affected because abundant dissolved nutrients available to microorganisms have been retained in treated effluents.

4 Conclusions

This work used sewage sludge as a raw material to prepare cationic aggregates via the HTC process coupled with a graft copolymerization procedure and explored the flocculation performance of obtained products. Results showed that as-prepared aggregates behaved very well for organic matter recovery from wastewater, displaying great application potential in the CEPT process for wastewater treatment and valuable organic matter capture.

Reference

[1] Wan, J., Gu, J., Zhao, Q., Liu, Y., 2016. COD capture: a feasible option towards energy self-sufficient domestic wastewater treatment. Scientific reports. 6, 1-9.

[2] Chakraborty, T., Gabriel, M., Amiri, A.S., et. al., 2017. Carbon and phosphorus removal from primary municipal wastewater using recovered aluminum. Environ. Sci. Technol. 51, 12302-12309.

The 11th International Symposium on Water Environment Systems
----- with Perspective of Global Safety (Nov. 16th ~ 17th, 2023)

GP-RSS & SyDE
Tohoku University

Carbon-neutral potential in anaerobic treatment of high-strength industrial organic wastewater

ZHE KONG[1, 2*]

[1] School of Environmental Science and Engineering, Suzhou University of Science and Technology, Suzhou, 215009, China

[2] National & Local Joint Engineering Laboratory for Municipal Sewage Resource Utilization Technology, Suzhou University of Science and Technology, Suzhou, 215009, China

*E-mail: zhekong@mail.usts.edu.cn

Abstract

The feasibility of anaerobic membrane bioreactor (AnMBR) for the treatment of N, N-dimethylformamide (DMF)-containing wastewater was theoretically compared with the conventional activated sludge (CAS) process in this study. The electricity consumption and expenditure, bio-energy production and CO_2 emission were investigated using the operational results of a lab-scale AnMBR operated in a long-term operation. The AnMBR was capable of producing bio-methane from wastewater and generated 3.45 kWh/m^3 of electricity as recovered bio-energy while the CAS just generated 1.17 kWh/m3 of electricity from the post-treatment of excessive sludge disposal. The large quantity of bio-methane recovered by the AnMBR can also be sold as sustainable bioresource for the use of household natural gas with a theoretical profit gain of 29,821 US$/year, while that of the CAS was unprofitable. The AnMBR was also demonstrated to significantly reduce the carbon emission by obtaining a theoretical negative CO_2 production of -2.34 kg CO_2/m^3 with the recycle of bio-energy while that for the CAS was 4.50 kg CO_2/m^3. The results of this study demonstrate that the AnMBR process has promising potential for the carbon-neutral treatment of high-strength DMF-containing wastewater in the future.

Keywords: Anaerobic digestion; AnMBR; anaerobic membrane bioreactor; industrial wastewater; bio-energy production; carbon neutrality.

1 Introduction

DMF is hazardous and toxic to humans due to its hepatotoxicity and potential carcinogenicity, which is also likely to cause eutrophication since this organic matter is a nitrogenous compound. Since the high-strength industrial wastewater typically contains various types of organic pollutants and its total COD concentration can be up to 10,000-30,000 mg/L, in which the concentration of DMF is typically over 10,000 mg DMF/L, accounting for the majority of the total COD. DMF is considered as a persistent organic matter with a low degradability, thus, it is quite essential to realize the effective treatment of industrial DMF-containing wastewater (DCW). With the rapid spread of the concept of carbon neutrality in wastewater treatment process in recent years, which aims at succeeding in energy conservation and recovery along with the reduction of carbon emission during the processing of wastewater treatment, the development of a sustainable and low-carbon treatment process for DCW has been on the list of concerns for the carbon-neutral goal.

In this study, a lab-scale AnMBR fed the synthetic DCW was conducted for a long-term operation to investigate the feasibility of the AnMBR. The operational results and data were processed for evaluating the potential of energy recovery, CO_2 emission reduction and electricity expenditure based on theoretical calculations. The performance results of the AnMBR were compared with the empirical results of a theoretical CAS process, which were assumed to share the same operational conditions, parameters and efficiencies with that of the AnMBR. A comparison was conducted between the two processes to give new insights into the engineering application of the AnMBR process in the treatment of DCW. The objectives of this study are to: 1) Demonstrate the sustainability of energy conservation in the carbon-neutral treatment of DCW through the AnMBR process; 2) Quantitatively compare the reduction of carbon emission during the treatment of DCW through the AnMBR and CAS process; 3) Assess the theoretical expenditure cost and potential profit for the treatment of DCW through the AnMBR and CAS process. The new findings of this work facilitate the popularization of this promising bio-technology in the future treatment of high-strength industrial wastewater.

2 Materials and methods

2.1 Experimental apparatus

A small lab-scale flat-sheet AnMBR was designed and set up for the long-term treatment of synthetic DCW. A flowchart of CAS process is assumed in comparison with the AnMBR system. A long-term continuous operation of 200 days was conducted for both the AnMBR and CAS system. The AnMBR obtains an operational volume of 7 L and a headspace of 8 L. The reactor was made of polyvinylidene fluoride (PVDF), in which a flat-sheet membrane module with a total area of 0.122 m^2, made of chlorinated polyethylene (CPE) (Kubota Membrane Cartridge, Japan), was inserted and settled inside the AnMBR. The sludge produced from both systems was further digested using a lab-scale continuous stirred tank reactor (CSTR) with an operational volume of 12 L for the post-treatment of wasted sludge. It should be noted that the CAS process in this study was assumed as a conceptual process, which had the ability to effectively degrade DMF. Since the CAS process is commonly used as a biological treatment process for industrial wastewater and has been investigated for years, the results obtained from the CAS process in this study is based on the same data of DMF concentration, removal efficiency and other parameters obtained from a lab-scale AnMBR. Some of the results are even "ideal" assumptions for the CAS process, so as to estimate the maximum ability of this process

The 11th International Symposium on Water Environment Systems
----- with Perspective of Global Safety   (Nov. 16th ~ 17th , 2023)

GP-RSS & SyDE
Tohoku University

for the treatment of DCW. The CSTR process is also assumed to have the reported performance of an effective digestion of the excessive sludge yielded during the treatment of DCW.

2.2 Chemical reagents and synthetic wastewater

All the analytically pure chemical reagents used in this study were purchased from Wako Co. Ltd., Japan. As can be seen in the supplementary information, an average concentration of approximately 2,105 ± 82 mg DMF/L (equivalent to 3,219 ± 124 mg COD/L) was obtained for the synthetic high-strength DCW, which was reserved in a 120 L plastic bucket that played the role of a substrate reserve tank. It should be noted that although the real typical concentration of DMF can be up to over 10,000 mg/L, it might be too high for a lab-scale experiment. It is improper to set the initial concentration too high in case that the AnMBR is unable to degrade the high-concentration COD or that toxic organic matters might inhibit the microbial activity when the concentration is too high. Therefore, for the lab-scale experiment in this study, it is common to use a relatively low concentration like 2,000 mg/L for theoretical investigations. The synthetic wastewater was prepared using DMF as the sole substrate, which was diluted with tap water.

3 Results and discussion

3.1. Operational results

The lab-scale attempt on the application of an AnMBR to the anaerobic treatment of high-strength DCW was proved successful, and the detailed operational results were also discussed in a previous study. At a relatively long HRT of 12-24 h, a high COD removal of over 97% was obtained through the AnMBR. The HRT of 8 h was considered as the shortest HRT for the stable operation of the AnMBR with an affordable limit OLR of 10.2 kg COD/m^3/d. Under this circumstance, the AnMBR was capable of degrading the majority of DMF contained in the synthetic wastewater from 2,105 ± 82 mg/L to 52.5 ± 9.1 mg/L, and a high methane yield of 990 L/m3 was simultaneously obtained, demonstrating an effective methanogenic degradation of DMF. The majority of influent COD was converted into bio-methane which accounted for 80% of the total COD, and the residual COD in the effluent just accounted for 5%. It is known that the biomass growth during the AD process is much lower than that through the aerobic CAS process, with a determined coefficient of 1.035 g MLSS/g COD, the sludge-COD conversion efficiency of DMF was calculated as a very low level of 5.4-6.5% (selected as 6.5%). In contrast, it has been widely reported that 30-50% of the influent COD turns out to be sludge instead of being degraded through the CAS process. In this study, the sludge-COD conversion efficiency was assumed as a high level of 50%, suggesting that under an ideal condition that a thorough aerobic degradation of DMF was obtained through the CAS process, half of the total influent COD of DCW was converted into CO$_2$ while the rest of it directly became part of the sludge.

3.2. Bio-methane and bio-energy recovery

As shown in **Fig. 1**, in this study, since the AnMBR process was designed as a lab-scale reactor, the flowchart of the entire system was simplified. The electricity consumed for maintaining the AnMBR at the mesophilic condition of 35 °C was calculated as 13.95 kWh/m^3. While the reactor heating accounted for the largest energy consumption, which could be majorly covered by the rest of combustion heat. As

is mentioned previously, the CSTR for the post-treatment of excessive sludge was typically operated at a higher thermophilic temperature of 55 °C to realize a higher COD removal and biogas production, and the electricity consumed for heating the CSTR was up to 1.58 kWh/m3. The electricity consumed by digester heating for the AnMBR was summed as 13.78 kWh/m^3, while that of the CAS was 1.22 kWh/m^3.
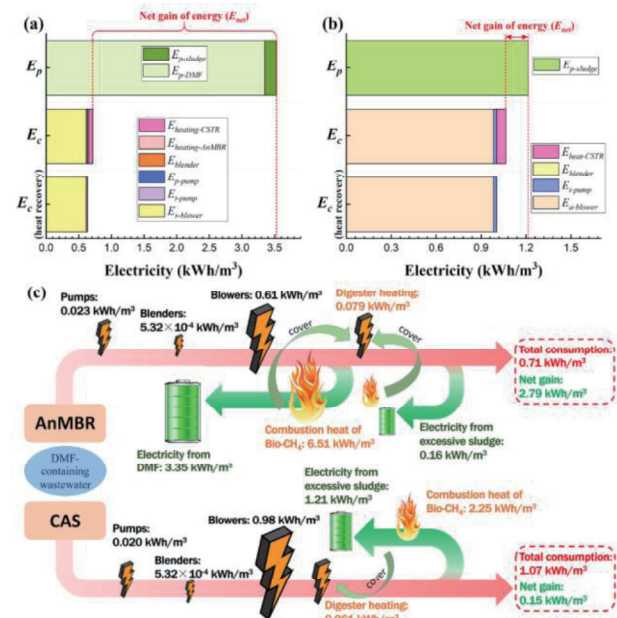

Fig. 1. A brief evaluation of energy conservation for the treatment of high-strength DMF-containing wastewater by the AnMBR (a) and CAS (b) processes along with the energy flowchart (c) for the comparison of two process.

4 Conclusions

The AnMBR process was proved as a promising alternative of the CAS process for carbon-neutral treatment of DCW with theoretical evaluation of energy, economy and carbon reduction. The AnMBR process could significantly save electricity in comparison with the energy-intensive CAS process. The future application of wastewater treatment process engineering for the AnMBR is considerd to have the potential of gaining net profit by selling the recycled bio-methane as household natural gas. The AnMBR process could also significantly reduce the carbon emission by lowering the CO$_2$ production during the wastewater treatment process. This study revealed the remarkable merits of the AnMBR process, also helping to popularize this carbon-neutral technology to the anaerobic treatment of industrial wastewater.

Reference

[1] Kong, Z., Xue, Y., Hao, T., Zhang, Y., Wu, J., Chen, H., Song, L., Rong, C., Li, D., Pan, Y., Li, Y., Li, Y.-Y., 2022. Carbon-neutral treatment of N, N-dimethylformamide-containing industrial wastewater by anaerobic membrane bioreactor (AnMBR): Bio-energy recovery and CO2 emission reduction. Bioresour. Technol. 358, 127396.

[2] Kong, Z., Xue, Y., Zhang, Y., Hao, T., Chen, H., Sun, J., Pan, Y., Li, D., Li, Y., Huang, Y., 2022. Insights into the carbon neutrality for the treatment process engineering of municipal wastewater by anaerobic membrane bioreactor integrated with partial nitritation-anammox: CO2 reduction and energy recovery. J. Water Process Eng. 49, 102996.

The 11th International Symposium on Water Environment Systems
----- with Perspective of Global Safety   (Nov. 16th ~ 17th , 2023)

GP-RSS & SyDE
Tohoku University

Occurrence of Viable but Non-Culturable (VBNC) state *Escherichia coli* in anaerobic digestion of high solid pig manure

〇Jia-Hao ZHANG[1], Min LIN[1], Wei QIAO[1,2*] & Renjie DONG[1]

[1]College of Engineering, Biomass Engineering Center, China Agricultural University, Beijing 100083, China; [2]Sanya Institute of China Agricultural University, Sanya, Hainan Province, 572025, China

*E-mail: qiaowei@cau.edu.cn; wayqiao@sina.cn

Abstract

Cost-effective hygienization of manure through anaerobic digestion was a long-standing challenge. Two-stage AD process introducing 55 and 70 °C biological hydrolysis following a 37 °C reactor was thus studied and compared to a parallelly operated mesophilic reactor at the same total HRT. The numbers of *E. coli* and fecal coliforms in the effluent of both the two-stage AD systems were much lower and comparable. However, live cells detected by RT-qPCR method, it was found that the proportion of VBNC cells increased by 26-42% after exposure under both 55 and 70°C condition. In contrast, the 37°C treatment was effective in reducing the presence of VBNC cells. Through observation of the cellular microstructure, it was discovered that the cell membranes of *E. coli* remained mostly intact after the 55/70°C treatment, and the cells were elongated and deformed, confirming the presence of VBNC cells. This study suggests that the high-temperature AD may lead to the entry of pathogens into the VBNC state, posing significant ecological safety risks.

Keywords: anaerobic digestion, pig manure, pathogens, VBNC

1 Introduction

Anaerobic digestion (AD) is a widely used technology to treat manure for pollution control, energy recycling, and pathogen inactivation. However, mesophilic AD (MAD) cannot effectively eliminate pathogens [1]. Two-stage AD that introduces high temperatures for pathogen inactivation and the subsequent mesophilic methane formation for process stability control and saving energy input is therefore more practical. In disinfection treatments for food and water, it has been observed that pathogens can enter a dormant state known as Viable But Non-Culturable (VBNC). In this state, the ability of bacteria to reproduce is greatly reduced, thus losing the ability to form colonies on the medium and escaping routine monitoring with false negatives; however, it remained pathogenic.

Therefore, this study aimed to improve the sanitization of two-stage AD by introducing thermal treatment and then analyze the occurrence of VBNC in manure and the changing pattern in AD.

2 Materials and methods

2.1 Two-stage AD systems

All reactors were CSTR with a working volume of 4 L and a stirring speed of 100 rpm and were fed once a day.

Table 1 The design of AD systems.

AD systems	1	2	3
T (℃)	37	55/37	70/37
HRT (d)	30	5/25	5/25
Feed TS (%)		10.0	
Feed VS (%)		7.7	
OLR (gVS·L⁻¹·d⁻¹)	2.6		15.4

2.2 Biological analysis

Pig manure and AD effluent were sampled for biological analysis during the stable period. The enumeration of *E. coli* was conducted according to GB 4789.38-2012 using VBR Agar-MUG.

2.3 RT-qPCR

Quantification of viable pathogens was performed by RT-qPCR in a previous report [3].

Briefly, the primer sequences used for tufa in RT-qPCR analysis was: F: ACTTCCCGGGCGACGACACTC; R: CGCCCGGCATTACCATCTCTAC. Calculate the VBNC change rate (%) for each AD using Equation (1).

$$VBNC\ change(\%) = \frac{reduction_{ficial} - reduction_{real}}{reduction_{ficial}} \quad (1)$$

2.4 SEM

The enriched bacterial suspension was inoculated into the filtered biogas slurry incubated at 37, 55, and 70°C for 5 days, respectively. The microstructure of *E. coli* was determined using a scanning electron microscope (JEOL, SU3500, Hitachi, Tokyo, Japan).

3 Results and discussion

3.1 The fermentation and hygienization performance

The long-term experiment lasted 571 days, and the stable time was as long as 260 days (more than 8 HRTs). Table 1 shows the fermentation performance of each AD system during the stable period. In the 2 and 3 systems, VS removal were increased by 18.5% and 2.7%, respectively, with residual TVFAs ranging from 0.4 to 0.6 g/L. However, the increase in Total Methane yield was relatively modest, at 6.7% and 3.3%, respectively.

In Figure 1, the fecal coliforms and *E. coli* in MAD effluent remained at 10^3-10^4 CFU or MPN/ml, while two-stage AD systems reduced the fecal coliforms and *E. coli* that were below the limit of China and the European Commission. Although a small number of fecal coliforms was still present in the 55°C reactor, they became undetectable in the subsequent mesophilic reactor. A study reported that the number of fecal coliforms and enterococci in sludge remained high after 60 minutes of pasteurization at 80°C. The recovery of coliform bacteria and *Enterococcus* spp. during the process of storage and farm utilization after the MAD with 60 minutes of pasteurization at 70°C was reported by Bagge and De. These results are inconsistent with this study, possibly because the longer thermal treatment time and other chemical factors have a positive effect on inactivating pathogens, which makes hygienization performance better.

The 11th International Symposium on Water Environment Systems
----- with Perspective of Global Safety   (Nov. 16th ~ 17th , 2023)

GP-RSS & SyDE
Tohoku University

Table 2 Fermentation performance of ADs.

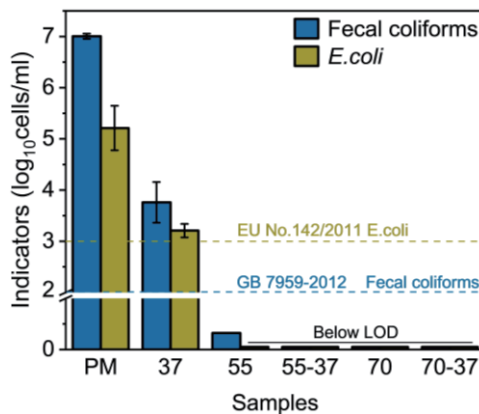| AD system	37°C	55-37°C	70-37°C
Total Methane yield (L/gVS)	0.30	0.32	0.31
VS removal (%)	48.7	57.7	50.0
pH	7.90	7.89	7.77
TAN (g/L)	2.5	2.7	2.4
TVFA (g/L)	0.4	0.6	0.4

Figure 1 Reduction of fecal coliforms and *E. coli*

3.2 The VBNC occurrence of *E. coli* in AD systems

Superficial reduction and real reduction of *E. coli* were detected by culturing and RT-qPCR methods, respectively. It can be observed that in the high-temperature phase of two-stage AD, the differences between the two methods reached 1.47 - 1.65 $\log_{10}$, which were further increased during the subsequent 37°C phase. This could be attributed to the thermal shock at 55°C and 70°C leading to the majority of *E. coli* entering the VBNC state. These bacteria have undergone some physiological changes, such as reduced cell membrane fluidity, which grants them environmental resistance. As a result, they can continue to grow in the subsequent MAD reactor. In the MAD, the real removal was 1.75 $\log_{10}$ higher than the superficial removal. This difference might be because there were already many VBNC cells present in untreated animal manure that couldn't be detected by culturing, and these VBNC cells were significantly removed during MAD. The results in Figure 2 show that 88% of the VBNC cells were removed in MAD, while after exposure to 55/70°C treatment, VBNC cells increased by 26-42%.
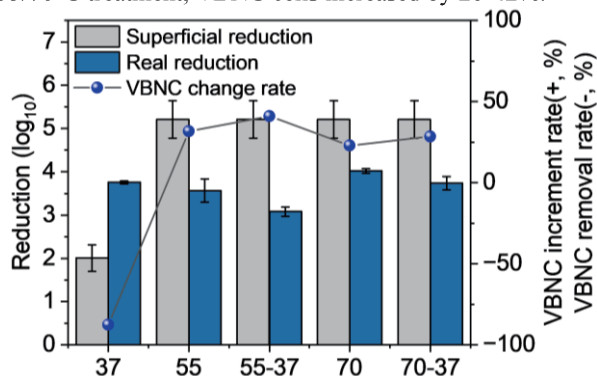

Figure 2 VBNC change rate of *E.coli* in AD systems

3.3 The microstructures of *E. coli* in digestate filtrates

In this section, the microstructure changes of *E. coli* were further investigated. The liquid phase of the digestate is used to simulate the effect of the AD environment on the inactivation of *E. coli*, eliminating the influence of particulate matter from animal manure on SEM observations. Fig. 3 shows that some *E. coli* cells elongated to nearly three times their original size (Fig. c) and transform into spherical shapes (Fig. d) after 5 days of treatment at 55°C and 70°C. However, these deformed cells had intact cell membranes and were not killed. The individual 70°C treatment exhibited the highest real reduction and the lowest VBNC increment rate (Fig. 2). This can be substantiated by SEM images, where it is evident that some cells underwent lysis and released their contents after treatment (Fig. 3d, yellow arrows). At 37°C (Fig. b), some *E. coli* cells also elongated and entered the VBNC state, confirming that the environment of animal manure itself can lead to the presence of VBNC cells.
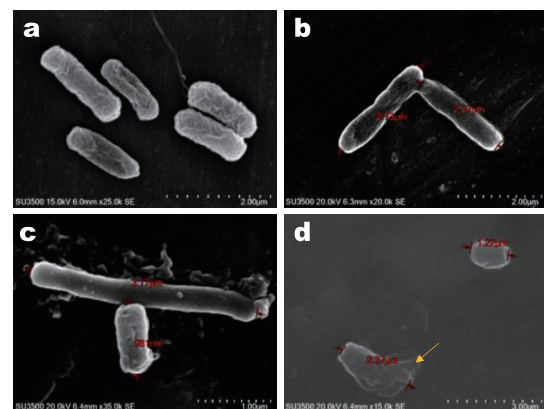

Figure 3 SEM image of *E. coli* in digestate filtrates.
a: initial; **b**: 37°C in 5 d; **c**: 55°C in 5 d; **d**: 70°C in 5 d.

4 Conclusions

For culture-detected methods, the hyperthermophilic temperature was not necessarily adopted since the thermophilic already has acceptable hygienization performance. However, high-temperature treatment leads to the majority of *E. coli* entering the VBNC state, resulting in a facial reduction far lower than the real reduction. In contrast, the MAD without thermal shock can effectively reduce the proportion of VBNC cells. In the future, more consideration should be given to innovative athermal AD processes for the sanitation of animal manure, and further studies are recommended to investigate the mechanisms of the VBNC occurrence in AD systems.

Reference

[1] Jiang Y, Xie SH, Dennehy C, Lawlor PG, Hu ZH, Wu GX, et al. Inactivation of pathogens in anaerobic digestion systems for converting biowastes to bioenergy: A review. Renewable and Sustainable Energy Reviews 2020;120:109654.

[2] Chen S, Li X, Wang Y, Zeng J, Ye C, Li X, et al. Induction of *Escherichia coli* into a VBNC state through chlorination/chloramination and differences in characteristics of the bacterium between states. Water Research 2018;142:279–88.

[3] Sheridan GEC, Masters CI, Shallcross JA, Mackey BM. Detection of mRNA by Reverse Transcription-PCR as an Indicator of Viability in *Escherichia coli* Cells. Appl Environ Microbiol 1998;64:1313–8.

Quantitaive microbial risk assessment for antibiotic resistant pathogenic bacteria contaminating hydroponic vegetables

◯ Shun TAKAYAMA[1] , Qian ZHANG[2], Ye Htut ZWE[2], Dan LI[2], Daisuke SANO[1]

[1]Department of Civil and Environmental Engineering, Tohoku University, Aoba 6-6-06, Aramaki, Aoba-ku, Sendai, Miyagi, Japan.

[2] Department of Food Science & Technology, National University of Singapore, Science Drive 2, Singapore

*E-mail: shun.takayama.r7@dc.tohoku.ac.jp

Abstract

Hydroponics is playing an important role to achieve the food security concerns, particularly in countries aiming to increase food self-sufficiency. However, hydroponics is vulnerable to microbial contamination, and the biofilm formed in hydroponic facilities may promote horizontal gene transfer (HGT) of antibiotic resistance genes (ARGs). Eventually the bacteria can become internalized into the edible parts of the vegetable through the roots, which could lead to human exposure of antibiotic resistant pathogenic bacteria. In this study, quantitative microbial risk assessment of hydroponics vegetable was performed, using literature values regarding the concentration of *Salmonella* spp. in hydroponics, efficiency of HGT, probability and rate of internalization, vegetable consumption patterns, and dose-response relationships. The estimated annual probability of infection per person by all *Salmonella* spp. was 1.1×10^{-2}, while the probability of infection from *Salmonella* spp. that acquire ARGs was estimated to be 1.2×10^{-7}. The results of this study emphasize the significant health risks posed by hydroponic vegetables.

Keywords: QMRA; Hydroponics; Antibiotic Resistant Genes; *Salmonella*.

1 Introduction

Hydroponics is a cultivation method in which crops are grown by nutrient solution without the use of soil [1]. Hydroponics is playing an important role in achieving food security because it brings us a variety of advantages, including the ability to control nutrients, utilize space more efficiently, and reduce the use of fertilizer and water [2]. However, there are some concerns regarding the microbiological safety of hydroponics and hydroponically grown vegetable. Hydroponics can be contaminated with pathogenic bacteria and antibiotic resistant bacteria (ARB) via irrigation water used for nutrient solution [3]. Leafy vegetables, a common vector of foodborne illness [4], are produced using a hydroponic method called the nutrient film technique (NFT), which allows for rapid spread of bacteria because the nutrient solution is constantly circulating in the facility [5]. In addition, the major foodborne bacteria, *Salmonella* spp., have a high biofilm-forming capacity and can persist in the facility for a long time [6]. Furthermore, biofilm is considered a hot spot for horizontal gene transfer (HGT) of antibiotic resistance genes (ARGs) via conjugation, one of the main mechanisms for HGT of ARGs [7]. Bacteria in the facility may eventually be taken up by the edible parts of the crop through the roots, and this phenomenon is referred to as internalization [8].

The objective of this study was to estimate quantitatively the risk caused by hydroponically grown vegetables and provide a framework for risk assessment to adequately fill current research gaps regarding hydroponics and ARB in the future.

2 Materials and methods

We employed a quantitative risk assessment (QMRA) framework [8]. Based on the assumed infection scenario, relevant data were extracted from previous studies in Google Scholar and used as input values for the QMRA model. In this study, it was assumed that the nutrient solution is contaminated with *Salmonella* spp. [10], and they acquire ARGs through conjugation in the biofilm [11]. Bacteria are eventually internalized into the edible parts of vegetables through the plant roots [12]. The harvested vegetables are then transported to retail stores [14], where they are sold and consumed raw by each household. We also performed several regression analyses and introduced new assumptions to determine input parameters. The bacterial concentration in the nutrient solution follows a Poisson distribution, and the average value (λ) is expressed as a function of time. Furthermore, the value (C_H) obtained by integrating λ over the period from about 7 days before the harvest (t_1) to the day of the harvest (t_2) was assumed to be the total number of bacteria that could be internalized in vegetables. We also assumed that internalization is determined by two factors: the internalization probability (P), which indicates the probability that internalization occur [12], and the internalization rate (R), which indicates how many bacteria in the nutrient solution are internalized into the edible parts [13]. Internalization was assumed to correlate with the bacterial concentration of nutrient solution for the elapsed time since bacterial contamination began, and internalization probability (P) was assumed to follow a binomial logistic curve [12]. Regarding the food supply chain, it was assumed that the temperature was always kept for the bacteria to die when they were transported or stored after harvest. After estimating the single exposure dose from these calculations, the probability of infection per exposure event was estimated using the beta Poisson model [17]. Furthermore, we calculated the annual infection probability considering each person's annual consumption frequency of leafy vegetables. All calculations in this study were performed using the statistical software R v.4.2.2. In the QMRA model, Monte Carlo simulations was performed with 10^6 iterations. In Poisson and binomial logistic regression analysis,

The 11th International Symposium on Water Environment Systems
----- with Perspective of Global Safety   (Nov. 16th ~ 17th , 2023)

GP-RSS & SyDE
Tohoku University

coefficients were estimated using Bayesian estimation. The main input values for the QMRA are listed in Table 1.

Table 1. Summary of variables and parameters used in the QMRA model (*: calculated in this study)

Symbol [source]	Variable	Distribution, value, or formula	Unit
λ [10]	Concentration of *Salmonella* spp. in the nutrient solution at time t	$\dfrac{\exp(a_0 + a_1)}{100}$	log CFU /mL
C_H*	total number of bacteria that could be internalized in vegetables.	$\int_{t_1}^{t_2} \lambda \; dt$	log CFU ×day /mL
η [11]	Conjugation efficiency	1.0×10^{-5}	-
P [12]	Internalization probability	$1/1 + e^{-(b_0 + b_1 \times CH)}$	-
R [13]	Internalization rate	2.0×10^{-4}	-
D_H*	Dose right after harvest when internalization occurs	$C_H \times R$	Log CFU/g
V [15]	The amount of vegetable per meal	Lognormal (4.35, 1.27) ×0.3	g
k [16]	Death rate parameter	0.0128	log CFU g^{-1}h^{-1}
G_{Tran} [14]	Change in concentration during transportation	$-k \times t_{Tran}$	log CFU/g
D_o*	Dose when internalization does not occur	0	CFU
D_1*	Dose by all *Salmonella* spp.	$10^{\wedge}(D_H + G_{Tran}) \times R \times V$	CFU
D_2*	Dose by all *Salmonella* spp. with ARGs	$10^{\wedge}(D_H + G_{Tran}) \times R \times \eta \times V$	CFU
D*	Dose	$D_o + D_1$, D_2	CFU
$P_{inf/event}$ [17]	Probability of infection per exposure event	$1 - \left(1 + \dfrac{D}{\beta}\right)^{(-\alpha)}$	-
F [18]	Number of days a person eats vegetables in a year	Uniform (105, 150)	day
$P_{inf/year/person}$*	Annual probability of infection per person	$1 - \prod_{i=1}^{F}(1 - P_{i\;inf/event})$	-

3 Results and discussion

The calculated risk values by all *Salmonella* spp. in hydroponically grown vegetables and by *Salmonella* spp. that acquired ARGs were summarized in Fig. 1 and Table 2. The annual probability of infection by all *Salmonella* spp. (1.1×10^{-2}) was higher than the allowable probability of infection (1.0×10^{-4}) [19], while the annual probability of infection by *Salmonella* spp. with ARGs (1.2×10^{-7}), was lower than the allowable value. These results indicated a potential health

risk from hydroponically grown vegetables where internalization had occurred. However, this study has a lot of assumptions and does not necessarily reflect accurate values. Therefore, in the future, the QMRA framework in this study should be used to appropriately fill the research gap by conducting surveys on the occurrence of internalization and the identification of factors that promote internalization in actual hydroponics facilities, rather than at the laboratory level. Furthermore, a detailed evaluation of the dynamics of ARGs during hydroponics cultivation is needed.
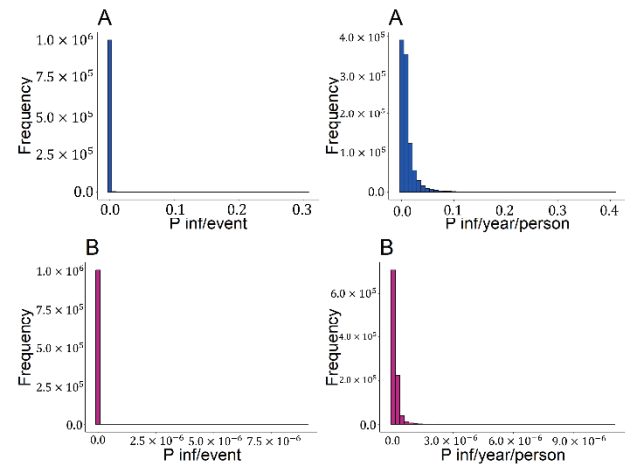

Fig.1. Histograms of the calculated risk values (A: *Salmonella* spp., B: *Salmonella* spp. with ARGs)

Table 2. Summary of mean risk values

	$P_{inf/event}$	$P_{inf/person/year}$
Salmonella spp.	8.8×10^{-5}	1.1×10^{-2}
Salmonella spp. with ARGs	9.7×10^{-10}	1.2×10^{-7}

Reference
[1] Vineeth et al., 2023, *ICESC 2023, 369-373*.
[2] Fimbres-Acedo et al., 2023, *Agronomy*, 13(1).
[3] Avila-Vega et al., 2014, *J. of Food Protection*, 77(11)
[4] Uyttendaela et al., 2015, *Comprehensive Reviews in Food Science and Food Safety*, 14(4), 336–356.
[5] Sela Saldinger et al., 2023, *In Horticulturae* (Vol.9, 1).
[6] Agnès et al., 2014, *In F. in Microbiology (Vol.5, IssueDEC)*.
[7] Blausein et al., 2016, *E. M. and Assessment, 188(1)*
[8] Riggio et al., 2019, *In Horticulturae* (Vol.5, 1).
[9] Owens et al., 2020, In *Water Research* (Vol. 174)
[10] Ilic et al., 2022, *Foods, 11(21)*.
[11] Qing Wang et al, 2015, PLOS ONE, 10(5), e0126784
[12] Koseki et al., 2011, *J. of Food Protection, 74(9)*
[13] Franz et al., 2007, *Food Microbiology, 24(1), 106–112*.
[14] Pang et al., 2017, *J. of Food Protection, 80(2), 302–311*.
[15] Mok et al., 2014, *Risk Analysis, 34(4), 602–613*.
[16] Mishra et al., 2017, *Food Control, 71, 32–41*.
[17] WHO, 2002, *Risk assessments of Salmonella in eggs and broiler chickens*.
[18] Farhadkhani et al., 2022, *Microbial Risk Analysis, 21*.
[19] Henao-Herreño et al., 2017, *Risk Analysis, 37(4), 733-743*

The 11th International Symposium on Water Environment Systems
----- with Perspective of Global Safety   (Nov. 16th ~ 17th , 2023)

GP-RSS & SyDE
Tohoku University

Using smoke condensed liquids during smoldering wasted fruit-tree branches for mosquito larva control

○ Dun-Sheng Yang[1]* & Shyi-Tien Chen[2]

[1] Ph.D. Program in Engineering Science and Technology, College of Engineering, National Kaohsiung University of Science and Technology, Kaohsiung City 82445, Taiwan.
[2] Department of Safety, Health and Environmental Engineering, National Kaohsiung University of Science and Technology, Kaohsiung City 82445, Taiwan.
*E-mail: i108109110@nkust.edu.tw

Abstract

Some mosquitos are disease-causing vectors. Existence of some disease-causing mosquitos poses a great threat to disease control worldwide. Finding an effective, low-cost alternative for mosquito population control is desperately needed. Pruned branches from three fruit trees of date, pomelo, and guava were collected, chopped, dried, and smoldered to form biochar and at the meantime generating smoke. The smoke was condensed at 6°C to form a smoke condensed liquid (SCL) and used as a larvicide for mosquito larva control. The SCL had a smoky smell, minimal nutrients, and little metal contents, yet contained plenty of phenolic molecules commonly used as biocides. As for larvicidal effects, a ten percent solution of the date and pomelo SCLs killed all tested larvae within 2 hrs.
Keywords: mosquito larvae; fruit-tree branches; smoke condensed liquid (SCL); larval mortality

1 Introduction

Mosquitos are annoying, yet a disease-carrying mosquito could be deadly. People in Southeast Asia and many other places have suffered from mosquito-borne diseases for a long time. Dengue fever in Kaohsiung City in Taiwan caused by Aedes mosquitoes is a good example. With distinctive black and white bands on their bodies and legs, Aedes aegypti and Aedes albopictus are known for transmitting several diseases in tropical and subtropical regions [1]. Several methods have been adopted to control these dangerous pathogen carriers, among which whole or part of the plant's extracts or essential oils [2-4] are commonly studied and have received various degrees of success. Among the studied plants, some are used as food or medicine [5], some are rare or costly to collect [6], and some use solvents to manufacture plant extracts or essential oils. These mosquito repellent alternatives may worsen food shortages or be considered environmentally unfriendly operations. Kaohsiung City in Taiwan, a tropical city in Southeast Asia, grows well-known fruits such as date, pomelo, and guava; however, the city also suffers from Aedes mosquito-related diseases. For fruit planting, trimming the fruit-tree branches is necessary for high yields. The massive, pruned branches were burned in the open field to provide extra nutrients to the farmland, and some were burned around residential areas to generate smoke to repel mosquitos. Burning branches in the open field is banned now for air pollution control, and since then, the fruit growers often encounter difficulties disposing of those pruned branches with sharp thorns. This study aimed to treat the fruit-tree branches in a combustion chamber to form smoke condensed liquid (SCL) as a bactericide as well as a mosquito larvicide. The goal of this study was to manufacture the SCLs of three pruned branches from date, pomelo, and guava trees, to analyze the ingredients of each SCL, and to study the SCLs' mosquito larvicidal effects.

2 Materials and methods

2.1. Preparations of Mosquito Larvae and Fruit-Tree Branches

Wild, not laboratory-bred, mosquito larvae were collected and tested. The tested Aedes mosquito larvae were collected from purposely allocated water buckets in their wild urban habitats at around a neutral pH and an ambient temperature around 25-30°C. Collected mosquito larvae and some reared adults during the tests were compared with [1] website information and confirmed by visual and were proved to be the Aedes mosquitos. Furthermore, three kinds of fruit-tree branches were collected from local farmers during fruit tree trimming seasons. The obtained branches were chopped into less than 2 cm chips and air-dried before being smoldered.

2.2 Smoldering Reactor Design and Operation

The reactor was equipped with a one-liter chamber for wood chip smoldering and a smoke condensation process driven by a vacuum pump at a flow of 5 L per minute (Fig. 1). A water-cooling system was operated at 6°C once smoke was produced. During each smoldering, 500 g of air-dried wood chips was placed in the reactor and ignited on top till their completeness. The temperature of around 300-400°C. The collected SCL was deemed to be 100% SCL and was diluted to certain concentrations for use in the tests.
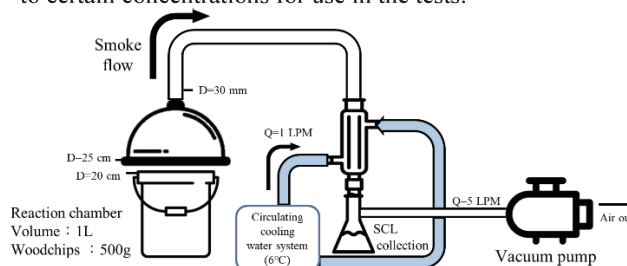

Fig. 1. Design and operating conditions of the fruit tree smoldering device.

The 11th International Symposium on Water Environment Systems
----- with Perspective of Global Safety   (Nov. 16th ~ 17th , 2023)

GP-RSS & SyDE
Tohoku University

2.3. Analysis of SCL Ingredients

SCL was extracted by hexane at sample/hexane (v/v) = 1.0. SCL ingredients in hexane were analyzed by a GC-MS device (GC-2010 Plus GCMS-QP2020, SHIMADZU CORPORATION, Kyoto, Japan) equipped with an Rtx-5MS capillary column from Restek™ (Bellefonte, PA, USA), and the content of each compound was reported as "abundance".

2.4. Larvicidal Test

To study the relations between the larval mortality and SCL dosage, each specimen was filled with 10 mL of 0-10% (v/v) SCL before a total of twenty larvae were randomly selected and put in each specimen at an ambient temperature. Water from the larva breeding bucket is used to adjust the needed SCL contents to avoid unnecessary interferences. The survival rate of the larvae in each specimen was recorded at time intervals from 0 to 144 h. Survived adults were checked to ensure their Aedes identity.

3 Results and discussion

3.1. SCL Properties

As showed in Table 1, total GC-MS abundances of the date, pomelo, and guava SCLs equaled to 44.8×10^6, 40.0×10^6, and 19.5×10^6, respectively. Their summarized SCL abundances were given in the following order (large to small) date, pomelo, then guava, and their percent abundances of their total were around 69, 62, and 82%, respectively. Meanwhile, the abundance of phenolic compounds in each SCL had a significant amount. Percent phenolic abundances of the date, pomelo, and guava SCLs were around 36, 32, and 46% of their total, respectively. It has been well noticed that phenolic compounds had anti-septic functions; however, the use of the SCL as a mosquito larvicide has not yet been reported and is to be further revealed below.

Table 1 Properties of three fruit-tree SCLs.

Eluted Time (min)	Standardized SCL Abundance ® and Percent of Total in Parenthesis			Compounds/Remarks
	Date	Pomelo	Guava	
4.367	1,803,840 (4.0)	1,695,168 (4.2)	-	Pyrazole, 1,4-dimethyl-
7.448	-	1,077,328 (2.7)	823,903 (4.2)	2(5H)-Furanone
9.233	390,152 (0.9)	-	-	Phenol
10.274	2,270,628 (5.1)	2,027,954 (5.1)	1,359,437 (7.0)	1,2-Cyclopentanedione, 3-methyl-
11.227	1,346,975 (3.0)	-	-	Phenol, 3-methyl-
11.468	5,047,432 (11.2)	4,907,177 (12.3)	2,671,629 (13.7)	Phenol, 2-methoxy-
12.044	1,368,125 (3.0)	571,430 (1.4)	921,379 (4.7)	Maltol
13.394	1,855,644 (4.1)	1,600,951 (4.0)	1,203,184 (6.2)	Creosol
13.572	4,318,762 (9.6)	3,347,830 (8.4)	1,310,554 (6.7)	Catechol
14.571	3,140,422 (7.0)	2,525,284 (6.3)	1,340,465 (6.9)	1,2-Benzenediol, 3-methoxy-
14.806	1,597,987 (3.6)	1,244,550 (3.1)	544,757 (2.8)	Phenol, 4-ethyl-2-methoxy-
15.947	7,201,005 (16.0)	5,289,310 (13.2)	5,735,301 (29.4)	Phenol, 2,6-dimethoxy-
19.483	600,658 (1.3)	327,768 (0.8)	-	Phenol, 2,6-dimethoxy-4-(2-propenyl)
Abundance of major compounds (% of total)	30,941,630(68.9%)	24,614,750 (61.6%)	15,910,610 (81.6%)	The abundance of major ingredients (Percent of the major ingredients with respect to the total)
Abundance of phenolics (% of total)	16,184,210 (36.1%)	12,838,647 (32.1%)	8,951,687 (45.9%)	The abundance of phenolic ingredients (Percent of the major ingredients with respect to the total)
Total abundance	44,881,227 (100)	39,970,517 (100)	19,503,967 (100)	Total abundance = total ions of the GC-MS chromatogram

3.2. SCL Larvicide Effect

Plots of larval survival rates over 144 h at various SCL concentrations ranging from 0 to 10% are given in Figure 2A-C for the date, pomelo, and guava cases, respectively. The results indicated that no larvae mortality was observed at Blank runs over the entire testing period, and the higher the SCL doses the fewer larvae survived at certain timespans. The dose–effect relations between each SCL content and the larvicidal effect were obvious. At a fixed SCL concentration, the larvae survival rate decreased as time went on. Similarly,

as the SCL concentration increased, the drop in larvae survival rate accelerated. In comparison, the guava SCL showed a less larvicidal effect than the date and pomelo SCLs, which appeared due to fewer compound abundances in the guava SCL than the other two (see Table 1).
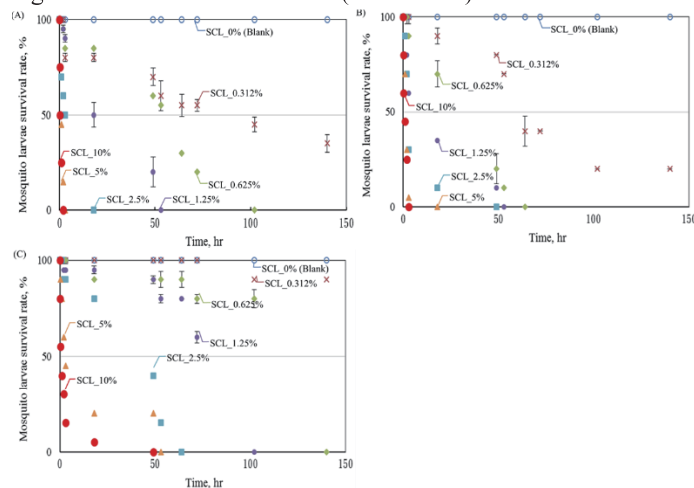

Fig. 2. Plots of larval survival rates over time at various concentrations (i.e., 0.312–10%) of (A) date, (B) pomelo, and (C) guava SCLs.

4 Conclusions

The SCL generated from the three fruit-tree branches appeared to have consisted of complex yet mostly similar compounds. The larvicidal effect was positively proportional to the amount of the SCL used as well. At 10% of the SCL, all of the tested larvae were killed in 2-3 h while using the date and pomelo SCLs.

Reference

[1] TWCDC. Dengue Fever; Taiwan Centers for Disease Control: Taipei, Taiwan, 2021.

[2] Pratheeba, T.; Vivekanandhan, P.; Faeza, A.K.N.; Natarajan, D. Chemical constituents and larvicidal efficacy of Naringi crenulata (Rutaceae) plant extracts and bioassay guided fractions against Culex quinquefasciatus mosquito (Diptera: Culicidae). Biocatal. Agric. Biotechnol. 2019, 19, 101137.

[3] Baskar, K.; Sudha, V.; Nattudurai, G.; Ignacimuthu, S.; Duraipandiyan, V.; Jayakumar, M.; Al-Dhabi, N.A.; Benelli, G. Larvicidal and repellent activity of the essential oil from Atalantia monophylla on three mosquito vectors of public health importance, with limited impact on non-target zebra fish. Physiol. Mol. Plant Pathol. 2018, 101, 197–201.

[4] Louis, M.L.M.; Pushpa, V.; Balakrishna, K.; Ganesan, P. Mosquito larvicidal activity of Avocado (Persea americana Mill.) unripe fruit peel methanolic extract against Aedes aegypti, Culex quinquefasciatus and Anopheles stephensi. S. Afr. J. Bot. 2020, 133, 1–4.

[5] Ali, S.I.; Gopalakrishnan, B.; Venkatesalu, V. Chicory (Cichorium intybus) and wormwood (Artemisia absinthium) extracts exhibit strong larvicidal activity against mosquito vectors of malaria, dengue fever, and filariasis. Parasitol. Int. 2018, 67, 781–786.

[6] Cheng, S.S.; Lin, C.Y.; Chung, M.J.; Liu, Y.H.; Huang, C.G.; Chang, S.T. Larvicidal activities of wood and leaf essential oils and ethanolic extracts from Cunninghamia konishii Hayata against the dengue mosquitoes. Ind. Crop. Prod. 2013, 47, 310–315.

The 11th International Symposium on Water Environment Systems
----- with Perspective of Global Safety   (Nov. 16th ~ 17th , 2023)

GP-RSS & SyDE
Tohoku University

Recycling of wetland plants in a novel constructed wetland – microbial fuel cell (CW-MFC) packed with suspended fillers for enhanced denitrification

○ Mengni TAO[1, 2], Zhaoqian JING[1*], Yu-You LI[2]

[1]Department of Civil Engineering, Nanjing Forestry University, Nanjing 210037, China.
[2] Department of Civil and Environmental Engineering, Graduate School of Engineering, Tohoku University,
6-6-06 Aoba, Aramaki-Aza, Sendai, Miyagi 980-8579, Japan
*E-mail: zqjing@njfu.edu.cn

Abstract

Substantial nitrogen in secondary effluent from wastewater treatment plants remains a threat to the aquatic environments, and therefore the deep treatment of secondary effluent is essential. In this research, the constructed wetland coupled with microbial fuel cells (CW-MFC) packed with suspended composite fillers were built to enhance nitrogen removal. Wetland plants were recycled as the additional carbon source in CW-MFC, and optimal adding position was evaluated. Results indicated that biomass adding in the anode of CW-MFC attained average total nitrogen removal of 90.67% and bioelectricity of 0.143 V. Suspended composite fillers and biomass addition contributed to the assembly of microbes related to nitrogen removal and organic degradation, and genera of *norank_o_Saccharimonadales* and *JGI_0001001_H03* showed high relative abundance in anodic region. Findings provide a potential way to develop a recycling CW-MFC and extend its application for wastewater treatment.
Keywords: plant biomass recycling; constructed wetland-microbial fuel cell; composite filler; nitrogen.

1 Introduction

The effluent from wastewater treatment plants (WWTPs) still contains a considerable nitrogen load, the remnants of which hold the potential to inflict detrimental consequences upon aquatic ecosystems. Considering diverse ecological intricacies, the comprehensive treatment of secondary effluent from WWTPs is essential. The constructed wetland-microbial fuel cell (CW-MFC) has received much attention as it promotes wastewater treatment and produces extra bioenergy simultaneously. Currently, the CW-MFCs have been analyzed to enhance nitrogen removal by changing operation conditions, filling materials, additional carbon sources, etc. Previous research utilized novel plastic fillers in CW and found that the nitrogen removal was higher than those with normal fillers, owing to the enhanced functional genera activity and abundance [1]. However, synthetic plastic fillers have been rarely applied in CW-MFC, and the related improvement of nitrogen removal should be further excavated.

In this study, the CW and CW-MFC packed with novel suspended plastic fillers were operated. Besides, the wetland plants were recycled and introduced as additional carbon sources. The related nitrogen removal, bioelectricity generation and microbial metabolisms were elucidated.

2 Materials and methods

2.1 The treatment of the wetland plants

The *Acorus calamus* was planted in December 2021, and was harvested in May 2022. After collection, the biomass was alkali-pretreated (6% NaOH, 12 h) and washed to neutral, then dried to the constant weight before use.

2.2 Operation of reactors

The CW, CW-MFC-1 and CW-MFC-2 were constructed as shown in **Fig. 1**. The filling materials composed of gravels (Φ8-12 mm, 40 cm of height) and suspended plastic fillers (K-1, Φ10 mm, 30 cm of height). The working volume was about 21.5 L, and the HRT of the reactors was 48 h. Graphite plates (200*100*8 mm) with small holes were installed as the anode and cathode, respectively, with the electrode spacing of 25 cm. The resistance box (set as 1000 Ω) was connected with anode and cathode, and the real-time voltage can be recorded by the paperless recorder. Before operation, the activated sludge (SV = 35%, MLSS = 3850 mg/L, SVI = 90.9 mL/g) was collected from oxidation ditch in Jiangning WWTPs (Nanjing, China), and then acclimated for 1 month.
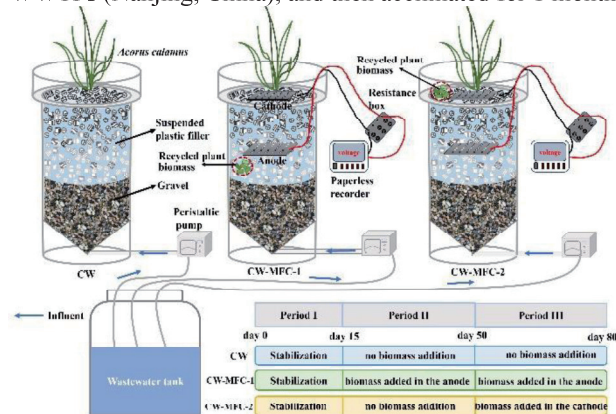

Fig.1 Schematic diagram of experimental reactors.

The synthetic wastewater was prepared by glucose, NH_4Cl, KNO_3, KH_2PO_4, NaCl, $NaHCO_3$ and other trace elements. The main concentrations are (mg/L): 45.5 ± 4.83 COD, 5.62 ± 0.65 NH_4^+-N, 10.7 ± 0.43 NO_3^--N, 0.5 TP. The dosage of the recycled plant biomass was 5 g, and the wrapped biomass was added in the anodic region (named CW-MFC-1) and cathodic region (named CW-MFC-2), respectively.

2.3 Analytical methods

The water samples were collected and filtered by 0.45-μm Millipore filter, and then determined through standard methods. Microbial samples around the anode and cathode

The 11th International Symposium on Water Environment Systems
----- with Perspective of Global Safety　　(Nov. 16th~17th , 2023)

GP-RSS & SyDE
Tohoku University

regions (same height in CW) were collected at the end of the experiments and were analyzed by high-throughput sequencing. The bacterial 16S rRNA gene region (V3-V4) was amplified by polymerase chain reaction (PCR) using primers 338F/806R.

3 Results and discussion

3.1 Overall COD and TN removal performance

The TN removals are shown in **Fig. 2 a-c**. In CW, the average TN removal was 76.99 ± 2.10%. The average TN removals of CW-MFC-1 during periods I, II and III were 73.7 ± 0.92%, 78.56 ± 5.36%, and 90.67 ± 8.38%, respectively. Biomass recycling significantly increased nitrogen removal. Besides, CW-MFC-1 showed higher and more stable nitrogen removal with the plant biomass added secondly (period III), indicating that the microbial activity was intensified after an adding cycle. In CW-MFC-2, the average TN removals in periods II and III were 76.60 ± 2.88%. and 82.77 ± 7.56%. Although the TN removal also increased, the maintenance was shorter than that in CW-MFC-1. It indicated that the plant biomass was suitable to be added in the anodic regions.
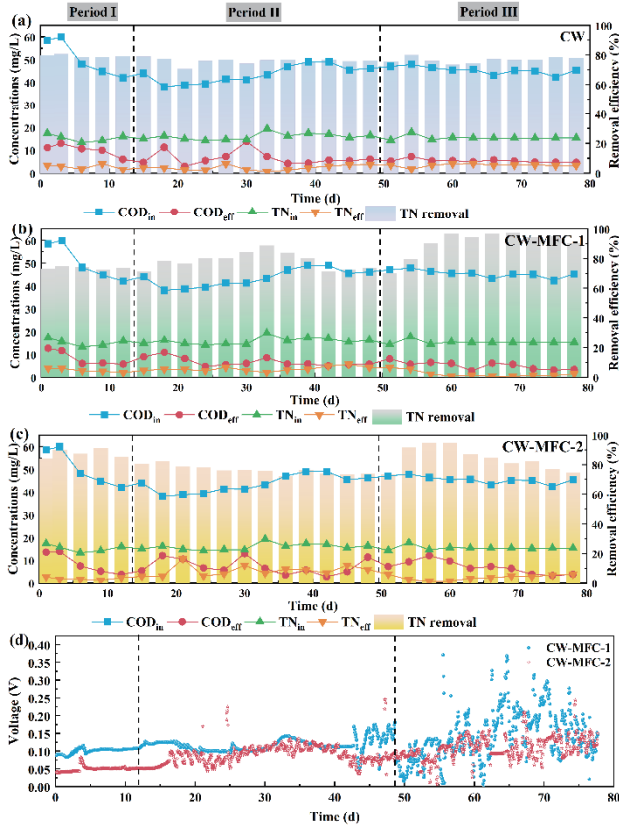
Fig. 2 COD and TN removal in CW (a), CW-MFC-1 (b), CW-MFC-2 (c) and bioelectricity generation (d)

With biomass addition, the effluent COD concentrations did not increase significantly, with maxima of 6.2, 10.9 and 8.1 mg/L in CW-MFC-1 **(Fig. 2a-c)**. Bioelectricity generation shows a similar trend to the TN removal. In CW-MFC-1, the average voltages were 0.101, 0.118, and 0.143 V **(Fig. 2e)**. In CW-MFC-2, the average voltages were 0.080, 0.090, and 0.118 V **(Fig. 2f)**. All above results revealed that recycling plant biomass in the anode was a better choice for CW-MFC.

3.2 Microbial community analysis

The dominant genera in three reactors are presented in **Fig. 3a**. Genera of *norank_o_Saccharimonadales* showed high

relative abundance (RA) in anodic region CW-MFC-1 (11.1%) and 2 (12.0%). It is reported that the gene was closely related to denitrification in biosystems [2]. The abundance of *JGI_0001001_H03* increased in CW-MFC, showing the role of the organic degradation under low nutrients conditions [3]. Co-occurrence networks showed the correlations of OTUs in CW and CW-MFCs. Fig. 3b presented 486 nodes and 7758 lines with 68.02% positive relations. Fig. 3c presented 482 nodes and 8795 lines with 66.07% positive relations. Main module (1-7) showed the higher abundance in CW-MFC (52.7%), while the total abundance was 46.29%. It indicated that biomass recycling contributed to the assembly of functional genes related to organic and nitrogen transformation.
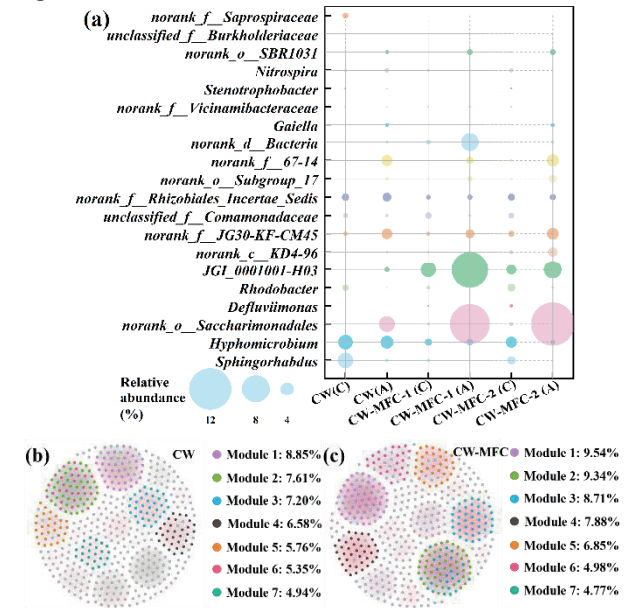

Fig. 3 Dominant genera (top 20) and co-occurrence networks of CW and CW-MFC by modularity class.

4 Conclusions

This study investigated the novel constructed wetland-microbial fuel cell with suspended fillers and recycled plant biomass to enhance nitrogen removal and bioelectricity generation simultaneously. Plant biomass added in the anode attained TN removal of 90.67% and voltage output of 0.143 V, respectively. Biomass addition contributed to increasing the abundance of functional genes related to nitrogen removal. Findings provide a promising method to improve nitrogen removal of secondary effluent and biomass recycling.

Reference

[1] Z Tao, et al. A novel filter-type constructed wetland for secondary effluent treatment: Performance and its microbial mechanism, Bioresource Technol., 380 (2023), 129075.
[2] Z Xue, et al. Integrated moving bed biofilm reactor with partial denitrification-anammox for promoted nitrogen removal: Layered biofilm structure formation and symbiotic functional microbes, Sci. Total Environ., 839 (2022), 156339.
[3] Sandrine Veloso, et al. Keystone microbial taxa organize micropollutant-related modules shaping the microbial community structure in estuarine sediments, J. Hazard. Mater., 448 (2023), 130858.

The 11th International Symposium on Water Environment Systems
----- with Perspective of Global Safety   (Nov. 16th ~ 17th , 2023)

GP-RSS & SyDe
Tohoku University

Environmental Impact of Anaerobic digestion on Sludge Disposal

◯ Sun Yizhu[1]* & Yu-You Li[1,2]

[1]Department of Civil and Environmental Engineering, Tohoku University, Miyagi 980-8579, Japan.
[2]Department of Graduate School of EngineeringTohoku University, Miyagi 980-8579, Japan..
*E-mail: sun.yizhu.q4@dc.tohoku.ac.jp

Abstract

Sewage sludge is a biomass that contains a large amount of energy. How to dispose of excess sludge is a very important problem. Anaerobic digestion is a popular method of sludge disposal in recent years. It can reduce the volume of sludge and recover a large amount of energy from methane. However, few studies have used actual sludge parameters from Japanese sewage plants to calculate the environmental impact of anaerobic digestion on sludge disposal. This study is based on the actual data of the Yamagata sewage plant and uses formulas to calculate the energy balance, greenhouse gas emissions, and comprehensive environmental impact of two disposal methods: direct incineration and anaerobic digestion followed by incineration. The results indicate that anaerobic digestion has significant beneficial impact on the environment. The Anaerobic digestion followed by incineration can save 856.92 kWh of electricity, reduce 340.55kg of carbon dioxide emissions and reduce 50.5% of the environmental impact than the incineration without Anaerobic digestion route for every 1t of dry sludge disposal.

Keywords: Sludge disposal; Anaerobic digestion; Energy balance; Incineration; Greenhouse gas emissions

1 Introduction

At present, the problem of global warming is becoming increasingly serious. Japan has set a goal of achieving carbon neutrality by 2050. To achieve this goal, it is necessary to reduce greenhouse gas emissions and increase the utilization rate of renewable energy.

Sewage sludge is a biomass rich in energy, and it is estimated that it contains approximately 12 billion kilowatt hours of energy each year in Japan. Therefore, how to dispose sludge and apply these energy is very important.

Anaerobic digestion (AD) is a biochemical process that converts organic materials into combustible biogas. In recent years, anaerobic digestion of sludge has been widely accepted as an environmentally friendly disposal method that can reduce sludge and recover energy. The organic matter in sludge is decomposed by anaerobic microorganisms under anaerobic conditions, producing biogas mainly composed of methane and carbon dioxide. Biogas can recover heat and electricity through cogeneration. However, anaerobic digestion also requires energy consumption and reduces the heat generated by subsequent sludge incineration. Research has shown that direct incineration is a more reasonable method of sludge disposal in China. For Japan, there is still a lack of validation based on actual sewage plant sludge data to determine whether anaerobic digestion is beneficial for sludge disposal. Therefore, this study selected the actual sewage sludge data of Yamagata sewage plant as the parameter,validated the beneficial effect of Anaerobic digestion on sludge disposal through calculation.

2 Materials and methods

2.1 Functional unit and system boundaries

This study is based on the calculation of each ton of dry sludge disposed, and two scenarios were selected. The sludge disposal method for Scenario 1 is direct incineration without digestion, while Scenario 2 is anaerobic digestion followed by incineration. The system boundaries are shown in **Fig. 1** and **Fig. 2.**
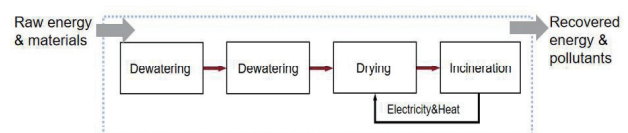

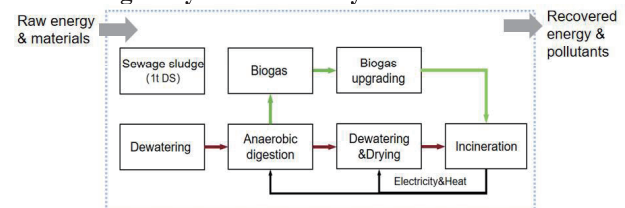
Fig. 1. System Boundary for Scenario 1

Fig. 2. System Boundary for Scenario 2

2.2 Research method

The energy balance and net greenhouse gas emissions of the two scenarios were calculated using the actual sludge parameters of the Yamagata sewage plant.

Energy consumption includes the electrical and thermal energy required for sludge disposal, while energy generation includes the electrical and thermal energy generated by anaerobic digestion and the heat generated by incineration. Greenhouse gas emissions include direct and indirect emissions, ultimately converted into carbon dioxide equivalent.

Finally, the comprehensive environmental impact was calculated using LIME2.

3 Results and discussion

3.1 Net energy balance

Scenario 2 consumed less energy and generated more energy than Scenario 1. This is mainly because thermal drying consumes the most electricity in sludge disposal, while anaerobic digestion greatly reduces the volume of sludge, thus greatly reducing the amount of electricity required for sludge during thermal drying. Moreover, the energy generated by anaerobic digestion of organic matter is greater than the heat generated by incineration.

The 11th International Symposium on Water Environment Systems
----- with Perspective of Global Safety   (Nov. 16th~17th, 2023)

GP-RSS & SyDe
Tohoku University

Table 1 Power consumption in Scenario 1

Scenario 1	Consumption (kW·h)	Generation (kW·h)	Total (kW·h)
Thickening	22.20	0.00	22.20
Anaerobic digestion	—	—	—
Dewatering	17.56	0.00	17.56
Thermal Drying	3275.64	0.00	3275.64
Incineration	153.33	2840.08	-2686.75
Total	3468.74	2840.08	**628.65**

Table 2 Power consumption in Scenario 2

Scenario 2	Consumption (kW·h)	Generation (kW·h)	Total (kW·h)
Thickening	22.20	0.00	22.20
Anaerobic digestion	661.41	1430.76	-769.35
Dewatering	19.00	0.00	19.00
Thermal Drying	1479.01	0.00	1479.01
Incineration	71.37	1053.50	-982.13
Total	2252.99	2484.26	**-231.27**
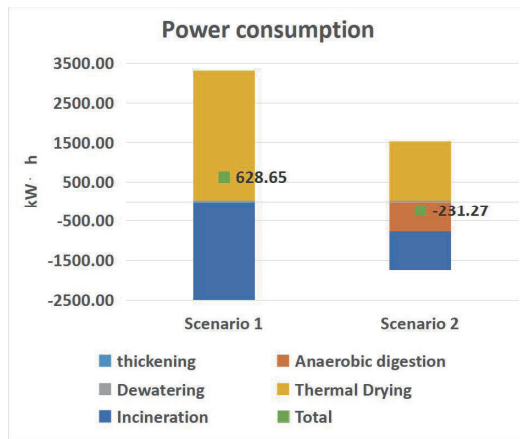
Fig. 3. Net energy balance

3.2 Net GHG emission

Scenario 2 emitted less greenhouse gases than Scenario 1. The N_2O generated by incineration accounts for approximately 47% of total GHG emissions. In AD process, some biogas escaped from biogas clean equipment, and the escaped biomethane would cause more greenhouse gas emissions.

Table 3 GHG emission of Scenario 1

Scenario 1	Direct emission (kg-CO₂eq/t)	Indirect emission (kg-CO₂eq/t)	Avoided emissions (kg-CO₂eq/t)	Total (kg-CO₂eq/t)
Thickening	0.00	11.54	0.00	11.54
Anaerobic digestion	0.00	0.00	0.00	0.00
Dewatering	0.00	35.13	0.00	35.13
Thermal Drying	0.00	1703.34	0.00	1703.34
Incineration	320.75	79.74	-1476.84	-1076.36
Total	320.75	1829.75	-1476.84	**673.65**

Table 4 GHG emission of Scenario 2

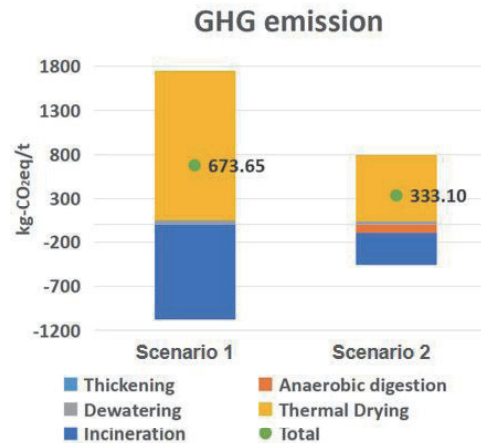| Scenario 2	Direct emission (kg-CO₂eq/t)	Indirect emission (kg-CO₂eq/t)	Avoided emissions (kg-CO₂eq/t)	Total (kg-CO₂eq/t)
Thickening	0.00	11.54	0.00	11.54
Anaerobic digestion	329.23	316.00	-744.99	-99.76
Dewatering	0.00	21.97	0.00	21.97
Thermal Drying	0.00	759.89	0.00	759.89
Incineration	150.11	37.16	-547.82	-360.54
Total	479.34	1146.57	-1292.81	**333.10**

Fig. 4. Net GHG emission

3.3 Integrated evaluation

In the process of incineration without AD, each ton of dry sludge disposed will cause a comprehensive environmental impact of 1100 yen.

In the process of Anaerobic digestion followed by incineration, each ton of dry sludge disposed will cause a comprehensive environmental impact of 544 yen.

Table 5 Integrated evaluation through LIME2

	Global Warming (kg-CO₂)	Human Health (DALY)	Social Assets (Yen)	Single Index (Yen)
Scenario 1	673.65	8.82E-05	2.18E+02	1100.07
Scenario 2	333.10	4.36E-05	1.08E+02	543.95

4 Conclusions

(1)The Anaerobic digestion followed by incineration route saved 856.92kWh of energy than the incineration without Anaerobic digestion route for every 1t of dry sludge disposal.

(2)The Anaerobic digestion followed by incineration route reduced 340.55kg of carbon dioxide emissions than the incineration without Anaerobic digestion route for every 1t of dry sludge disposal.

(3)The Anaerobic digestion followed by incineration route reduced the environmental impact by 50.5% compared with the incineration without Anaerobic digestion route.

(4)Based on the sludge data of Yamagata Sewage Plant, sludge Anaerobic digestion has a very significant beneficial impact on the environment.

Reference

[1] Shunan Zhao, et al. Does anaerobic digestion improve environmental and economic benefits of sludge incineration in China? Insight from life-cycle perspective. Resources Conservation and Recycling 188(15):106688.

[2] A, Xiaodi Hao , et al. Sustainable disposal of excess sludge: Incineration without anaerobic digestion. Water Research 170.

[3] Balasundaram, Gowtham. , et al. Energy feasibility and life cycle assessment of sludge pretreatment methods for advanced anaerobic digestion. Bioresource technology 357(2022):127345.

[4] Chao Rong , et al. Seasonal and annual energy efficiency of mainstream anaerobic membrane bioreactor (AnMBR) in temperate climates: Assessment in onsite pilot plant and estimation in scaled-up plant. Bioresource Technology,Volume 360, 2022, 127542.

The 11th International Symposium on Water Environment Systems
----- with Perspective of Global Safety   (Nov. 16th ~ 17th , 2023)

GP-RSS & SyDE
Tohoku University

The effect of recirculation on two-phase anaerobic fermentation system of food waste and paper waste

○ QINGKANG ZENG [1*], YUANYUAN REN [1] & YU-YOU LI [1]

[1]Department of Engineering, Tohoku University, Miyagi 980-8579, Japan.
*E-mail: zeng.qingkang.q4@dc.tohoku.ac.jp

Abstract

In the two-phase anaerobic fermentation system, organic matter is used by the acid generation bacteria in the first stage to produce VFAs and hydrogen, and the Methanogen in the second stage uses the VFAs generated in the first stage to generate methane. Therefore, the activity of acid generation bacteria in the first stage is always inhibited due to the low pH value caused by the accumulation of VFAs. In order to keep the stable operating of two-phase anaerobic fermentation system, additional alkaline substance need to be added into the hydrogen fermentation tank to control the pH in normal range. In this study, as to make the system become stable by itself, the sludge in methane fermentation tank will be recirculated into hydrogen fermentation tank which aims to dilute the substrate, provide alkalinity and microorganism for hydrogen fermentation tank. By conducting two long-term comparative experiments on whether sludge recirculation is added or not, it aims to research the effect of sludge recirculation on the gas generation capacity and organic matter degradation rate in each stage, and the organic matter degradation efficiency of the whole system.

Keywords: Co-fermentation; Food waste; Paper waste; Recirculation

1 Introduction

In the report of IEA in December 2022, it was forecast that "renewable energy will overtake coal as the world's largest power source by the beginning of 2025. From some viewpoints like global warming prevention, increasing prices of fossil fuel, and the goal of building decarbonized society, methods of generating hydrogen and methane from organic waste through anaerobic microorganisms are attracting attention. Among the different conversion technologies, anaerobic digestion (AD) is considered as the sustainable and environmental-friendly technology that stabilizes and deals with organic waste such as food waste and paper waste, reduces the amount of organic matter, and adds value of circulating fuel that simultaneously generates methane and hydrogen. Food waste and paper waste are two main components of solid waste, and the past researches have shown that co-digestion of FW and PW can effectively get stable biogas generation. In addition, it has also been informed that two-phase anaerobic digestion systems can provide ideal environmental conditions for different microbial groups in two reactors, increase substrate degradation and improve the stability of the whole system. However, due to the high TS in hydrogen fermentation reactor, it is difficult to mix sludge evenly, and the accumulation of VFA leads to the continuous decrease of pH value in sludge, which will inhibit the activity of microorganisms. Therefore, by recirculating the methane fermentation sludge to hydrogen fermentation tank, the purpose of dilution, addition of alkalinity and microorganisms will come true. So, in order to test the impact of sludge recirculation, we conducted the following research.

2 Materials and methods

The two-phase AD research of food waste and paper waste was conducted using the continuous experiment system shown in Figure 1. The experiment was conducted by mixed food waste and paper waste as the total solid mass ratio was 7:3 and the TS concentration was 10%. The hydrogen fermentation tank and methane fermentation tank were employed as the thermophilic reactor and mesophilic reactor respectively. 600 ml of substrate was supplied into the system every day during continuous experiment. It was controlled whether recirculation was added or not, and then analyzed the biogas production performance and organic matters degradation efficiency in two different situations, in order to explore the effect of sludge recirculation on the two-phase anaerobic fermentation system. The concrete experiment flow is shown in Figure 2.
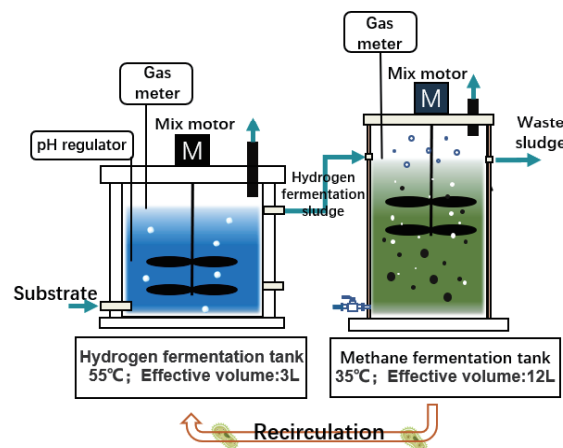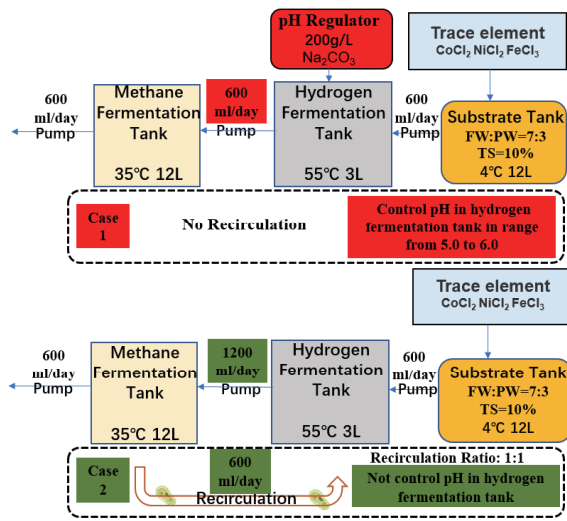

Fig. 1. Continuous experiment device.

The 11th International Symposium on Water Environment Systems
----- with Perspective of Global Safety   (Nov. 16th ~ 17th , 2023)

GP-RSS & SyDE
Tohoku University

Fig. 2. Continuous experiment process.

3 Results and discussion

The biogas production and composition in the hydrogen fermentation tank and methane fermentation tank were respectively analyzed every day and some parameters such as pH, alkalinity, the concentrations of COD, carbohydrates, protein, ammonia, VFAs and so on were measured for analyzing the substrate degradation efficiency, biogas production rates both in the two fermentation tanks. Figures 3 and 4 respectively showed the data of some parameters in hydrogen fermentation tank and methane fermentation tank before and after adding   recirculation during the long-time and continuous operating. For two-phase anaerobic fermentation systems, adding recirculation can significantly improve the generation rate and yield of hydrogen and methane. When adding the recirculation in system, the concentration of TAN and alkalinity in hydrogen fermentation tank increased, while TS/VS   decreased. And in methane fermentation tank, these parameters do not change obviously after adding recirculation.

4 Conclusions

(1) The long-term continuous experiment had verified that the recirculation ratio of 1:1 can maintain stable biogas production and system itself stability, without the need for additional alkaline solution to control the pH of hydrogen fermentation tank. The biggest advantage of adding recirculation is that it can make the two-phase anaerobic fermentation system stably produce biogas by itself which would significantly reduce the cost of system.

(2) Adding recirculation significantly reduced the concentration of VFAs in hydrogen and methane fermentation tanks, which indicated the reduced risk of acidification, more complete utilization of VFAs and higher microbial activity in system.

(3) It significantly reduced the TS and VS of sludge in hydrogen fermentation tank, supplemented the alkalinity, and improved the degradation rate of various organic matters when added sludge recirculation in two-phase AD system.
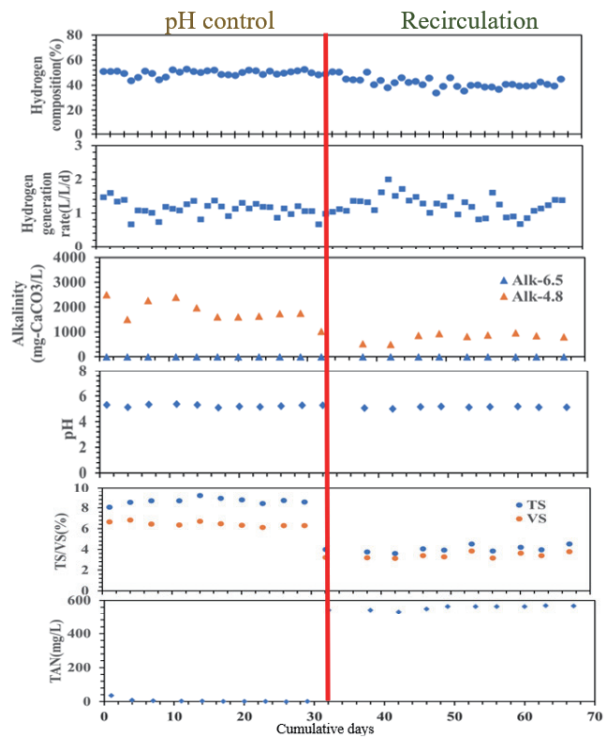

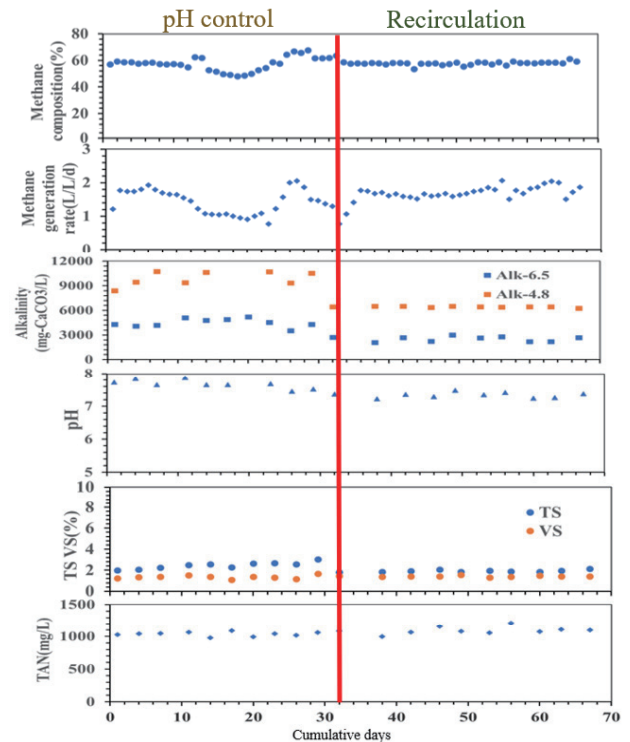
Fig. 3. Hydrogen fermentation tank.

Fig. 4. Methane fermentation tank.

Reference

[1] Yu Qin, Yu-You Li, Co-production of biohydrogen and biomethane from food waste and paper waste via recirculated two-phase anaerobic digestion process: Bioenergy yields and metabolic distribution, Bioresource Technology, Volume276, 2019.

The 11th International Symposium on Water Environment Systems
----- with Perspective of Global Safety   (Nov. 16th ~ 17th , 2023)

GP-RSS & SyDe
Tohoku University

Biomethanation of H_2 and CO_2 in an anaerobic membrane reactor

○Juntong Ha[1]*, Min Ye[2], Yu Qin[2] & Yu-You Li[1,2]

1 Department of Frontier Science for Advanced Environment, Graduate School of Environmental Studies, Tohoku University, Miyagi 980-8579, Japan.
2 Department of Civil and Environmental Engineering, Tohoku University, Graduate School of Engineering, Miyagi 980-8579, Japan

Abstract

Efforts toward biomethanation technology are accelerating as measures for Carbon Capture, Usage, and Storage (CCUS) technology. However, few studies are related to microbial competition for H_2/CO_2 consumption between hydrogenotrophic methanogens and homoacetogens. The aim of this study was to study the competitive relationship between these two microorganisms under the condition that H_2/CO_2 is the only gaseous substrate. This study used a 15L AnMBR and flat film to maintain anaerobic microorganisms' growth. (1) Under the condition of pH 7.5, we conducted biomethanation by increasing the gas loading rate of the reactor in stage, to observe the maximum methane production or acetate production efficiency. (2) The relationship between CH_4 production, acetic acid accumulation, and HCO_3^- concentration was discussed by periodically detecting the HCO_3^- concentration in the reactor.

Keywords: Biomethanation, Bio-acidification, Homoacetogenesis, AnMBR, Decarburization.

1 Introduction

In the final stage of methane fermentation, hydrogenotrophic methanogens and homoacetogens compete for H_2 as a substrate. Biomethanation technology uses methanogenesis to convert H_2/CO_2 into CH_4 under anaerobic conditions. Homoacetogenesis can grow on gaseous substrates($H_2/CO_2/CO$) and produce acetic acid as the main product through a metabolic process called reductive acetogenesis. Acetic acid is an important material for industrial production, widely used in the fields of textiles, medicine, food, and so on. Furthermore, Bio-acidification technology produces 1 mole of acetic acid from 2 moles of CO_2, whereas the biomethanation process produces 1 mole of CH_4 from 1 mole of CO_2. Both technologies consume the same volumes of H_2, whereas bio-acidification doubles the volumes of CO_2 consumed. Thus, homoacetogenesis also can be seen as a strategy for biological CO_2 decarbonization.

$$CO_2 + 4H_2 \rightarrow CH_4 + 2H_2O \qquad \Delta G = -135.6 (KJ/mol) \quad (1)$$
$$2CO_2 + 4H_2 \rightarrow CH_3COOH + 2H_2O \quad \Delta G = -104.6 (KJ/mol) (2)$$

Factors affecting competition between the two microorganisms include pH, temperature, H_2 partial pressure, trace elements, gas solubilization efficiency, and alkalinity. For example, homoacetogens prefer weakly acidic environments, whereas hydrogenotrophic methanogens are better adapted to pH-neutral environments. However, due to the complexity of microbial diversity and interactions in actual industrial operation, as well as other microorganisms (sulfate-reducing bacteria) can also influence the competitive relationship. So an in-depth understanding of the competition between homoacetogens and hydrogenotrophic methanogens is required.

In order to deeply investigate the competition between homoacetogenesis and methanogenesis, firstly we explored the effect of gas loading rate on methanogenesis and acetic acid accumulation under pH 7.5. By staging increasing the gas flow rate, methane production rate, acetic acid concentration, and HCO_3^- concentration were discussed by periodically detecting the HCO_3^- concentration in the reactor.

2 Materials and methods

2.1 Long-term continuous experiment

The overview of the AnMBR reactor is shown in Figure 1. The AnMBR reactor with a liquid volume of 6 L and a top gas space of 9 L was operated at 35°C. The H_2/CO_2 ratio remains at 4:1. The mixed gas enters the reactor through the gas dispersion device at the bottom of the membrane unit. The inoculum was obtained from a UASB reactor treating methanol wastewater. The experiment was carried out for 40days and was divided into two phases. During Phase 1(day 0-24), the gas loading rate was maintained at 3.5 L/L/d and 5.3 L/L/d in Phase 2. The detailed operation conditions of the reactor are provided in Table 1.
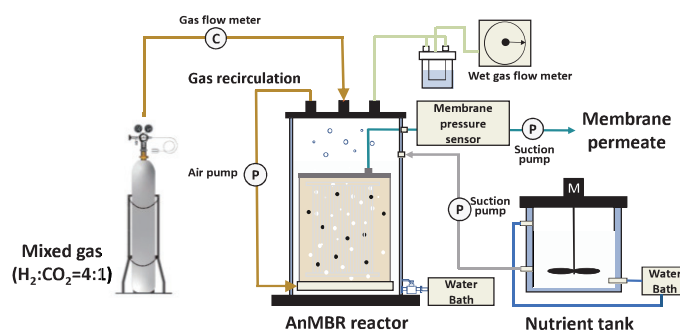

Fig.1. Schematic diagram of AnMBR

Table 1. Reactor operating conditions

Phase	I	II
Inject gas	H_2 & CO_2	
H_2:CO_2 ratio	4:1	4:1
H_2 loading rate(L/L/d)	2.96	4
CO_2 loading rate(L/L/d)	0.74	1
pH	7.5	7.5

2.2 Sampling and analytical methods

All samples of membrane permeate were analyzed after being filtrated through Millipore filter units with 0.45μm pore size. The composition of the biogas(H_2, CH_4, CO_2)was measured once daily using a gas chromatograph with a TCD detector. The volatile fatty acids(VFAs)were quantified by gas chromatography(Agilent 6890 series).

The 11th International Symposium on Water Environment Systems
----- with Perspective of Global Safety   (Nov. 16th ～ 17th , 2023)

GP-RSS & SyDE
Tohoku University

3 Results and discussion

3.1 Reactor performance

Fig.2 shows the results of a long-term continuous operation of the AnMBR. Table 2 shows the reactor performance at two different phases. The pH was stable in the range of 7.3-7.5 from phase 1 to phase 2. The CH_4 production rate also increased progressively with increasing gas loading rate. From the first day of operation, the VFA concentration in the system gradually decreases, which means that the accumulated acetic acid is quickly converted into methane. This may be because the methanogenic bacteria gradually adapted to the system. However, in phase 2, when the gas flow rate was increased to 5.3 L/L/d, there was a decreasing trend in gas utilization efficiency, H_2 was from 85% to 72%, and CO_2 was from 86.1% to 72%. and there was a decrease in CH_4 content to 31.5%.
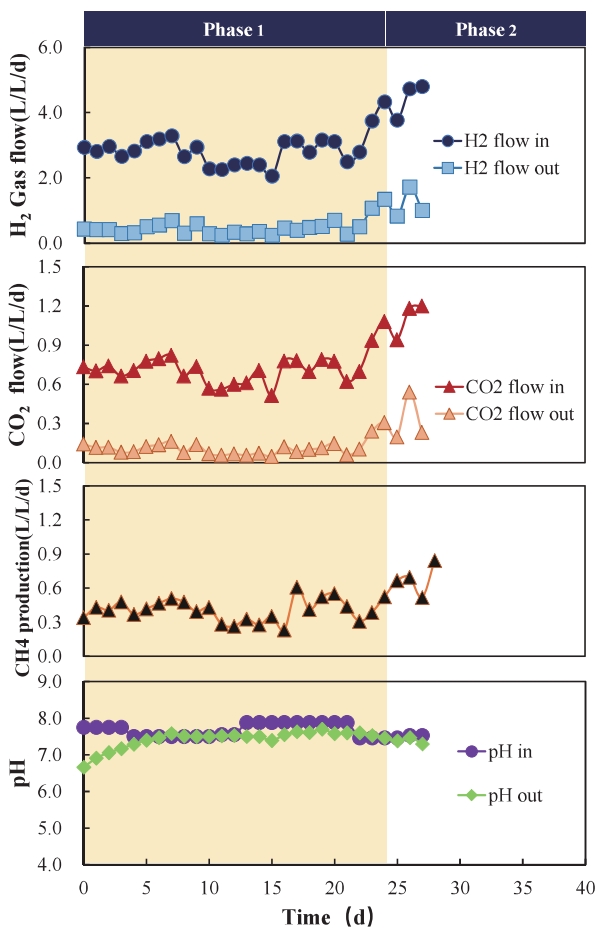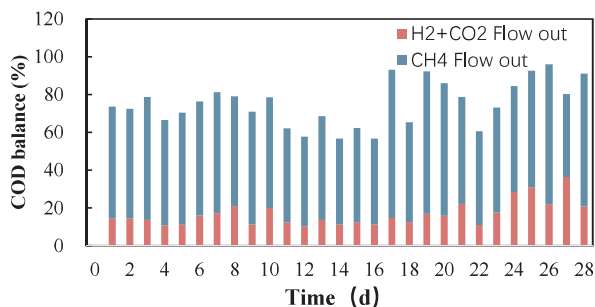
Table 2 Reactor performance at two different phases

	Phase 1	Phase 2
Operation days	0-24	24-now
Gas loading rate（L/L/d）	3.5	5.3
Gas loading rate （gCOD/L/d）	2.0	3.0
Biogas composition		
CH_4%	44.9	31.5
CO_2%	10.6	13.7
H_2%	44.5	54.8
CH_4 yield（mL/gVS/d）	91.6	147.4
CH_4 production（L/L/d）	0.40	0.65
H_2 flow in（L/L/d）	2.77	4.27
H_2 flow out（L/L/d）	0.41	1.19
CO_2 flow in（L/L/d）	0.70	1.07
CO_2 flow out（L/L/d）	0.10	0.30
H_2 utilization efficiency(%)	85.4	72.3
CO_2 utilization efficiency (%)	86.1	72.0

4 Conclusions

Increasing the gas loading rate led to an increase in the hydrogen partial pressure in the reactor. High hydrogen partial pressure is not conducive to the production of methane by hydrogenotrophic methanogenic bacteria, so methane production shows a downward trend. However, under high hydrogen partial pressure, the activity of homoacetogens was enhanced, so the acetic acid concentration in the system shows an upward trend. In the next operating phase, in order to further verify this speculation, the gas loading rate will continue to be increased.

Reference

[1]Chun-Yu Lai, Hydrogen-driven microbial biogas upgrading: Advances, challenges, and solutions[J]. Water Research, 2021, 197: 117120.
[2]Akira Hafuka, In-situ biogas upgrading with H_2 addition in an anaerobic membrane bioreactor (AnMBR) digesting waste activated sludge[J]. Science of The Total Environment, 2022, 828: 154573.
[3] Giorgio Pratofiorito. A membrane biofilm reactor for hydrogenotrophic methanation[J]. Bioresource Technology, 2021, 321: 124444.
[4]Díaz I. A feasibility study on the bioconversion of $CO2$ and $H2$ to biomethane by gas sparging through polymeric membranes[J]. Bioresource Technology, 2015, 185: 246-253.
[5]Alfaro N. $H2$ addition through a submerged membrane for in-situ biogas upgrading in the anaerobic digestion of sewage sludge[J]. Bioresource technology, 2019, 280: 1-8.

Fig. 2. Reactor performance of H_2 and CO_2.

Fig. 3. COD balance calculation

The 11th International Symposium on Water Environment Systems
----- with Perspective of Global Safety   (Nov. 16th ~ 17th , 2023)

GP-RSS & SyDE
Tohoku University

Utilizing Thermodynamics to Analyze methane production AnMBR System for Sulfate-Laden Wastewater Treatment

Zifan Wu[1], Tianwei Hao[1*]

[1]Department of Civil and Environmental Engineering, Faculty of Science and Technology, University of Macau, Macau, China.
*E-mail: twhao@um.edu.mo.

Abstract

In this AnMBR study, we achieved a remarkable organic carbon removal efficiency exceeding 90%. Intriguingly, methane production displayed fluctuations upon the addition of higher sulfate levels, resulting in yields ranging from 106.5 to 209.7 mL/g CODre. Our COD balance analysis unveiled intensified competition following the addition of sulfate. Our investigation also encompassed Gibbs energy changes ($\Delta_{rxn}G$) for pivotal reactions within the AnMBR, including H_2, acetate, and CO_2 generation, as well as methanogenesis and sulfidogenesis processes. These results are presented as $\Delta_{rxn}G$ curves over the experimental phases. It was observed that to promote significant syntrophic methanogenesis, the concentration of $H_2(aq)$ must exceed 2.87×10^{-6} M, ensuring a negative $\Delta_{rxn}G$. Consequently, our findings suggest that syntrophic methanogenesis could be substantially inhibited when H_2 falls below this threshold, leading to a reduction in methane production.

Keywords: AnMBR; Methane production; Gibbs energy change; Methanogenesis; Sulfidogenesis

1 Introduction

Recent advances in wastewater treatment extend beyond purification to focus on energy and resource recovery. The Anaerobic Membrane Bioreactor (AnMBR) is an innovative technology that combines anaerobic digestion with membrane separation, offering a novel approach (Ji et al., 2021). In influent wastewater with sulfate concentrations of 50-500 mg/L, effective sulfate management can boost methane production by aiding hydrolysis and propionic degradation.

This study aims to develop a quantitative thermodynamic model to enhance our understanding of anaerobic digestion with sulfate. The research posits that biological reactions adhere to thermodynamic principles and depend on a negative Gibbs energy change ($\Delta_{rxn}G$) for significant progress. Microorganisms serve as catalysts, accelerating reactions, but they don't influence the thermodynamics (Hansen, 2023). Enzyme-catalyzed reactions with low activation energies suggest that a more negative $\Delta_{rxn}G$ value in a faster reaction rate, making the rate directly proportional to $\Delta_{rxn}G$.

2 Materials and methods

The AnMBR system utilized a micro-filtration module with a flat-type polyvinylidene difluoride membrane, featuring a 0.45 μm pore size. Synthetic domestic wastewater was continuously moved by a peristaltic pump for influent and effluent management. Biogas produced was recirculated to clean the membrane via a gas diffuser, and gas production was quantified using a gas bag. Transmembrane pressure was monitored with an integrated pressure meter. In the initial startup phase (phase 1), municipal sewage treatment plant sludge was introduced. The mixed liquid volatile suspended solids concentration was maintained at 8-10 g/L, and the reactor's temperature was kept between 30-35 ℃.

3 Results and discussion

During phase 1, the AnMBR system operated with a hydraulic retention time (HRT) of 11-13 hours, processing synthetic sewage with COD concentrations of 428.6-532.2 mg/L and SO_4^{2-}-S content below 10 mg/L. This phase enabled microorganism acclimatization. In phase 2, with COD levels of 428.6-532.2 mg/L and SO_4^{2-}-S content of 23.6-26.8 mg/L, the AnMBR maintained an HRT of 11-13 hours. Phase 3, with COD spanning 458.8-511 mg/L and SO_4^{2-}-S at 37.8-41.8 mg/L, preserved the same HRT. Phase 4, with COD within 432.5-531.9 mg/L and SO_4^{2-}-S at 37.8-41.8 mg/L, saw the HRT reduced to 5-7 hours. In phase 5, COD ranged from 433.1 to 526.1 mg/L, with SO_4^{2-}-S content between 105.2 and 116.6 mg/L, and the HRT was adjusted to 5-7 hours for treatment optimization (Table 1).

Table 1 The characteristics of AnMBR

Phases (day)	HRT (hours)	COD Conc.(mg/L)	SO_4^{2-}-S Conc.(mg/L)
1(1-32)	12±1	472.4±41.8	9.8±1.8
2(33-70)	12±1	480.4±51.8	25.2±1.6
3(71-94)	12±1	484.9±26.1	39.8±2.0
4(95-172)	6±1	482.2±49.7	40.9±3.2
5(173-204)	6±1	478.1±45.8	110.9±5.7

Over the 200-day experimental duration, the AnMBR system consistently exhibited remarkable organic matter removal efficiency, consistently surpassing 90% (Fig. 1). This level of performance represents a substantial improvement over the conventional anaerobic bioreactors, which typically achieve around 60% COD removal. Moreover, sulfate-S removal, particularly in the initial stages, approached 40%, gradually escalating to exceed 80% with the rise in sulfate-S concentration.
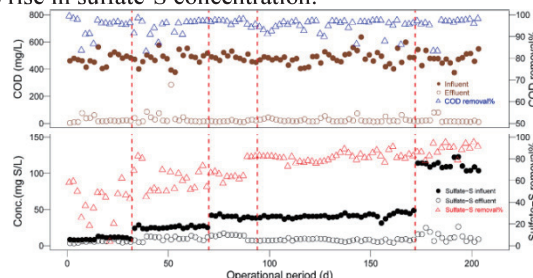

Fig. 1. AnMBR performance of long-term experiment

In both phase 1 and phase 2, the methane yield surpassed 200 mL/g CODre. Notably, when a higher sulfate-S dosage was employed, a considerable decrease in CH4 yield was observed. Conversely, at lower sulfate-S concentrations, no substantial alteration in CH4 production occurred (Fig. 2).

The 11th International Symposium on Water Environment Systems
----- with Perspective of Global Safety   (Nov. 16th ~ 17th , 2023)

GP-RSS & SyDE
Tohoku University

Based on organic matter balance analysis, the conversion of COD through sulfate reduction exhibited a remarkable shift, escalating from <1% in phase 1 to over 30% in phase 5. This indicates a substantial intensification in the competition for organic substrates. Furthermore, in cases involving lower sulfate-S dosages, nearly 60% of COD was transformed into methane, a percentage that dropped to under 40% with increased sulfate-S supplementation (Fig. 3). Nonetheless, the specific pathway affected by sulfate addition remains unclear.
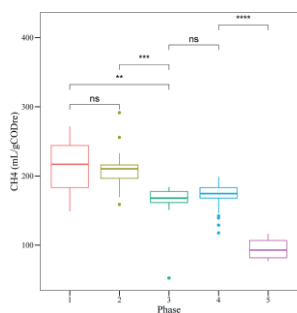

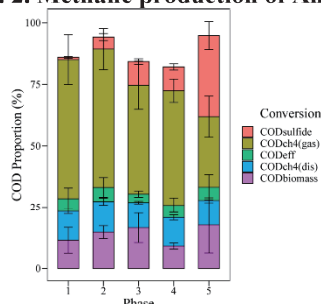**Fig. 2. Methane production of AnMBR**

Fig. 3. COD balance of long-term experiment

The $\Delta_{rxn}G$ calculations indicate that sulfidogenic reaction by acetoclastic SRB is anticipated to exhibit significantly faster rates compared to acetoclastic methanogenesis reaction across all sulfate concentrations. The acetoclastic methanogenesis reaction closely approximates the syntrophic methanogenesis reaction at various sulfate concentrations, a similarity that might be influenced by the H_2 concentration within the reactor. Notably, the syntrophic sulfidogenesis reaction yields substantially lower rates than the other three types of reactions, as depicted in Figure 4. Based on these findings, a preliminary inference can be drawn that the addition of sulfate has the potential to induce competition for acetate and consequently influence the H_2 utilization pathway. To trigger a substantial occurrence of syntrophic methanogenesis, it is imperative that the concentration of $H_2(aq)$ remains above the threshold indicated by the black dashed line, $\log_{10}(2.87*10^{-6}$ mol/L) (Fig. 5). Acetate, propionate, butyrate, and valerate all play pivotal roles in facilitating syntrophic methanogenesis under our experimental conditions. It's worth noting that acetate serves as a byproduct of H_2 production resulting from VFAs degradation. As such, any reduction in acetate removal tends to enhance H_2 production. Consequently, it can be anticipated that the rate of H_2 production will increase as acetate consumption intensifies due to competition with acetoclastic SRB.

H_2 plays a crucial role as an intermediate in the degradation of organic matter through methanogenesis, and it is rapidly cycled within this process, as evidenced by $\Delta_{rxn}G$ value. Additionally, it is essential to note that hydrogenotrophic

SRB have a lower Ks value than hydrogenotrophic methanogens, which gives them a competitive advantage, as highlighted in previous studies(Conrad, 1999).
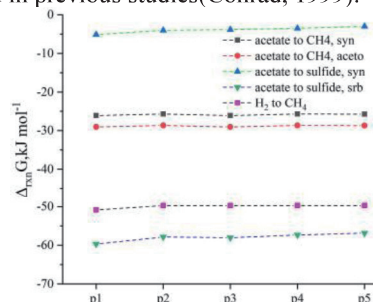

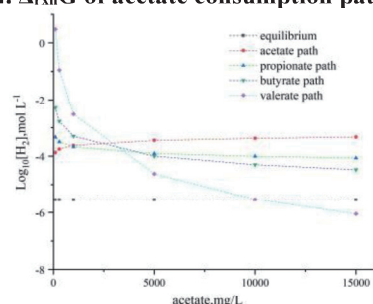**Fig. 4. $\Delta_{rxn}G$ of acetate consumption pathways**

Fig. 5. Logrithmn of the molar concentration of $H_2(aq)$ at equilibrium for VFAs

When the concentration of $H_2(aq)$ falls below the critical threshold concentration for hydrogenotrophic methanogenesis, this microbial activity comes to a halt. Following the introduction of sulfate, where the rates of H_2 utilization for methanogenesis and sulfate reduction are both existed, steady-state conditions shift from exclusive methanogenic H_2 utilization to simultaneous utilization by both methanogenesis and sulfate reduction. This transition results in a drop in the steady-state H_2 concentration below the threshold required for methanogens, leading to the cessation of CH_4 production.

4 Conclusions

The AnMBR system consistently demonstrated exceptional organic matter and sulfate-S removal efficiency. The introduction of higher sulfate levels notably impacted methane production. The analysis of the organic carbon balance and Gibbs free energy suggests that competition for organic substrates occurred following sulfate addition. Hydrogenotrophic methanogenesis ceased when the H_2 concentration dropped below a critical equilibrium level.

Reference

Conrad, R., Contribution of hydrogen to methane production and control of hydrogen concentrations in methanogenic soils and sediments. FEMS Microbiology Ecology 28 (1999), 193–202.

Hansen, L.D., Thermodynamic method for analyzing and optimizing pretreatment/anaerobic digestion systems. Biofuel Res. J. 10 (2023), 1816–1829.

Ji, J., Chen, Y., Hu, Y. et al., One-year operation of a 20-L submerged anaerobic membrane bioreactor for real domestic wastewater treatment at room temperature: Pursuing the optimal HRT and sustainable flux. Science of The Total Environment 775 (2021), 145799.

The 11th International Symposium on Water Environment Systems ----- with Perspective of Global Safety   (Nov. 16th ~ 17th , 2023)

GP-RSS & SyDE
Tohoku University

Enhanced methanogenesis for dry anaerobic digestion of chicken manure with in-situ ammonia stripping

○ Yapeng Song[1,2], Wei Qiao[1,2]* & Renjie Dong[1]

[1]College of Engineering, Biomass Engineering Center, China Agricultural University, Beijing 100083, China;
[2]Sanya Institute of China Agricultural University, Sanya, Hainan Province, 572025, China.
*E-mail: songyapeng202109@126.com

Abstract

Dry anaerobic digestion of chicken manure faces the bottleneck of ammonia inhibition. In-situ ammonia stripping was investigated to alleviate ammonia inhibition in the dry anaerobic digestion of chicken manure (feeding a total solid 20%). This study examined the influence of the in-situ ammonia stripping process on the fermentation performance through digester operation for 550 days. The results obtained in this study demonstrated that the stripping process effectively decreased the concentration of ammonia nitrogen (TAN) from 8.0 to 3.0 g/L, resulting in a methane yield of up to 0.3 L/g-VS. The removal efficiencies of COD, carbohydrates, and proteins were 72%, 92%, and 57%, respectively. In conclusion, ammonia stripping is a promising approach for alleviating ammonia inhibition, and it holds the potential for industrial application due to its simple operation.

Keywords: Dry anaerobic digestion; Chicken manure; ammonia stripping.

1 Introduction

Ammonia inhibition poses a significant challenge in the anaerobic digestion of high-solid chicken manure. The primary approach to mitigate this inhibition is by reducing ammonia levels. In-situ ammonia stripping has shown promising results in effectively decreasing ammonia concentrations, achieving a 30% removal efficiency, and increasing methane yield by 34%[1]. Therefore, ammonia stripping holds excellent potential for improving ammonia removal and methane production.

This study aims to verify the feasibility of the in-situ ammonia stripping process through a long-term continuous operation in the dry anaerobic digestion of chicken manure with a total solid (TS) feeding rate of 20%. The findings from this study may provide valuable insights into the industrial application of anaerobic treatment for chicken manure.

2 Materials and methods

2.1 Substrate and inoculum

Chicken manure comes from large chicken farms. Collect chicken manure and place it in a refrigerator at 4 °C with a 21-25% TS. TS was diluted to 20% as substrate. The inoculum was taken from a mesophilic digester (37°C, fed with chicken manure, 10% TS, hydraulic retention time (HRT) of 30 d), and the chemical properties of the substrate and inoculum were shown in Table 1.

2.2 Setup of in-situ stripping CSTR system

A continuous stirred-tank reactor (CSTR) was employed with a working volume of 4.0 L and a total volume of 6.0 L. The digester was maintained at 37±1℃. The HRT was 60-120 d, and the OLR was 1.4-2.8 g-VS/(L· d). The in-situ ammonia stripping system includes a biogas circulation pump and an ammonia absorption bottle. The ammonia absorption bottle contained 400 mL of 6 M phosphoric acid. The ammonia stripping pump operates continuously at 4.0 L/min and 1 d interval (1 d-on/1 d-off) under HRT 120-90 d and continuous stripping for HRT 60 d. The ammonia stripping process of the reactor is shown in Figure 1.
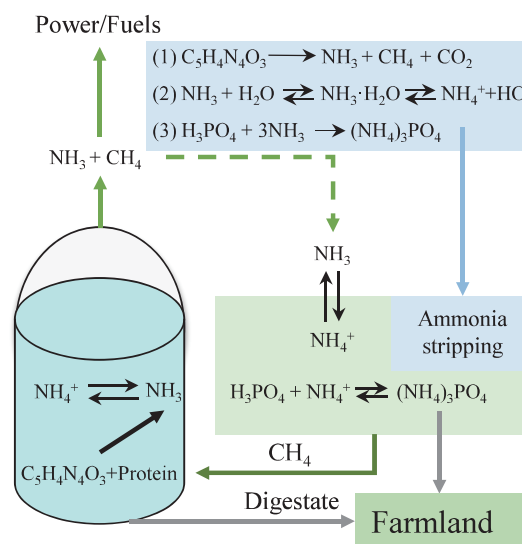

Power/Fuels

(1) $C_5H_4N_4O_3 \longrightarrow NH_3 + CH_4 + CO_2$

(2) $NH_3 + H_2O \rightleftarrows NH_3 \cdot H_2O \rightleftarrows NH_4^+ + HO^-$

(3) $H_3PO_4 + 3NH_3 \longrightarrow (NH_4)_3PO_4$

$NH_3 + CH_4$

NH_3

NH_4^+

Ammonia stripping

$NH_4^+ \rightleftarrows NH_3$

$H_3PO_4 + NH_4^+ \rightleftarrows (NH_4)_3PO_4$

$C_5H_4N_4O_3 + Protein$

CH_4

Digestate

Farmland

Fig. 1. Ammonia stripping process of reactor

3 Results and discussion

3.1 Methane production performance under stripping

The reactor operates for about 500 days. There was no ammonia stripping. The TAN concentration exceeded 8.0 g/L after 150 days, and biogas production stopped. Ammonia stripping was used in HRT 120, and TAN was stable at about 3.8 g/L. The methane yield reached 0.30 L/g-VS. Although the HRT was 90 d, the TAN increased a litter (4.7 g/L), and the biogas production performance was excellent. The HRT was 60 d, and a lower TAN concentration (3.0 g/L) was achieved due to the continuous stripping operation. The methane yield reached 0.29 L/g-VS. The methane yield of different HRT phases reached 72%-77% of the theoretical potential of chicken manure. The biochemical methane potential (BMP) of chicken manure was around 0.3 L/g-VS [2]. This indicates that ammonia inhibition did not occur during the study.

The 11th International Symposium on Water Environment Systems
----- with Perspective of Global Safety   (Nov. 16th ~ 17th , 2023)

GP-RSS & SyDE
Tohoku University

The TVFA concentration was between 0.5-1.7 g/L under stripping conditions, demonstrating the efficient conversion of organic acids to methane at low ammonia conditions. VFA accumulation causes additional stress, especially in high-ammonia systems. It is not recommended that the OLR was more significant than 3 g-VS/(L·d) for the anaerobic digestion of chicken manure. In this study, although the OLR increased to 2.8 g-VS/(L·d), the lower VFA concentration (0.5 g/L) illustrates the excellent methane production performance in low ammonia conditions.
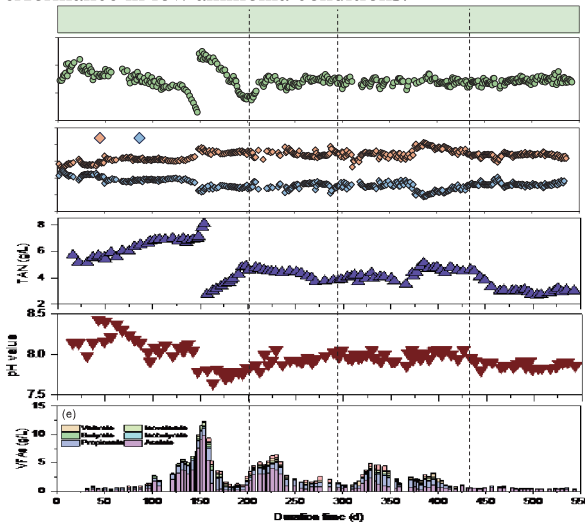

Fig. 2. Operation performance under ammonia stress

Table 1. Performance of methane production performance of high solid chicken manure.

Parameters	Unit	HRT 120 d	HRT 120 d	HRT 90 d	HRT 60 d
Duration	d	1-204	205-295	296-431	431-500
Operation	/	No stripping	With stripping	With stripping	With stripping
Biogas production	L/L/d	/	0.59	0.74	1.18
CH4 in biogas	%	/	69	73	67
TAN	g/L	8.2	3.8	4.7	3.0
FAN	g/L	0.7	0.4	0.3	0.3
pH	/	8.01	7.92	7.72	7.79
Total VFA	g/L	11.9	1.7	0.9	0.7
Acetate	g/L	9.5	0.7	0.5	0.5
Propionate	g/L	1.3	0.6	0.2	0.1
Other acids	g/L	1.1	0.4	0.2	0.1
TS removal	%	/	71	67	65
VS removal	%	/	84	83	82
COD removal	%	/	73	71	72

3.2 Matter conversion flow under different ammonia stress

The material flow and balance of different ammonia stress are shown in Figure 3. The higher TS, VS, and COD removal efficiencies were mainly attributed to the low ammonia level and long HRT in this study. The higher carbohydrate and protein degradation efficiencies also explained the higher material conversion. The TAN concentration increased from 2.8 to 9.0 g/L, the degradation efficiency of carbohydrates decreased by 28%, and 92% for protein [3]. In addition, the contribution rates of carbohydrates and proteins to methane production were 46%-48% and 24-27%, respectively, and both account for 71%-73%. The contribution of protein degradation to methane production increased the methane yield due to the higher methane production potential of proteins compared with carbohydrates (0.53 vs 0.42 L/g-VS) for the anaerobic digestion of rich nitrogen substrate. The stripping process overcomes ammonia inhibition and enhances the degradation of proteins and carbohydrates.

Hydrolysis, acidogenesis, acetogenesis, and methanogenesis efficiencies were 57%-59%, 63-70%, 68%-71%, and 67%-70% under ammonia stripping operation. The acidogenesis was the same as the methanogenesis efficiency, which indicates that VFAs could be converted into methane effectively. The IC50 (50% inhibition) of the hydrolysis and acidogenesis process was around 5.3-5.7 g/L, while it was 5.0 g/L for the methanogens in thermophilic anaerobic digestion chicken manure[4]. Therefore, the main reasons for the accumulation of VFA were the different responses of anaerobic consortia to high ammonia levels and hydrolysis/acidogenesis bacteria continuing to produce organic acids. In-situ stripping can reduce the concentration of TAN to achieve high-efficiency material conversion of high-solid chicken manure, which provides new insights for the engineering application of high-solid chicken manure.
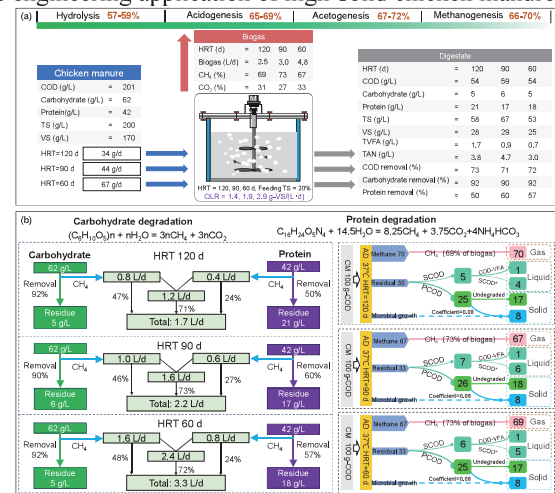

Fig. 3. Material balance, conversion efficiency, and methane production contribution

4 Conclusions

Through the long-term operation of a continuously operated reactor, ammonia stripping effectively reduced the concentration of TAN, resulting in enhanced methane production. Additionally, the volatile fatty acids were maintained at a low level. The changes observed in the dominant methanogens provided helpful information for understanding the impact of reducing ammonia concentration on process performance.

Reference

[1] S. Bi, W. Qiao, L. Xiong, A. Mandy, S.M. Wandera, D. Yin, R. Dong, Improved high solid anaerobic digestion of chicken manure by moderate in situ ammonia stripping and its relation to metabolic pathway[J]. Renewable energy, 2020, 146: 2380-2389.

[2] Y. Song, W. Qiao, M. Westerholm, G. Huang, M.J. Taherzadeh, R. Dong, Microbiological and Technological Insights on Anaerobic Digestion of Animal Manure: A Review[J]. Fermentation, 2023, 9: 436.

[3] Q. Niu, Y. Takemura, K. Kubota, Y.Y. Li, Comparing mesophilic and thermophilic anaerobic digestion of chicken manure: Microbial community dynamics and process resilience[J]. Waste Management, 2015, 43: 114-122.

[4] Q. Niu, T. Hojo, W. Qiao, H. Qiang, Y.-Y. Li, Characterization of methanogenesis, acidogenesis and hydrolysis in thermophilic methane fermentation of chicken manure[J]. Chemical Engineering Journal, 2014, 244: 587-596.

The 11ᵗʰ International Symposium on Water Environment Systems
----- with Perspective of Global Safety   (Nov. 16ᵗʰ ~ 17ᵗʰ , 2023)

GP-RSS & SyDE
Tohoku University

Ozone pretreatment combined with partial denitrification-anammox process for efficient nitrogen removal from nanofiltration concentrate of landfill leachate

Haoran Zhao[1], Lianpei Zou[1], Mengting Jiang[1], Yu-You Li[2], Jianyong Liu[1*], Yuanyuan Shi[1]

[1]School of Environmental and Chemical Engineering, Shanghai University, 333 Nanchen Road, Shanghai 200444, China
[2]Department of Civil and Environmental Engineering, Graduate School of Engineering, Tohoku University, 6-6-06 Aza, Aramaki, Aoba-ku, Sendai, Miyagi 980-8579, Japan.
*E-mail: liujianyong@shu.edu.cn

Abstract

  Treatment of nanofiltration concentrate (NFC) from landfill leachate is challenging due to its complex composition and high concentration of refractory organic matter. This study proposed a combined process of ozone pretreatment and partial denitrification/anammox (PD/A) for treating NFC, exploring the feasibility of using ozone-oxidized NFC as a carbon source for partial denitrification. The ozone oxidation process was employed to degrade the refractory organic compounds. With an ozone flow rate of 1.2 L/min and a reaction time of 50 min, the chemical oxygen demand (COD) removal efficiency of NFC was 20.83%, and the volatile fatty acid (VFA) content reached a maximum value of 104.37 mg/L. Meanwhile, the process significantly increased the ammonia and nitrate concentrations in the NFC. Then, PD/A process was applied to remove nitrogen from the NFC. Results showed that PD/A can effectively remove nitrogen from the NFC without additional carbon source. Using VFA produced in the ozone oxidation stage as carbon source, the reactor achieved a nitrogen removal efficiency of approximately 70%, resulting in an effluent with a total nitrogen below 40 mg/L, which satisfied the relevant standards in China. This study provides new insights into the application of ozone oxidation and PD/A in treating NFC from leachate.
Keywords: Nitrogen removal; Ozonation; PD/A; Refractory organic matter; Wastewater treatment.

1 Introduction

  As the amount of municipal solid waste increases, so does the production of landfill leachate. Membrane advanced treatment technologies, such as nanofiltration (NF) and reverse osmosis (RO), are commonly used for landfill leachate treatment, but the resulting nano filtration concentrate (NFC) can account for up to 30% of the total leachate generated. NFC is a complex wastewater with high organic content, poor biodegradability, and a complicated composition that presents challenges in its treatment, which may pose potential environmental risks.

  In developing countries, such as China, it is common to treat NFC by recycling it back into the landfill. However, this practice results in the accumulation of salts and recalcitrant pollutants, which in turn makes the treatment of leachate more challenging[1]. To address these challenges, advanced oxidation processes (AOPs) have gained attention for treating NFC due to their ability to remove refractory organic compounds and improve biodegradability. Specifically, Ozone-based advanced oxidation has emerged as a popular choice for the advanced treatment of landfill leachate or NFC. Reports indicate that ozone oxidation is not only effective in eliminating some organic pollutants from NFC, but it also promotes the transformation of refractory organic compounds and enhances the biodegradability of the concentrate.

  Typically, after being treated by ozone oxidation, the NFC is recycled back into the biological system for conventional nitrification–denitrification process, which still requires large amount of aeration and additional carbon source, resulting in high energy consumption. 25% and save

100% of organic matter, but their practical application is limited by the requirement for nitrite. With the concept of Partial denitrification (PD) being proposed and widely recognized in recent years, the coupling process of Partial denitrification Anammox (PD/A) has become an effective method for achieving advanced nitrogen removal of landfill leachate. As shown in the equation, the PD process is suitable for treating wastewater rich in ammonia and nitrate, but still requires a small amount of additional carbon source.

  In this study, an innovative process was proposed to treat NFC by combining ozone oxidation with PD/A. Firstly, ozone oxidation was utilized to remove refractory organic substances from the NFC and greatly enhance its biodegradability. It is noteworthy that ozone oxidation is usually considered to cause an increase in ammonia nitrogen, but in this study, the concentrations of both ammonia and nitrate in the NFC increased significantly after ozone oxidation, which is favorable for the subsequent PD/A process. Then, the ozone-treated NFC was subjected to the PD/A process in an Expanded Granular Sludge Bed (EGSB) reactor without external carbon source addition, achieving advanced nitrogen removal by transforming the ammonia and nitrate in the ozone-treated NFC into nitrogen gas, resulting in their removal.

2 Materials and methods

  Ozone was generated by an ozone generator and delivered into the ozone oxidation tank through a hose, where it reacted with NFC. Residual gas was absorbed by a KI solution.

The 11th International Symposium on Water Environment Systems
----- with Perspective of Global Safety   (Nov. 16th ~ 17th , 2023)

GP-RSS & SyDE
Tohoku University

In this study, an expanded granular sludge bed (EGSB) reactor was set up with a working volume of 2 L. The reactor was made of organic glass with a diameter of 80 mm and height of 500 mm. The influent was introduced into the reactor via a bottom inlet using a peristaltic pump, while the effluent was discharged from an upper three-phase separator outlet. The reactor was operated at a con stant temperature of 35 ± 1 ^{0}C. Furthermore, the reactor was covered with black sponge to protect it from sunlight and minimize heat loss.

The inoculated sludge of EGSB reactor is Anammox granular sludge, which has been cultured for a long time in Zhuyuan Sewage Treatment Plant (Shanghai, China). The granular sludge has a particle size of 2–3 mm, with MLVSS and MLSS values of 15.54 g/L and 57.00 g/L, respectively.

3 Results and discussion

3.1 Evaluation of ozone oxidation process for the pretreatment of NFC

To investigate the potential of ozonated NFC as a carbon source for denitrification, the transformation of refractory organic matter in the concentrate was examined under varying ozone treatment times at a constant flow rate of 1.2 L/min. Analysis of the volatile fatty acid (VFA) content in NFC before and after ozone oxidation (Fig. 1) showed that the total VFA content in the NFC prior to ozone oxidation was 18.14 mg/L, which increased to 101.70 mg/L after ozone oxidation, which was similar to the phenomenon observed in previous reports.

The present investigation revealed an unexpected and surprising observation that the ozone oxidation process, which typically converts organic nitrogen to ammonia, results in a significant increase in both ammonia and nitrate in the NFC. Fig. 3 demonstrated a remarkable surge in the concentrations of both NO_3^--N and NH_4^+-N during the initial 60 min of the reaction, followed by a gradual increase in nitrate and a decline in ammonia.Of the VFAs measured, acetic acid and butyric acid showed the most significant changes. These findings demonstrate the significantly improved biodegradability of NFC after ozone treatment, indicating that ozone-treated NFC is a promising denitrification carbon source that can provide an electron donor for partial denitrification.
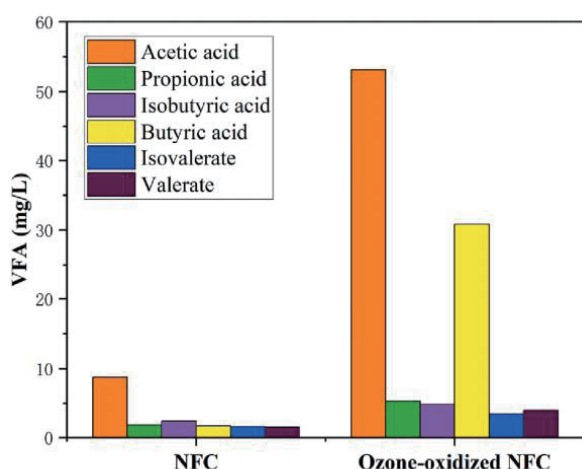

Fig. 1. Changes of VFA concentration in NFC before (a) and after (b) ozone oxidation.

3.2 Nitrogen removal performance

The nitrogen removal performance in the PD/A-EGSB reactor is shown in Fig. 4. The stage I (day 1–42) corresponds to the start-up period. Batch experiments on day 43 (Fig. 5) indicated a considerable decline in nitrate and COD concentration, accompanied by the accumulation of nitrite up to 32.23 mg/L. In the stage II (day 43–55), ultrafiltration effluent containing nitrate was used instead of sodium nitrate to evaluate the performance of the PD/A reactor. The outcomes revealed that the nitrogen removal efficiency (NRE) remained above 95%, thereby affirming the PD/A-EGSB reactor's stable operation.

In general, the PD/A process exhibited excellent performance in treating ozone-oxidized NFC, achieving significant nitrogen removal without the need for external carbon sources, and maintaining long-term stability. Furthermore, the integration of ozone pre-treatment with PDA eliminates the need for aeration and external carbon sources, resulting in substantial economic advantages, resulting in substantial economic benefits.

3.3 Transformation and utilization mechanism of organic matter

The initial COD concentration of the NFC was measured to be 1750 ± 150 mg/L and the organic matter in the NFC after ozone oxidation was still mainly composed of humic substances and fulvic acid. Ozone oxidation effectively degraded the refractory organic matter in the NFC.

To investigate the conversion of organic matter in the PD/A process, the concentration of VFA in the influent and effluent of the reactor was measured. It was observed that the VFA concentration in the NFC significantly decreased from 101.70 mg/L in the influent to 24.61 mg/L in the effluent, with a utilization rate of 83.82% after treatment in the PD/A reactor. This suggests that the VFA generated during the ozone oxidation process was fully utilized in the PD/A process. Moreover, the ozone oxidation process not only decomposed refractory organic matter but also produced VFAs, which were fully utilized as a carbon source for the PD/A process to achieve advanced nitrogen removal of the NFC.

4. Conclusions

The integration of ozone pretreatment and PD/A technology in this study achieved efficient nitrogen removal of the NFC. After ozone pretreatment, the concentration of VFA reached a maximum of 104.369 mg/L, which mainly served as a carbon source for the subsequent PD/A process, indicating that ozone oxidation effectively degraded the refractory organic matter in the NFC and enhanced its biodegradability. Moreover, the ozone oxidation process induced substantial increases in both ammonia and nitrate concentrations within the nanofiltration concentrate, thereby facilitating subsequent PD/A reactions.

Reference

[1] F.L. Bai, H.T. Dr, C.W. Dr, J. Ma, *Treatment of nanofiltration concentrate of landfill leachate using advanced oxidation processes incorporated with bioaugmentation*, Environ. Pollut. 318 (2023) 12.

[2] A.M. Ch´avez, O. Gimeno, A. Rey, G. Pliego, A.L. Oropesa, P.M.´Alvarez, F.J. Beltr´an, *Treatment of highly polluted industrial wastewater by means of sequential aerobic biological oxidation-ozone based AOPs*, Chem. Eng. J. 361 (2019) 89–98.

The 11th International Symposium on Water Environment Systems
----- with Perspective of Global Safety   (Nov. 16th ~ 17th , 2023)

GP-RSS & SyDE
Tohoku University

Towards sustainable wastewater treatment by chemically enhanced primary treatment and mainstream anammox: Challenges and solutions forward

○ Ruolan Wen [1*], Huan Yang [1] Hui Cheng[1], Lianpei Zou[1], Yu-You Li[2]& Jianyong Liu[1]

[1] School of Environmental and Chemical Engineering, Shanghai University, 333 Nanchen Road, Shanghai 200444, China.

[2] Department of Civil and Environmental Engineering, Graduate School of Engineering, Tohoku University, 6-6-06 Aza, Aramaki, Aoba-ku, Sendai, Miyagi 980-8579, Japan.

Abstract

The conventional activated sludge process poses a notable challenge to wastewater treatment plants (WWTPs) because of its intensive energy requirement. Therefore, there is an urgent need to develop sustainable wastewater treatment methods. Chemically enhanced primary treatment (CEPT) has been explored for organics and phosphorus capture, and mainstream anaerobic ammonium oxidation (anammox) has been designed to remove nitrogen from wastwater due to its advantages of no aeration and organic matter and low sludge production. However, in today's continuous development of sustainable sewage treatment plants, there are still some challenges in the application of these processes. Herein, this study summarised and discussed the barriers to establishing sustainable WWTPs from a plant-wide operational perspective. To realise carbon neutralisation in wastwater treatment plants, this study proposed an anaerobic digestion and sulphate reduction combined with a sludge oxidation process to optimize chemical recovery in CEPT, as well as a strategy to upgrade and provide nitrite to the mainstream anammox via partial nitrification of sidestream digester liquor. Based on these proposals, this review designed a novel wastewater treatment scheme to achieve sustainable WWTPs and accounted for the scheme's energy recovery, chemical reuse, and quantified the nitrogen removal contribution rates of mainstream and sidestream.

Keywords: Mainstream anammox; Sidestream partial nitrification; Energy recovery; Phosphorus recovery; Coagulant recovery.

1 Introduction

The conventional activated sludge (CAS) process is the most commonly used technology for municipal wastewater treatment. However, the high energy input is required to remove organics and nutrients. Sustainable wastewater treatment involves removing pollutants and recovering energy and resource. An innovative wastewater treatment process—the A-B process—has been proposed and widely discussed. The A-stage is designed to capture organics from wastewater for energy recovery, and the B-stage is tailored for energy-efficient nutrient removal.

In the A-stage, the carbon capture processes mainly include chemically enhanced primary treatment (CEPT), high-rate activated sludge (HRAS), and anaerobic processes. Compared with the last two processes, CEPT has stable organic matter capture efficiency, approximately >90% of the total phosphorus (TP) can also be effectively recovered. However, CEPT requires many coagulants, significantly increasing the cost of chemicals and the production of chemical sludge.

In the B-stage is primarily dedicated to removing nitrogen. Notably, anaerobic ammonium oxidation (anammox)—an emerging autotrophic nitrogen removal technology—may be preferable for the B-stage. Anammox has been successfully applied at full scale for treating various types of high-strength wastewater. Nevertheless, applying mainstream anammox in municipal wastewater remains challenging. The stable and economical provision of nitrite is a critical bottleneck for mainstream anammox application in wastewater with low nitrogen concentrations.

This review critically analysed and discussed the most recent advances in A-B processes for sustainable wastewater treatment. Based on the effective recovery of organic matter (C) and phosphorus (P) and partial capture of organic nitrogen (N) from wastewater by CEPT, the most suitable mainstream anammox process was discussed based on the C/N ratio and carbon source type of the CEPT effluent, and the contribution of nitrogen captured by CEPT to the mainstream denitrification was calculated in detail.

2 CEPT for phosphorus and energy recovery:

Challenges and solutions

CEPT has been used for capturing organics from municipal wastewater and can remove 50–87% of the COD by coagulation-flocculation and sedimentation. Since higher COD can be concentrated from wastewater into sludge by CEPT, higher energy recovery was achieved (0.29 kWh/m^3 of wastewater). Therefore, CEPT may be a more reasonable option for maximising the energy recovery of WWTPs.

However, fresh coagulants need to be added constantly, increasing the operational cost of WWTP. The coagulant contributed 55% of the total cost of the CEPT-based WWTP. Moreover, owing to the efficient carbon capture efficiency and coagulant addition, there is also significant amounts of chemical sludge are produced. Consequently, this will increase the operating pressure of the wastewater plants, including logistical and financial challenges. Meanwhile CEPT can capture almost all phosphorus in wastewater. However, the addition of flocculants containing metal ions can affect the efficiency of phosphorus release[1].

The 11th International Symposium on Water Environment Systems
----- with Perspective of Global Safety   (Nov. 16th ~ 17th , 2023)

GP-RSS & SyDE
Tohoku University

Based on the above discussion, an anaerobic digestion and sulphate reduction combined with sludge oxidation (AD-SR/O) process was proposed to recover bioenergy, phosphorus, and coagulant from CEPS. First, Fe salts and polyacrylamide were used to capture organic matter and phosphorus in wastewater. Subsequently, sulphate was added to the anaerobic digestion reactor to achieve simultaneous and efficient recovery of methane and phosphorus. Next, an oxidation unit is configured to oxidise the FeS in the digestate. Notably, both ferric iron-rich sludge and regenerated sulphate can be recycled. The AD-SR/O process provides opportunities for recycling coagulants, reducing operating costs and improving WWTP sustainability.

3 Mainstream anammox: Optimal solution for efficient nitrogen removal with low C/N

Conventional nitrification and denitrification processes require a C/N of approximately seven for biological nitrogen removal. Notably, if the CEPT process is used in the A-stage of the A-B process, the concentration of organics would be insufficient for downstream nitrogen removal in the B-stage. Therefore, innovative autotrophic nitrogen removal processes should be developed to address this challenge towards achieving sustainable wastewater treatment. Consequently, the anammox process has gained increasing interest for treating low C/N wastewater in the B-stage.

Partial nitrification, in which ammonium is partially oxidised to nitrite by AOB, has been commonly explored as a nitrite supply pathway for anammox. However, its application in municipal wastewater treatment faces many challenges[2]. The PD/A process has been proposed as another pathway to achieve mainstream anammox. In this process, nitrate is reduced to nitrite by denitrifying bacteria. Subsequently, ammonium and nitrite are removed using the anammox process. Additionally, PD can achieve NO_2^--N accumulation by metabolically controlling the denitrification process or the partial denitrifying bacterial community to provide a substrate for the mainstream anammox process.

A strategy was proposed to upgrade and provide nitrite to mainstream anammox by the PN of sidestream digester (S-PN/M-A) to reduce the energy consumption of wastewater plants and improve the sustainability of WWTPs. First, the carbon capture unit is essential before anammox. Subsequently, the organics in the sludge are recovered as bioenergy (CH_4) by anaerobic digestion, and nitrogen in the sludge is released into the digester liquor during anaerobic digestion. Lastly, the nitrogen in the digester liquor is converted to nitrite by PN, providing another stable nitrite supply route for mainstream anammox.

4 A novel sustainable wastewater treatment scheme based on CEPT and mainstream anammox

A novel sustainable wastewater treatment scheme based on the optimised carbon and phosphorus recovery process and upgraded mainstream anammox were proposed (Fig. 1).

According to some experimental data, CEPT can remove 80% COD and 95% phosphorus from wastewater. Additionally, it is assumed that 70% of organics in CEPS could be converted into methane during the AD-SR because CEPS exhibits better digestion characteristics than traditional secondary sludge. Ferric chloride (30 mg/L) is added to the primary settling tank, and the corresponding sulphate causes the SRB to consume 9.8% of the organic matter in the sludge. Theoretically, the chemical energy derived from 1 g

methane-COD is approximately 13.9 kJ; therefore, the total recoverable energy in the sludge can be estimated as 3071.9 kJ/m³. Therefore, the proposed scheme can recover 1075.2 kJ/m³ energy from wastewater, equivalent to 0.3 kWh/m³. Notably, the energy consumption in conventional WWTPs is 0.3–0.6 kWh/m³. In the final step of AD-SR/O process, the oxidation of digestate rich in FeS is designed to regenerate and recycle iron coagulant and sulphate. The oxidation process can achieve approximately 80% oxidation efficiency.

In the proposed scheme, this study hypothesised that CEPT removes 30% of the TN in wastewater. Moreover, the C/N ratio of the CEPT effluent is 2.3 since organics are captured, indicating suitability for subsequent PD/A units. Furthermore, the PN of the digester liquor process could provide 14.25 kg/d of nitrite for the mainstream anammox. This means that in the proposed scheme, S-PN/M-A rather than PD/A can remove 70% of TN in the mainstream. According to the calculation, the sidestream contributes approximately 54% of the nitrogen removal rate to the mainstream anammox.
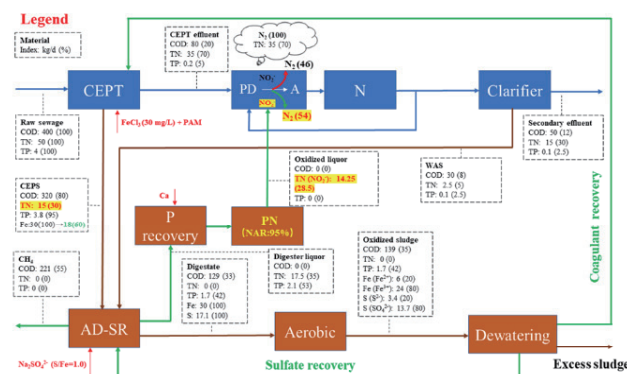

Fig. 1. Material flow and mass balance in the proposed wastewater treatment scheme.

6 Conclusions and perspectives

The innovative AD-SR/O technology proposed by our research team will significantly increase the bioenergy (CH_4 55%) and phosphorus (over 50%) derived from CEPS. Moreover, it recovers chemical (Fe and S 80%) reduces the operational cost of WWTPs. Furthermore, S-PN/M-A provides a stable nitrite supply pathway for mainstream anammox, and the sidestream supply of nitrite contributes approximately 54% of nitrogen removal to the mainstream. Future studies should focus on how to enrich nitrogen into the sidestream (for example, ammonium adsorption), the effect of CEPT and organic matter redirection on PD/A, and development of supporting control strategies to promote the practical application of this scheme.

Reference

[1] Yu, B., et al., Species, fractions, and characterization of phosphorus in sewage sludge: A critical review from the perspective of recovery. Sci Total Environ, 2021. 786: p. 147437.

[2] Guo, Y., et. al., Towards more efficient nitrogen removal and phosphorus recovery from digestion effluent: Latest developments in the anammox-based process from the application perspective. Bioresour Technol, 2020. 299: p.122560.

The 11th International Symposium on Water Environment Systems
----- with Perspective of Global Safety (Nov. 16th ~ 17th , 2023)

GP-RSS & SyDE
Tohoku University

Optimizing Organic Loads in High-Rate Activated Sludge for Partial Nitritation/Anammox Integration in a Novel Municipal Treatment Process

○ Weizhe Xia[1]*, Yanxiao Wei[1], Min Ye[1], Yu-You Li[1, 2]

[1]Department of Civil and Environmental Engineering, Tohoku University, Miyagi 980-8579, Japan.
[2]Department of Frontier Science for Advanced Environment, Graduate School of Environmental Studies, Tohoku University, Miyagi 980-8579, Japan.
*E-mail: xia.weizhe.r5@dc.tohoku.ac.jp.

Abstract

Due to the high COD and low nitrogen concentration of municipal wastewater, which pose a challenge for partial nitritation/anammox (PN/A) process, a novel municipal treatment process was set up to efficiently redirect COD resource and remove nitrogen. The process consists of two parts: high rate activated sludge (HRAS) in A-stage that is designed for COD capture, whereas PN/A is tailored in B stage for nitrogen removal. Hydraulic retention time (HRT) was alternated to various organic loads to optimize both COD and nitrogen concentrations for PN/A stability. The HRAS reactor was operated for 200 days and achieved stable treatment performance with 25.31 ± 5.86 mg- NH_4^+-N/L, approximately 0.09 mg-NO_2^--N/L and 0.19 mg-NO_3^--N/L in the effluent. Furthermore, 81% COD removal efficiency (CRE) was obtained when organic loading rate (OLR) was 94.74 ± 35.21 mg $COD \cdot L^{-1} \cdot d^{-1}$. This study presents a promising way to integrate the PN/A process for the novel municipal wastewater treatment process.

Keywords: High rate activated sludge; Partial nitritation/anammox; Organic loading rate; Energy recovery.

1 Introduction

Nitrification-denitrification process, a widely used municipal wastewater treatment process, has mature practical application and can effectively remove ammonia nitrogen. However, the discovery of the anammox bacteria at the end of the 20th century provided a new way to remove nitrogen of wastewater. Compared with traditional process, partial nitritation/anammox (PN/A) process is a much more cost-effective and environmentally friendly way, due to its less oxygen demand, no COD requirement, and greenhouse gas emission reduction. Recently, more and more wastewater treatment plants applied anammox process to accomplish nitrogen removal in sidestream. However, the research on application of anammox process in mainstream is still insufficient. Mainstream anammox process faces much more challenges, such as low ammonia nitrogen concentration, organic matter, and nitrite-oxidizing bacteria (NOB)[1].

To deal with the problems faced by anammox process, a novel municipal treatment process was set up, consisting of two parts, A-stage and B-stage. A-stage is designed for COD capture, while B-stage, PN/A, is tailored for nitrogen removal. Compared to the conventional activated sludge process, the high rate activated sludge (HRAS) system not only conserves energy and emits fewer greenhouse gases but also facilitates energy recovery, making it an exemplary choice for the B-stage of a novel two-step municipal wastewater treatment process. To determine optimal HRAS operation conditions for the PN/A process, COD removal rate, various nitrogen concentration and nitrogen distribution were analyzed. Furthermore, organic loading rate (OLR) was alternated to optimize the performance of HRAS, fitting for PN/A process.

2 Materials and methods

2.1 Reactor configuration

The experimental apparatus comprised three components: the main body of the airlift reactor, water influent system, and aeration system, being shown in Fig. 1. An airlift reactor was used in this study, featuring a reaction zone with a 10 L (5 L in phase 1–2) effective volume. The temperature was maintained at 25°C.
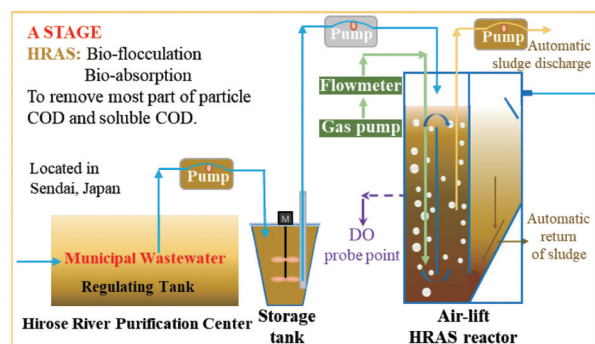

Fig. 1 Schematic diagram of HRAS reactor

The reactor was placed at the Hirose River Purification Center (Sendai, Japan), and ran continuously for 200 days with a total of 7 phases (Table. 1). HRAS process started with phase 3 with a 10 L reactor which can provided more effluent for the PN/A reactor in stage B. A peristaltic pump was used to automatically discharge excess sludge from the reactor based on timed settings.

2.2 Analysis methods

Influent and effluent samples were filtered by 0.45 μm filter. Capillary electrophoresis (Agilent 7100) was used to measure NH_4^+-N, NO_2^--N, NO_3^--N, PO_4^{3-}-P, and Ca^{2+} concentrations. Sludge concentration and settling properties were determined using previously described methods. Total nitrogen (TN) concentrations and COD were analyzed according to APHA standard method[2].

The 11th International Symposium on Water Environment Systems
----- with Perspective of Global Safety   (Nov. 16th~17th , 2023)

GP-RSS & SyDE
Tohoku University

Table 1 Operation Conditions

Phases	Day (d)	HRT (h)	V (L)	OLR (g COD·L^{-1}·d^{-1})	CRE (%)
1	1–16	6	5	1.26 ± 0.24	97.66
2	17–38	3	5	3.89 ± 0.69	92.91
3	39–117	3	10	2.27 ± 0.85	80.95
4	118–163	2	10	3.65 ± 0.89	68.41
5	164–180	1	10	10.99 ± 2.70	77.80
6	181–188	0.5	10	21.93 ± 7.84	50.28
7	189–200	2	10	5.40 ± 0.08	67.59

3 Results and discussion

As shown in table. 1, reactor started as HRAS in phase 3, in which the organic load rate is 2.27 ± 0.85 g COD·L^{-1}·d^{-1}, with COD removal efficiency (CRE) came to 80.95%. At phase 4 and 5, OLR rose to 3.65 ± 0.89 and 10.99 ± 2.70 g COD·L^{-1}·d^{-1} presentively, with the decreasing CRE. In phase 6 and 7, the CRE was even worse, dropping to 50.28% and 67.59%. Therefore, the organic removal was the best at HRT of 3 h.
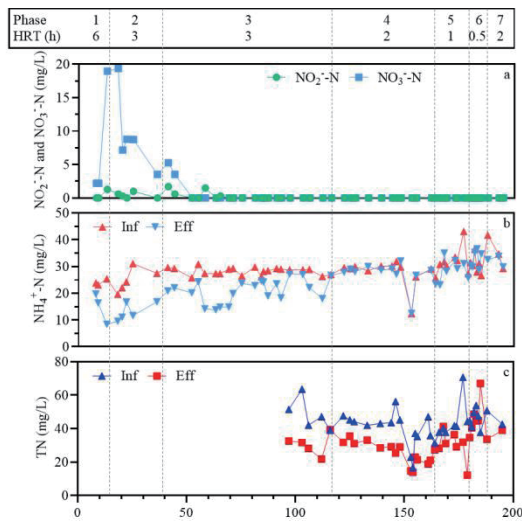

Fig. 2. Operation performance of HRAS reactor

The nitrogen distribution of the effluent is shown in Fig. 2. In phase 1, the reactor was operated as conventional activated sludge process, resulting in the oxidization of nitrogen and high concentration of NO$_3^-$-N (7.79 ± 7.91 mg/L), and ammonium nitrogen concentration (14.82 ± 4.74 mg/L) in the effluent. With the OLR increasing in phase 2, the reactor was transformed into HRAS process. Thereafter, the reactor has achieved stable long-term operation in phase 3. NO$_2^-$-N, NO$_3^-$-N concentration dropped to 0.09 ± 0.34 mg/L and 0.19 ± 0.91 mg/L. These results can be attributed to short SRT and low aeration operation of HRAS, inhibiting NOB activity. The concentration of NO$_2^-$-N and NO$_3^-$-N both in influent and effluent of HRAS is close to 0 mg/L from phase 3 to 7. In addition, NH$_4^+$-N concentration slightly decreased. However, the TN concentration reduced significantly. It can be figured out that the removed TN was caused by the organic matter degradation.
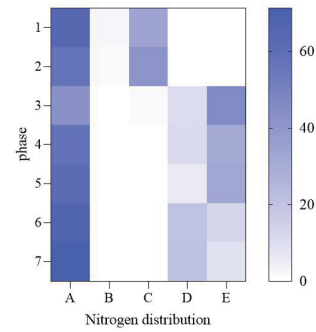
A: NH$_4^+$-N; **B:**NO$_2^-$-N; **C:** NO$_3^-$-N; **D:** ON; **E:** Assimilation.

Fig. 3. Nitrogen distribution of HRAS effluent

The nitrogen distribution has been calculated, which is illustrated in Fig 3. In phases 1 and 2, as the reactor is operated at low OLRs. The high COD removal rate was corresponding with a significant accumulation of NO$_3^-$ in the effluent (33.79% and 41.30%, separately). After the transformation of HRAS was completed (phase 3), the ratio of NO$_2^-$and NO$_3^-$ in the effluent decreased to 0.42% and 0.90%, respectively. Meanwhile, the proportion of cellular assimilation increased to 46.03%. In phase 4, due to lower HRT, the activity of NOB has been minimized, further increasing NH$_4^+$-N proportion. However, when HRT came to 1h in phase 5, though the proportion of ON reduced with the rising of NH$_4^+$-N proportion, the stability of effluent quality decreased, because of the deterioration of hydraulic stability in the reactor caused by the shortened HRT. In phase 6, HRT was further shortened to 0.5 h, leading to rapid increasing of the proportion of ON in effluent. It can be attributed to the short HRT leading to wash out of the sludge, which is also the reason for insufficient biological adsorption. HRT was changed to 2 hours in phase 7 for recovery. However, due to short recovery time and negative effects on sludge in phase 6, the performance was poor. In summary, the reduced proportion of NO$_2^-$-N and NO$_3^-$-N in phases 3, 4, and 5, indicates that nitrogen oxidation is limited, and the activity of NOB is also inhibited.

4 Conclusions

(1) HRAS is a promising and suitable process for pretreatment in novel municipal treatment process. The effluent nitrogen distribution in phase 3, 4, 5 exhibits steady stability performance and complies with the subsequent PN/A treatment criteria for none NO$_2^-$-N and NO$_3^-$-N proportion and comparative high NH$_4^+$-N proportion (42.44%, 57.76% and 61.43%, respectively).

(2) Considering the results of CRE, ammonia concentration in effluent, COD recovery as sludge, phase 3 (HRT: 3h) is the best condition, corresponding with 2.27 g COD·L^{-1}·d^{-1} OLR, achieving 80.95% CRE.

Reference

[1] Lisheng Wang, Wancong Gu, Yanchen Liu, Peng Liang, Xiaoyuan Zhang, Xia Huang, Challenges, solutions and prospects of mainstream anammox-based process for municipal wastewater treatment, Science of The Total Environment, Volume 820, 2022.

[2] APHA, 2005. Standard Methods for the Examination of Water and Wastewater. APHA-AWWA-WEF, Washington, DC, USA.

The 11th International Symposium on Water Environment Systems
----- with Perspective of Global Safety   (Nov. 16th ~ 17th , 2023)

GP-RSS & SyDE
Tohoku University

Agricultural drought assessment in the tropical humid region: A case study of Indonesia

◯ Amalia Nafisah Rahmani IRAWAN[1*] & Daisuke KOMORI[1,2]

[1]Graduate School of Environmental Studies, Tohoku University, Miyagi 980-0845, Japan.
[2]Green Goals Initiative, Tohoku University, Miyagi 980-8572, Japan.
*E-mail: amalia.nafisah.rahmani.irawan.q3@dc.tohoku.ac.jp

Abstract

In tropical-humid regions, wet farming crops, such as paddy, are a common agricultural commodity that demand substantial water resources. These crops are primarily cultivated in the Asian monsoon region, where there is a high rate of precipitation. The cultivation cycle of these crops is usually divided into wet and dry cropping seasons. During the dry cropping season, they are particularly susceptible to agricultural drought, as consequence of reduced precipitation. This research focuses on Indonesia as a case study, aiming to evaluate the risk of agricultural drought on wet farming crops during the dry cropping season by analyzing the relationship between drought hazard and its risk. To assess the hazard, the Standardized Precipitation Index (SPI) was used by utilizing the Global Satellite Mapping of Precipitation (GSMaP) dataset, which offers a spatial resolution of $0.1° × 0.1°$. The correlation analysis between SPI and drought-affected areas at a city scale indicated that SPI-3 in August is the most suitable timescale for evaluating agricultural drought in Indonesia. And for the assessment of agricultural drought risk, it was carried out on a grid scale, involving the development of a crop yield estimation model utilizing the Normalized Difference Vegetation Index (NDVI). The correlation analysis between SPI-3 and the detrended crop yield, as indicators of drought risk, revealed that areas with an r-value ≤ 0.6 experienced higher yield losses, signifying greater vulnerability to drought. Conversely, areas below the threshold value exhibited lower crop yield losses, even in regions severely affected by drought, because the existing irrigation system was able to resist the drought's impact on crop yield loss.

Keywords: Agricultural Drought; Rice; Tropical Humid; Indonesia; SPI

1 Introduction

The Intergovernmental Panel on Climate Change (IPCC) reported that the world's temperature is expected to increase by around 1.5°C in 2030. One of the impacts of this temperature increase is the variability of the rainfall pattern and the distribution, which is not evenly distributed globally. This condition can lead to more severe drought disasters in some parts of the world. The Food and Agriculture Organization (FAO) mentioned that the agricultural area absorbs around 80% of drought direct's impact especially in developing countries.

Refer to the 4 types of droughts, agricultural drought is preceded by meteorological drought or where there is deficiency of precipitation and over time can lead to the depletion of soil moisture that affected crop production. From this understanding, many precipitation-based indexes were developed for drought assessment, one of which is Standardized Precipitation Index (SPI).

The Standardized Precipitation Index (SPI), introduced by McKee et al. in 1993, is a useful tool for assessing drought conditions. It only requires long-term precipitation data, typically spanning 20-30 years. By employing probability density functions and normalization, SPI can evaluate both wet and dry conditions in various regions, with drought indicated by SPI values of -1 or lower. SPI offers flexibility in terms of time scales, allowing it to be calculated according to the user's preferences. Thus, SPI has been widely applied in drought assessment, including for agricultural drought. For instance, Ali (2001) found that in Turkey, SPI-3 is sensitive to soil moisture levels, which, in turn, impact crop growth. However, there is no consensus on the most suitable time

scale for drought assessment using SPI. This study was conducted to assess the impact of agricultural drought to paddy in the tropical-humid region with objectives as follows: i) examine the temporal response of wet crop to various SPI index, ii) developing the crop yield estimation model with 250-m resolution as indicator of agricultural drought risk, and iii) assessing the correlation between SPI and crop yield on the grid scale to determine the spatial response wet crop to agricultural drought.

This research was conducted in West Java as one of the provinces in Indonesia with the rainy season from October - March and the dry season from April - September. According to Maryati et al., (2012), 50.02% of the land is an agricultural area, dominated by paddy fields, which is very vulnerable to drought events. The results of this study will be helpful to get a better understanding about the use of SPI for agricultural drought assessment in tropical-humid regions.

2 Materials and methods

The flowchart in Fig. 1. outlines the two main parts of this research, represented in blue and green colours. the blue section focuses on temporal assessment, it starts by evaluating drought using the SPI based on the daily precipitation data obtained from the GSMaP with 0.1° resolution from April 2000 – March 2021. SPI was computed for 60 different scenarios, considering various SPI aggregation timeframes (SPI-1, SPI-3, SPI-6, SPI-9, and SPI-12) and month references from January to December. Subsequently, a correlation analysis was performed between the SPI index and areas affected by drought, as detailed in Dai et al. (2020), to identify the most suitable SPI index with the strongest correlation.

The 11th International Symposium on Water Environment Systems
----- with Perspective of Global Safety   (Nov. 16th ~ 17th , 2023)

GP-RSS & SyDE
Tohoku University

The green section is dedicated to spatial assessment, where the dry crop yield on a grid-scale was estimated using multiple linear regression method between the Normalized Difference Vegetation Index (NDVI) obtained from MODIS with 250-m resolution and subround crop yield data obtained from the Statistical Bureau of West Java during the dry cropping season. Finally, the correlation between the selected SPI index and detrended crop yield value is analysed to assess the spatial response of the wet farming crop during the dry cropping season to agricultural drought.
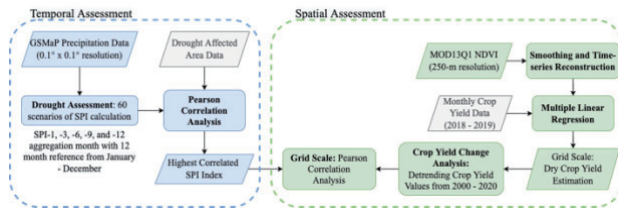
Fig. 1. Research flowchart.

3 Results and discussion

Based on the result on Fig. 2. the heatmap analysis indicates that all scenarios of the SPI index produced negative correlations, represented by the red colour. Please note that the black color in the heatmap involved only a wet season, which is not a target period of this study, so the result was excluded. This result can be interpreted that the decrease in SPI index, or a dry condition, is associated with an increase of drought-affected areas in the agriculture region. In addition, the highest negative correlation was produced during the SPI-3 in August (r-value = -0.6 and p-value <0.05). Thus, it can be concluded that this index can be used to examine the impact of agricultural drought because in all the regencies, the drought condition that was represented by this index, was corresponding with the drought-affected areas. Moreover, the index's timescale is coincided with the peak of the dry season, which is very significant to crop production during the dry cropping period.
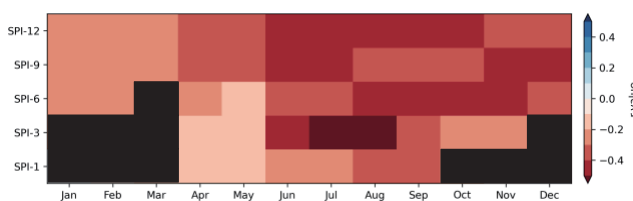

Fig. 2. Heatmap of Mean of Correlation Value between SPI Index and Drought-Affected Areas.

For the spatial assessment, we first created a model for estimating crop yield at the grid level using multilinear regression analysis in Python. This process involved selecting the most important NDVI images. We followed the recommendation of Freund and Littell (1991) by removing variables that weren't significant, based on their high p-values, through a step-by-step elimination process. The crop yield, after removing any trends, served as the dependent variable. It was determined using monthly crop production data from the dry cropping season. Meanwhile, the independent variables were the smoothed NDVI values from the same period.

Then, the correlation between the SPI index and detrended crop yield, as an indicator of agricultural drought risk, was assessed. Fig. 3. where the triangle-shaped marker indicates

the irrigated area, and the hexagonal shaped marker indicates the local water resources-irrigated area. The blue color indicates the area with a r-value less than 0.6, meanwhile the red color indicated the r-value larger than 0.6. The vertical line represents the error bar for detrended crop yield, indicating the variability of agricultural drought risk, which could result in crop yield gain (if larger than 1) or crop yield loss (if less than 1). On the other hand, the horizontal line represents the error bar for the SPI index, indicating the different degrees of hazard among all grids.
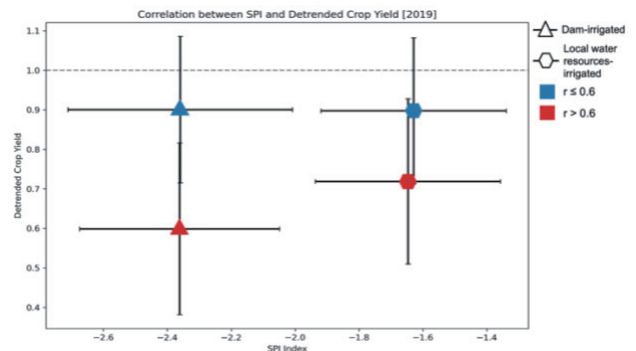

Fig. 3. Correlation between SPI Index and Detrended Crop Yield based on The Existence of Irrigation System.

The analysis revealed that irrigated areas were primarily situated on the left side or in regions experiencing more severe drought conditions. This suggests that the irrigation system effectively provided water in drought-prone areas. In areas with an r-value exceeding 0.6 (shown in red), which were more susceptible to drought, more significant droughts resulted in greater crop yield losses, highlighting the impact of drought as a key factor. On the other hand, regions with an r-value below 0.6 (indicated in blue) showed no significant difference in crop yield loss. This indicates that the presence of an irrigation system helped mitigate the impact of agricultural drought, resulting in similar crop yield losses to areas with local water resources, even in the face of severe drought. Nevertheless, hazard assessment alone cannot fully explain the variations in wet farming crop responses during the dry cropping season, necessitating further research.

4 Conclusions

This research suggested that SPI-3 can be used to assess the agricultural drought assessment in the tropical-humid region. The spatial assessment on the grid-scale revealed that there is a negative correlation between the SPI index and detrended crop yield, indicating that crop yield loss is associated with dry conditions. This finding revealed that areas with an r-value ≤ 0.6 experienced higher yield losses, signifying greater vulnerability to drought. Conversely, areas below the threshold value exhibited lower crop yield losses, even in regions severely affected by drought, because the existing irrigation system was able to resist the drought's impact on crop yield loss.

Reference

[1] Dai, Meng, et al. "Assessing agricultural drought risk and its dynamic evolution characteristics." *Agricultural Water Management* 231 (2020): 106003.
[2] Freund R. J Littell R. C 1991 *SAS System for Regression*, 2nd edn (Cary, NC: SAS Institute Inc.)
[3] Maryati, S., A. N. S. Humaira, and F. Pratiwi. "Spatial pattern of agricultural land conversion in West Java

The 11th International Symposium on Water Environment Systems
----- with Perspective of Global Safety　　(Nov. 16th~17th , 2023)

GP-RSS & SyDE
Tohoku University

Province." *IOP Conference Series: Earth and Environmental Science*. Vol. 131. No. 1. IOP Publishing, 2018.

[4] McKee, Thomas B., Nolan J. Doesken, and John Kleist. "The relationship of drought frequency and duration to time scales." *Proceedings of the 8th Conference on Applied Climatology*. Vol. 17. No. 22. 1993.

[5] Umran Komuscu, Ali. "Using the SPI to analyze spatial and temporal patterns of drought in Turkey." *Drought Network News (1994-2001)* (1999): 49.

The 11th International Symposium on Water Environment Systems
----- with Perspective of Global Safety   (Nov. 16th ~ 17th , 2023)

GP-RSS & SyDE
Tohoku University

Remote sensed vegetation for flood modeling

◯ Andre ARAUJO FORTES[1*], Masakazu HASHIMOTO[1] & Keiko UDO[1]

[1]Department of Civil and Environmental Engineering, Tohoku University, Miyagi 980-8579, Japan.
*E-mail: andre.araujo.fortes.p6@dc.tohoku.ac.jp

Abstract

Flood modeling is a common practice for most flood studies. Modeling with traditional calibration methods can provide acceptable results when compared to real events. However, using a single static value of roughness coefficient for an entire river environment or even different static values for multiple locations within the river environment does not comprehend the actual phenomena of hydraulic resistance. Vegetation plays a key role in the determination of the Manning roughness in floodplain areas, where its value varies dynamically with the change of flow conditions. Despite its effect, vegetation is often neglected in flood modeling due to its difficulty to acquire for vast environments, but remote sensing, along with machine learning, has facilitated this work, allowing researchers to map different vegetation characteristics in river environments. This research presents a methodology for acquiring the distributed vegetation parameters of leaf area index (LAI) and vegetation height, by combining satellite and UAV imagery with machine learning. Flood simulations were performed considering these parameters to dynamically calculate the roughness in the floodplains and the results were compared with the traditional static roughness method. The results have shown that using the dynamic roughness model can provide better results than the static model, allowing for shortening the calibration time in flood modeling.

Keywords: Flood modeling; vegetation; remote sensing; machine learning; Manning coefficient.

1 Introduction

On October 12, 2019, Japan was hit by typhoon Hagibis, which caused extreme rainfall and floods all over Japan [1]. River management is tasked with providing security to the population near rivers and applying flood control strategies, which can be decided through studies that require flood modeling. Among all the inputs of flood models, the roughness parameter is critical, with great variation depending on many factors.

Vegetation is the primary determinant of the roughness value in the floodplain areas of river environments [2], where its density is the main parameter acting in the resistance while in the emergent state [3], and the ratio of water depth and vegetation height (degree of submergence) determines the roughness in the submerged state [4].

Despite the number of studies demonstrating the effect of vegetation on flow dynamics, the use of vegetation data in flood modeling is not a common practice in the industry, due to the great time and cost required for acquiring this data. Recent technologies have facilitated this work. The use of UAV photogrammetry from optical cameras has enabled the mapping of distributed vegetation height in river environments [5]. Besides UAV technology, studies combining machine learning with satellite imagery have mapped vegetation height for wide areas [6] and increased the resolution of important parameters like the leaf area index (LAI) for entire areas [7]. The great advantage of UAV imagery is the centimeter scale resolution it can generate. Satellite imagery, on the other hand, has a lower resolution of data, but with higher temporal frequency, and can be obtained for free.

The objective of this research is to assess the usefulness of remote sensed vegetation parameters in flood modeling and to verify the effect of considering the vegetation parameters on a 2D hydraulic simulation of typhoon Hagibis in a UAV observed stretch of the Nanakita River, in the Miyagi prefecture of Japan.

2 Materials and methods

The 2D hydraulic simulation was performed in a 2km stretch of the Nanakita River, a class B river, managed by Miyagi prefecture. The river has 45 km of length with a catchment area of 244 km². The UAV observation of the stretch was performed in September 2019, one month before the typhoon event.

Three simulations were performed in the stretch, one used static roughness values for the channel and floodplains, the static Manning simulation (SMS), and two used the dynamic Manning calculation in the vegetated areas. The Manning value was calculated by a routine added to the 2D hydraulic model [8] that calculated the roughness in the vegetated cells for two different scenarios, the emergent and submerged state. In the emergent scenario, the vegetation LAI was used to represent the vegetation density, as suggested in Jalonen et al. [9], The LAI values of each vegetated cell were used to calculate the Darcy-Weisbach friction factor based on a formula proposed by Järvelä [3], and later converted to the Manning roughness coefficient. In the submerged state, the Manning was calculated from the degree of submergence of the vegetation, using a formula obtained from regression analysis from data obtained from Japan Institute of country-ology and engineering [10]. In a partial dynamic Manning simulation (PDMS), only the submerged state was considered, blocking the flow while the vegetation was emergent. In the full dynamic Manning simulation (FDMS) both emergent and submerged states were considered.

The vegetation parameters used in the model were obtained using two different methods. The LAI was obtained in a moderate resolution by downscaling the MODIS LAI data with 500 m resolution with machine learning. As in Gokool et al. [7], the 500m resolution MODIS NDVI and EVI were used as input variables, and MODIS LAI as target variable to train a machine learning model. After training, NDVI and EVI were calculated from sentinel-2 satellite images with 10 m resolution and used to obtain the LAI with the same

The 11th International Symposium on Water Environment Systems
----- with Perspective of Global Safety   (Nov. 16th ~ 17th , 2023)

GP-RSS & SyDE
Tohoku University

resolution. The vegetation height was obtained from the UAV observation. As explained in Araújo Fortes et al. [8], the point cloud data from the observation was used to generate the RGB orthoimage of the stretch. A sample of this orthoimage was selected and a k-means cluster was used to make clusters based on the RGB values. The clusters were classified into vegetation and not-vegetation by visual supervision and a machine learning model was trained using the RGB as input and the classification as output. After training, the model was applied to the entire image, mapping the vegetation location in the stretch. With the vegetation location, the height was obtained by normalizing the digital surface model (DSM) with the digital elevation model (DEM) of the stretch.

The data DEM used in the simulations was generated by interpolation of 21 cross-sections provided by Miyagi prefecture. The discharge used was obtained from a previous simulation that used the RRI model [11]. The difference in the simulations was restricted to the Manning applied. Table 1 shows the manning setting for all simulations.

Table 1 Manning setting for the simulations.

Simulation	Channel	Floodplains/vegetation
SMS	0.022	0.038
PDMS	0.022	Dynamic
FDMS	0.022	Dynamic

3 Results and discussion

The vegetation parameters could be successfully obtained in the study area. The machine learning model used to map vegetation used a multi-layer perceptron (MLP) algorithm. The accuracy of the model was 0.99. The vegetation covered 18% of the stretch and its average height was 1.7 m. The LAI model also used an MLP algorithm, the average LAI obtained in the stretch was 2.43. Figure 1 shows the vegetation LAI and height in the stretch.
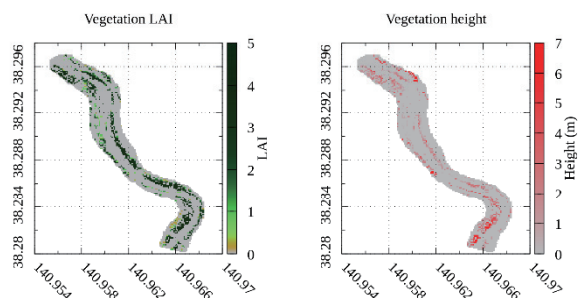

Fig. 1. Vegetation LAI and height in the stretch.

The hydraulic simulation considering the vegetation parameters in both emergent and submerged states (FDMS) achieved the best result among all simulations. The RMSE between the water level of 5 observed points in the stretch and all the simulations were calculated. Table 2 shows the RMSE of all simulations.

Table 2 RMSE for all simulations.

Simulation	RMSE
SMS	0.141
PDMS	0.189
FDMS	0.137

The FDMS and SMS had a very similar water level profile, while the PDMS achieved a higher water level profile, due to the blocking of flow during the emergent state of the vegetation. The FDMS results indicate that the method used

can substitute the traditional static methodology, shortening the calibration process.

4 Conclusions

The use of remotely sensed vegetation in flood modeling has been shown to be effective. Application of machine learning techniques on satellite and UAV imagery can produce results useful for flood simulations. The consideration of vegetation parameters in the roughness dynamic calculation in the 2D hydraulic model has improved the results when considering both the emergent and submerged state of the vegetation.

Reference

[1] M. Kazama et al., Disaster report on geotechnical damage in Miyagi Prefecture, Japan caused by Typhoon Hagibis in 2019, Soils and Foundations, 61 (2021), 549–565.

[2] N. G. Ebrahimi, M. Fathi-Moghadam, S. M. Kashefipour, M. Saneie, and K. Ebrahimi, Effects of Flow and Vegetation States on River Roughness Coefficients, Journal of Applied Science, 8 (2008), 2118–2123.

[3] J. Järvelä, Determination of flow resistance caused by non-submerged woody vegetation, International Journal of River Basin Management, 2 (2004), 61–70.

[4] V. Nikora, S. Larned, N. Nikora, K. Debnath, G. Cooper, and M. Reid, Hydraulic Resistance due to Aquatic Vegetation in Small Streams: Field Study, Journal of Hydraulic Engineering, 134 (2008), 1326–1332.

[5] W. van Iersel, M. Straatsma, E. Addink, and H. Middelkoop, Monitoring height and greenness of non-woody floodplain vegetation with UAV time series, ISPRS Journal of Photogrammetry and Remote Sensing, 141 (2018), 112–123.

[6] W. Li, Z. Niu, R. Shang, Y. Qin, L. Wang, and H. Chen, High-resolution mapping of forest canopy height using machine learning by coupling ICESat-2 LiDAR with Sentinel-1, Sentinel-2 and Landsat-8 data, International Journal of Applied Earth Observation and Geoinformation, 92 (2020), 102163.

[7] S. Gokool, R. P. Kunz, and M. Toucher, Deriving moderate spatial resolution leaf area index estimates from coarser spatial resolution satellite products, Remote Sens Appl, 26 (2022), p. 100743

[8] A. Araújo Fortes, M. Hashimoto, K. Udo, K. Ichikawa, and S. Sato, Dynamic Roughness Modeling of Seasonal Vegetation Effect: Case Study of the Nanakita River, Water (Basel), 14 (2022), 3649.

[9] J. Jalonen, J. Järvelä, and J. Aberle, Leaf Area Index as Vegetation Density Measure for Hydraulic Analyses, Journal of Hydraulic Engineering, 139 (2013), 461–469.

[10] Japan Institute of country-ology and engineering, Manual of plans for river channel (in Japanese), in Manual of plans for river channel, Sankaidou, 2002.

[11] T. Sayama, G. Ozawa, T. Kawakami, S. Nabesaka, and K. Fukami, Rainfall–runoff–inundation analysis of the 2010 Pakistan flood in the Kabul River basin, Hydrological Sciences Journal, 57 (2012), 298–312.

The 11th International Symposium on Water Environment Systems
----- with Perspective of Global Safety   (Nov. 16th ~ 17th , 2023)

GP-RSS & SyDE
Tohoku University

Evaluation of the Amount of Hydraulic Energy in Irrigation Reservoirs Based on Structural Characteristics in Western Japan

○ Atsuya IKEMOTO[1]*, So KAZAMA[1] & Takeo YOSHIDA[2]

[1]Department of Civil and Environmental Engineering, Graduate of School of Engineering, Tohoku University, Miyagi 980-8579, Japan.
*E-mail: ikemoto.atsuya.s1@dc.tohoku.ac.jp
[2] National Agriculture and Food Research Organization

Abstract

The study aimed to estimate the electricity generated by irrigation reservoirs in each prefecture. This study estimated the potential for power generation from reservoirs in western Japan, where there are a large number of reservoirs. As a result, Hiroshima, Hyogo, Okayama, Yamaguchi and Kagawa prefectures generated the most electricity. In addition, the greater the reservoir storage, the greater the electricity generation. In the future, hydropower generation will have to be estimated on the basis of inflows into reservoirs. some prefectures, particularly Okinawa, Miyazaki, and Kagoshima, exhibited low power generation despite having tall dams per reservoir, warranting further research of power generation potential in relation to water storage capacity.

Keywords: irrigation reservoir; hydro power; structural characteristics.

1 Introduction

In order to achieve carbon neutrality by 2050[1], there is a push to promote the installation of small-scale hydropower systems in irrigation reservoirs. The ability to generate energy from water stored in irrigation reservoirs is seen as an effective way to mitigate global warming. Although the electricity generated on an individual basis is small, the applicability of using irrigation reservoirs during disasters has been proposed[2]. The effects and implications of using irrigation reservoirs for purposes other than their primary function need to be assessed. Goto et al.[3] and Uesaka et al.[4] suggest that reservoirs have potential for multipurpose use. There is little research on hydropower generation in reservoirs[3],[5], and no studies have assessed their hydropower potential throughout Japan. This study estimated the potential for power generation from reservoirs in western Japan, where there are a large number of reservoirs.

2 Data set

The study's primary objective is to assess the impact of hydropower generated by irrigation reservoirs. Initially, the amount of hydro energy generated during pre-discharge was determined, and the factors influencing the electricity output were analyzed. Additionally, an investigation into the reduction of carbon dioxide emissions was undertaken.

In this study, the data for the reservoir disaster prevention support system were provided by the National Agriculture and Food Research Organization (NARO). As irrigation-only dams not listed in the data of the reservoir disaster prevention support system were identified, irrigation-only dams not listed in the data of the reservoir disaster prevention support system were added from the dam data (W01-05) for 2014 published by the National Land Numerical Information[6]. In order to ensure the inclusion of different data, irrigation-only dams not listed in the reservoir data were defined as dams that were at least 1 / 60 degrees away from the coordinates listed in the reservoir data with respect to latitude and longitude, and that the difference between the total water storage capacity of the reservoir and that of the irrigation-only dam was at least 20% of the total water storage capacity of the reservoir. The dams were selected to satisfy the following conditions. In this study, the data obtained from the reservoir disaster prevention support system plus the irrigation-only dams obtained from the national land survey data were used as the reservoir data. Note that the reservoir data in this study are the data of agricultural reservoirs with the addition of irrigation dams.

3 Methods

The study aimed to estimate the electricity generated by irrigation reservoirs in each prefecture. To achieve this, we estimated the amount of electricity produced by each reservoir using equation (1).

$$P = \gamma \rho g Q H_e = 0.8 \cdot \gamma \rho g Q H \qquad (1)$$

where P denotes power production [W], γ represents the turbine's efficiency, g denotes acceleration due to gravity [m/s^2], Q denotes flow rate [m^3/s], He denotes effective head [m], and H represents total head [m]. It should be noted that γ is set at 0.6. It is a challenge to determine an irrigation reservoir storage rate for each reservoir due to the varying reservoir storage rate. They established the level of half the embankment height for each irrigation reservoir. It is noteworthy that the Reservoir Disaster Prevention Support System data did not identify the embankment height for 26701 reservoirs. The flow rate was established to deplete the storage capacity of each reservoir to zero within three days. Pre-flood releases are implemented three days before the flood to control its impact. The authors[7] estimated the impact of reservoirs with zero storage capacity on flood control. To relate this study to their work, the researchers determined the amount of water released when storage was set to zero. The maximum possible impact of setting the storage volume to zero was assessed.

The 11th International Symposium on Water Environment Systems
----- with Perspective of Global Safety　(Nov. 16th～17th , 2023)

GP-RSS & SyDE
Tohoku University

4 Results and discussions

In terms of size, the most electricity in western Japan was generated by Hiroshima, Hyogo, Okayama, Yamaguchi and Kagawa prefectures. Fig.1 illustrates the correlation between reservoir storage and electricity production across the prefectures. Fig.1 illustrates the correlation between reservoir storage and electricity production across the prefectures. Fig.1 illustrates the correlation between reservoir storage and electricity production across the prefectures. It is evident from the diagram that higher reservoir storage corresponds with greater electricity generation. Eq(1) suggests that reservoir embankment height can also impact the amount of electricity produced, not just reservoir storage volume. This study examined the structure of agricultural reservoirs, specifically water storage volume and embankment height, and analysed the correlation between water storage volume, embankment height, and power output across each prefecture. Fig.2 illustrates the connection between total water storage capacity and power output of reservoirs in each prefecture, while Fig. 3 shows the relationship between bank height per reservoir and power output in each prefecture. As illustrated in Fig.2, prefectures with greater water storage capacities, including Hyogo and Kagawa, exhibited higher electricity generation. Fig.3 indicates that some prefectures, particularly Okinawa, Miyazaki, and Kagoshima, exhibited low power generation despite having tall dams per reservoir, warranting further research of power generation potential in relation to water storage capacity.

5. Conclusions

This study estimated the potential for power generation from reservoirs in western Japan, where there are a large number of reservoirs. As a result, Hiroshima, Hyogo, Okayama, Yamaguchi and Kagawa prefectures generated the most electricity. In addition, the greater the reservoir storage, the greater the electricity generation. In the future, hydropower generation will have to be estimated on the basis of inflows into reservoirs.
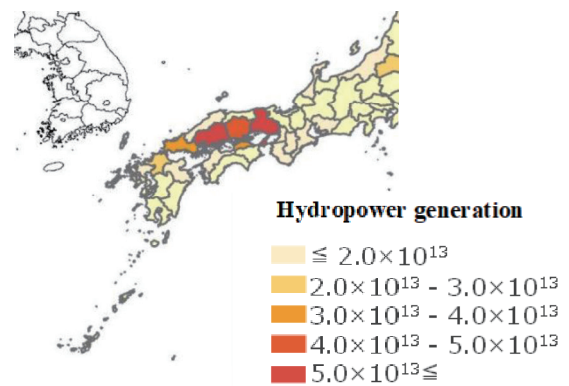
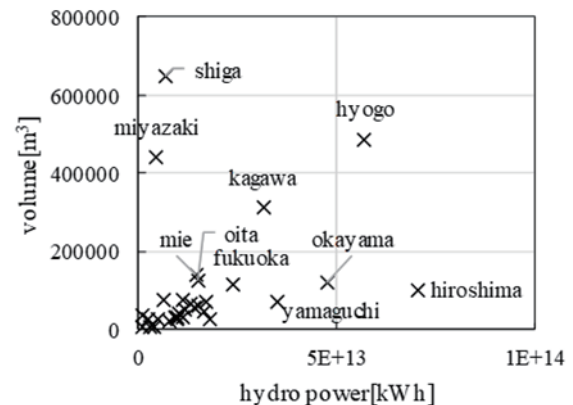## Acknowledgement

Fig.1 Hydropower generation by province

Fig.2 Relationship between total irrigation reservoir storage and electricity generation

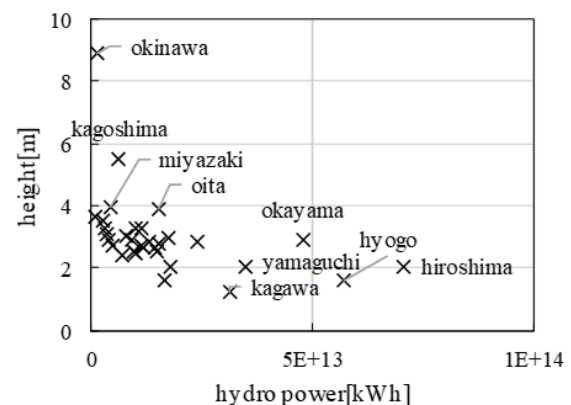Fig.3 Relationship between height and power generation

Reference

[1] Ministry of Land, Infrastructure and Transport, Promoting the introduction of renewable energy such as small hydropower, 2021.

[2] Onishi et al., A Case Study on Small Scale Hydropower Generation Using Agricultural Water Supply Facilities in Gifu and Aichi Prefectures, Journal of the Society of Agricultural and Rural Engineering, Vol.81, Issue 2, pp.15-18, 2013.

[3] Goto et al., How to utilize agricultural irrigation facilities by introducing small hydropower generation, Journal of the Society of Agricultural and Rural Engineering, Vol.81, Issue 2, pp.710, 2013.

[4] Uesaka : Problem and Directionality Concerning Small-scale Hydropower Utilizing Agricultural Water, Water, land and environmental engineering, Vol. 78, Issue 8, pp.36, 2010.

[5] Tanji et al. : Prospects for paddy irrigation systems that respond to future changes in energy supply, Japan society Hydro and Water Resources., Vol.23, No.1, pp.4356, 2010.

[6] Ministry of Land, Infrastructure and Transport, Digital National Land Information, https://nlftp.mlit.go.jp/ksj/, 2023/10/06.

[7] Ikemoto et al., POTENTIAL OF IRRIGATION RESERVOIRS FOR FLOOD PREVENTION AND EVALUATION OF THE REDUCTION RATE OF FLOOD DAMAGE COST FOR EACH PREFECTURE, Journal of Japan Society of Civil Engineers, Ser. B1 (Hydraulic Engineering), Vol.78, No.2, I_265-I_270, 2022.

The 11ᵗʰ International Symposium on Water Environment Systems
----- with Perspective of Global Safety   (Nov. 16ᵗʰ ~ 17ᵗʰ , 2023)

GP-RSS & SyDE
Tohoku University

Factor Analysis of People Migration to Flood Damage Using Municipality Data

Ayaka Okamoto[1], So Kazama, Hayata Yanagihara, Yusuke Hiraga

[1]Department of Civil and Environmental Engineering, Tohoku University, Miyagi 980-8579, Japan.

*E-mail: okamoto.ayaka.s3@dc.tohoku.ac.jp

Abstract

As an initial study to clarify the impact of flood disasters on population change, this study quantitatively analyzes the impact of flood damage on the rate of change in the social population in all municipalities in Japan in the case of recent flood damage. The variables selected to represent the scale of flood damage were the area inundated, the percentage of households inundated under the floor, inundated above the floor, and the percentage of households completely destroyed in each municipality. The results of both multiple regression and DID analyses showed that the rate of households inundated under the floor, the rate of households inundated above the floor, and the rate of households completely destroyed had a negative impact on the rate of change in the social population ($p<0.05$). Floods have a negative impact on social population change at the municipal level in recent flood disasters in Japan.

Keywords: population change; flood damage; municipalities; analysis of statistics; throughout Japan.

1 Introduction

Understanding the dynamics of the social population is important from the viewpoint of social infrastructure development, and is particularly important in Japan, which has entered a society with a declining population. According to a report by the International Displacement Monitoring Centre (IDMC), approximately 76% of Japan's population movements due to natural disasters between 2008 and 2020 will be caused by floods and typhoons. One example of the impact of flood damage on population decline in Japan is the disappearance of the Yatsumen residential community in Gotsu City, Shimane Prefecture, following torrential rains in western Japan. Previous studies[1),2)] have mainly analyzed a small number of municipalities, and there is no analysis of the impact of the scale of flood damage on population change across the whole of Japan. The purpose of this study is to clarify the impact of the scale of flood damage on the rate of change of the social population in recent years, as a basic study to clarify the impact of flood damage on population change in all municipalities in Japan.

2 Target area and used data

In the analysis in Chapter 3, all municipalities that experienced flood damage between 2014 and 2020 were included in the analysis. In the analysis in Chapter 4, all Japanese cities, towns, and villages, regardless of whether they were inundated or not, were included in the analysis for the period from 2014 to 2020. As a result, 2220 cities, wards, towns, and villages were included in the analysis. Details of the data are shown below.

a) Population and number of households

Data on the rate of social change in each municipality were obtained from the Population, Demographic and Household Census based on the Basic Resident Registers for the period from 2015 to 2021. Data on habitable area and the number of households by municipality were obtained from the General Contact Point of Government Statistics for the period from 2014 to 2020. Data on the number of households under the floor, households above the floor, and households completely destroyed were obtained from the Flood Damage Survey by municipality from 2014 to 2020.

b) Inundated area ratio

The inundated area ratio is calculated by dividing the area of residential and other flooded areas by the habitable area in the flood damage by municipality in the Flood Damage Survey.

c) Inundated household ratio

The inundation rate of households inundated under the floor, the inundation rate of households inundated above the floor, and the rate of households completely destroyed were calculated. The number of households inundated under the floor, the number of households inundated above the floor, and the number of households completely destroyed were used to calculate the ratio of each to the number of households in each municipality.

3 Multiple regression analysis

(1) Data and methods

In multiple regression analysis, the objective variable was the social increase/decrease rate. The explanatory variables were the rate of households inundated under the floor, the rate of households inundated above the floor, and the rate of households completely destroyed, excluding the rate of inundated area. Independence among the explanatory variables was checked, and it was confirmed that there was no multicollinearity among the variables.

(2) Results

Table 1 shows the results of multiple regression analysis. All explanatory variables for the rate of households inundated under the floor, the rate of households inundated above the floor, and the rate of households completely destroyed fulfilled $p < 0.05$. The coefficients of each explanatory variable were negative, confirming that they act to decrease the social population. The coefficients of each explanatory variable were all negative, suggesting that not only large-scale damage such as completely destruction, but also inundation damage under the floor can decrease the social population.

The 11th International Symposium on Water Environment Systems
----- with Perspective of Global Safety   (Nov. 16th~ 17th , 2023)

GP-RSS & SyDE
Tohoku University

4 DID Analysis

(1) Methodology

In this study, DID analysis was used to analyze the impact of flood damage on the social increase/decrease rate. Equation (1) shows the regression equation used in the DID analysis. A weighted least squares method was used, considering the population of each municipality as a weight. For a more detailed explanation of the DID analysis, please refer to the previous report3).

$$Y_{st} = \alpha + \delta_{rDD}FLOOD_{st} + \sum_{k=1}^{2220} \beta_k DIST_{ks} + \sum_{j=2015}^{2020} \gamma_j YEAR_{jt}$$

$$+ \sum_{k=1}^{2220} \theta_k (DIST_{ks} \times t) + e_{st} \qquad (1)$$

Y_{st} : Social increase/decrease rate

α : Slice

δ_{rDD}, γ_j, β_k, θ_k : Coefficient

s : [1, 2, 3, . . . ,2219] : District

t : [2014, 2015, . . . , 2020] : Year

e_{st} : error term

$DIST_{ks}$: Variable that is 1 when j=t (District dummy)

$YEAR_{jt}$: Variable that is 1 when j=t (Year dummy)

$FLOOD_{st}$: Five variables (Flooded area rate, Rate of households inundated under the floor, Rate of households inundated above the floor, Rate of households completely destroyed and washed away)

(2) Results

Figure1 shows the results of the DID analysis when parallel trends are considered and weighting by population is taken into account. Figure1 shows the relationship between $FLOOD_{st}$ and δ_{rDD} in equation (1). The error bars in Figure 1 are 95% confidence intervals. The p-values for each variable are shown at the top of the figure. Figure 1 shows that the effects of the presence or absence of flooding and the rate of inundated area on the social increase/decrease rate are not statistically significant. On the other hand, the rates of households inundated under the floor, households inundated above the floor, and households completely destroyed had a negative impact on t the social increase/decrease rate at the 5% level of significance.

In order to analyze in detail the non-linearity between flood magnitude and the social increase/decrease rate, a DID analysis was conducted using a binary variable with multiple threshold values as a cross term, focusing on the rate of completely destroyed houses, which showed statistically significant and influential results in Figure 2, following Naoi et al3). A dummy variable was defined as 1 when the variable of interest was greater than the threshold value and 0 when the variable was less than the threshold value, and a DID regression analysis was conducted using this dummy variable as a cross term. The threshold value was set to divide the sample into 10 parts. Figure 2 shows the relationship between the threshold of the rate of households completely destroyed and the coefficient δ_{rDD} in the DID analysis. The error bars in Figure 2 are 95% confidence intervals. Figure 2 shows that the coefficient of the dummy variable for the percentage of households with completely destroyed houses tends to increase as the threshold value of the variable increases.

Table 1 Results of multiple regression analysis
（ Sample size: 2903 municipalities ）.

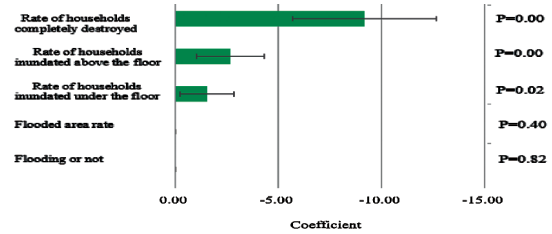|	Coefficient	Standard error	t-value	p-value	Lower limit 95	Upper limit 95
Slice	0.00	0.02	0.00	1.00	-0.04	0.04
Rate of households inundated under the floor	-0.10	0.02	-4.50	0.00	-0.14	-0.06
Rate of households inundated above the floor	-0.05	0.02	-2.28	0.02	-0.10	-0.01
Rate of households completely destroyed	-0.10	0.02	-4.77	0.00	-0.14	-0.06

Fig. 1. Coefficient (δ_{rDD}) for each variable in DID regression analysis (weighted by population).
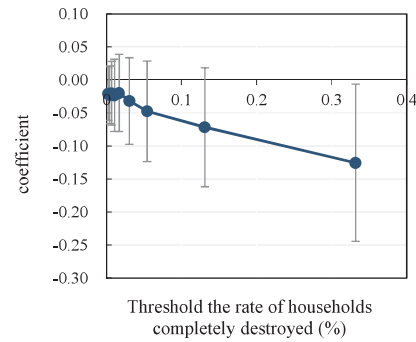

Fig. 2. Threshold and coefficient (δ_{rDD}) of the rate of households completely destroyed in DID analysis.

The significance level of 5% is met when the threshold value of the percentage of households with completely destroyed houses is 0.3%.

5 Conclusions

As an initial study to clarify the impact of flood disasters on people migration, this study analyzes the impact of flood damage on the social increase/decrease rate in all municipalities in Japan. The results suggest that flood damage has a negative impact on the social increase/decrease rate at the municipal level in recent flood disasters in Japan. In the future, we would like to analyze the relationship between flood damage and the social increase/decrease rate on a smaller scale.

Reference

[1] Murai, T., Watanabe, S., Yamada, M. and Chibana, T.: Characterization of population loss due to flooding based on population projections, Japan society of hy-drology and water resources, 2019 Research and Presen-tation Abstracts, pp. 262-263, 2019.

[2] Namikawa, Keigo, Naoki Koyama, and Tadashi Yama-da: Analysis of the impact of large-scale disasters on lo-cal population and its causes, Journal of River Engi-neering, Vol. 28, 2022.

[3] JOSHUA D. ANGRIST and JORN-STEFFEN PISCHKE: MASTERING METRICS THE PATH FROM CAUSE TO EFFECT, pp. 178-203, 2015.

The 11th International Symposium on Water Environment Systems
----- with Perspective of Global Safety   (Nov. 16th ~ 17th , 2023)

GP-RSS & SyDE
Tohoku University

Geomatics for Monitoring Rehabilitation Status in Aruwakkalu Limestone Quarry Sri Lanka

◯ Chaminda SP[1*] ,Waravita CS[1], Madhuranga AU[1] , Rodrigo MAJ[1], Jayawardena CL[1] &

Samarakoon KGAU[1]

[1]Department of Earth Resources Engineering, University of Moratuwa, Sri Lanka.
*E-mail: chaminda@uom.lk.

Abstract locations

Mine rehabilitation involves recreating lands damaged by mining activities, and mine rehabilitation monitoring plays an important role in achieving successful mine rehabilitation programs, thereby mitigating environmental impacts through mining activities. The objective of this study is to investigate the applicability of geomatics for monitoring the rehabilitation process in the Aruwakkalu limestone quarry. Aerial imagery is collected using a UAVs equipped with a multispectral sensor, and the acquired data undergoes thorough post-processing through software tools like Pix4D, ENVI, and ArcGIS. Vegetation indexes are developed from this processed data, and areas are categorized based on the year of replanting. Subsequent studies have revealed the existence of factors hindering the growth of vegetation cover. The analysis of the terrain models in the research area has uncovered irregular drainage patterns and erosions, both of which have had an adverse impact on the development of vegetation in the region. To address this issue, it is necessary to implement measures such as grading and forming improved landforms. The results offer significant insights that can be harnessed through geomatics techniques to effectively monitor and enhance rehabilitation endeavors in comparable mining locations, thus making a useful contribution to the promotion of sustainable mining practices.

Keywords: UAVs; hydrology; NDVI; vegetation; topography.

1 Introduction

Aruwakkalu limestone quarry, situated in Sri Lanka, is a substantial limestone deposit that is owned and managed by Siam City Cement (Lanka) Limited. It stands as one of the most extensive limestone reserves in the country. Due to the relatively shallow depth of the limestone deposit, open-cast mining techniques are being employed for its excavation. The primary objective of utilizing excavated limestone is to manufacture cement.

The rehabilitation process of Aruwakkalu limestone quarry consists of several stages. The initial phase of the rehabilitation process involves the implementation of land restoration measures, wherein the excavated regions are replenished by reintroducing the overburdened material that was previously removed. In order to get the ultimate landform, the process of replantation is employed, wherein native trees are strategically planted atop the re-filled land area.

Conventional methods for monitoring revegetation involve the designation of multiple sampling locations to quantitatively assess parameters such as tree density, which is essential for evaluating tree growth, height, and girth [1]. Although these techniques can demonstrate effectiveness in the surveillance of minor quarries, their application to larger areas becomes unfeasible and demands significant labor resources [2]

In contrast, the utilization of geomatics for monitoring rehabilitation progress presents a substantially more efficient alternative in comparison to conventional practices. The integration of Unmanned/Unpiloted Aerial Vehicles (UAVs) surveying techniques within geomatics for the evaluation of rehabilitation status in open pit mining is a relatively novel approach that holds the potential for substantial improvements in both precision and efficiency in the assessment process [2], [3].

2 Materials and methods

2.1 Study Area

The Aruwakkalu Limestone Quarry is situated precisely at the coordinates of 8°15'4.14 N latitude and 79°49'10.45E longitude. The study area comprises an extensive land expanse, encompassing a total area of 1.024 km^2 (102.44 hectares). Different sections within this study region have undergone reforestation initiatives in varying years as shown in Figure 1. It is important to underscore that this study is limited to the areas where reforestation activities were carried out specifically between the years 2002 and 2021.

2.2 Data Collection

The missions conducted for this study entailed the utilization of a DJI Phantom 4 Pro V2 Unmanned Aerial Vehicle (UAV) equipped with a multispectral camera. Throughout the survey mission, a total of 12,258 images were systematically captured across six

The 11th International Symposium on Water Environment Systems
----- with Perspective of Global Safety (Nov. 16th ~ 17th , 2023)

GP-RSS & SyDE
Tohoku University

Fig. 1- Map showing different areas that are replanted in different years.

distinct spectral bands, encompassing Red Edge, Near-Infrared, Green, Red, Blue, and Visible Light, employing the multispectral camera. The drone's flight path was pre-programmed to maintain a consistent altitude of 120 meters, a choice made to strike a harmonious balance between image resolution and the extent of the surveyed area. To ensure comprehensive data coverage and the precision of collected information, a side overlap ratio of 60% and a front overlap ratio of 80% were implemented. These systematic measures were implemented with the overarching objective of effectively monitoring and assessing the progress of quarry site rehabilitation efforts.

2.3 Data Processing

The processing of UAV images, utilizing Pix4D, involves importing images, initial processing, generating a dense point cloud and Digital Surface Model (DSM), quality control, and data extraction. Color correction using ENVI software was employed to address color variation in the maps. Georeferencing of UAV ortho image maps was performed in ArcMap, which improved accuracy and suitability for spatial analysis. Both Pix4D and ArcMap contributed to aligning the orthoimages with real-world geographic coordinates, enhancing spatial accuracy and enabling integration with other geospatial datasets. NDVI maps were created based on replantation years to assess vegetation density. This approach involved orthophoto correction and pixel-by-pixel NDVI computation,

yielding insights into vegetation distribution and dynamics. NDVI maps for individual replanted areas were also generated, aiding rehabilitation evaluation. To establish NDVI map threshold values, comparisons were made between NDVI readings and RGB photos. This allowed for the classification of different vegetation conditions, enhancing the interpretability of NDVI maps.

The application of the Digital Terrain Model (DTM) facilitated the generation of drainage path maps for both rehabilitated areas and their surroundings. These maps were instrumental in revealing the hydrological characteristics of the study area, allowing for the identification of surface water flow directions. This information is crucial for understanding hydrological processes within both rehabilitated and neighboring landscapes, ultimately contributing to the evaluation of rehabilitation effectiveness with respect to water flow dynamics.

3 Results and discussion

Considering that the studied areas were planted at varying times, an analysis of their growth progress can be conducted by evaluating their respective advancements up to the image acquisition date. This analysis aims to determine the current vegetation coverage and mean Normalized Difference Vegetation Index (NDVI) values, as presented in Table 1

Table 1- Vegetation cover and the mean NDVI values of the study area in 2023

Replanted Year	Replanted Area (ha)	Current (2023) Vegetation Cover %	Mean NDVI
2002	2.73	61.27	0.46
2003	2.21	74.02	0.43
2004	3.07	79.09	0.42
2005	3.77	84.34	0.42
2006	1.71	82.50	0.38
2007	1.91	80.95	0.44
2008	10.38	76.09	0.43
2009	11.22	77.70	0.44
2010	8.03	90.03	0.47
2011	4.57	86.58	0.42
2014	2.35	46.35	0.41
2016	2.10	62.02	0.43
2017	3.04	59.46	0.38
2018	2.04	36.04	0.37
2020	6.09	35.78	0.38
2021	3.37	40.44	0.35

The 11th International Symposium on Water Environment Systems
----- with Perspective of Global Safety   (Nov. 16th ～ 17th , 2023)

GP-RSS & SyDE
Tohoku University

It is noted that current vegetation cover percentage and mean NDVI values are higher in the regions where replantation done in earlier years. The highest and lowest vegetation cover and mean NDVI values are observed in the 2010 & 2021 plantation areas respectively. However, there are no significant relations on vegetation cover percentage and mean NDVI values with plantation years. Some areas where trees are planted earlier years not showing well growth due to various reasons such as soil fertility level, moisture conditions and erosion due to irregular drainage pattern. Computed NDVI mean values clearly noted that the areas where it needed replanting again to accomplished success rate of rehabilitation process.

A drainage map produced using acquired images used to analyze impacts on hydrological characteristics [4] of the rehabilitated area and its surrounding region. This map facilitates the interpretation of water flow patterns as of the date of image acquisition, as depicted in Figure 2. The study also noted irregular hydrological conditions and streams converging towards the rehabilitated area. This resulted from topographical changes due to decommissioning, affecting water drainage patterns. In some cases, a low vegetation cover is observed in the vicinity of surface pathways, as depicted in the above figure. This decline in vegetation can be attributed to erosion induced by the presence of water pathways. UAVs provided detailed monitoring information, with multispectral images offering insights into various environmental aspects and site conditions.
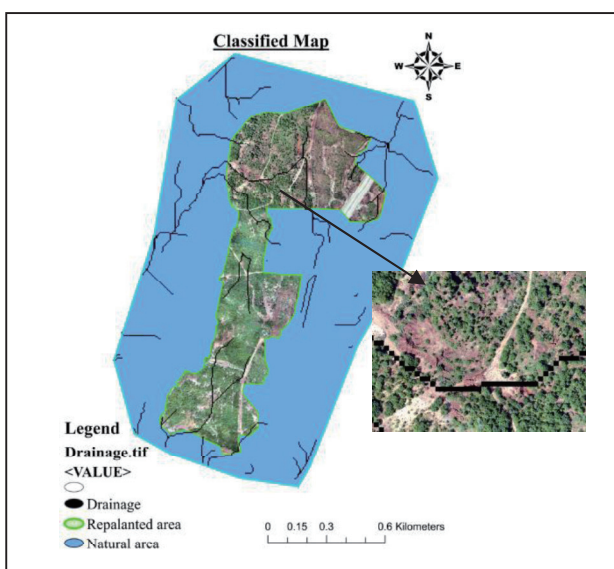

Figure 2- Drainage map of the Study and the Surrounding area.

4 Conclusions

The analysis of vegetation cover in the rehabilitated areas of the Aruwakkalu limestone quarry reveals substantial disparities based on the year of plantation. The highest vegetation cover is observed in the 2010 plantation area, associated with well-distributed hydrogeology and minimal erosion. A potential correlation between hydrogeology and vegetation cover suggests the need for verification via area-specific rainfall data. These findings emphasize the necessity for targeted interventions and further investigations to enhance rehabilitation effectively.

The effective utilization of UAVs, image processing techniques and vegetation indices are in monitoring the rehabilitation of the Aruwakkalu limestone quarry has demonstrated notable efficiency. UAV technology provides detailed and extensive information, particularly beneficial for overseeing expansive areas. Geomatic-based monitoring enables a comprehensive understanding of rehabilitation progress, facilitating enhanced decision-making and adaptive strategies to improve overall rehabilitation outcomes.

References

[1] N. Perera, "Annual monitoring report for INSEE rehabilitation sites at Aruwakalu Lime Stone Quarry Site and Kuratiyamohotte, Puttalam 2022 IUCN, International Union for Conservation of Nature, Sri Lanka Country Office," 2022.

[2] K. Johansen, P. D. Erskine, and M. F. McCabe, "Using Unmanned Aerial Vehicles to assess the rehabilitation performance of open cut coal mines," *J Clean Prod*, vol. 209, pp. 819–833, Feb. 2019, doi: 10.1016/j.jclepro.2018.10.287.

[3] F. S. Nascimento, M. Gastauer, P. W. M. Souza-Filho, W. R. Nascimento, D. C. Santos, and M. F. Costa, "Land cover changes in open-cast mining complexes based on high-resolution remote sensing data," *Remote Sens (Basel)*, vol. 12, no. 4, Feb. 2020, doi: 10.3390/rs12040611.

[4] C. S. Patabendige, S. Kazama and Y. S. Kondage, "Spatial and Temporal Variation of Runoff Trend in Sri Lanka During the Past Decades," *2019 Moratuwa Engineering Research Conference (MERCon)*, Moratuwa, Sri Lanka, 2019, pp. 751-756, doi: 10.1109/MERCon.2019.8818782.

The 11th International Symposium on Water Environment Systems
----- with Perspective of Global Safety   (Nov. 16th ~ 17th , 2023)

GP-RSS & SyDE
Tohoku University

History of Tsunami Prevention Policies in Miyagi Prefecture

◯ Chise NISHIWAKI*, Makoto OKUMURA

International Research Institute of Disaster Science, Tohoku University, Miyagi 980-0845, Japan.
*E-mail: chise.nishiwaki.a6@tohoku.ac.jp.

Abstract

Tsunami countermeasures have been considered as a result of countermeasure selection aiming at protecting the lives and property of residents as much as possible. We conducted a historical survey of the selection process of tsunami countermeasures implemented in Miyagi Prefecture for past tsunamis mainly based on the newspapers published in the region at the time as sources of information. It shows that for all tsunamis, not all of available measures were investigated in the selection process, but that selections were strongly limited from the smaller set of measures which directly contribute to solve the problems faced by the local government at the time; industrial development issue, for example. The Miyagi Prefectural Government prioritized the swift recovery of fishery industry, protection of public roads as industrial infrastructure, preparation of tsunami-free costal area for industrial development in each tsunami, rather than evaluating an single purpose, such as people's life protection.

Keywords: Tsunami; countermeasures; modern history; entity.

1 Introduction

The Sanriku coastal area is known as a tsunami prone area, and has repeatedly experienced large-scale tsunamis. Since the Meiji Era (1868-1912), the Meiji Sanriku Tsunami (1896), the Showa Sanriku Tsunami (1933), and the Chilean Earthquake Tsunami (1960) had left deadly damages, before the Great East Japan Earthquake and Tsunami (2011).

A historical review of the tsunami countermeasures implemented after each of these tsunamis shows that the content of them has changed with each one. While at the time in Meiji, the implementation of measures and the cost burden were left to the affected areas, after the Chilean tsunami, seawalls and breakwaters were constructed in many areas with National Government subsidies.

These changes are often explained from a technical point of view in previous studies. Or it has been generally accepted that tsunami countermeasures were selected to reduce future damage to the lives and properties of residents as much as possible, within the limits of scientific knowledge, engineering technology and economic constraints of the time.

However, a closer look at the process of selecting each countermeasure reveals that technology and cost are not always the main factor that can explain the choice of them. In these cases, social problems faced by the local government at the time may strongly affect the policy selection process. That has been overlooked so far, and may give a new perspective on the selection of tsunami countermeasures.

Although there have been many studies on tsunami countermeasures in the past, none of them has been able to explain the reasons for the selection other than technical and economic perspectives. The study by Kentaro Okamura [1], in particular, has a common viewpoint with this study, since it compares and analyzes the process of village reorganization in each tsunami in the past, especially the Showa Sanriku Tsunami (1933), and also refers to the background of the reorganization. However, the study only deals with the reorganization of villages and does not cover other tsunami countermeasures. In other previous studies, there is no explanation of the reasons for the selection of tsunami countermeasures other than engineering knowledge, technology, and economic viewpoints.

In this study, we focus on the three tsunamis; Meiji Sanriku (1986), the Showa Sanriku (1933), and the Chilean(1960), and analyze how the countermeasures were selected after each tsunami. We also review the main objectives behind the selection, and reexamine the prioritization of tsunami protection.

2 Materials and methods

The purpose of this study is to clarify how tsunami countermeasures were selected in Miyagi Prefecture after the three tsunamis. For this purpose, it is necessary to grasp over time what kind of discussions were held, but it is not appropriate with the data compiled later.

In order to confirm the policy selection process, we mainly used newspapers published in the area at the time of the tsunami as useful materials. Specifically, the "Ou-u Nichinichi Shimbun" was used for the Meiji Sanriku (1896), and the "Kahoku Shimpo" was used for the Showa Sanriku (1933) and the Chilean earthquake tsunami (1960).

Because disaster stories were widely read, newspapers sent correspondents to the affected areas and published numerous articles on the tsunami on a daily basis. In addition, reporters from local newspapers were familiar with the area and had many acquaintances there. Therefore, the content of the newspaper articles was diverse and informative, and can be analyzed over time.

Furthermore, these newspapers also provide articles, not directly reporting the tsunamis. Such articles sometimes provide information on the historical background of the time and events that occurred in the affected areas and prefectures at the same time, which can be combined to clarify the situation from multiple perspectives.

However, the accuracy of the information cannot be guaranteed with newspaper data alone, we conducts a comprehensive analysis using official documents of the national government and Miyagi Prefecture, as well as other literary sources, in order to collect information that cannot be obtained from newspapers.

The 11ᵗʰ International Symposium on Water Environment Systems
----- with Perspective of Global Safety   (Nov. 16ᵗʰ ~ 17ᵗʰ , 2023)

GP-RSS & SyDE
Tohoku University

3 Results and discussion

At the time of the Meiji Sanriku Tsunami (1896), there was no national or prefectural funding for policies aimed at mitigating future tsunami damage, and implementation was left to the affected communities. Therefore, engineering tsunami countermeasures were technically and financially difficult. Nevertheless, it is known that in Miyagi Prefecture, some of the affected villages moved to higher ground, and that the prefecture dispatched officials to the affected areas and took part in the administrative aspects of the relocation, such as the selection of relocation sites.

On the other hand, a survey of newspaper articles on the discussions leading up to the decision to relocate to higher ground reveals that a plan for mass relocation to other areas was discussed immediately after the tsunami. At the time, national policy recommended that people move to Hokkaido and Taiwan, and it was not uncommon for communities that were severely damaged by the disaster to move together as a group. This background was probably the reason for the proposal.

The reason why people chose to live on higher ground in spite of such circumstances was that the governor of Miyagi Prefecture had a policy of maintaining villages, no matter how badly damaged they were, and prevented people from moving out of their homes. Furthermore, the governor had also instructed that no change of occupation would be allowed. These facts clearly indicate that Miyagi Prefecture placed importance on the maintenance of local industries, particularly fisheries, which is one of the major industries, and that assistance measures were taken to prevent migration to other areas, subsidize the continuation of families, and otherwise maintain the community.

After the Showa Sanriku Tsunami (1933), the national government took the lead in conducting on-site surveys by researchers and experts, and various disaster prevention measures such as seawalls, breakwaters, and tide embankments were discussed, in addition to relocation to higher ground, according to previous studies.

By this time, the government was subsidizing not only the cost of disaster recovery, but also the cost of preventative measures. It is known that many disaster-stricken areas were relocated to higher ground as a result of these subsidies. In these days, measures to improve farming, mountain and fishing villages were underway as a relief for those villages that were economically exhausted due to the Showa Depression and bad harvests. It was confirmed that, the relocation to higher ground was planned as an application of this measure, and as a result, the government budgeted for the relocation. At the time, the national government considered the economic rehabilitation of the region to be an urgent issue, and was therefore receptive to the project.

On the other hand, it was found that Miyagi Prefecture planned to construct breakwaters and coastal levees other than relocation to higher ground, but most of these measures were not budgeted by the national government, and in the end, only a small portion of them were implemented. Our close look of these prefectural plans of coastal levees revealed that the planned locations did not correspond to the scale of damage to settlements or human lives. Rather, they were planned mainly where prefectural roads existed as industrial infrastructure or where new roads were to be constructed. This indicates that Miyagi Prefecture gave priority to the contribution to the economic and industrial development in selecting tsunami countermeasures.

After the Chilean tsunami (1960), it is known that tsunami countermeasures mainly consisted of structures such as seawalls. On the other hand, there were various discussions on tsunami countermeasures during this period, especially among scholars in Miyagi and Iwate prefectures. In particular, since the Chilean tsunami was a "distant tsunami", which occur far away, it was pointed out that it was necessary to take into account past near-shore tsunamis such as the Meiji Sanriku and Showa Sanriku tsunamis. And Miyagi Prefecture has established a tsunami countermeasures study group led by researchers.

However, Miyagi Prefecture focused on structure-based tsunami countermeasures at an early stage and planned structure-centered tsunami countermeasures, without waiting for the discussion of the study group.

At that time, "Tohoku Development Promotion Law" were enacted, and the promotion of the Tohoku region was at a turning point. Furthermore, industrialization was being promoted by the national government, and new industrial sites were being requested due to the shortage of existing sites. Tohoku, which had been a backward region since the Meiji Era, was also trying to keep up with industrialization. Miyagi Prefecture was also promoting industrialization by building suitable factory sites and developing new economic plans. In this context, the tsunami countermeasures that would lead to the securing of industrial sites in the waterfront area were selected as a priority.

4 Conclusions

By looking at the process of how tsunami countermeasures were selected in Miyagi Prefecture since the Meiji Era, we have clarified the thinking behind these choices.

The results show that, although the purpose of protecting people's lives and property is a prerequisite, the measures were selected to directly contribute to solving the problems faced by the local government, rather than selected based on technological improvement or economic factors, as considered so far. The prefecture, in particular, has always prioritized the maintenance and promotion of industry.

Even in the immediate aftermath of a disaster, the national, prefectural, and local governments tended to give priority to solving different problems that they had faced just before the disaster, rather than working together to solve the common problem of improving their ability to cope with the tsunami that is expected to hit in the future. There were pressing issues, then it was difficult to take tsunami countermeasures for a single purpose.

This history of tsunami countermeasure selection can be seen as an inspiration for the reconstruction efforts that are expected to be initiated by the local residents in the future.

Reference

[1] Kentaro Okamura, "Sanriku-tsunami" to shuraku saihen(The "Sanriku Tsunami" and the Reorganization of Villages), 2017.

The 11th International Symposium on Water Environment Systems
----- with Perspective of Global Safety   (Nov. 16th ~ 17th , 2023)

GP-RSS & SyDE
Tohoku University

Effects of Gravel Mining and Dam Sediment Trapping on Long-Term Sediment Dynamics in Yoshino River, Japan

○ Daisuke Nakahara[1]*& Keiko Udo[1]

[1]Department of Civil and Environmental Engineering, Tohoku University, Miyagi 980-8579, Japan.
*E-mail: daisuke.nakahara.q2@dc.tohoku.ac.jp

Abstract

Gravel mining and dam construction alter sediment transport and river morphology, leading to river channel instability. Previous studies have shown how human activity changed the river environment, but the underlying sediment transport mechanisms remain unclear. This study evaluates the effects of gravel mining and sediment trapping by the Ikeda dam on riverbed morphology and sediment dynamics in the Yoshino River, Japan, utilizing one-dimensional model. The variation in sediment load resulting from gravel mining may have continued after the 1970s when the frequency of gravel mining decreased. The reduction in bedload in the lower reaches may be a result of the decreased frictional velocity due to riverbed incision. The sediment trapping of Ikeda dams could affect sediment transport not only in the nearby area of the dam, but also far downstream to the estuary.

Keywords: Anthropogenic activity; Sediment transport; Gravel mining; Dam construction; Yoshino River.

1 Introduction

Gravel mining and dam construction alter sediment transport and river morphology, leading to river channel instability, for example, reduction of sediment load in rivers, channel erosion, coarsening and habitat alteration [1].

In Japan, large-scale human alterations had occurred decades ago [2-3]. Previous studies have identified changes caused by human activity; however further research is needed to comprehend the mechanisms of sediment transport behind these changes.

This study aims to evaluate the effects of previous gravel mining and sediment trapping by Ikeda dam on riverbed morphology and sediment dynamics in the Yoshino River, Japan, utilizing a one-dimensional model.

2 Materials and methods

2.1 Study area

Yoshino River has been used extensively for gravel mining. During the 1950s and 1960s, the process was conducted in the downstream region. However, government regulations caused such extraction activities to decrease.

Ikeda Dam is located about 78 km from the estuary and has a catchment area of 1,904 km². It started operating in 1975.

2.2 One-dimensional model analysis

This study used the one-dimensional riverbed deformation model of Takebayashi and Fujita (2011) [4].

The analysis section is the 77.8 km section between the mouth of the Yoshino River and the Ikeda Dam. The initial riverbed elevation for the numerical analysis is measured in 1965. There are 390 points in the 0.2 km intervals in the longitudinal direction.

The initial grain size distribution for the numerical analysis was measured from 1997 to 1998. This measured grain size distribution was divided into thirteen classes.

The upstream boundary discharge for 1965-1974 is the average daily flows at Ikeda (Mu-Tei). The discharge for 1975-1999 is the hourly releases from the Ikeda Dam. The target runoffs are larger than 1,000 m³/s to reduce the computational cost. The duration of the covered runoffs spans 3,857 hours. The boundary condition of the water level
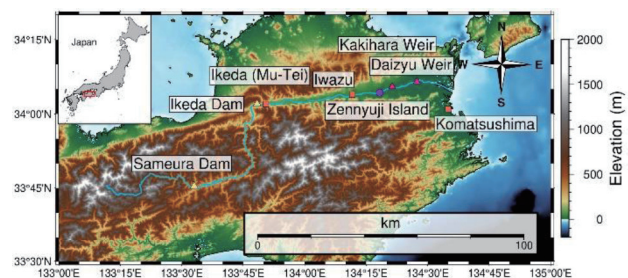

Figure 1. Yoshino River Basin

at the estuary is the hourly tide level at the Komatsushima Station in Tokushima Prefecture.

2.3 Gravel mining

This study subtracted an estimated amount of riverbed lowering due to mining from a value of the riverbed elevation at the beginning of each year's analysis. The estimated amount of riverbed degradation is calculated by dividing the annual amount of gravel mining for each section by area of that section. The amount of gravel mining before regulations is said to be two to three times the permitted amount [3]. Therefore, the amount of gravel mining from 1965 to 1974 is assumed to be two or three times the permitted amount.

2.4 Sediment trapping by the Ikeda dam

Estimated sediment trapping rates are utilized to set sediment passage rates relative to equilibrium sediment load for upstream end. The sediment capture rate of the Ikeda Dam is estimated to be 22% from Brown's equation [5], 15% from Dendy's equation [6], and 28% from Kira's equation [7].

2.5 Analysis Cases

The thirteen scenarios are classified and averaged into four cases based on the presence of gravel mining and/or the dam.

3 Results and discussion

3.1 Riverbed elevation

The model's reproducibility of the riverbed elevation is considered adequate, as it is consistent with the measurement, except for the areas close to the river mouth, upstream of the Kakihara weir, and at 76 km from the river mouth.

The analysis with gravel mining and the measurement show that the riverbed has lowered by a maximum of

The 11th International Symposium on Water Environment Systems
----- with Perspective of Global Safety   (Nov. 16th ~ 17th , 2023)

GP-RSS & SyDE
Tohoku University

approximately 2 m, whereas non-gravel mining results indicate that the scale of riverbed reduction is small. The riverbed reduction occurred primarily in the 1960s and 1970s during extensive gravel mining.

In contrast, riverbed variations are small depending on the presence or absence of the Ikeda dam. The small sediment trapping rate of the Ikeda Dam may be a factor.

3.2 Sediment load

Fluctuations in sediment load associated with gravel mining may have continued after the 1970s, when the abundance of gravel mining declined. Bedload increased in the middle reaches and decreased in the other reaches. Bedload at the river mouth decreased by 42% compared to no mining.

In addition, the sediment trapping of the Ikeda dam may affect sediment transport not only near the dam but also far downstream. The suspended sediment load was decreased throughout the study section. Bedload tends to decrease the closer to the Ikeda dam. However, bedload near the river mouth also decreases, albeit to a lesser degree.

3.3 Friction velocity

In general, an increase in friction velocity coincides with an increase in the sediment transported.

Gravel mining reduced friction velocity around the river mouth. This reduction may have contributed to the decrease in bedload at river mouth. This reduction in bedload can be explained by an increase in cross-sectional area and hydraulic depth due to riverbed incision by mining and tidal levels that are uncorrelated with riverbed elevation. The reasons for the decrease in suspended sediment load in the upper reaches and the rise in bedload in the middle reaches remain unknown.

The variation in friction velocity resulting from sediment trapping by the dam is minor. This minor change can be related to the slight change in riverbed elevation with and without the dam. To clarify the changes in sediment transport, we will discuss the sediment grain size distribution and critical shear stress, in addition to friction velocity.

4 Conclusions

Sediment load variations resulting from the implementation of gravel mining may have continued after the 1970s, when gravel mining settled down. The reduction in bedload in the lower reaches may be a result of riverbed incision and decreased frictional velocity. The Ikeda dam's sediment trapping could affect sediment transportation not only in the nearby dam area, but also far downstream to the estuary.

Reference

[1] G. M. Kondolf, "PROFILE: Hungry Water: Effects of Dams and Gravel Mining on River Channels," *Environmental Management*, vol. 21, no. 4, pp. 533–551, Jul. 1997, doi: 10.1007/s002679900048.

[2] R. Itsukushima, "Historical development and the present status of Japanese dams," *River Research and Applications*, vol. 39, no. 6, pp. 1136–1147, 2023, doi: 10.1002/rra.4129.

[3] Y. Muramoto, "River Disasters due to River Channel Process —On Recent Trends of River Bed Variation in Japan—," *Kyoto Daigaku Bosai Kenkyujo Nenpo*, vol. 17A, 1974, [Online]. Available: http://hdl.handle.net/2433/69569

[4] Takebayashi H. and Fujita M., "One dimensional bed deformation analysis with general cross-section on bed composed of cohesive and non-cohesive 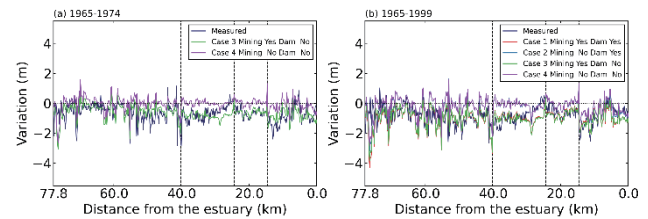materials," *Journal of the Japan Society of Erosion Control Engineering*, vol. 64, no. 2, 2011, doi: 10.11475/sabo.64.2_3.

[5] C. B. Brown, "Discussion of 'Sedimentation in reservoirs,'" *Proceedings of the American Society of Civil Engineers*, vol. 69, no. 6, pp. 1493–1500, Jan. 1943.

[6] F. E. Dendy, "Sediment Trap Efficiency of Small Reservoirs," *Transactions of the ASAE*, vol. 17, no. 5, 1974, Accessed: Apr. 02, 2023. [Online]. Available: https://doi.org/10.13031/2013.36994

[7] H. Kira, "On the Trap Efficiency of Reservoirs and Sediment Budget in Japan," *Transactions of The Japanese Society of Irrigation, Drainage and Reclamation Engineering*, vol. 1978, 1978, doi: 10.11408/jsidre1965.1978.78_16.

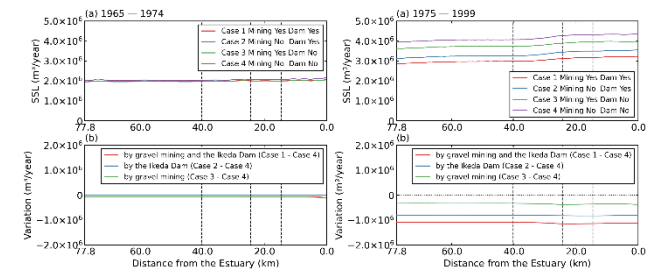**Figure 2. Cumulative change in riverbed elevation**

Figure 3. (a) Annual average suspended sediment load (b) Variation due to anthropogenic activities
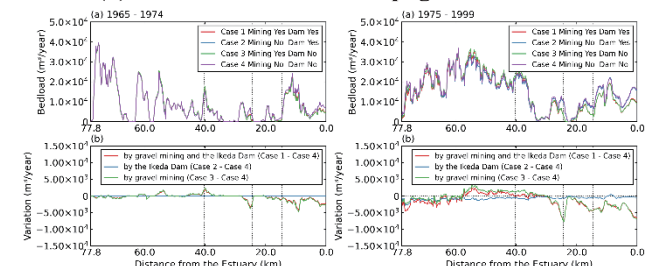

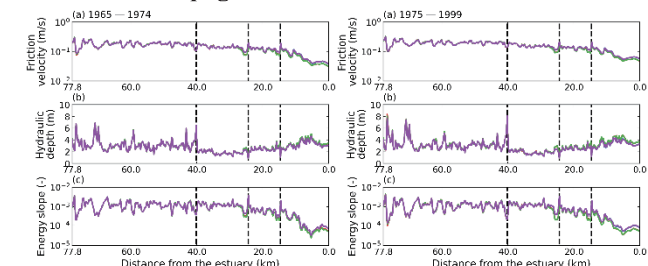**Figure 4. (a) Annual average bedload (b) Variation due to anthropogenic activities**

Figure 5. (a) Average friction velocity (b) Average hydraulic depth (c) Average energy slope Legend for this figure is the same as Figure 2.

The 11th International Symposium on Water Environment Systems
----- with Perspective of Global Safety   (Nov. 16th ~ 17th , 2023)

GP-RSS & SyDE
Tohoku University

Calibrating hydrology models in poorly gauged and heavily regulated basin with satellite data

○ Dung Trung VU[1,2*], Thanh Duc DANG[3], Francesca PIANOSI[4], & Stefano GALELLI[2,5]

[1]Global Hydrodynamics Lab, Institute of Industrial Science, University of Tokyo, Tokyo 153-8503, Japan
[2]Pillar of Engineering Systems and Design, Singapore University of Technology and Design, Singapore 487372, Singapore.
[3]Department of Civil and Environmental Engineering, University of South Florida, FL 33620, USA
[4]School of Civil, Aerospace and Design Engineering, University of Bristol, Bristol BS8 1TH, UK
[5]School of Civil and Environmental Engineering, Cornell University, NY 14853, USA
*E-mail: dtvu205@gmail.com.

Abstract

Calibrating large-scale hydrological models is often challenged by the lack of in situ data on river discharge and water infrastructure operations. This modeling backdrop creates a number of potential pitfalls for model calibration, potentially affecting the reliability of hydrological models. Here, we introduce a novel numerical framework to explore and overcome these pitfalls. Our framework consists of VIC-Res (a large-scale hydrological model setup for the Upper Mekong Basin) and a hydraulic model used to infer river discharge from satellite data. Using these two models and global sensitivity analysis, we show the existence of a strong relationship between the parameterization of the hydraulic model and the performance of VIC-Res — a codependence that emerges for a variety of performance metrics that we considered. Using the results provided by the sensitivity analysis, we propose an approach for breaking this codependence and informing the hydrological model calibration, which we finally carry out with the aid of a multi-objective optimization algorithm. The approach used in this study could integrate multiple remotely sensed observations and is transferable to other poorly gauged and heavily regulated river basins.
Keywords: hydrological models; poorly gauged basins; reservoir operation; satellite data.

1 Introduction

Large-scale hydrological models have gained popularity over the past few decades. Such models were implemented for a wide range of applications, such as quantifying the potential impact of climate change on water resources or predicting extreme events. Unfortunately, due to the lack of long and reliable time series data of observed discharge, large-scale hydrological models are rarely calibrated, or the calibration exercises are limited to a portion of the model domain [1]. Additionally, the absence of the operations of hydraulic infrastructures (i.e., reservoirs) in hydrological models, also due to the lack of in situ data, could affect the results of model calibration [2]. Some studies have dealt with the lack of observed discharge by converting altimetry water levels and/or river widths derived from satellite images to river discharge through hydraulic models in which the parameters need to be calibrated as well. Such hydraulic models are coupled with hydrological models, and the parameters of the two models are calibrated concurrently [3]. However, a potential pitfall is the fact that estimation errors in the hydraulic model may be compensated for by introducing parameter biases in the hydrological model, and vice versa. Considering the increase of remotely sensed hydrological data and that these satellite products are the only means to estimate river discharges in many regions of the world, the question arises as to how best use such remotely sensed data to support model calibration. Hence, the overarching questions are: (1) To what extent is it possible and helpful to calibrate a largescale hydrological model in ungauged basins using remotely sensed data? and (2) How do we deal with potential interactions between parameters of two models in model calibration?

2 Materials and methods

We implement VIC-Res model for the Upper Mekong River basin which is characterized by a shortage of observed discharge data and the hydrological alterations caused by the system of more than ten large reservoirs on the mainstream. VIC-Res is a novel variant of Variable Infiltration Capacity
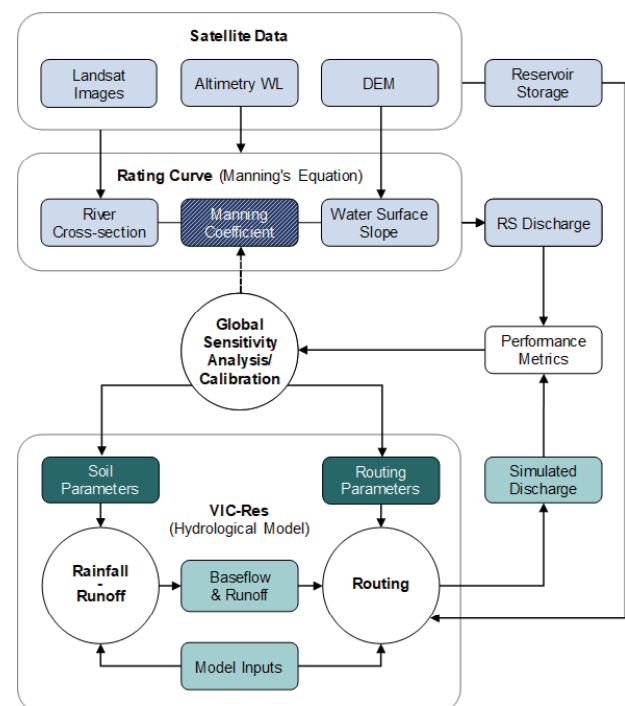

Fig. 1. Methodology.

The 11ᵗʰ International Symposium on Water Environment Systems
----- with Perspective of Global Safety (Nov. 16ᵗʰ ~ 17ᵗʰ , 2023)

GP-RSS & SyDE
Tohoku University

largescale hydrological model [4], that includes a module for representing reservoir operations, in which we use the time series of reservoir storage inferred from satellite data [5]. To generate discharge data for the calibration of VIC-Res, we use Jason-2 altimetry water levels at the virtual station (~280 km in downstream of Chiang Saen station considered as the basin outlet) and a hydraulic model (a rating curve containing Manning's coefficient (*n*) as a model parameter) that is also constructed using satellite data. In our framework, we first use global sensitivity analysis to demonstrate the existence of a pronounced codependence between *n* and the performance metrics of VIC-Res (NSE, TRMSE, MSDE, and ROCE). To break this codependence, we leverage the results of the sensitivity analysis to constrain the range of *n* and, thus, safely inform the calibration of VIC-Res.

3 Results and discussion

Fig. 2 illustrates the results of river cross-section (a), rating curve (b), and discharge (c) at the virtual station estimated using satellite data. In panel b, we highlight the three rating curves corresponding to the three special values of *n* in its recommended variability range. In panel c, we show the variability range of remotely sensed (RS) discharge (light blue band) and compare the discharge estimated with the average value of *n* (dark blue line) against the one obtained by scaling the observed discharge at Chiang Saen by the area ratio of 1.17 (dotted orange line).
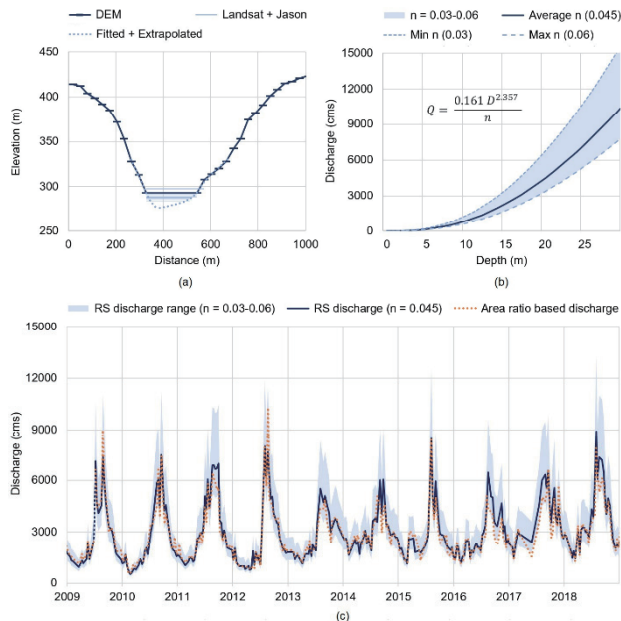

Fig. 2. River cross-section (a), rating curve (b), and remotely sensed discharge at the virtual station (c).

The results of the sensitivity analysis reveal a strong codependence between *n* and the performance metrics of VIC-Res. Specifically, by selecting the top 25% of model parameterizations (=250/1000 samples) yielding the best performance for each metric (e.g., highest NSE, lowest TRMSE) we receive different variability ranges of *n*, followed by different variability ranges of RS discharge. This can be explained by the fact that the performance metrics capture different aspects of model accuracy, which is affected by RS discharge estimated with *n* and used for calibration. To balance the aspects of model accuracy, we intersect the

four groups of top 25% of model parameterizations and receive 40 model parameterizations. The corresponding range of *n* is narrowed down significantly to [0.04, 0.052], also the variability range of RS discharge. Using RS discharge estimated with the new average value of *n* (0.046) for model calibration, we have a performance shown in panel a of Fig. 3. Finally, we provide model validation with observed discharge at Chiang Saen in panel b of Fig. 3.
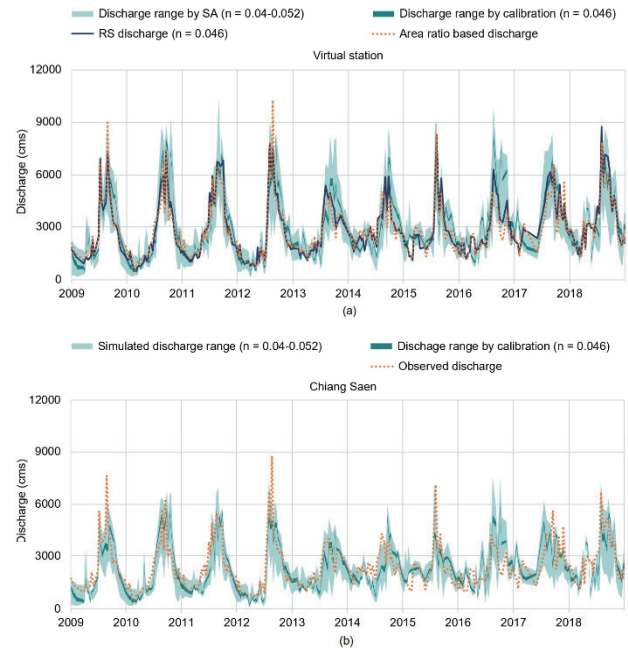

Fig. 3. Model calibration with remotely sensed discharge (a) and validation with observed discharge (b).

4 Conclusions

In this study, we develop an approach for calibrating large-scale hydrological models which use reservoir storage and river discharge data inferred from satellite data. Sensitivity analysis results show a strong codependence between *n* and the performance metrics of VIC-Res, that helps to narrow down the range of *n* and reduce the uncertainty in model calibration. Model calibration and validation results are reasonable when considering that no in situ data are used.

Reference

[1] Bierkens, M. F. P., Global hydrology 2015: State, trends, and directions, WRR, 51 (2015) 4923–4947.

[2] Dang, T. D., Chowdhury, A. K., & Galelli, S., On the representation of water reservoir storage and operations in large-scale hydrological models, HESS, 24 (2020) 397–416.

[3] Huang, Q., Long, D., Du, M., Han, Z., & Han, P., Daily continuous river discharge estimation for ungauged basins using a hydrologic model calibrated by satellite altimetry, WRR, 56 (2020) e2020wr027309.

[4] Dang, T. D., Vu, D. T., Chowdhury, A. K., & Galelli, S., A software package for the representation and optimization of water reservoir operations in the VIC hydrologic model, EMS, 126 (2020) 104673.

[5] Vu, D. T., Dang, T. D., Galelli, S., and Hossain, F., Satellite observations reveal 13 years of reservoir filling strategies, operating rules, and hydrological alterations in the Upper Mekong River basin, HESS, 26 (2022) 2345–2364.

The 11th International Symposium on Water Environment Systems
----- with Perspective of Global Safety   (Nov. 16th ~ 17th , 2023)

GP-RSS & SyDE
Tohoku University

Effects of Land Use Change to Canopy Interception, Evapotranspiration, and Water Balance in a Humid Tropical Hillslope of Sumatra, Indonesia.

○Eilif DJAMRES[1*], Takahiro SAYAMA[2], EvaYAMAMOTO[2] YoshitoSUGAWARA[2]

[1]Graduate School of Engineering, Kyoto University, Kyoto, Japan, 615-8530, Japan.
[2]Disaster Prevention Research Institute, Kyoto University, Kyoto, 611-0011, Japan
[*]E-mail: eilif.djamres.85x@st.kyoto-u.ac.jp.

Abstract

This study investigates the impact of land use change, specifically the conversion of forested areas to oil palm plantations, in a humid tropical hillslope of Sumatra, Indonesia. The research focuses on the changing of potential evapotranspiration (PET) and rainfall partitioning between jungle rubber (JR) and oil palm (OP) plantations impacts to the groundwater (GW) and water balance using the rainfall–runoff–inundation (RRI) model. By the Penman–Monteith model, we recorded the changing PET from 1422.45mm in JR to 1058.93mm in OP during one–year simulation. Moreover, we used Suzuki interception model to get the difference rainfall interception rate among JR and OP land cover. Interception rate on the JR was 69.6% of gross rainfall (Pg) while OP had 14.9%. The RRI model suggested that the increasing of the discharge after changing the land cover is mainly due to different of rainfall input in the model. If we compare the percentage of the discharge on the water balance, OP released slightly smaller percentage of discharge. The portion of evapotranspiration from JR to OP was remain consistent increased, even though OP had a larger PET.

Keywords: Humid tropical hillslope; Land use change; RRI model; Interception; Water balance.

1 Introduction

Land use change (LUC), particularly the conversion of forested areas to oil palm plantations, is a prevalent phenomenon in many humid tropical regions (Hansen et al., 2013; Gibbs et al., 2010; Margono et al., 2014). The global demand of the oil palm is projected to increase constantly up to 2050 following the historical expansion of 1990 to 2010 (Harris et al., 2013). In Southeast Asia, large areas of forests have been converted to oil palm, and other monoculture plantations over the last decades (Hansen et al. 2013, Margono et al. 2014, Clough et al. 2016. Such intense land use change is often followed by an impairment of ecohydrological functions (Bruijnzeel 2004, Bradshaw et al. 2007, Ellison et al. 2017) and has been acknowledged as the significant issue threatening water reservoir and watershed management (e.g.,Woldemichael et al. 2012; Yigzaw and Hossain 2016).

In order to encompass the complicated impacts of land use changes in a hillslope scale, this study further integrated some hydrological modeling techniques to quantify potential evapotranspiration (PET) variations, rainfall partitioning between jungle rubber (JR) and oil palm (OP) plantations that two dominant LUC in the area, and RRI model to get the GW dynamics and water balance changing. In the RRI model, we added the water storage-evapotranspiration relationship on canopy and soil to account the actual evapotranspiration rate. By quantifying and consolidating the results, this research aims to understand the impacts of LUC on hydrological processes in a humid tropical hillslope. While, for the specific objectives were: (a) To understand how the LUC will impact to rainfall partitioning, evapotranspiration, and groundwater dynamics of a humid tropical hillslope; (b) What is the impact of LUC to water balance in the hillslope scale.

2 Methods

The study hillslopes are located in the Batanghari River basin (42,690 km2) in Jambi Province, Sumatra, Indonesia.

The climate in Jambi Province is humid tropical with an average air temperature of 26.7 ± 0.2°C and annual precipitation of 2,235 ± 381 mm as recorded from 1991 to 2011 (Drescher, J. et al., 2016). The position of the hillslope is 2°15'31.1"S 102°10'20.6"E and covered by a secondary forest known as the 'jungle rubber agroforest' (Joshi et al., 2002), where rubber trees are planted without slash–and–burn techniques.

The GW monitoring period presented here was from December 2019 to December 2020. The gross rainfall (Pg) was measured by a tipping bucket (CPK-RAIN-1, Climatec; Phoenix, AZ, USA) that gauge every ten-minute. We used a barometric (DAIKI, DIK-615A-B1) for gauging GWs level in the boreholes. The GWs level were recorded every 10 minutes from the three observation boreholes (named JR1, JR2, and JR3) installed along the SK hillslope. Then, these data were compensated with temperature and pressure data (TD-Diver DI800, Van Essen; Delft, Netherlands). Moreover, the potential evapotranspiration calculated by Penman-Monteith and using meteorological data from the ERA5-Land dataset.

This research used Throughfall (TF) and stemflow (SF) data from other research that conducted in the same province (Jambi) and has similarity trees types (Bejo et al., 2015). We adopted their measurement results to our study area with our own gross rainfall (Pg) data. Then, by Suzuki conceptual model, we calculate the TF, SF, and interception (Ic).

The used hillslope hydrologic model is the rainfall-runoff-inundation (RRI) model that has a hillslope element to incorporate bedrock groundwater (Sayama et al. 2012, Sayama et al. 2015a, Sayama et al. 2015b). We conducted a numerical experiment to produced GW fluctuation and water balance of six simulations, called simulation A, B, C, D, E, and D, with different parameters and model settings.

The simulations A, C, and E were set as JR canopy, while simulation B, D, and F were OP canopy. Simulation A and B used Pg and simulation C–F employed net rainfall (Pn) that

The 11th International Symposium on Water Environment Systems
----- with Perspective of Global Safety   (Nov. 16th ~ 17th , 2023)

GP-RSS & SyDE
Tohoku University

results from the Suzuki model. To differentiate evapotranspiration from the soil, we assumed the root depth of mature oil palm as 0.3m (Lisma S., et al., 2018) and 0.55m for rubber root depth (Yang B., et al 2020). In term of suction head of the root, we assumed that rubber has -1m and -2.5 for OP.

3   Results and Discussions

This research calculated PET by using the obtained meteorological data and P-M equation. The total annual PET during period in JR was 1422.45mm and 1058.93mm in OP. Total Pg between 12 December 2019 to 12 December 2020 was 3343.2 mm with March being the wettest month, recorded 513.2 mm or 15.35% of the total Pg. Throughfall in JR comprises 69.6% of the Pg or 2328.2 mm. Only very small fraction of the rainwater appeared as stemflow that was 7.08 mm of the Pg.

Interception loss, calculated as the difference between the sum of throughfall and stemflow from the total Pg was 1007.91 mm or about 30.15%. Differently compare to the OP canopy, the TF in this land cover was 84.96% of Pg or 2840.27mm during a year calculation. Meanwhile the stemflow was 3mm with about a half of Ic percentage in the JR which recorded 14.95% (499.92mm).

During study period, the observed GW remained at a depth of ~300 cm from the soil surface in the early dry season (June), and decreased to 415 cm during the driest period (August–September). However, the persistent GW was observed even in the driest period, it indicates that evapotranspiration in the JR is energy limited rather than water limited.

The RRI model results suggested that without interception, the simulation "A" which used Pg as input data, in rainy season its GW was rose more than observation data and reached near the surface which the GW observation was not experience. Since the simulation "A" was not limiting the transpiration in the certain depth (assuming transpiration occur in all soil layer levels), in the driest season (July to September), no GW was not existed in the soil column.

With smaller rainfall input, simulation "C" had the deepest GW level. In the days with no rainfall as in the early of March and 4 to 7 July (Figure 6), its GW was no longer exist. This condition was worst in the driest period (July-September). In simulation "E", we used Pn and restricted the evapotranspiration that worked just on the certain level based on the root depth of the rubber which 0.55m. This evapotranspiration setting could reduce the GW sink in the dry season as simulation "C", otherwise the GW still existed and fluctuated similar as a GW from observation. The persistence of GW even in the driest season indicated that the model can reflect the humid tropical environment which characterized by wet conditions, where the total evapotranspiration largely depend on atmospheric energy supply (Wohl et al., 2012), and the soil is always moist as reflected by the persistence of GW throughout the year.

A summary of the annual water balance of each simulation is provided in **Figure 1**. Without limiting the evapotranspiration depth, LUC may have profound effects on discharges (Simulation A vs Simulation B and Simulation C vs Simulation D). Changing the land cover from JR to OP was elevated the discharge about 11% as shown by Simulation A and B. Simulation C and D were utilized a Pn coming from Suzuki model, in this case the discharge rose

prominently that recorded 13% or from 1165.31mm to 1798.5mm. The smaller rainfall inputs as used by simulation C and D were also impact on reducing the actual evapotranspiration.
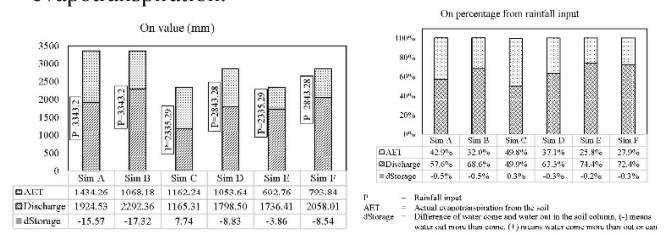

Figure 1 Water balance of model simulations

To reflect the actual condition, we set evapotranspiration from trees at a certain level based on its root characteristics. This setting could reduce the discharge comparing with previous simulations. The JR hillslope (Simulation E) had 1736.43mm of discharge during a year while OP hillslope (Simulation F) recorded 2058.01mm. However, it could not simply assuming that this increasing of discharge was just related to the LUC solely. If we see the percentage of the discharge, the Simulation F had a smaller discharge's percentage. It supposed the rising discharge in "Simulation F" was impact of the larger rainfall input. Regarding the actual evapotranspiration, OP created about 200mm more even though we input potential evapotranspiration in the model setting almost 400mm less than JR.

4 Conclusions

This research measured the effect of land cover change in a hillslope scale on the humid tropical environment. We got the difference rainfall partitioning among JR and OP land cover. JR had a higher interception rather than OP, it comprised 69.6% of Pg while OP had 14.9%. By utilizing net rainfall and actual evapotranspiration in the RRI model, we successfully replicated the observed GW. Moreover, the model suggested that the increasing of the discharge after changing the land cover is mainly due to different of net rainfall input in the model.

Reference

[1] Bejo, S., (2015) Intersepsi dan Aliran permukaan Pada Transformasi Hutan hujan Tropika Dataran Rendah Jambi. (Doctoral dissertation, Graduate School of IPB University) accessed from https://www.uni-goettingen.de/de/document/download/39fa62856e82ac32fc2cd85051c9a868.pdf/Dissertation_Bejo_Slamet_IPB_2015.pdf.

[2] Li H, Chen R, Han C, Yang Y. Evaluation of the Spatial and Temporal Variations of Condensation and Desublimation over the Qinghai–Tibet Plateau Based on Penman Model Using Hourly ERA5-Land and ERA5 Reanalysis Datasets. Remote Sensing. 2022; 14(22):5815. https://doi.org/10.3390/rs14225815

[3] Sayama T, Kosugi K, Iwami Y, (2015a) Development of a distributed rainfall-runoff model simulating for mountainous groundwater, JSCE B1 (Hydraulic Engineering) 71(4):331-336.

[4] Suzuki, M, (1980) Evapotranspiration from a small catchment in hilly mountains (I) Seasonal variations in evapotranspiration, rainfall interception and transpiration, Journal of the Japanese Forestry Society, 62(2):46-53.

The 11th International Symposium on Water Environment Systems
----- with Perspective of Global Safety   (Nov. 16th ~ 17th , 2023)

GP-RSS & SyDE
Tohoku University

Sensitivity Analysis of Extreme Precipitation Over Western Tohoku Using TIGGE Ensembles

◯ Sawitree ROJPRATAK[1]* & Yusuke HIRAGA[2]

[1]Department of Civil Engineering, Rangsit University, Pathum Thani 12000, Thailand.
[2]Graduate School of Civil Engineering, Tohoku University, Miyagi 980-8579, Japan.
*E-mail: fiatsawitree@gmail.com, sawitree.r61@rsu.ac.th.

Abstract

Flood occurs frequently in Japan and effects damage to both lives and properties. At the beginning of August 2022, an extreme precipitation even in the southwestern Tohoku (SWT) region and causes the great flood disaster. This research is in the SWT region. The purpose of this research is to analyze the sensitivity of precipitation by applying Ensemble Sensitivity Analysis (ESA) for establishing a linear relationship between average precipitation of SWT region and 6 variables at 925hPa. They are specific humidity, temperature, geopotential height, u of wind, v of wind, and moisture flux. The averaged 48 hour accumulated precipitation and variables of forecast data are obtained from The Interactive Grand Global Ensemble (TIGGE) of European Centre for Medium-Range Weather Forecasts (ECMWF). The result of the research found the moisture flux and u of wind are positively correlated with the increase in precipitation in the same direction, and ES values are 8.17 and 7.36. However, the sensitivity of specific humidity is not affected highly to precipitation in negative trend. Finally, the areas of v of wind are affected to precipitation in negative trend, and the values are mid to low.

Keywords: Ensemble Sensitivity Analysis; Extreme precipitation; TIGGE; Ensemble forecast; Southwestern Tohoku region.

1 Introduction

Japan is a country surrounded by the sea. It is often affected by natural disasters such as typhoons, volcanic eruptions, earthquakes, and floods. The south western Tohoku (SWT) region is located in the northern part of Japan. According to the Japan Meteorological Agency (JMA) report, in August 2022, the most severe event in this northern region occurred. The amount of rainfall increased by more than 70% in the entire Tohoku region [1]. The TCC (2022) report [2] states that extreme precipitation was mainly due to a stationary front that occurred from early to mid-August. Although the front slowly shifted north to south with different shapes and orientations, its eastern part often remained in the northern part of Japan, maintaining a strong moisture transport into Tohoku and ultimately leading to extreme precipitation.

Ensemble Sensitivity Analysis (ESA) has been widely used as a tool to understand and predict the meteorological conditions associated with severe weather events. Torn and Hakim (2008) [3] proposed a method that utilizes ensemble statistics to estimate the sensitivity of initial conditions in predicting the event using ESA. ESA is commonly used to examine the predictability of weather events. Guo et al. (2019) [4] examined heavy rainfall events in Beijing and found that the low-level southwestly moist flow in the lower atmosphere plays a significant role in heavy rainfall in Beijing. There have been other heavy rainfall events studied using ESA [5]; [6]; [7].

2 Materials and methods

At the beginning of August 2022, SWT region was one of the areas impacted by Typhoon No. 6 [8], leading to extreme precipitation. Therefore, it became an area of interest for study. This study utilizes forecast data from The Interactive Grand Global Ensemble (TIGGE) of European Centre for Medium-Range Weather Forecasts (ECMWF). The ensemble forecasts initialized at 1200 UTC 31 July 2022.

There are 50 members of ensemble forecasts in the ECMWF. The data is gridded $0.14° \times 0.14°$. The averaged accumulated precipitation of the forecast is during the 48th hour to the 96th hour (1200 UTC 02 August 2022 to 1200 UTC 04 August 2022) over SWT region. In addition, 48th hour forecast 6 variables of interest at the 925 hPa level encompass specific humidity, temperature, geopotential height, u of wind, v of wind, and moisture flux.

The sensitivity of a forecast metric j and variable x are performed in this Eq. (1)

$$ES = \frac{\partial J}{\partial x_i} = \frac{cov(J, x_i)}{var(x_i)} \sigma_{x_i} \qquad (1)$$

From equation, J and x are 1xM estimates of the scalar forecast metric referred to the response function and variable of ith, sequentially. Moreover, cov represents the covariance between an argument and var denotes variance of M ensemble members. The above equation expresses linear regression. The independent variable is an analysis grid point, and the dependent variable is the forecast metric.

The sampling errors of regression coefficient are valued between with a limited number of ensemble members and the number of state variables. Hence, a statistical significance test is performed using the method outlined [3]. ESA serves the purpose of establishing linear correlations between the average precipitation within the SWT region and a set of 6 variables measured.

3 Results and discussion

The computation of ES using the 48-hour averaged accumulated precipitation in the SWT region and various variables at 925 hPa reveals the sensitivity of the response function to geopotential height displays a positive sensitivity at a relatively modest level, peaking at 2.24 from Fig. 1 (a). This indicates the geopotential height enhances the lower-level precipitation responsibly. For the sensitivity to precipitation of moisture flux (Fig. 1 (b)), it is observed a response in the same direction as high precipitation, yielding

The 11th International Symposium on Water Environment Systems
----- with Perspective of Global Safety   (Nov. 16th ~ 17th , 2023)

GP-RSS & SyDE
Tohoku University

a high ES value of up to 8.17. For the sensitivity to precipitation of specific humidity, it is found to have a relatively low sensitivity in the negative direction, with the highest value at -4.53. However, it except in the southern and southwestern parts of the SWT region where there is a high positive sensitivity response, reaching a maximum value of 7.47, as shown in Fig. 1 (c).

From Fig. 1 (d), it is evident about the majority of the temperature exhibits a positive sensitivity response to precipitation at a lower level which the highest value is 3.01. There are exceptions in the areas of edges from the northwest down to the southwest of the SWT region, which show a negative sensitivity response at a mid-level. The maximum value is at -4.23. For the sensitivity of the sensitivity of horizontal air movement towards the east (u of wind), the response is clearly seen to be positively correlated with precipitation in the same direction which the highest value is 7.36. In other words, the horizontal speed of air moving towards the north (v of wind) exhibits an opposite relationship with precipitation which the lowest value at -4.14. However, there is a positive correlation in the northern and northwestern of the SWT region. The highest value at 4.35, as shown in Fig. 1 (e) and 1 (f), respectively.
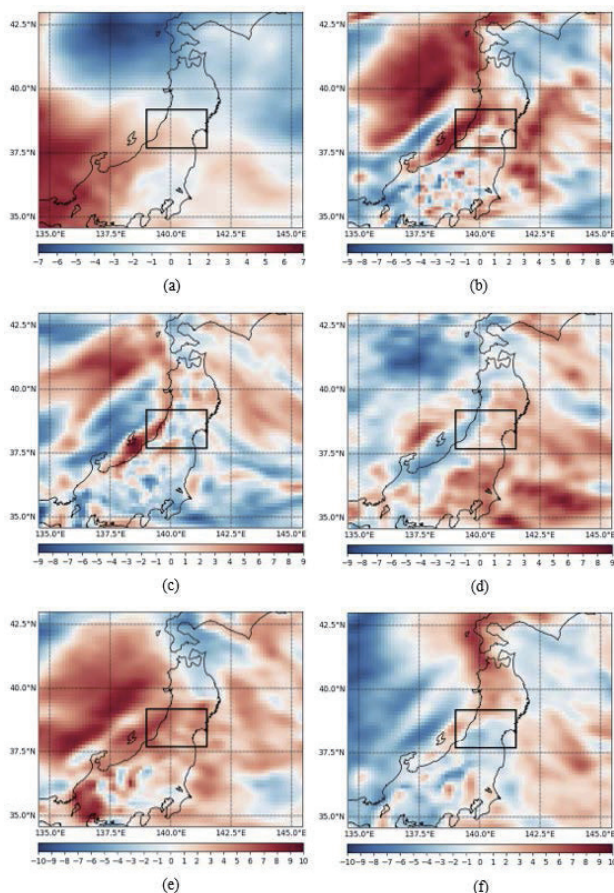

Fig. 1. Sensitivity of averaged 48 hours accumulated precipitation over southwestern Tohoku (SWT) region with time 48th hour to 96th hour forecast by initializing at 1200 UTC 31 July 2022 and 6 forecast variables at 925 hPa: (a) geopotential height, (b) moisture flux, (c) specific humidity, (d) temperature, (e) u of wind and (f) v of wind

4 Conclusions

In the analysis of the sensitivity to the averaged 48-hour accumulated precipitation, the correlated factors with an increase in precipitation are moisture flux, u of wind, and geopotential height. The ES values are 8.17, 7.36, and 2.24 respectively.   Another variable with positive sensitivity to precipitation is geopotential height. The highest geopotential height is 2.24. The sensitivity of specific humidity is not high responsibly to precipitation in negative trend, and the highest of specific humidity is -4.53. Moreover, temperature has mostly a positive impact on precipitation. The highest value is 3.01. V of wind affects precipitation across the area negatively. The maximum values are -4.14.

Reference

[1] Japan Meteorological Agency (JMA). (2022). Weather in August (in Japanese). https://www.data.jma.go.jp/obd/stats/data/stat/tenko202208.pdf.

[2] Tokyo Climate Center (TCC), Japan Meteorological Agency (JMA). (2022). Climate characteristics and factors behind record-high temperatures in late June/early July 2022 and subsequent weather conditions, 1–12. https://www.data.jma.go.jp/tcc/data/news/press_20220914.pdf.

[3] Torn RD, Hakim GJ (2008) Ensemble-based sensitivity analysis. Monthly Weather Rev 136, 663–677. https://doi.org/10.1175/2007MWR2132.1

[4] Guo, Y., Wang, Y., Dai, K., Zhang, X., & Shen, Y. (2019). Ensemble Sensitivity Analysis Applied to a Heavy Rainfall Event in Beijing. Environment and Information Engineering (SEEIE 2019), 132-135.

[5] George, B., & Kutty, G. (2021). Ensemble sensitivity analysis of an extreme rainfall event over the Himalayas in June 2013. Dynamics of Atmospheres and Oceans, 93, 101202, 1-16.

[6] George, B., & Kutty, G. (2022). Sensitivity analysis applied to two extreme rainfall events over Kerala using TIGGE ensembles. Meteorology and Atmospheric Physics, 134(2), 2-22.

[7] Wang, C. C., Li, M. S., Chang, C. S., Chuang, P. Y., Chen, S. H., & Tsuboki, K. (2021). Ensemble-based sensitivity analysis and predictability of an extreme rainfall event over northern Taiwan in the Mei-yu season: The 2 June 2017 case. Atmospheric Research, 259, 105684, 1-22.

[8] Japan Meteorological Agency (JMA). (2022). Yamagata Prefecture Disaster Meteorological Information: Heavy rain associated with low pressure and fronts (August 2nd to 5th, 2020), 1-28. https://www.data.jma.go.jp/yamagata/pdf/support/storm/2022_1.pdf.

The 11th International Symposium on Water Environment Systems
----- with Perspective of Global Safety   (Nov. 16th ~ 17th , 2023)

GP-RSS & SyDE
Tohoku University

Where should riparian vegetation be cut from for effective flood damage reduction?

○ Hayata YANAGIHARA[1*], So KAZAMA[1]

[1]Department of Civil and Environmental Engineering, Graduate School of Engineering, Tohoku University, Miyagi 980-8579, Japan.
*E-mail: yanagihara.hayata.r1@dc.tohoku.ac.jp

Abstract

This study evaluated the effect of the order of riparian vegetation removal on flood damage reduction in class A river systems throughout Japan to understand where riparian vegetation should be cut from for effective flood damage reduction. Flood inundation analyses were carried out using roughness coefficients to reflect the condition before and after riparian vegetation removal, and the flood damage costs were calculated based on the inundation depths. The results show that the flood damage reduction effects differ depending on the order of riparian vegetation removal. The number of river systems with the highest damage reduction rate was 13 in the case of upstream → midstream → downstream, 39 in the case of downstream → midstream → upstream, 14 in the case of midstream → upstream → downstream and 38 in the case of midstream → downstream → upstream. We therefore conclude that where riparian vegetation should be cut from depends on the river system.

Keywords: riparian vegetation; flood damage reduction; removal order; adaptation measure.

1 Introduction

In Japan, the frequency of extreme rainfall is predicted to increase due to global warming [1]. Therefore, there are concerns about future increases in flood damage [2], and adaptation measures need to be implemented to reduce the adverse effects of climate change. Previous studies have evaluated the effectiveness of adaptation measures. For example, Yamamoto et al. [2] assessed flood damage reduction effects of land-use control, piloti building and improvement of flood control levels across Japan considering climate change. Previous studies have pointed out the limitations of adaptation measures. Mitigation measures, including reductions in greenhouse gas emissions, should therefore be promoted in parallel with adaptation measures. In this context, riparian vegetation removal has recently attracted attention as a countermeasure that combines adaptation and mitigation measures. Riparian vegetation removal is expected to reduce channel roughness and increase the cross-sectional area of rivers. In addition, the cut riparian vegetation can be utilized for biomass power generation, which can also contribute to mitigation measures. The Mogami River Public-Private Partnership Platform is utilising cut riparian vegetation for biomass power generation [4]. For sustainable biomass power generation from riparian vegetation and effective flood damage reduction, it is necessary to assess where riparian vegetation should be cut from: upstream, midstream or downstream. However, no evaluation of flood damage reduction by the order of riparian vegetation removal has been carried out. This study therefore evaluated the impact of the order of riparian vegetation removal on flood damage reduction.

2 Methodology

The assessment of flood damage reduction by riparian vegetation removal was carried out by applying the method of Yanagihara et al. [4]. Yanagihara et al. [4] carried out flood inundation analyses using roughness coefficients to reflect the condition before and after riparian vegetation removal

Table 1. Scenarios for the order of riparian vegetation removal.

Scenario	Stage	Condition of riparian vegetation		
		Upstream	Midstream	Downstream
Upstream → midstream → downstream	1	Non-luxuriance	Luxuriance	Luxuriance
	2	Growth	Non-luxuriance	Luxuriance
	3	Luxuriance	Growth	Non-luxuriance
Downstream → midstream → upstream	1	Luxuriance	Luxuriance	Non-luxuriance
	2	Luxuriance	Non-luxuriance	Growth
	3	Non-luxuriance	Growth	Luxuriance
Midstream → upstream → downstream	1	Luxuriance	Non-luxuriance	Luxuriance
	2	Non-luxuriance	Growth	Luxuriance
	3	Growth	Luxuriance	Non-luxuriance
Midstream → downstream → upstream	1	Luxuriance	Non-luxuriance	Luxuriance
	2	Luxuriance	Growth	Non-luxuriance
	3	Non-luxuriance	Luxuriance	Growth

and calculated the flood damage costs based on inundation depths. To assess the differences in flood damage reduction effects depending on the order of riparian vegetation removal, scenarios for the order of riparian vegetation removal were set up (Table 1). In the scenarios for the order of riparian vegetation removal, the river channel was divided into upstream, midstream and downstream sections, with cutting from upstream, downstream and midstream. There are two scenarios for cutting from midstream: midstream to upstream and midstream to downstream. Each scenario consists of three riparian vegetation stages. To consider the case of riparian vegetation growth and re-luxuriance after cutting, it was assumed that the section that was cut and non-luxuriance

The 11th International Symposium on Water Environment Systems
----- with Perspective of Global Safety   (Nov. 16th ~ 17th , 2023)

GP-RSS & SyDE
Tohoku University

in Stage 1 was assumed to be growth in Stage 2 and re-luxuriance in Stage 3. By considering the growth process in the scenarios for the order of riparian vegetation removal, it is possible to reflect the time elapsed since cutting and to evaluate differences in the order of riparian vegetation removal. It was assumed that the re-luxuriance condition was the same as the luxuriance condition. The biomass potential was calculated by multiplying the riparian vegetation area by the normalised vegetation index. The upstream, midstream and downstream sections of the river channel were determined so that the biomass potential was approximately the same in each section. Roughness coefficients reflecting each riparian vegetation condition were determined by the method of Yanagihara et al. [5].

3 Results and discussion

The expected annual damage reduction rate for each scenario is the average of the expected annual damage reduction rates for stages 1, 2 and 3 of the riparian vegetation. The river systems with the highest expected annual damage reduction rate for each scenario were the Tokachi River system (7.5%), Seki River system (6.6%) and Tenjin River system (5.3%) in the case of upstream → midstream → downstream, the Seki River system (9.4%), Tokachi River system (8.4%) and Oita River system (6.8%) in the case of downstream → midstream → upstream, the Tokachi River system (7.5%), Seki River system (6.7%) and Oyabe River system (5.4%) in the case of midstream → upstream → downstream and the Seki River system (9.3%), Tokachi River system (8.4%) and Oita River system (6.9%) in the case of midstream → downstream → upstream. Although the ranking of the river systems with the highest expected annual damage reduction rate varies according to the order of riparian vegetation removal, high flood damage reduction by riparian vegetation removal is expected in the river systems mentioned above.

Fig. 1 shows the scenario with the highest expected annual damage reduction rate for each class A river system. The number of river systems with the highest expected annual damage reduction rate for each scenario was 13 in the case of upstream → midstream → downstream, 39 in the case of downstream → midstream → upstream, 14 in the case of midstream → upstream → downstream and 38 in the case of midstream → downstream → upstream. These results indicate that the flood damage reduction effect differs depending on the order of riparian vegetation removal. Similarly, the scenario for the order of riparian vegetation removal that resulted in the highest expected annual inundation area (maximum inundation depth of 10 cm or more) reduction rate was examined (Fig. 2). The results showed that in 65 out of 109 river systems, the results were different from those for the annual expected damage reduction rate.

4 Conclusions

This study estimated the flood damage reduction effects by the order of riparian vegetation removal on class A river systems across Japan. The results showed that the flood damage reduction effect varied depending on the order of riparian vegetation removal. We therefore conclude that
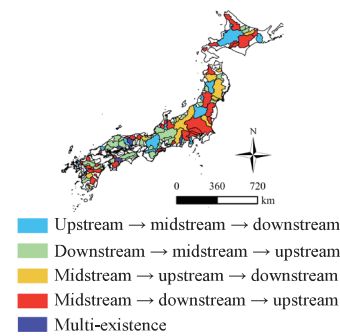

Fig. 1. Scenario with the highest expected annual damage reduction rate by class A river system.
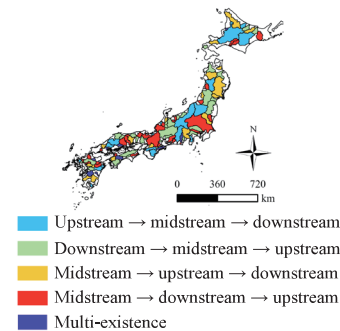

Fig. 2. Scenario with the highest expected annual inundation area rate by class A river system.

where riparian vegetation should be cut from depends on the river system.

Reference

[1] Yanagisawa, H. et al., Spatial frequency analysis of annual extreme daily precipitation across Japan, *Journal of Hydrology: Regional Studies*, Vol. 42 (2022), 101131.
[2] Yamamoto, T. et al., Evaluation of flood damage reduction throughout Japan from adaptation measures taken under a range of emissions mitigation scenarios, *Climatic Change*, Vol. 165 (2021), 60.
[3] Yamagata Office of Rivers and National Highways, Mogami River Public-Private Partnership Platform, https://www.thr.mlit.go.jp/yamagata/river/mogamigawa-platform/index.html (accessed 15 October 2023).
[4] Yanagihara, H. et al., Nationwide evaluation of potential flood damage reduction by riparian vegetation removal in Japan, *Journal of Japan Society of Civil Engineers*, Ser. G (Environmental Research), Vol. 79, No. 5 (2023), In press.
[5] Yanagihara, H. et al., Evaluation of flood adaptation and mitigation measure by the order of riparian vegetation removal, *Journal of Japan Society of Civil Engineers*, Special issue (Hydraulic Engineering), In press.

The 11th International Symposium on Water Environment Systems
----- with Perspective of Global Safety   (Nov. 16th ~ 17th , 2023)

GP-RSS & SyDE
Tohoku University

Optimal Selection and Bias Correction of Satellite Precipitation Datasets in the Data-Scarce Upper Indus Basin

○ Hira SATTAR[1*], Tsuyoshi KINOUCHI[1]

[1]Department of Transdisciplinary Engineering, Tokyo Institute of Technology, Yokohama 226-0026, Japan.
*E-mail: hira_sattar@hotmail.com

Abstract

Satellites and remote sensing have emerged as a crucial asset in hydrological investigations and estimation of river flows, particularly in regions with limited data availability. However, ensuring the accuracy of satellite instruments is challenging, especially in the snow-covered peaks of underdeveloped high-elevation mountain ranges. Additionally, disparate satellite products yield varying estimates for the same hydrological components, leading to the question of which product is best suited for a specific river basin. To address this, we propose a water balance closure technique using GRACE dual satellite data and various precipitation and evapotranspiration datasets for the Upper Indus basin (UIB). After comparing four precipitation and two evapotranspiration datasets, we identified the combination of TRMM precipitation and GLDAS evapotranspiration as having the lowest closure error. Subsequently, we applied bias correction using a proportional redistribution technique to assess errors in individual water balance components based on their proportional contributions to the overall water balance.

Keywords: water balance; satellite datasets; precipitation; evapotranspiration; Upper Indus Basin

1 Introduction

The Upper Indus basin holds significant importance in the management of regional water resources and environmental preservation in Pakistan. As a sub-basin of the Indus River, the flows from the UIB contribute to Pakistan's agricultural, industrial, and domestic water supply. The Indus River system relies heavily on runoff from snow and glacier melt from the UIB, accounting for over 50-80% of its total flow (Liu et al.,2017). The basin hosts more than 11,000 glaciers (ICIMOD, 2012), making it highly vulnerable to climate change. Avalanche-fed glaciers dominate the region, limiting measurements to a select few with extensive, high-altitude accumulation basins (Hewitt, 2011). This results in significant data scarcity in the basin.

Addressing this data scarcity, the utilization of satellite and remote sensing data emerges as a promising alternative for conducting hydrological investigations and assessing water resources. However, before undertaking any hydrological investigation, it is crucial to assess the satellite dataset's performance specific to the given river basin. While many researchers have cross-validated satellite precipitation data with observed gauge data to select the best satellite dataset, in the case of high-elevation, snow-fed basins like the Upper Indus basin, rain gauge measurements are known to potentially underestimate precipitation, especially snowfall (Sevruk, 1984; Baudouin et al., 2020).

In such circumstances, the utilization of the water balance closure technique becomes a reliable approach for selecting the most suitable dataset for the basin. This study aims to integrate the water balance technique with the GRACE terrestrial water balance estimates, satellite weather data, and observed discharge. The goal is to identify the optimal precipitation dataset for the Indus River basin and to apply necessary corrections to the satellite data.

2 Materials and methods

We use the water balance closure method to choose the most suitable precipitation and evapotranspiration dataset for the Upper Indus Basin during the period from 2011 to 2017. This method takes into account various water balance components, including precipitation, evapotranspiration, streamflow, and changes in terrestrial water storage. Among the datasets analyzed, we select those that result in the smallest water balance closure residue, denoted as "r." These chosen datasets are then applied in the following phases of our research. At the basin scale, the terrestrial water budget can be expressed as follows:

$$\Delta S = P - ET - Q \qquad (1)$$

where ΔS is the change of water storage averaged over the entire basin, P is precipitation, ET is evapotranspiration, Q is streamflow at the basin outlet.

The selected precipitation and evapotranspiration datasets are then corrected from their errors. In this study, the proportional redistribution technique is applied due to its simplicity and satisfactory results for the corrected values of P, ET, Q and ΔS (Abolafia-Rosenzweig et al., 2021). This technique redistributes the residual errors proportionally to the individual water budget components, thus achieving closure of the water budget. The method redistributes the residual error to each water budget component by adding respective errors (ε) (Eq. 4) to enforce the closure as follows:

$$P-ET-\Delta S-Q = r \neq 0 \qquad (3)$$

$$(P+\varepsilon_P)-(ET+\varepsilon_{ET})-(\Delta S+\varepsilon_{\Delta S})-(Q+\varepsilon_Q) = r' = 0 \qquad (4)$$

where ε represents the error associated with each water balance component with its respective subscript and r' represents the residual after the water budget is closed.

3 Results and discussion

3.1. Selection of best performing satellite data

The monthly rate of change in terrestrial water storage, obtained from GRACE satellite data, is compared to P-ET-Q (as per equation 1) to assess water balance closure. This comparison involves maintaining a constant value for ET in each analysis and comparing the results of equation 1 using all four precipitation datasets (as shown in Figure 1). The figure illustrates P (TRMM, IMERG, GPCP, & MERRA-2)-

The 11th International Symposium on Water Environment Systems
----- with Perspective of Global Safety   (Nov. 16th ~ 17th , 2023)

GP-RSS & SyDE
Tohoku University

ET (GLDAS) - Q (Observed). Similarly, the same analysis was conducted using P (TRMM, IMERG, IMERG & MERRA-2) - ET (MERRA-2) - Q (Observed).
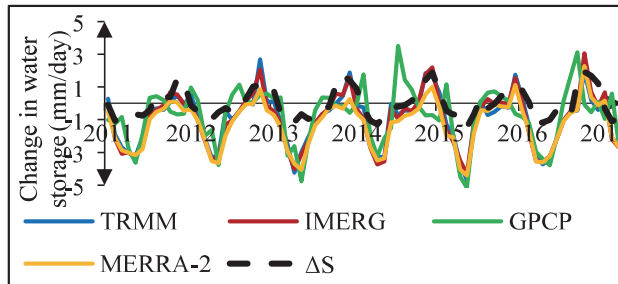

Fig. 1. Water balance closure of UIB using GLDAS evapotranspiration and four different precipitation datasets.

From the figure, it is evident that the TRMM and IMERG precipitation datasets yield significantly better results in terms of closure error and correlation compared to the other two datasets, with GPCP showing the weakest correlation.

Table 1 Performance comparison of four precipitation datasets using GLDAS and MERRA-2 evapotranspiration.

		Precipitation dataset			
		TRMM	IMERG	GPCP	MERRA-2
GLDAS	r	-0.82	-0.86	-0.61	-1.15
ET	R^2	0.81	0.84	0.45	0.81
MERRA	r	-0.72	-0.76	-0.51	-1.04
ET	R^2	0.81	0.84	0.43	0.82

A comparison of the closure error "r" and the coefficient of correlation "r2" for all 16 combinations of precipitation and evapotranspiration used in Equation 1 is presented in Table 1. In the case of the evapotranspiration datasets, GLDAS consistently produces better results than MERRA-2 for all precipitation datasets. For the subsequent steps in this study, TRMM and GLDAS are selected as the best performing datasets.

3.2. Error correction of datasets

The correction was applied to the selected datasets: TRMM for precipitation and GLDAS. The results are shown in Figure 2.
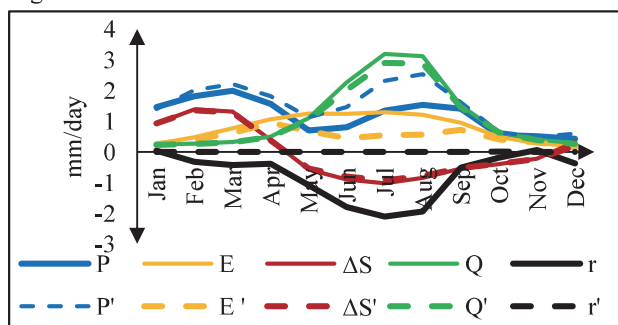

Fig. 2. Monthly water balance components from 2011 to 2017 before and after applying correction.

The figure displays the monthly values of the original water balance components P, ET, ΔS, Q, and the water balance residual (r) alongside their respective corrected counterparts P', ET', ΔS', Q', and r', following the application of the correction technique. Notably, a larger error in precipitation and evapotranspiration is evident during the summer months, coinciding with the wet season in the basin. Conversely, there is less error observed during the dry months, which occur from October to February. This seasonal variation in error levels suggests that satellite performance is influenced by changing weather conditions.

The corrected values for precipitation and evapotranspiration indicate that the satellites tend to underestimate precipitation while overestimating evapotranspiration. After the application of the correction, the maximum monthly water budget residual, previously at -2 mm/day in July, was significantly reduced, approaching near-zero levels.

4 Conclusions

In this study, we demonstrated the significance of satellite and remote sensing technology in hydrological investigations, especially in data scarce regions. We addressed the challenge of satellite data accuracy, particularly in high-elevation, snow-fed mountainous areas. Through a rigorous evaluation of various precipitation and evapotranspiration datasets, we identified the combination of TRMM precipitation and GLDAS evapotranspiration as the most suitable for UIB.

To enhance data accuracy further, we applied a bias correction technique based on proportional redistribution. This methodology allows us to assess and correct errors in individual water balance components, contributing to a more accurate overall water balance.

This research serves as a valuable step toward better understanding and managing water resources in the region, particularly in high-elevation, snow-fed basins like the Upper Indus basin where data scarcity remains a big problem. Ultimately, our efforts contribute to sustainable water resource management and environmental preservation in Pakistan.

Reference

[1] Liu, T., Tsuda, M., & Iwami, Y. (2017). A study on flood forecasting in the upper Indus basin considering snow and glacier meltwater. *Journal of Disaster Research*, 12(4), 793-805..

[2] ICIMOD (2012). Status of Glaciers in the Indus Basin.

[3] Hewitt, K. (2011). Glacier change, concentration, and elevation effects in the Karakoram Himalaya, Upper Indus Basin. *Mountain Research and Development*, 31(3), 188-200.

[4] Sevruk, B. (1984). International comparison of national precipitation gauges with a reference pit gauge. *WMO Instrument and Observing Methods Report, No. 17*, 111.

[5] Baudouin, J. P., Herzog, M., & Petrie, C. A. (2020). Cross-validating precipitation datasets in the Indus River basin. *Hydrology and Earth System Sciences*, 24(1), 427-450..

[6] Abolafia-Rosenzweig, R., Pan, M., Zeng, J. L., & Livneh, B. (2021). Remotely sensed ensembles of the terrestrial water budget over major global river basins: An assessment of three closure techniques. *Remote Sensing of Environment*, 252, 112191.

The 11th International Symposium on Water Environment Systems
----- with Perspective of Global Safety   (Nov. 16th ~ 17th , 2023)

GP-RSS & SyDE
Tohoku University

Maximizing Atmospheric River-induced precipitation in the Maipo River Basin, Chile

○ Yusuke Hiraga[1*] & Joaquin Meza[2]

[1]Department of Civil Engineering, Tohoku University, Sendai, Japan.
[2]Department of Civil Engineering, Universidad Técnica Federico Santa María, Valparaiso, Chile
*E-mail: yusuke.hiraga.c3@tohoku.ac.jp

Abstract

In Chile where extreme floods caused significant damages, Probable Maximum Precipitation (PMP) estimate is important for flood risk management. Conventionally, PMP has been estimated using the statistical approach in Chile due to its applicability for sparsely-gauged basins. However, for complex terrain such as Andes Mountain Range, the statistical method is not appropriate since it cannot deal with non-linear orographic effects and precipitation observations are usually not dense. Thus, there is an urgent need to improve the conventional PMP estimates over Chile. This study used the model-based PMP estimation approach to maximize the target historical precipitation over the Maipo River Basin, Chile. This study further deals with the recently raised questions on the model-based PMP estimation: (1) How can one estimate PMP with the range (not deterministically)? (2) How can one evaluate the frequency of the estimated PMP? This study attempts to answer the raised questions above and estimate maximum precipitation scenarios in the Maipo River Basin, Chile.

Keywords: Probable Maximum Precipitation (PMP); WRF model; Atmospheric Rivers.

1 Introduction

Flood disaster-related risk has increasingly become a global concern. Chile, located in South Ameica, is not an exception and has experienced several flood disasters in recent years. In February 2017, heavy rains struck central and northern Chile, causing landslides and flooding. This storm left three dead and 19 missing, according to the country's disaster agency. More recently, in January 2021, heavy rainfall associated with a zonal atmospheric river triggered disastrous flooding and landslides in the Maipo River Basin with severe social impacts and economic losses. Due to its significant impact on the society, there is an urgent need to improve flood management measures for Chile.

It is imperative to estimate design precipitation and floods to achieve flood control measures. Probable Maximum Precipitation (PMP) and Probable Maximum Flood (PMF) approaches are widely used for estimating design precipitation and floods. PMP is defined as the theoretical maximum precipitation for a given duration under possible meteorological conditions [1]. Several approaches have been proposed to rigorously estimate PMP, including the statistical approach [2], storm maximization approach [3], and numerical model-based approach [4,5]. Conventionally, PMP has been estimated using the statistical approach in Chile in practice. However, statistical approach has been challenged in various aspects. Koutsoyiannis (1999) [6] stated that the upper bound of precipitation cannot be estimated using the statistical approach as it fundamentally estimates precipitation with large return periods. Statistical approach is not appropriate for complex terrain since (1) precipitation observation is usually not available in complex terrains and (2) it is particularly challenging to reasonably estimate spatial distribution pattern based on the limited number of stations.

Numerical model-based approach maximizes precipitation depths by numerically solving the nonlinear governing equations of the regional atmospheric processes over the complex terrain. In recent years, numerical model-based approach has been drawing considerable attention due to its potential to overcome the major limitations in the traditional PMP estimation. Despite its benefits, none of previous works attempted to estimate PMP using numerical weather models for South America, harvoring the Andes Mountain Range. Thus, the objective of this study was to estimate maximum precipitation for the target storm events, using a numerical weather model. Furthermore, this study deals with the recently raised questions on the model-based PMP estimation: (1) How can one estimate PMP with the range (not deterministically)? (2) How can one evaluate the frequency of the estimated PMP?

2 Materials and methods

Figure 1 shows the shape and location of the Maipo River Basin (MRB), Chile. The MRB locates in the central Chile between latitudes 32°55' and 34°15' S with an area of 15,157 km². Four important topographic characters are Andes, Central Valley, Coast Range, and Coastal Plains in the basin. Atmospheric Rivers (ARs), long and narrow corridors of high
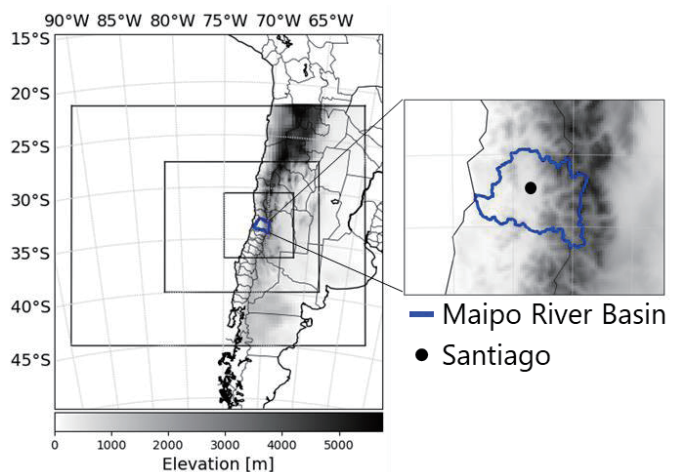

Fig. 1. Maipo River Basin and WRF model domains

The 11th International Symposium on Water Environment Systems
----- with Perspective of Global Safety   (Nov. 16th ~ 17th , 2023)

GP-RSS & SyDE
Tohoku University

moisture transport, is the dominant storm type on extreme precipitation in this region.

This study used the Weather Research and Forecasting (WRF) model to simulate and maximize the target 72-hr precipitation events. This study used the Climate Forecast System Reanalysis (CFSR) dataset as initial and boundary conditions of the WRF model. Figure 1 shows the 2-way nesting domain of the WRF model with the resolutions of 36km, 12km, and 4km.

This study first simulates the target 72-hr precipitation events with various combinations of physical parameters. Then, this study maximizes the simulated precipitation based on the moisture optimization method [5] and atmospheric boundary condition shifting (ABCS) method [5]. The moisture optimization method increases relative humidity at the modeling boundary as follows:

$$RH = \begin{cases} \min(\beta RH_0, 97\%), & \text{if } RH_0 < 97\% \\ RH_0, & \text{if } RH_0 \geq 97\% \end{cases} \quad (1)$$

where RH is the modified relative humidity (%), RH_0 is the initial relative humidity (%), and β is a unitless multiplier. The ABCS method geospatially shifts the atmospheric boundary conditions in latitudinal directions so that the moisture inflow can be transposed to where its contribution to the basin precipitation is maximized. This study computes the integrated water vapor transport (IVT) as follows:

$$IVT = \sqrt{\left(\frac{1}{g}\int_{1000}^{300} q\boldsymbol{u} \; dp\right)^2 + \left(\frac{1}{g}\int_{1000}^{300} q\boldsymbol{v} \; dp\right)^2} \quad (2)$$

where g is the gravitational acceleration, $\boldsymbol{u}$ and $\boldsymbol{v}$ is the horizontal wind vector determined by its meridional and zonal wind components, q is the specific humidity, and dp is the pressure difference between adjacent pressure levels.

3 Results and discussion

Figure 2 shows the precipitation maximization result for the target precipitation event (UTC 1200 12th June-UTC 1200 15th June, 2000). By combining the RHP method and ABCS method, one can generate ensemble patterns of the target precipitation, leading to the maximum estimate with its range as in Figure 2. The maximum precipitation depth (282.4 mm; 35.1 % increase from CTL) was obtained by shifting atmospheric boundary condition to 1.5 degree south and increasing RH with β=1.3. Figure 3 shows the spatial distributions of the differences in (a) IVT and (b) 72-hr precipitation between the maximum case and CTL case. Figure 3 shows that the maximization procedure increased the IVT over the basin in which the IVT field shows the corresponding change to 1.5 degree south shifting. As a result of the IVT increase over the entire basin, precipitation
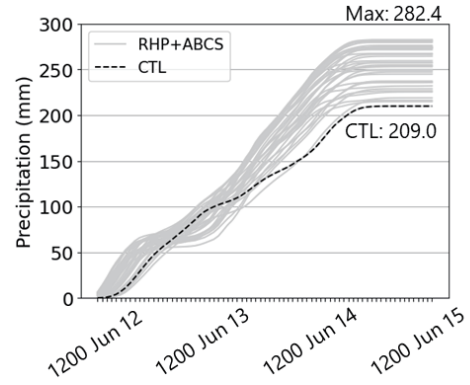

Fig. 2. Precipitation maximization by means of moisture optimization and ABCS methods

increased in most parts of the basin. Our further analysis shows that the time series of precipitation difference and IVT difference over the basin between the maximum case and CTL case were highly correlated each other: R^2=0.85 (p<0.01). This high significant relationship between IVT and precipitation is consistent with the previous studies on extreme precipitation mechanisms in Chile.

Although it is not presented here in this paper, the frequency of the maximum precipitation was estimated based on the long-term record of the basin-average IVT. Furthermore, the estimated maximum precipitation was compared to the conventional statistical method-based PMP values in the Maipo River Basin. Overall, this study is the first attempt to maximize historical precipitation using a numerical model-based approach in South America.

References

[1] WMO. 2009. Manual on estimation of Probable Maximum Precipitation (PMP), WMO-No. 1045.
[2] Hershfield, D.M. 1961. Estimating the probable maximum precipitation. J. Hydraul. Div. 87, 99–116.
[3] Hansen, E.M., Fenn, D.D., Corrigan, P., Vogel, J.L., Schreiner, L.C., Stodt, R.W. 1994. Probable maximum precipitation -Pacific Northwest states: Columbia River (including portions of Canada), Snake River and Pacific coastal drainages. NWS Hydrometeorological Rep. 57, 353.
[4] Ohara, N., Kavvas, M.L., Kure, S., Chen, Z., Jang, S., Tan, E. 2011. Physically based estimation of maximum precipitation over American River Watershed, California. J. Hydrol. Eng. 16, 351–361.
[5] Hiraga, Y., Iseri, Y., Warner, M.D., Frans, C.D., Duren, A.M., England, J.F., Kavvas, M.L. 2021. Estimation of Long-duration Maximum Precipitation during a winter season for large basins dominated by Atmospheric Rivers using a Numerical Weather Model. J. Hydrol. 598, 126224.
[6] Koutsoyiannis, D. 1999. A probabilistic view of Hershfield's method for estimating probable maximum precipitation. Water resources research, 35(4), 1313-1322.
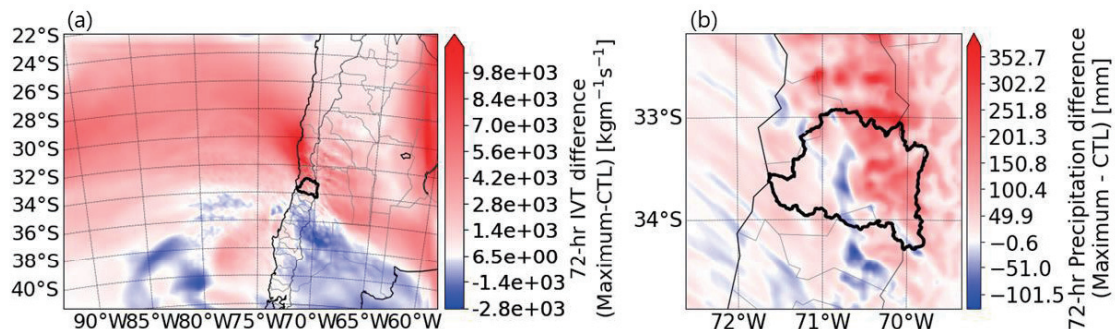
Fig. 3. Difference in (a) 72-hr IVT and (b) precipitation between the maximum case and CTL

The 11th International Symposium on Water Environment Systems
----- with Perspective of Global Safety   (Nov. 16th ~ 17th , 2023)

GP-RSS & SyDE
Tohoku University

Development of an edge computing-based sensory network to mitigate the impact of natural disasters in pond aquaculture

Hsiang-Hsuan LI[1], Tsun-HuaYANG[1*]

[1]Department of Civil Engineering, National Yang Ming Chiao Tung University, Hsinchu City, Taiwan.
*E-mail: tshyang@nycu.edu.tw

Abstract

Natural disasters have caused great damage to the inland fishing industry, which is most concentrated in the western coastal regions of Taiwan. This research proposed a combination of structural and non-structural measures to mitigate the impact of natural disasters on inland fisheries. First, this research focuses on the development of a temperature model for the temperature modeling of inland fishponds. Unlike other existing temperature models, ENFIM is designed to be embedded in a microcontroller unit (MCU). Second, a customized MCU sensor was developed and ENFIM was installed in the sensor to perform edge computing for temperature prediction. The user can get the information from the sensor locally and directly in a timely manner. Finally, fishermen in Taiwan usually pump warmer water from the underground to the fishpond to maintain the temperature. This is a problem for a region known for its severe land subsidence. Therefore, it is proposed to grow fish in greenhouses. It will not only mitigate the effects of low temperature, but also reduce operating costs. This research is still in progress and hopefully the result can benefit Taiwan's aquaculture and fisheries and help them mitigate the impact of extreme weather events in the future.

Keywords: temperature model; aquaculture; edge computing; sensor; greenhouse.

1 Introduction

Climate change has been linked to an increase in the frequency of natural disasters such as floods and cold snaps, which have caused inconvenience to residents and damage to property and infrastructure in Taiwan's coastal regions. According to Fisheries Agency, Ministry of Agriculture, Taiwan[1], the annual production value of inland fisheries in Taiwan is 336 billion NTD in 2019, which is the most among distant, offshore, and inland fisheries. Natural disasters have caused tremendous damage to the fisheries industry. For example, the loss of aquaculture and fisheries in Chiayi County was 460 million NTD due to a flood event on August 23, 2018. Another damage caused by a cold current in January 2016 in Taiwan was estimated at 2.19 billion NTD. The same problems are plaguing other countries all over the world. For example, 84.5% of the damage to the fishing industry in the United States was due to natural disasters [2]. Extreme weather events will become more frequent in the future, according to the latest prediction report [3] and the economic losses to fisheries from natural disasters are also expected to increase. In order to enhance the adaptability of the fisheries industry to extreme weather conditions, the Taiwanese government has made efforts to promote "Intelligent Fisheries 4.0" to ensure the sustainability and social benefits of Taiwan's aquaculture industry and to achieve the United Nations' goals of a sustainable society and coexistence with disasters [4]. However, researches related to "Intelligent Fisheries 4.0" focus on aquaculture water quality and process automation. There is no research on the integration of weather forecasting information and sensors to mitigate the impacts of natural disaster.

This study developed an **E**nergy balance based **FI**shpond **M**odel (ENFIM), which can be installed in sensors, through the assumption of heat energy conservation, and then customized a sensor with the capability of edge computing, which can collect environmental information such as water temperature and water depth. The combination of the sensor and ENFIM not only provides monitoring information, but also actively simulates the future changes of water temperature and water level in the fish pond when weather forecast data is available. Many studies have focused on the development of fishpond temperature models [5, [6]. Recently, the application of Internet of Things (IoT) has attracted much attentions, and many studies have implemented it in the monitoring of water quality in fishpond [7, 8, 9]. Looking at many studies, there are no studies that have developed on-board water temperature models for sensors that can perform edge computing in the fishpond. Furthermore, if the temperature model is embedded in the sensor, a detailed investigation must be performed due to limited computing power. Finally. Zhu et al. [10] showed that the application of greenhouse can maintain fishpond temperature. Hessberg and Alberto [11] confirmed that the greenhouse like plastic sheet can not only maintain temperature in fishpond but also prevent predation from birds. In Taiwan, greenhouse is commonly used in Farming of shellfish. This study proposed the application of greenhouse to mitigate the impact of natural disasters with the advantages of environmental friendliness and low operating cost. In addition, because monitoring and forecasting information is available locally, fishermen can take mitigation measures with more lead time, and the efficiency of the greenhouse is expected to improve.

2 Materials and methods

This study assumed that the temperature in a fishpond is completely fixed and a thermal energy conservation equation is listed as Eq. 1.

The 11th International Symposium on Water Environment Systems
----- with Perspective of Global Safety   (Nov. 16th~17th, 2023)

GP-RSS & SyDE
Tohoku University

$$\frac{dE}{dt} = q_{solar} - q_{back} + q_{sky} - q_{evap} + q_{rain} \mp q_{conv} \mp q_{soil} \mp q_{other} \qquad \text{Eq. 1}$$

E is the total amount of heat energy at any time t, and q_{solar} is the solar radiation, q_{back} is the radiant heat from the pond, qsky is the long-wave radiation from the sky, q_{evap} is the pond evaporation, and q_{conv} is the air convection. Others such as q_{rain}, q_{soil} represent the energy from rainfall and soil respectively, while q_{other} is the source or sink of other heat sources. Assuming that the total thermal energy of the fishpond is as Eq. 2, where ρ is the density of the water, while V is the volume of the water in the fishpond, C_p is the specific heat of the water, and T is the temperature of the water.

$$E_{pond} = \rho V C_p T \qquad \text{Eq. 2}$$

These equations can be differentiated and T at $t + \Delta t$ is solved using the 4th order Runge-Kutta method.

3 Results and discussion

An experiment was conducted to test the model performance on the roof of Engineering Building II on the NYCU campus (Fig. 1). Preliminary results are shown in Figures 2 and 3. Overall, the trend of temperature variation for cases with and without greenhouse can be simulated. The RMSEs are 1.29, 1.83, and 1.14, respectively.
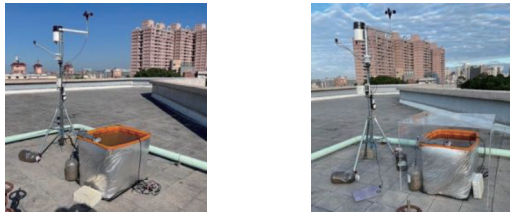

Fig. 1. Experimental setup with (left) and without (right) greenhouse on the roof of Engineering Building II on the NYCU campus
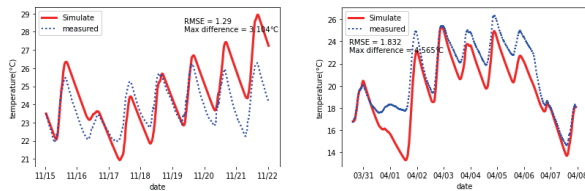

Fig. 2 Comparison of simulated results and observations for the period from November 15 to November 22, 2022 (left) and for the period from March 31 to April 8, 2023 (right).

The effect of greenhouse is significant in Fig. 3, There is a 5 degree difference in temperature in both experiments. The model successfully simulated the difference of temperature in the pond by neglecting the q_{conv} and q_{evap} terms.
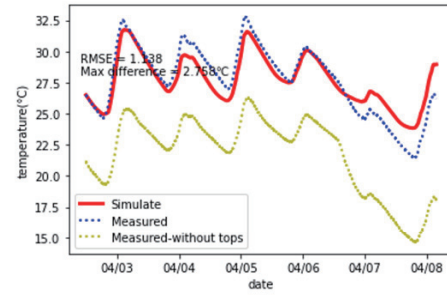

Fig. 3 Comparison of greenhouse simulated results and observations for the period from April 3 to April 8, 2023

4 Conclusions

The preliminary results have shown the potential of ENFIM for temperature modeling in fish ponds. However, further studies in a real fishpond and under different weather conditions need to be conducted to confirm the further performance of ENFIM in the future.

Reference

[1]   Fisheries Agency, Ministry of Agriculture, Long-term Development Strategy for Fisheries Policy Report, 2022.

[2]   The Natural Conservancy, Extreme Climate Events Threaten US Fisheries, Fishermen, and Coastal Communities, 2021.

[3]   Chow, Winston, et al. IPCC Sixth Assessment Report (AR6): Climate Change 2022-Impacts, Adaptation and Vulnerability: Factsheet Human Settlements. 2022.

[4]   United Nations. The UN Sustainable Development Goals. United Nations, New York, 2015. Available at (accessed 05 October 2023): https://sdgs.un.org/goals.

[5]   Klemetson, S. L., Rogers, G. L., Aquaculture Pond Temperature Modeling, Aquacultural Engineering, 4(3), 191-208., 1985.

[6]   Lamoureux, J, Heat Transfer in Outdoor Aquaculture Ponds. Louisiana State University and Agricultural & Mechanical College, 2003.

[7]   Fastie, C., Vernal Pool Data Logging. Available at (accessed 05 October 2023): http://fastie.net/vernal-pool-logger/.

[8]   Abinaya, T., Ishwarya, J., Maheswari, M., A novel methodology for monitoring and controlling of water quality in aquaculture using Internet of Things (IoT). In 2019 International Conference on Computer Communication and Informatics (ICCCI) (pp. 1-4). IEEE, 2019, January.

[9]   Teja, K. B. R., Monika, M., Chandravathi, C., Kodali, P., Smart Monitoring System for Pond Management and Automation in Aquaculture. In 2020 International Conference on Communication and Signal Processing (ICCSP) (pp. 204-208). IEEE., 2020, July

[10]   Zhu, S., Deltour, J., Wang, S., Modeling the thermal characteristics of greenhouse pond systems. Aqua cultural Engineering. 18: 201-217, 1998.

[11]   Hessberg, H., Alberto. C., Evaluation of greenhouses in fish production. 20. 124-137, 2016.

The 11th International Symposium on Water Environment Systems
----- with Perspective of Global Safety   (Nov. 16th ~ 17th , 2023)

GP-RSS & SyDE
Tohoku University

Peak flow reduction by the upstream inundation and afforestation in small rivers

○ Yuki INOSHITA[1*], So KAZAMA[1]

[1]Department of Civil Engineering, Environmental Tohoku University, Miyagi 980-8579, Japan.
*E-mail: yuki.inoshita.q6@dc.tohoku.ac.jp.

Abstract

This study quantitatively evaluated the impact of population decline on stream flows in three small and medium-sized river basins in the Tohoku region by conducting runoff and inundation analyses, assuming changes in land use and channel conditions in response to the progressive stages of population decline. The results showed that the annual maximum flow decreased by 6.85% in the Sukawa River and by 6.59% in the Ootani River when land use was changed. The reduction of the annual maximum flow decreases the flood risk and reduces the damage downstream. Drought flow increased by 1.25% in the Sugawa River and by 6.57% in the Ootani River. The findings of this study will contribute to future river management planning in small and medium-sized river basins where population decline is significant.
.

Keywords: depopulation, runoff analysis, distributed runoff model, land-use

1 Introduction

In recent years, Japan has experienced heavy rainfall disasters every year, and it is expected that flood damage will become more severe and more frequent in the future. In addition, tax revenues are decreasing in rural areas due to population decline, making it difficult to maintain and manage infrastructure facilities. In the future, river management is expected to be forced to cope with severe disasters while reducing costs. In small and medium-sized rivers with rapidly declining populations, it may be necessary in the future not to manage them. There have been no studies on runoff analysis considering population decline, and changes in hydrological processes due to population decline are still unknown. Population decline promotes land use change, such as the abandonment of fields and settlements, and vegetation change due to the abandonment of forests. *Chiba and Kazama*[1]) evaluated changes in the flow of small and medium-sized rivers due to land use change, taking into account differences in roughness, evapotranspiration, and infiltration rates by land use. The results showed that forestation and inducement of inundation in uninhabited watersheds promote the reduction of flood risk downstream.

However, the study did not take into account past land-use changes and the uncertainty of flow fluctuation due to such changes. Therefore, this study statistically analyzed past and present land use change trends in uninhabited areas and small- and medium-sized river basins, and evaluated flow fluctuations due to the associated changes in the river basins. The impact of population decline was quantitatively evaluated by conducting runoff and inundation analyses, changing the predicted use and channel change, respectively, to correspond to the progressive stages of population decline.

2 Materials and methods

2.1 Region and Materials

The target watersheds are the upper reaches of the Sukawa River flowing through Kaminoyama City, Yamagata Prefecture, and the Dangosawa and Ohtani River watersheds

Fig.1.Dataset

Data	References
Temperature, Snow Depth, Wind Speed, Sunshine Duration	Sukawa : Yamagata AMeDAS Observatory Ohtani River, Dangosawa : National Institute for Environmental Studies
Elevation	Basic map information
River, Land Use	National Land Value Information

flowing into the Tadami River through Mishima Town, Fukushima Prefecture. The Dangosawa watershed is a rare watershed where the National Research Institute has observed the flow of the Dangosawa River despite the fact that it has no population. The watershed area is approximately 72.6 km² in Sukawa, 48.6 km² in Ohtani River, and 3.1 km² in Dangosawa.

The period covered was from July 1, 2019 to June 30, 2020. The data used in the analysis are shown in Table 1. The analysis was conducted using a mesh size of 100 m × 100 m.

2.2 Methods

The distributed runoff model was estimated using the continuity equation and Manning's equation for direct runoff and river runoff, and the storage function method for baseflow, following Chiba and Kazama[1]) .

$$\partial A/\partial t + \partial Q/\partial x = (R + SM - R_{in} - E)B_m \quad (1)$$

$$Q = \frac{1}{n} A^{5/3} I^{1/2} S^{-2/3} \quad (2)$$

$$R_{in} = k_{in} \times h \quad (3)$$

$$\partial s/\partial t = R_{in} - q_b \quad (4)$$

$$s = k_s q_b^{p_s} \quad (5)$$

where A is cross-sectional area (m²), Q is flow rate (m³/s), t is time (s), x is distance in the direction of flow (m), R is rainfall (m/s), SM is snow melt (m/s), R_{in} is infiltration (m/s),

The 11th International Symposium on Water Environment Systems
----- with Perspective of Global Safety   (Nov. 16th ~ 17th , 2023)

GP-RSS & SyDE
Tohoku University

E is evapotranspiration (m/s), Bm is mesh width (m), n is Manning's roughness coefficient (s/m$^{1/3}$), I is the riverbed gradient, S is the wetted area (m), kin is the model constant (/s), h is the water depth (m), s is the apparent storage height (m), qb is the runoff velocity in the soil (m/s), ks and ps are model constants. As in Chiba-Kazama, the model constants were set as $kin=9.0\times10^{-5}$/s, $ks=100$, $ps=0.3$ for the Dangosawa and Ohtani River watersheds, and $kin=4.8\times10^{-4}$/s, $ks=80$, $ps=0.5$ for the Sukawa River watershed.

The situation of overgrowth of vegetation due to inadequate river management was represented by the occurrence of inundation in the river channel. Based on the relationship between the channel water level and the floodplain water level, the amount of runoff due to inundation and the amount returning to the river channel were determined using the overflow formula following *Takeda et al.*[2] .

$$Q_o = 0.35 B_m \times |h_d| \sqrt{2g|h_d|} \qquad (6)$$

$$h_d = h_f + h_o - h \qquad (7)$$

where Qo: overflow rate (m^3/s), hd: overflow depth (m), hf: floodplain depth (m), ho: flooding depth (m).

3 Results and discussion

3.1 Results and discussion

When the population reaches zero, the land use of the watershed is assumed to gradually decline and eventually change to forest. The analysis was conducted assuming that all land use is converted to forest and that the river channel is covered with vegetation. The vegetated channel was represented by increasing the channel roughness from 0.030 s/m$^{1/3}$ to 0.100 s/m$^{1/3}$. The annual maximum and low flows of the current land use and the land use with the entire area forested were examined.

The annual maximum flows decreased by 6.85% in the Sukawa River and by 6.59% in the Ootani River when land use was varied. The reduction of the annual maximum flow decreases the flood risk and reduces the damage downstream. Drought flow increased by 1.25% in the Sukawa River and by 6.57% in the Ootani River. The increase in drought flow leads to a stable supply of water resources. On the other hand, the annual maximum flow in the Dangosawa increased by 3.34% and the drought flow decreased by 18.0%. Flooding occurred in the Sukawa and Ohtani Rivers, but not in the Dangosawa stream.

When all land use is converted to forest, flood risk is reduced and water resources are stabilized in the two watersheds where the population is expected to decrease. On the other hand, in the Dangosawa watershed, flood risk increased and water resources became unstable. The current land use in the Sukawa and Ohtani River watersheds has a population of only a few hundred people, and land uses such as building sites exist. Compared to forests, these land uses have a low storage function and precipitation runs off quickly. The change to forest land use increases the storage function and suppresses runoff. Therefore, the annual maximum flows in the Sukawa and Ohtani Rivers are considered to have decreased and the flood risk is considered to have decreased. On the other hand, Hanawa-Kozawa, with a population of zero, has only forests, rice fields and other agricultural land. Rice fields have a higher storage function than forests, and converting rice fields to forests would amplify runoff. Therefore, it is assumed that the annual maximum flow in
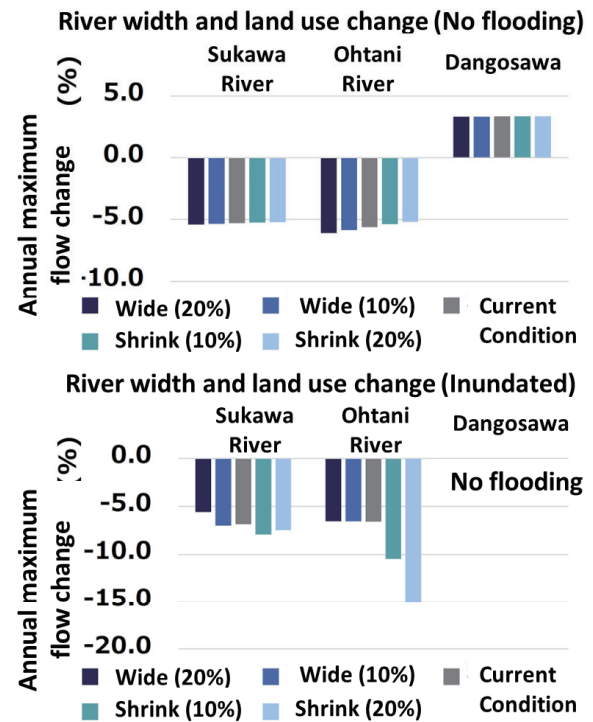

Fig.2. Comparison of annual maximum flow change

the Dangosawa stream is increased and the flood risk is increased.

3.2 Results and discussion

Abandonment of river management encourages bank failure and overgrowth of vegetation. In addition to the assumptions made in the previous section, we assumed river widening/reduction, revetment cut-off, and changes in channel roughness. Figure 1 shows the results of the comparison of annual maximum flow change due to river width and land use change. When inundation is not taken into account, the decrease in the annual maximum flow rate becomes smaller as the river width decreases. When inundation is taken into account, the decrease in annual maximum flow increases as the river width decreases. This is because the reduction in river width promotes inundation and increases the amount of water stored in the floodplain. In addition, it was shown that revetment cutbacks and increased channel roughness reduce peak discharge downstream when inundation is taken into account. Channel alteration due to abandonment of river management promotes the occurrence of inundation. The perception of uninhabited small and medium-sized river basins as flood plains and their frequent inundation may lead to the control of downstream flood risk.

4. References

[1] Chiba.,K. and Kazama, S.:As sessment of changes in the flow of small river basins due to depopulation using a distributed runoff model, JSCE, B1, Vol78, No2, pp535-540, 2022.

[2] Takeda, M. and Uetsuka, T. and Inoue, K. and Toda, K. and Hayashi, H.: Numerical analysis of overland flood flow due to storm surge in an urban area, Annuals, Disas. Prev. Res. Inst.,Kyoto Univ., No. 39 B-2, 1996.

The 11th International Symposium on Water Environment Systems
----- with Perspective of Global Safety   (Nov. 16th ∼ 17th , 2023)

GP-RSS & SyDE
Tohoku University

An initial assessment of mobile LiDAR scanning for river topographic survey

○ Mio Ishikawa[1]*, Keisuke ONO[1], Toru NEMOTO[2], Naotsugu YAMAMOTO[2],

Kohei TAKEMURA[2],Yasutaka KOUSAKA[2]

[1]Department of Civil Engineering and Management, Tohoku Institute of Technology,
Miyagi 982-8577, Japan.
[2]CTI Engineering Co., Ltd., Miyagi 980-0811, Japan.
*E-mail: s2014105@st.tohtech.ac.jp

Abstract

Reliable inland flood simulation demands accurate cross section data of canals. However, acquisition of cross section data of small canal requires field measurement and takes tremendous amount of effort especially for a large watershed. As an initial assessment, this study conducted 3D scanning with viDoc RTK rover in Zaru river in Sendai, Miyagi, and evaluated its applicability for river cross section survey. The result showed that elevation derived from LiDAR measurement was closed to that of official elevation data, suggesting that the proposed 3D scanning method was applicable even in river cross section survey.

Keywords: river cross section survey; LiDAR; inland flood inundation

1 Introduction

In a changing climate, floods are becoming more frequent throughout the world. In Japan, serious floods are causing inundation damage almost every year and inland flood is critical especially in city areas. As a non-structural countermeasure against inland flood, Japanese river administrators, such as the Ministry of Land, Infrastructure, Transport and Tourism (MLIT), and municipal governments, designate potential areas of inland flood inundation as "inland flood inundation areas".

Small canals or streams plays an important role to simulate inland flood in the watershed since significant amount of water pass through the water path. Therefore, reliable inland flood simulation demands accurate cross section data of canals. However, cross section data of small canals are rarely measured and archived, and acquisition of the cross section data requires field measurement and takes tremendous amount of effort especially for a large watershed.

Recently, several affordable mobile LiDAR scanning devices became available in consumer market. Some of them use the LiDAR sensor of iPhone Pro or iPad Pro, which popularize the 3D scanning due to its affordable price and its handy application in a smartphone platform. Commercial LiDAR solutions like the viDoc RTK rover become attractive to engineers as they promise absolute centimeter-level accuracy, removing the need for heavyweight GNSS rovers to conduct GCP measurements [1].

These state-of-the-art scanning technologies has a potential to be applied into topographic survey such as cross section survey of canals. However, further assessment of such solutions would be needed, especially in situations where target area is large and includes water surface. As an initial assessment, this study conducted 3D scanning with viDoc RTK rover in Zaru river in Sendai, Miyagi, and evaluated its applicability for river cross section survey.

2 Materials and methods

(1) Study area

The study area is Zaru river in Sendai, Miyagi. The river cross section survey was conducted in the location of 0.8km and 1.0km upstream of the conjunction with Natori river. Figure 1 is an overview of study area.

(2) Scanning method

As a scanning device we used iPad Pro 11inch coupled with a group of PIX4D applications. It delivers the absolute centimeter-level accuracy of photogrammetry deliverables achieved by using the viDoc RTK rover synchronized with the mobile image acquisition software: Pix4Dcatch. RTK (Real-Time Kinematic) is a technique used to increase the accuracy of GNSS positions using a fixed base station, that wirelessly sends out correctional data to a moving receiver. GNSS refers to a constellation of satellites providing signals from space that transmits position and timing data. The receivers then use this data to determine their location. An RTK technique requires two receivers: A stationary "base
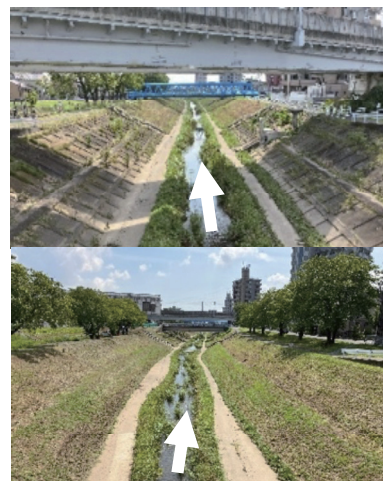

Fig. 1. Study area of river cross section survey
(Top: 0.8km, Bottom: 1.0km)

The 11th International Symposium on Water Environment Systems
----- with Perspective of Global Safety   (Nov. 16th ~ 17th , 2023)

GP-RSS & SyDE
Tohoku University

station" with a known location, and a mobile "rover". The communication between the base station and the rover is carried out through an NTRIP service. An NTRIP service is used in areas with strong 3G/LTE cellular coverage and a vast network of NTRIP mount points nearby.

(3) Post-processing of data

After the field survey with PIX4Dcatch and PIX4D viDoc RTK rover, data was exported to post-processing in PIX4Dmatic and then PIX4Dsurvey. PIX4Dmatic is a software optimized for accurate and fast photogrammetric processing for large scale, corridor, and terrestrial projects. It is designed to handle and process thousands of images with ease while maintaining survey-grade accuracy, coupled with Pix4D catch and viDoc RTK rover. PIX4Dsurvey is a software combining power of images and point clouds to extract key elements from photogrammetry, laser scanning or LiDAR data. It is often used to filter objects from point cloud data, such as vegetation, and generate accurate digital terrain models (DTM).

(4) Validation data

Field measurement of river cross section survey was provided by the Ministry of Land, Infrastructure, Transport and Tourism (MLIT) [2]. This is one of the official topographic data of river derived by leveling survey in the field.

3 Results and discussion

(1) Point cloud data with filtering vegetation

Original data generated by PIX4Dmatic provides point cloud data of surface of target objects which includes surface of ground as well as vegetation on the riverbank. Therefore, filtering function is applied in PIX4Dsurvey to remove the noise of vegetation. After removal of vegetation, digital terrain model (DTM) was developed. Figure 2 depicts the effect of filtering of the noise due to vegetation. The points in blue color were removed by the filtering with a threshold value of 0.2m. Figure 3 shows the point cloud data after the filtering of vegetation.

(2) Extraction of river cross section

River cross section was extracted from digital terrain model (DTM) generated by the filtered point cloud at the location of 0.8km and 1.0km, then compared with field measurement of MLIT. Figure 4 shows the comparison of river cross section. The graph shows that elevation derived from LiDAR measurement is closed to that of official elevation data, suggesting that the proposed 3D scanning method is applicable even in river cross section survey in this size of river. At the location of 0.8km, lowest elevation in the cross section were 7.57m in official data, 7.96m in LiDAR measurement after filtering. At the location of 1.0km, lowest elevation in the cross section were 9.04m in official data, 8.72m in LiDAR measurement after filtering. The lowest elevation derived LiDAR measurement is consistently higher than that of official data since LiDAR cannot go through the water surface and cannot capture the bathymetry under the water.

4 Conclusions

As an initial assessment, this study conducted 3D scanning with viDoc RTK rover in Zaru river in Sendai, Miyagi, and evaluated its applicability for river cross section survey. The
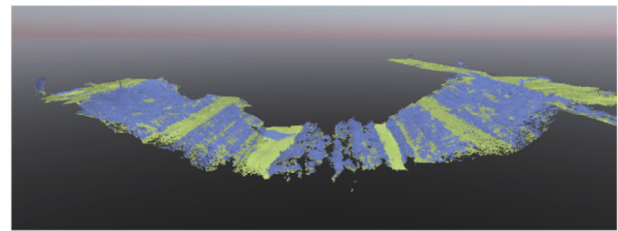

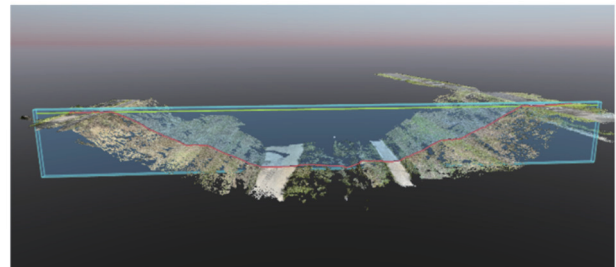**Fig. 2. Image of filtering vegetation from point cloud data in PIX4Dsurvey**

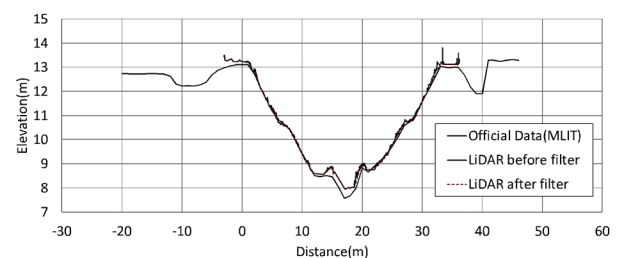**Fig. 3. Image of extraction of cross section from filtered point cloud data in PIX4Dsurvey**

Fig. 4a. comparison of river cross section at 0.8km
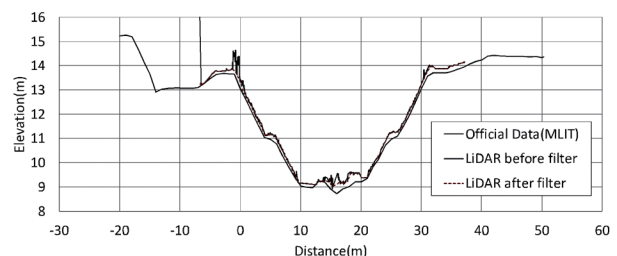

Fig. 4b. comparison of river cross section at 1.0km

result showed that elevation derived from LiDAR measurement was closed to that of official elevation data, suggesting that the proposed 3D scanning method was applicable even in river cross section survey.

Reference

[1] Yuen, R. Z. M., Boehm, J. (2022), Potential of consumer-grade cameras and photogrammetric guidelines for subsurface utility mapping, ISPRS TC II 7th International Workshop LowCost 3D - Sensors, Algorithms, Applications, p. 243–250.

[2] Ministry of Land, Infrastructure, Transport and Tourism, Annual river cross-section survey data of fiscal year 2022.

The 11th International Symposium on Water Environment Systems
----- with Perspective of Global Safety   (Nov. 16th ~ 17th , 2023)

GP-RSS & SyDE
Tohoku University

Estimation and analysis of population in river spaces using mobile spatial statistics data

Kazuya Ito[1*], Yusuke Hiraga So Kazama

[1]Department of Civil and Environmental Engineering, Tohoku University, Miyagi 980-8579, Japan.
*E-mail: kazuya.ito.s7@dc.tohoku.ac.jp.

Abstract

This study aims to understand the demographic dynamics of river space use using mobile spatial statistics, and examines a method for estimating the river space use population from mobile spatial statistics data, and analyzes the factors of the estimated use population. The proposed method for estimating the river population using river space obtained values for 41.6% of the target rivers that were 1 to 5 times higher than those obtained from the survey of river space use. Hourly analysis of population dynamics at the time of flood damage in the doumeki district of Yamagata Prefecture, which suffered flood damage in 2020 and 2022, showed that the population concentrated between the time of the flood warning and the peak flood level in both years. Furthermore, it was confirmed that the number of population at the time of the issuance of the flood warning in 2022 was smaller than that in 2020. This suggests that the residents' evacuation awareness may have increased as a result of past disaster experiences.

Keywords: Mobile spatial statistics, demographics, component analysis

1 Introduction

In order to realize good conservation and maintenance of river space, it is important to understand the actual status of river space utilization in detail. For this purpose, the Ministry of Land, Infrastructure, Transport and Tourism conducts a survey on the actual status of river space use in first-class rivers in Japan approximately once every three years (once every five years from 2010) to determine the population using river space. However, the survey is of limited use due to the following problems: the number of people using the river space can only be obtained every few years and for each season; the number of people using the river space as a whole is estimated based on the number of people at a limited number of survey points along the river space; and the survey is very costly to conduct. On the other hand, mobile spatial statistical data is currently available for all of Japan, with a spatial resolution of 500 meters and an estimated number of people per hour. In recent years, studies utilizing mobile spatial statistics have been conducted in various fields, such as evacuation behavior analysis during disasters[1] and in combination with person-trip surveys[2]. However, there are few cases in which mobile spatial statistics have been utilized in river space. The purpose of this study is to estimate the population using river space using mobile spatial statistics, and to clarify the actual conditions of river use through component analysis of the estimated population.

2 Materials and methods

2.1   Target Area

In this study, a total of 12 first-class rivers in the Tohoku region: the Iwaki, Takase, Mabuchi, Kitakami, Naruse, Natori, Abukuma, Yondai, Omono, Koyoshi, Mogami, and Akagawa Rivers were included. Of the meshes bordering each river system, those with a river channel area greater than 50% of the mesh area were selected, and the average population of these meshes was used as the target population. The period covered was from January 1, 2019 to December 31, 2022.

3 Methods

3.1   Methods for estimating the population using river space

First, the annual average population of the target mesh from 22:00 to midnight is assumed to be the permanent population of the mesh, and the permanent population is subtracted from the estimated population for each hour to obtain the hourly current population of the target mesh. The riverine population is then multiplied by the ratio of the area of the river channel to the area of the target mesh to estimate the riverine population using the river. When converting the hourly riverine population into a daily population, the daily riverine population was calculated for each two-hour period between 7:00 and 18:00 (7:00, 9:00, 11:00, ...). This is due to the fact that the river space use survey is conducted from sunrise to sunset, and the average stay time of river users is assumed to be 2 hours. Equations (1) and (2) summarize the above estimation method.

$$P_p = {}^1\!/\!_{365} \sum_{d=1}^{365}(P_{d,22} + P_{d,23} + P_{d,24})/3 \qquad (1)$$

$$P_d = \sum_{h=1}^{24}\left(P_{d,h} - P_p\right) \times R \qquad (2)$$

$$\text{Est} = \sum_{d=1}^{365} P_d \qquad (3)$$

where $P_{d,h}$: population at day d, time h (persons), P_p: annual average permanent population of the target mesh (persons), P_d: estimated user population (persons), R: ratio of river channel area to total area of the target mesh, Est: annual river space user population (persons), U: annual number of river users from the river use survey (persons); however, when $(P_{d,h} - P_p)$ is negative in (2), it is calculated as 0.

3.2   Demographic Analysis of Disasters

In order to analyze the population dynamics around a river during a disaster, three cells in the doumeki district of Yamagata Prefecture were analyzed hourly during the flooding of the Mogami River in 2020 and 2022. The three

The 11th International Symposium on Water Environment Systems
----- with Perspective of Global Safety   (Nov. 16th ～ 17th , 2023)
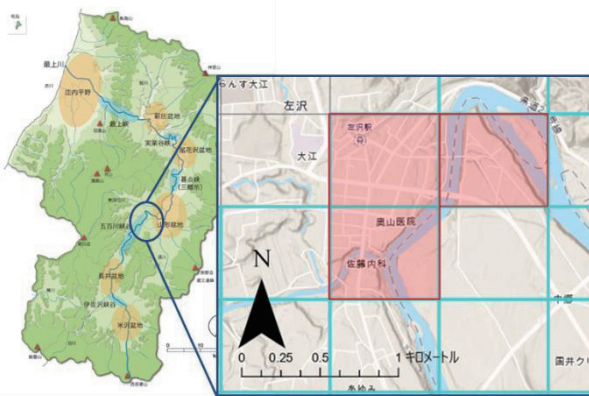
GP-RSS & SyDE
Tohoku University

Figure 1 Target mesh for the doumeki area

selected cells are all adjacent to each other and were severely flooded in 2022. The analysis period was five days before and after the disaster in both years. The analysis focused on the time periods when flood warnings were issued and peak flood levels were reached, and the changes in the water level of the population in the two years were compared.

4 Results and discussion

4.1   Estimation of population using river space

Figure 2 shows the results of the population use estimation. Figure 2 compares the estimated population of annual river space users based on the mobile space statistics in this study with the values obtained from the survey on river space use. The results of Ito et al.'s analysis, in which the target mesh was limited to four cells around the sea, are also displayed in the graph. As shown in Figure 2, the estimated values obtained by this study's method were in the range of 1 to 5 times those of the river space use survey in 5 of the 12 target rivers, obtaining estimates of the same order of magnitude. However, in other rivers, there were cases where the estimated values deviated significantly from the actual river space use survey (Kitakami River). However, in some rivers, such as the Aka River, the mesh was expanded from 4 meshes to the entire river basin, and the estimated values were closer to those of the river space utilization survey. However, the values are still overestimated compared to the values from the survey of river space use, and further correction is considered necessary.

4.2   Demographic Analysis of Disasters

Figures 3 and 4 show the population dynamics of the target mesh in the doumeki area during the Mogami River inundation in fiscal 2020 and 2022, respectively. Figures 3 and 4 summarize the hourly population movements during the inundation for a total of five days (two days before and after the inundation). These results show that the number of people in the former year was smaller than that in the latter year when the flood warning was issued. This is presumably due to the fact that fewer people approach rivers during floods, based on the past experience of flood damage in 2020. Furthermore, in both years, the population increased from the time the flood warning was issued, with the maximum population recorded at the time of the peak flood level. This may be due to the fact that local residents who were alerted
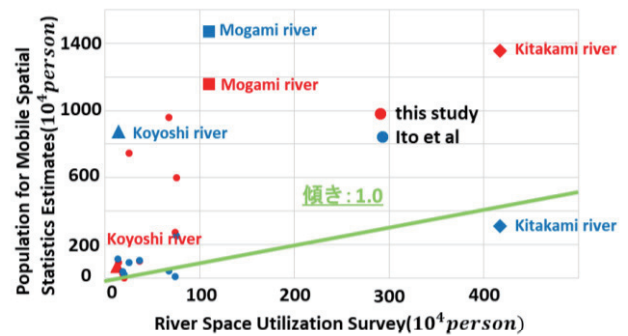

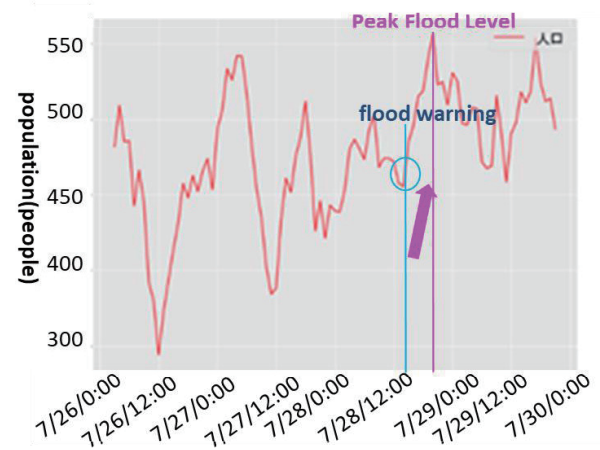Figure 2 Comparison results of estimated values

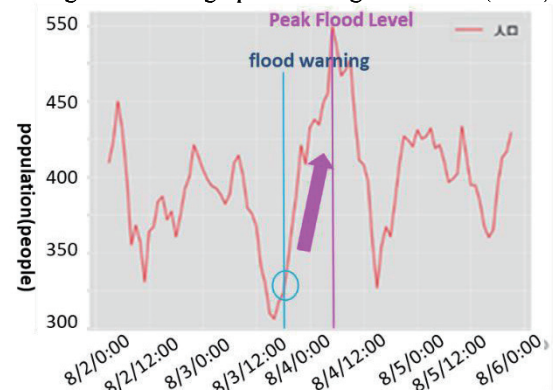Figure 3: Demographics during inundation (2020)

Figure 4: Demographics during inundation (2022)

to the danger by the flood warnings evacuated to evacuation centers and fire brigades were dispatched to rescue people. These results suggest that it may be possible to confirm the demographic situation at the time of a disaster using cell phone location data, and to quantify the impact of past disaster experiences on the demographic situation.

Reference

[1] Fuminori Sato, Makoto Rikiishi, Akimasa Fujiwara: Independent component analysis of recovery and reconstruction processes using mobile spatial statistics: the case of the August 2014 Hiroshima landslide disaster, Proceedings of the 55th Annual Conference on Civil Engineering Planning.

[2] Atsushi K. Morio et al.: Comparative Analysis of Mobile Spatial Statistics and Person Trip Surveys in the Tokyo Metropolitan Area: Toward Application to the Urban Transportation Field, 52nd Annual Conference on Civil Engineering and Planning, Proceedings

The 11th International Symposium on Water Environment Systems ----- with Perspective of Global Safety   (Nov. 16th ~ 17th , 2023)

GP-RSS & SyDE
Tohoku University

Flood Susceptibility Mapping Using Explainable Machine Learning Models

◯ Kumudu Madhawa KURUGAMA[1*], So KAZAMA[1] , Yusuke HIRAGA[1] & Chaminda SAMARASURIYA[2]

[1]Department of Civil and Environmental Engineering, Tohoku University, Miyagi 980-8579, Japan.
[2] Department of Earth Resources Engineering, University of Moratuwa, Katubedda 10400, Sri Lanka
*E-mail: kurugama.arachchige.kumudu.madhawa.r4@dc.tohoku.ac.jp

Abstract

Floods are among the most devastating natural disasters and may cause immeasurable damage. Thus, identifying flood-prone areas is necessary. Data-driven models have been showing their ability of flood susceptibility mapping (FSM) in data-scare regions as an alternative to traditional hydrological models, but they are not widely used by stakeholders due to their black-box nature. This research suggests utilizing the Shapley additive explanation (SHAP) method to interpret the results generated by the CatBoost machine learning model and to assess the influence of different variables on FSM. A geodatabase with a flood inventory (445 flooded locations) and thirteen flood conditioning factors were used to implement the model and results were validated using area under curve (AUC) method, which showed a success rate and prediction rate of 93.1% and 92.5%, respectively. SHAP plots indicated that the regions with lower elevations and topographic roughness values, gentler slopes, moderate rainfall, and closer proximity to rivers are more susceptible to flooding. According to the results obtained, we suggest incorporating SHAP-based data-driven models in forthcoming studies on FSM to enhance the interpretations of model outcomes.
Keywords: AUC, Flood susceptibility mapping, GIS, SHAP, Machine learning.

1 Introduction

Floods rank among the most devastating and catastrophic calamities on a global scale due to their immense damage to the infrastructure and the natural environment [1]. Therefore, prior identification of flood prone regions and factors that drive flood occurrences, is one of the critical steps in developing flood mitigation strategies to reduce the impact of floods and effectively allocate resources to future flood events.

In recent years data-driven models have been showing their ability of FSM and found to be more accurate than other traditional FSM models particularly in data-scare regions. While ML models often yield more accurate outcomes, they are commonly referred to as "black boxes" owing to their limited model interpretability, therefore rarely selected by stakeholders [2]. The Shapley additive explanation (SHAP) model is widely utilized as a transparent and interpretable model in diverse areas of geo-hazard studies. In this study, we used an ensemble tree based CatBoost ML model to develop a flood susceptibility map for Rathnapura and then applied SHAP to interpret the model outcomes.

2 Materials and methods

2.1 Study area

The study area is Rathnapura district, which is in the upper catchment of Kalu river, Western province, Sri Lanka. In Rathnapura district, the most devastating floods occurred during the following years 2003, 2008, 2012, and 2017 resulting in hundreds of fatalities and economic losses.

2.2 Flood inventory and spatial data

The A total of 445 flood location points was chosen as the flood inventory based on documentary sources and field survey data collected from disaster management center (DMC), Sri Lanka. The flood inventory data was divided into 70% and 30% sections for training and testing, respectively. Thirteen FCFs; elevation, curvature, aspect, slope, normalized difference vegetation index (NDVI), topographic roughness index (TRI), topographic wetness index (TWI), sediment transportation index (STI) distance from river, distance from road, land cover (LULC), soil, and rainfall with 30m spatial grid resolution were considered.

2.3 CatBoost model

CatBoost algorithm is an enhanced approach of gradient boosting decision trees (GBDT) [2]. This model is created incrementally through a stagewise approach, with each stage refining the approximation more precisely. The primary goal of the learning method is to develop a function $H : \mathcal{R}^n \rightarrow \mathcal{R}$ that reduces the expected loss which can be depicted as in following equation.

$$L(H) := \mathbb{E}L(y, H(X))$$

where $L(.,.)$ represents a smooth loss function, X and y are training samples. The process generates a series of successive estimations $H^t : \mathcal{R}^m \rightarrow \mathcal{R} (t = 0, 1, ..)$ through iterative steps.

$$H^t = H^{t-1} + \alpha g^t$$

where α is the step size and the function $g^t : \mathcal{R}^n \rightarrow \mathcal{R}$ is a base predictor which is chosen from a group of functions G, used to limit the expected loss can be explained as in following equation.

$$g^t = arg \, min_{g \in G} \mathbb{E}L(y, H^{t-1}(X) + g(X))$$

2.4 SHapley Additive exPlanations (SHAP)

The explainability of ML models comes under Explainable Artificial Intelligence (XAI) which demonstrates the importance of conditioning factors to overall predicted results, allowing the analyst to determine what the ML model considers when assessing flood susceptibility [2]. The Shapley value is calculated based on the average marginal

65

The 11th International Symposium on Water Environment Systems
----- with Perspective of Global Safety   (Nov. 16th ~ 17th, 2023)

GP-RSS & SyDE
Tohoku University

contribution across all possible permutations of the features, as following equation.

$$\phi_i(f,x) = \sum_{S \subseteq N \backslash \{i\}} \frac{|S|!\,(n-|S|-1)!}{n!}[\upsilon(S \cup \{i\}) - \upsilon(S))]$$

where ϕ_i is the contribution of feature i, N is the set of all features, n is the number of features in N, S is the subset of N containing feature i, and $\upsilon(N)$ is the base value.

2.5 Model validation

In this study, the model outcomes were validated using the success and prediction rate curves, developed using area under curve method (AUC) using the training and testing data sets, respectively.

3 Results and discussion
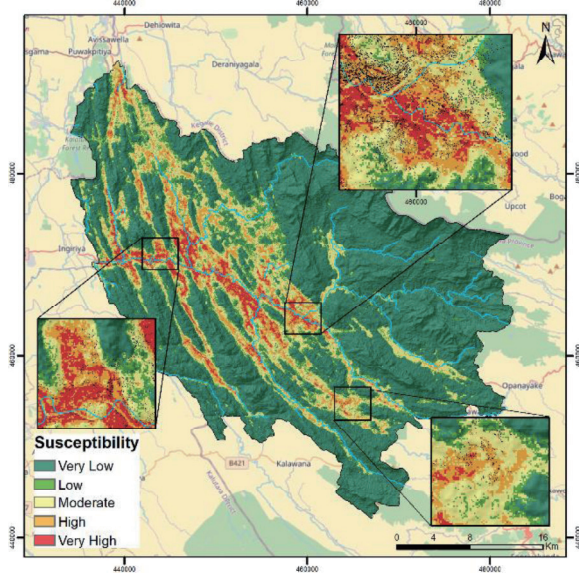
3.1 Flood susceptibility map

Fig.1. Flood susceptibility map of Rathnapura

The flood probability map, which was obtained as the model outcome was then classified into five flood susceptible zones using natural breaks classification technique (Fig. 1). According to figure 1, 8.9% of the study area was covered with high and very high susceptibility classes where 15% of the total area was classified as moderate risk area and most of the region (75.6%) was classified as low and very low susceptible to flooding.

3.2 Model validation

In the model validation stage, support vector machine (SVM) and modified frequency ratio (MFR) methods were used to compare the model performance and, Table 1 provides evidence of the impressive performance exhibited by the CatBoost model (Table 1) where success and prediction rate values were 93.1% and 92.5%, respectively.

Table 1. Success and prediction rate curve values

Model	Success Rate (%)	Prediction Rate (%)
CatBoost	93.1	92.5
SVM	89.6	85.6
MFR	84.3	83.5

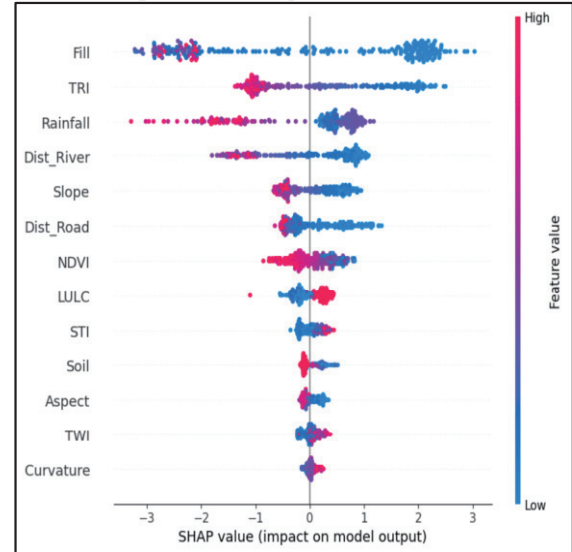**3.2 Feature importance using SHAP method**

Fig.2. SHAP summary plot

According to the results (Fig.2) elevation, TRI and rainfall were the main contributors. Both elevation and TRI determine the natural flow of water and identify areas that can impede or redirect the flow of water during floods. Areas at higher elevations generally act as water sources, while low-lying areas with more residential density tend to accumulate water causing floods. Furthermore, TRI indirectly reflects the infiltration capacity of the land. The city area experiences moderate rainfall, and the surrounding mountains experience high levels of rainfall due to orographic lifting. Thus, the river water level increases, as well as cities located in the valley area (downstream of these mountains) inhibit the rapid runoff of water and tend to have an increased risk of flooding. In summary, Elevation, TRI, Rainfall, distance from the river, and slope variables show a greater impact on flood occurrence, distance from road, NDVI, LULC and soil variables show moderate effect while STI, TWI and Curvature show the least importance.

4 Conclusions

This research revealed that the CatBoost model attained a 92.5% AUC value, indicating a high level of accuracy and approximately 9% of the area is classified as high and very high flood susceptibilities. Based on SHAP analysis, these zones are mainly distributed in regions with lower elevations and TRI values, gentler slopes, moderate rainfall, closer proximity to rivers and residential areas. Using the SHAP model alongside ML models in FSM can enhance our comprehension of the fundamental mechanisms and factors influencing flood risk, particularly in regions where data is limited.

Reference

[1] Duan, Le, et al. "Susceptibility Assessment of Flash Floods: A Bibliometrics Analysis and Review." *Remote Sensing*, Vol. 14, Issue 21(2022), p. 5432.

[2] B. Pradhan, S. Lee, A. Dikshit and H. Kim, "Spatial flood susceptibility mapping using an explainable artificial intelligence (XAI) model." *Geoscience Frontiers*, Vol. 14, Issue.6 (2023).

The 11th International Symposium on Water Environment Systems
----- with Perspective of Global Safety   (Nov. 16th ~ 17th , 2023)

GP-RSS & SyDE
Tohoku University

Analyzing Climatic Variations and Their Implications for Cereal Cultivation Potential in Afghanistan

○ Mohammad Naser SEDIQI[1*], Daisuke KOMORI[1,2]

[1] Green Goal Initiative, Tohoku University, Sendai 980-8579, Japan
[2] Graduate School of Environmental Studies, Tohoku University, Miyagi 980-8579, Japan.
[*]E-mail: ediqi.mohammad.naser.c8@tohoku.ac.jp.

Abstract

This study assessed the shifts in agricultural climate boundaries and the identification of potential future agricultural regions in Afghanistan, emphasizing the critical influences of climate change and elevation. Employing Geographic Information System (GIS) techniques and climate models, the research meticulously evaluated future changes in climatic boundaries and the potential assessment of agricultural areas, specifically focusing on two significant crops, winter wheat and rice. The analysis utilized historical data from 1975 to 2014 and future projections for 2060 to 2099 across Afghanistan's distinct climatic regions. A key finding of the study was the inverse correlation between maximum temperature (Tmx) and elevation, a relationship that suggests a possible upward shift in climate boundaries, which could necessitate cultivation at higher elevations in the future. Regional disparities in precipitation changes were also observed, further emphasizing the need for region and crop-specific planning. The research's findings illuminate the multifaceted impacts of climate change on Afghanistan's agricultural potential and highlight the urgency for adaptive strategies tailored to variations in regional and elevation factors. By taking into account essential components such as temperature, precipitation, and particularly the role of elevation in dictating agricultural potential, the study contributes significant insights toward sustainable water resource management, climate change mitigation, and the formulation of effective adaptation measures.

Keywords: Climate Change, Elevation, Agricultural Potential, Climate Boundary, Afghanistan.

1 Introduction

Climate change presents a multitude of challenges for the agricultural sector worldwide. One of the most notable impacts is on crop productivity, with many regions experiencing reduced yields as a result of altered precipitation patterns and temperature fluctuations (IPCC, 2014).

A significant and often overlooked consequence of climate change is the shift in agricultural zones. As the globe warms, certain regions may become less suited for their traditional crops while others may emerge as new agricultural frontiers (Morton, 2007).

However, it is also important to recognize that climate change is not merely a harbinger of challenges but can also usher in opportunities for the agricultural sector. For instance, the opportunity that arises from changing climatic patterns is the creation of additional potential areas for agricultural cultivation, based on agricultural climate boundaries (Challinor et al., 2014).

Historically, various methodologies have been employed to gauge potential agricultural areas. Crop Simulation Models, as discussed by Hodson et al (2010), use software to predict the effects of climate change on crop yields. Another avenue for understanding land potential is through Soil Testing, a method where soil samples are analyzed to determine their composition and thus their suitability for agriculture (Van Noordwijk et al., 1993).

However, a notable gap exists in the literature regarding the future potential areas based explicitly on the range of climate boundaries of crops. Moreover, the influence of elevation on these shifting agricultural climate boundaries remains underexplored, despite its significance in regions with varied topographies like Afghanistan.

Afghanistan, with its unique climatic regions ranging from hot arid to cold temperate zones, stands at the forefront of these challenges and opportunities.

In light of these identified research gaps, the objectives of this study is to assess the shifts in agricultural climate boundaries in Afghanistan, giving particular emphasis to the profound influence of elevation. Furthermore, our research will venture into identifying the potential regions in Afghanistan that might emerge as agricultural hotspots in the evolving context of climate change.

2 Materials and methods

This study aims to evaluate the potential shifts in climatic boundaries and the prospects for agricultural areas in Afghanistan, taking into account the interplay of elevation and climate change. Focusing on winter wheat and rice crops. Making use of key climate variables derived from the ensemble of the Coupled Model Intercomparison Project Phase 6 (CMIP6) General Circulation Models (GCMs) – namely, maximum (Tmx) and minimum temperatures (Tmn) and precipitation (Pre) – the study contrasts the historical period (1975-2014) with future projections (2060-2099) under the Shared Socioeconomic Pathways 5-8.5 (SSP5-8.5) pathway.

Historical agricultural locations serve as the baseline for past analysis, while the emphasis for future scenarios encompasses a comprehensive examination across all climatic zones.

The 11th International Symposium on Water Environment Systems
----- with Perspective of Global Safety   (Nov. 16th ~ 17th , 2023)

GP-RSS & SyDE
Tohoku University

3 Results and discussion

3.1 Elevation-Dependent Climatic Variations: An Overview on Agriculture in Afghanistan

Figure S1 presented the correlation of maximum temperature (Tmx) with elevation across climatic zones for the wheat crop season during the periods 1975-2014 and 2060-2099 under the SSP5-8.5 pathway. A stark rise in future temperature averages was observed, especially in the hot arid climatic region, reflecting anticipated global warming trends. This suggests that due to global warming, existing climates at lower altitudes may shift to higher elevations, potentially influencing future agricultural practices.

Using the 95% interval above the historical Tmx average as a threshold, potential agricultural regions were pinpointed. Regions surpassing this boundary, however, could witness climates unfamiliar to current agricultural practices, emphasizing the necessity for adaptive approaches.

3.2 Projected Climate Boundary Exceedances and Potential Agricultural Regions for Wheat and Rice Crops

Figure 1 and 2 depict potential agricultural regions across Afghanistan expected to exceed the acceptable climatic boundaries for wheat and rice cultivation, respectively. These figures were enhanced to include the current agricultural regions, color-coded in black.

For wheat cultivation, Figure 1 showcased regions projected to experience unfamiliar climate extremes, with color codes for ease of understanding: red denoted temperature extremes, orange signified precipitation extremes, and yellow indicated regions likely to grapple with both precipitation and temperature extremes. Regions that remained uncolored denoted potential agricultural areas projected to stay within the climate boundaries, primarily located at higher elevations and within the cold temperate climate zone. The observed trends in data indicate that while a few regions might experience combined extremes of temperature and precipitation, the majority of regions will likely face temperature extremes alone. Therefore, these potential shifts in temperature can have a significant influence on the productivity and viability of wheat cultivation.
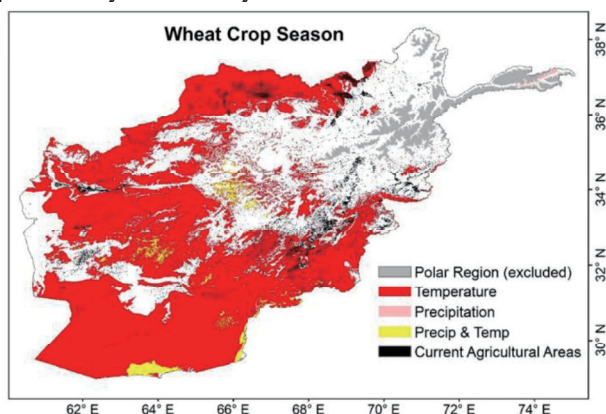

Fig. 1. Geographic representation of areas predicted to experience unfamiliar climate extremes for wheat cultivation.

In contrast, Figure 2, dedicated to the rice cultivation season, presented a more challenging scenario. Compared to the wheat season, a larger fraction of Afghanistan's agricultural regions was projected to face unfamiliar climate extremes during the rice cultivation period

However, considering an alternative perspective, "wet" crops like rice, which require significant amounts of water and are often grown in flooded conditions, might actually be less vulnerable to increasing temperatures. The rationale is that irrigation can help alleviate heat stress, allowing these crops to be grown even in regions with higher temperatures. This is in alignment with the findings by (Hendrawan et al., 2023), which indicate that the role of irrigation in rice farming can help mitigate the impacts of heat stress or drought on crop yield.
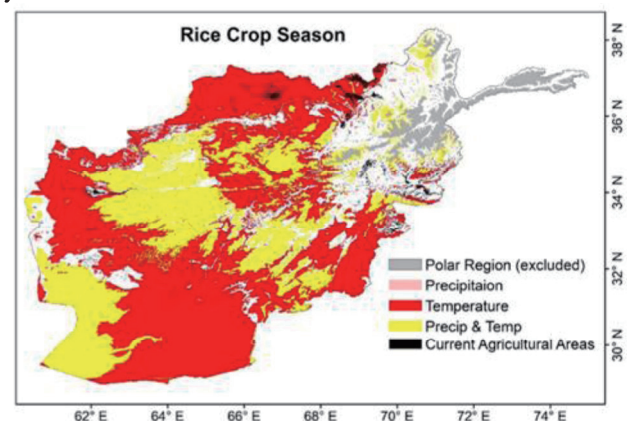

Fig. 2. Geographic representation of areas predicted to experience unfamiliar climate extremes for wheat cultivation.

4 Conclusions

The research underscores the dynamic interplay between climate change and elevation in Afghanistan's agricultural landscape. With global warming trends suggesting an upward shift in climatic boundaries, cereal cultivation, particularly wheat and rice, may soon need to transition to higher elevations. Regional disparities in precipitation further emphasize the need for targeted agricultural strategies. In areas predicted to surpass historical climate norms, adaptive measures are crucial to safeguard food security. Overall, the study's findings emphasize the urgency for tailored, adaptive agricultural planning in the face of impending climatic changes in Afghanistan.

Reference

1. IPCC, 2014. Climate Change 2014: Impacts, Adaptation, and Vulnerability.
2. Morton, J.F., 2007. The impact of climate change on smallholder and subsistence agriculture.
3. Challinor, A. J., Watson, J., Lobell, D. B., Howden, S. M., Smith, D. R., & Chhetri, N. (2014). A meta-analysis of crop yield under climate change and adaptation. Nature Climate Change
4. Meine van Noordwijk, Gerard Brouwer, Klaas Harmanny, (1993). Concepts and methods for studying interactions of roots and soil structure.
5. Hendrawan, V. S. A., Komori, D., & Kim, W. (2023). Possible factors determining global-scale patterns of crop yield sensitivity to drought. PLoS ONE, 18(2 February), 1−20. https://doi.org/10.1371/journal.pone.0281287

The 11th International Symposium on Water Environment Systems
----- with Perspective of Global Safety   (Nov. 16th ～ 17th , 2023)
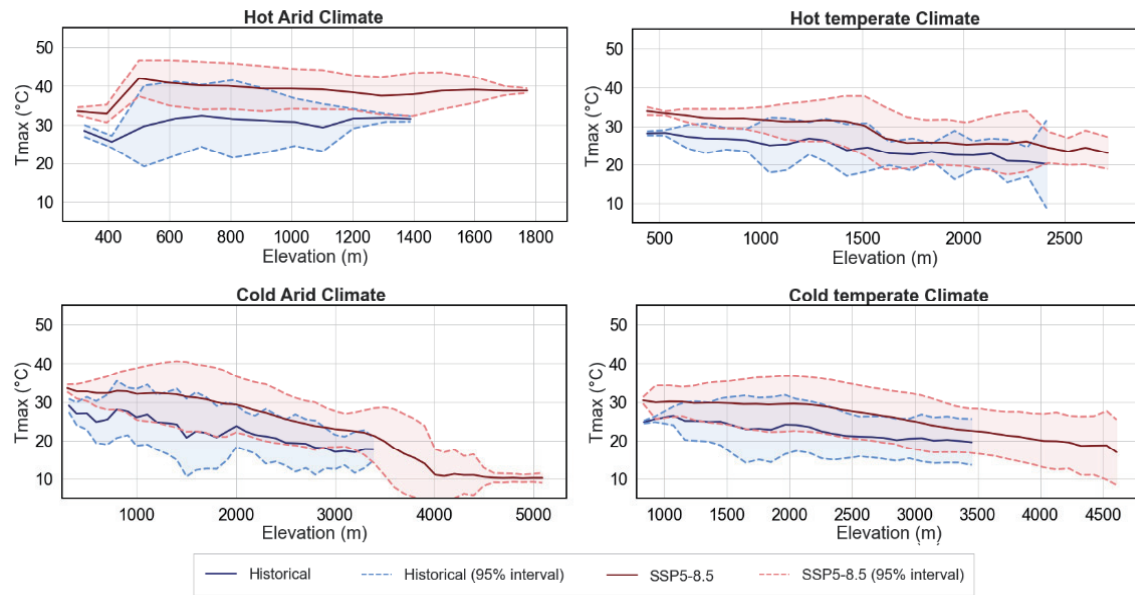
GP-RSS & SyDE
Tohoku University

APPENDIX

Figure S1. Historical average (1975-2014) and projected future average (2060-2099) of Tmx variation with elevation across different climate regions during wheat crop season.

The 11th International Symposium on Water Environment Systems
----- with Perspective of Global Safety   (Nov. 16th ~ 17th , 2023)

GP-RSS & SyDE
Tohoku University

Modeling The Interaction of Flood Hazard and Society in Citarum Watershed, Indonesia: A Socio-hydrological Perspective

○ Muthiah SADIDAH[1*], Daisuke KOMORI[1]

[1]Graduate School of Environmental Studies, Tohoku University, Miyagi 980-8572, Japan.
[2]Green Goals Initiative Laboratory, IRIDES building, Tohoku University, Miyagi 980-8572, Japan.
*E-mail: Muthiah.sadidah.t2@dc.tohoku.ac.jp

Abstract

In this study, the SH modeling of flooding in Karawang has provided valuable insights into the memory dynamics and impacts of flood events. Two important effects related to flood damage, the "adaptation effect" and the "levee effect," were investigated. The adaptation effect was found in the target area driven by accumulated societal memory of past flood events. On the other hand, the reduction in flood memory led to a slight increase in damage when river flooding occurred in 2019 after the absence of floods following the 2016 event. Therefore, the levee effect was not found instead the adaptation effect remained in the target area. In addition, in the process of this study, a new method of extracting memory loss rate has been proposed. This method was conducted using significance test focusing on memory using a certain initial value of memory loss rate as a benchmark. This method resulted in a range of memory loss rates of this study (0.05 until 0.42). Using this range with memory loss rates of previous study to be compared with GDP (Gross Domestic Product) gave this study new insights. This comparison involved looking at how economic factors, as indicated by GDP, connect with the way people remember flood events. This analysis helps us gain a deeper understanding of how economic conditions influence the way people remember floods, and it provides valuable insights into the wider socio-economic consequences of flood memory patterns.

Keywords: socio-hydrological modeling; socio-hydrology; flood hazard; society.

1 Introduction

Based on National Agency for Disaster Countermeasure of Indonesia (BNPB), Karawang regency is the most flooding-prone area in Citarum watershed with the highest number of flood events compared to the upper areas. Recent research has explored the impact of human interventions to floods including urbanization, land-use change, etc [Di Baldassarre et al., 2009; Heine and Pinter, 2012; Remo et al., 2012]. However, all these works have been looking only at one side of the interaction between floods and societies [Di Baldassarre et al., 2013].

This study aims to develop a socio-hydrology model to quantitatively explain the coevolution of human-flood systems. We proposed a dynamic analysis using socio-hydrological (SH) model to Indonesia. The SH model was applied in Karawang Regency of Citarum Watershed which is known as the largest watershed in West Java, Indonesia. In addition, no prior research has employed the SH model in Indonesia, specifically within the Karawang Regency.

2 Materials and methods

This research used hydrological (water level) and societal data (population data); this research also used historical flood event data derived from Based on National Agency for Disaster Countermeasure of Indonesia (BNPB).

The SH model, developed by Di Baldassarre in 2015, used a set of differential equations to understand the interactions between human activity, technology, and flooding. The model uses the variable F to represent the severity of a flood event, the variables and parameters used in Equations (1) are

$$F_{\_} = 1 - \exp\left(-\frac{W + \xi_H H_{\_}}{\alpha_H}\right) if\ W + \xi_H H_{\_} > H_{\_} \quad (1)$$

$$\frac{dD}{dt} = \rho_d\big(1 - D(1 + \alpha_D M)\big) - \Delta(\Psi(t))FD_{\_} \quad (2)$$

$$\frac{dH}{dt} = -\Delta(\Psi(t))R - K_T H \quad (3)$$

$$\frac{dM}{dt} = \Delta(\Psi(t))FD_{\_} - \mu_S M \quad (4)$$

Fig.1. Socio-hydrological modeling equations

W: high water level, $H_{\_}$: flood protection level before the flooding event, ξH: proportion of flood level enhancement due to the presence of levees and αH: parameter related to the slope of the floodplain and the resilience of the human settlement. The Equations (2)– (4) show the dynamics of the human-floodplain system. The D, H and M represent the population density, flood protection level and flood memory of the community respectively. The parameters in the set of equations are ρD: mean relative growth rate, αD: ratio preparedness/awareness, κT : protection level decay rate and μS : memory loss rate, $\Delta(\Psi(t))$: a function which is always 0 and becomes 1 in flood occasion.

3 Results and discussion

The results of SH model applied in Karawang Regency show that flood events happened in 2013 and 2014 result in damage ratio (the ratio of people evacuated and modelled flood damage) around 1. These consecutive flood events accumulated societal memory and lead to a decreased damage resulted in 2016 flood event with damage ratio 0.43. The results of SH model applied in Karawang Regency show

The 11th International Symposium on Water Environment Systems
----- with Perspective of Global Safety   (Nov. 16th ~ 17th , 2023)

GP-RSS & SyDE
Tohoku University

that flood events happened in 2013 and 2014 result in a damage ratio (the ratio of people evacuated and modelled flood damage) around 1. These consecutive flood events accumulated societal memory and lead to a decreased damage resulted in 2016 flood event with damage ratio 0.43. The results of SH model applied in Karawang Regency show that flood events happened in 2013 and 2014 result in damage ratio (the ratio of people evacuated and modelled flood damage) around 1. These consecutive flood events accumulated societal memory and lead to a decreased damage resulted in 2016 flood event with damage ratio 0.43. Consequently, it is speculated that the damage from river flooding has reduced due to the accumulation of memories as the effect of flood events in 2013 and 2014, this situation is called adaptation effect. On the other hand, a decrease of flood memory occurred in 2019, this is resulted by no flood events after 2016 flood. In addition, it can be seen in Figure 2, a river flooding occurred in 2020 has damage ratio 0.5 which is slightly increased from damage ratio in 2016 (0.43). However, in comparison to damage change that occurred in adaptation effect, the decrease of memory in this case is not significant. Therefore, it is speculated that there is no levee effect found in this study as society still maintains the adaptation effect.
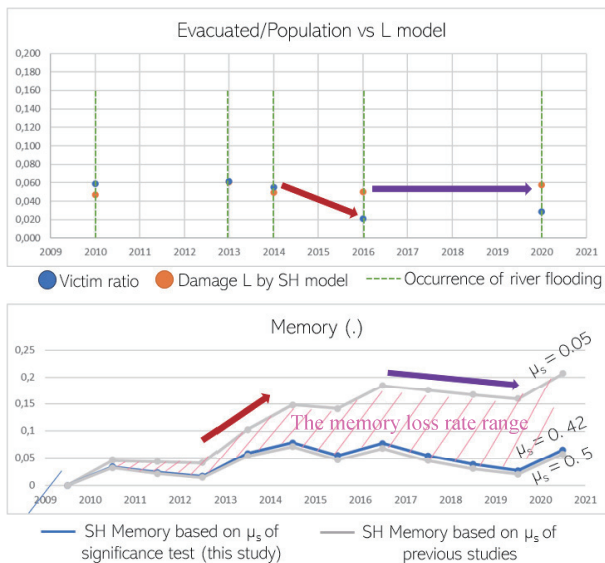

Fig.2. SH model results and memory loss rate range

This research used a significance test to assess whether the observed changes in the memory loss rate, as determined by my model, genuinely reflect variations in the damage ratio or if they could have occurred randomly. The findings indicate that the memory loss rate of this study ranged from 0.05 to 0.42. This calculation of memory loss rate range has not been applied in the previous study and one of the findings in this study. The visualization can be seen in Figure 2.

This study discussed the results of the comparison of the memory loss rates of the previous studies including this study and the GDP of each country of the study cases. Figure 3 depicts two groups which are low GDP countries and high GDP countries. In the first group, countries with lower GDP have lower memory loss rates, they tend to keep memory because they are still growing economically so they have low mitigation systems like flood protection, they are still focusing on their economic growth, so they tend to remember past flood events more clearly. Then as GDP gets higher, they

are growing economically, and have better flood protection, so they have more sense of security, then this memory loss rate becomes higher as they more easily forget past flood
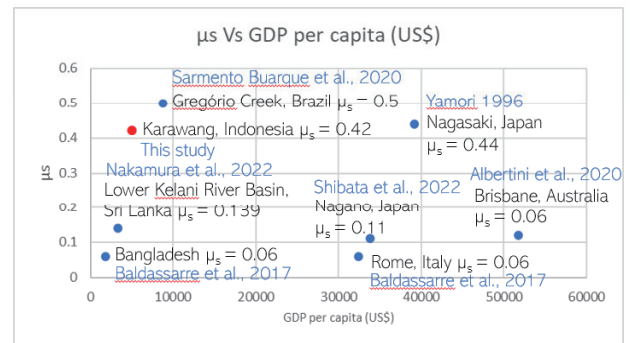

Fig.3. Memory loss rate Vs GDP per capita (US$)

events. This statement suggests that when disaster prevention measures are implemented in places that are prone to disasters (like floods), it makes these areas safer. Because of this increased safety, people from other regions have started moving to these safer areas. The assumption here is that these newcomers have not previously experienced flooding in these places, so they tend to forget about the possibility of floods more quickly compared to the long-time residents. In essence, newcomers might not have strong memories or higher memory loss rate of past floods because they have not lived through them in that specific area.

In the second group, this increase phase is the same as explained before but this group has a decrease phase, this means that after one point, when they are economically stable and economically satisfied, they are more aware of flood education, flood early warning system, they have more flood mitigation training, so when the memory becomes lower again, they become more aware again of the past flood evens, they more focus on things like disasters, and safety. To be clearly understood, the memory loss rate for the second group is similar to that of Bangladesh and Sri Lanka in the first group. This suggests that Bangladesh and Sri Lanka may not encourage people to settle in high-risk areas because these regions lack investments in disaster prevention infrastructure. In contrast, the second group appears to have implemented restrictions on land use in high-risk areas due to substantial investments in disaster prevention infrastructure. These land use restrictions are believed to also influence how quickly people forget about flood events.

4 Conclusions

Overall, adaptation effect has been found in this study. Moreover, in the process of this study, a new method of extracting memory loss rate has been proposed. This method was conducted using significance test. Using this range with memory loss rates of previous study to be compared with GDP (Gross Domestic Product) gave this study new insights about how economic factors, as indicated by GDP, connect with the way people remember flood events.

Selected References

[1] Di Baldassarre, G., Viglione, A., Carr, G., Kuil, L., Salinas, J.L. and Blöschl, G., 2013. Socio-hydrology: conceptualising human-flood interactions. Hydrology and Earth System Sciences, 17(8), pp.3295-3303.
[2] Di Baldassarre, G., Viglione, A., Carr, G., Kuil, L., Yan, K., Brandimarte, L. and Blöschl, G., 2015. Debates—Perspectives on socio-hydrology: Capturing feedbacks between physical and social processes. Water Resources Research, 51(6), pp.4770-4781.

The 11th International Symposium on Water Environment Systems
----- with Perspective of Global Safety   (Nov. 16th ~ 17th , 2023)

GP-RSS & SyDE
Tohoku University

The Impact of the 2018 Ranch Fire on Extreme Runoff Scenarios and Downstream Flood Risk in the Lake County of North-Central California

○ Dilshan MWRR[1*], Hiraga Y[1] , Kazama So[1] & Chaminda SP[2]

[1]Department of Civil Engineering, Tohoku University, Miyagi 980-8579, Japan.
[2]Department of Earth Resources Engineering, University of Moratuwa, Sri Lanka.
[*]E-mail: munipurage.wasitha.randeepa.ranga.dilshan.p5@dc.tohoku.ac.jp.

Abstract

Wildfires and extreme precipitation are in an increasing trend in the global context. Elevated risks of floods are expected to occur due to fire-induced land cover alterations. Hence, it is important to identify the impact of wildfire upon flood downstream, under changing climate. This study focuses on the impact of the 2018 Ranch fire on the downstream runoff in the Lake County of North - Central California. The Soil and Water Assessment Tool (SWAT) is used to simulate runoff downstream of the Lake County. Using gridded hydrological and meteorological data from 2015-2018 and 2019-2022, two SWAT models were set up and calibrated on a daily and monthly basis, to reflect pre and post wildfire land surface conditions respectively. Model calibration was performed after identifying 9 sensitive parameters, including the Soil Conservation Service curve number (SCN-CN). Curve number appeared to be one of the three most sensitive parameters, in terms of the parameter relative importance, both in pre-and post-wildfire simulations   on daily and monthly basis. Further studies are needed to better understand the effect of fires on the flood magnitude and occurrence.

Keywords: curve number ; hydrology ; post-fire runoff ; SWAT model ; wildfires

1 Introduction

Wildfires have a significant influence on ecosystems because they provide nutrients for ecological regeneration while also resulting in disasters.   Climate change is increasing the frequency of wildfires across the world, notably in the United States, South America, Central Asia, Southern Europe, Southern Africa, and Australia [1]. More than 90% of fires are caused by humans. Meanwhile, extreme precipitation, is a major worry because of the broad repercussions it can cause, such as soil erosion, landslides, and urban flash floods [2].

Sequential disaster scenarios are becoming more common in California due to the increasing frequency and severity of wildfires and precipitation. The Thomas Fire, a sizable wildfire that affected Ventura and Santa Barbara Counties, was the worst of the several wildfires that broke out in southern California in December 2017. At the time, it was the biggest wildfire in California's recorded history. A total of around 281,893 acres were burnt (440 sq mi; 114,078 ha). Following this large fire event, a significant amount of rain fell in southern California's coastal. The unstable terrain led to a massive landslide. Buildings in the Californian town of Montecito were hit by rocks, and a roadway was several feet deep in mud .The consequential mud and debris flow on January 9, 2018, has killed at least 21 people, destroyed over 100 homes, and shut down a major freeway between southern and central/northern California for 12 days.

Studies have shown that the western United States is more susceptible to the combined impacts of wildfire and excessive rainfall since it frequently experiences both threats [3]. Although several research have shown the influence of wildfires-induced land surface conditions on runoff mainly focusing on water resource perspective [4] or short duration flash flood [5], relatively little attention has been paid to understanding how the wildfires can alter the design flood in the basins, which is usually estimated in a single storm scale.

As extensive wildfires may completely alter the basin land surface conditions, the design flood estimated under the forested land surface conditions may drastically change post-fire. This impact needs an urgent investigation since the fire-rain sequential events are in increasing trend. As a first step of the afore-mentioned objective, this study examines   how extensive wildfires can change watershed characteristics, which can then be used to examine the possible significant change in pre- and post-fire runoff. This study used the Soil and Water Assessment Tool (SWAT) model forced by gridded climate dataset to simulate the runoff in the selected basins and to estimate the difference in the land surface parameters.

2 Materials and methods

The North Fork Cache Creek, in Lake County California, USA was chosen as the area of interest. It is a mountainous region in California's Lake County which features diverse landscapes and drains into Clear Lake. The Ranch Fire, California's second-largest wildfire, burned 410,203 acres in 2018, causing significant damage and impacting the North Fork Cache Creek watershed. The fire burnt area has been extended with the support of hydrological and meteorological vapor pressure deficit, horizontal wind speed and wind gust speed [6].

The Soil and Water Assessment Tool (SWAT), a distributed hydrological model with a physical basis that simulates the effects of land use, management techniques, and climatic variables on water, sediment, and nutrient yields in watersheds, is utilized in this study. Pre- and post-wildfire SWAT models were developed using meteorological and topographic data from 2015-2018 and 2019-2022, respectively, to assess the wildfire's impact on the watershed's hydrological processes. SWAT model outputs were calibrated using SUFI-2 algorithm in SWAT-CUP,

The 11th International Symposium on Water Environment Systems
----- with Perspective of Global Safety   (Nov. 16th ~ 17th , 2023)

GP-RSS & SyDE
Tohoku University

considering daily discharge data, and identifying sensitive parameters for further modifications.

3 Results and discussion

Two models were calibrated separately for daily and monthly time steps. The monthly-based scenario showed R^2, Nash-Sutcliffe efficiency coefficient and mean square error (MSE) values of 0.88,0.82 and 4.40 for pre fire model and 0.96,0.94 and 0.99 for post-fire models respectively. The daily -based scenario showed the corresponding statistical values of 0.63,0.62 and 12.00 for pre fire and 0.68, 0.68 and 12.00 for post fire model respectively.
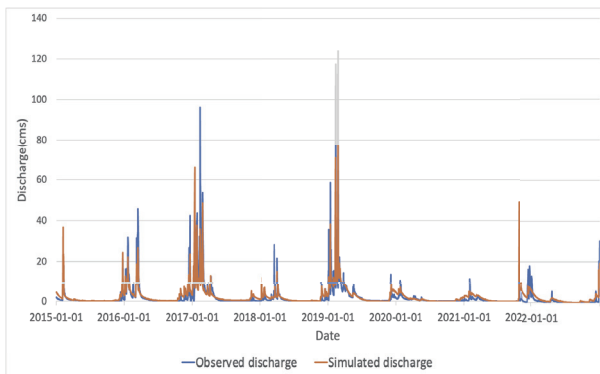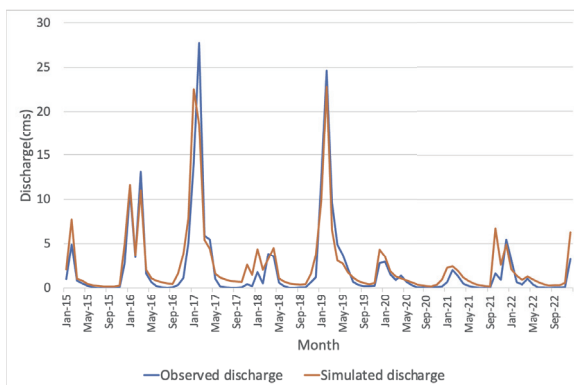

Fig.1. Discharge simulation for daily time scale.

Fig.2. Discharge simulation for monthly time scale.
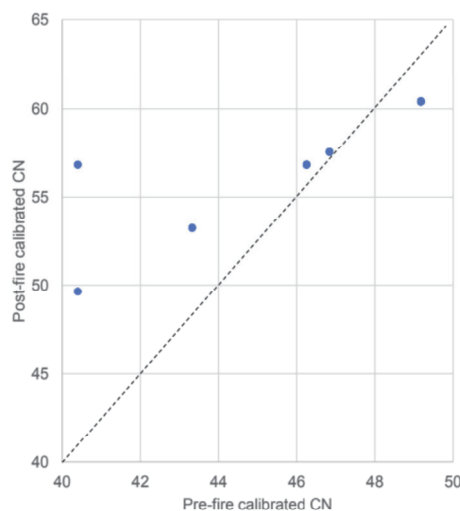

Fig 3. CN comparison

In both temporal scales, the post-wildfire model was more statistically in agreement with the observed discharge data, as indicated by the NSE and RMSE.

A higher CN2 value indicates that a greater proportion of rainfall will runoff and a smaller proportion will infiltrate into the soil. (Arnold et al.,1990) The CN comparison of pre and post wildfire scenarios, for the 75 HRUs indicated a clear increment of CN in the post-wildfire scenario, pointing out the influence of CN as a sensitive parameter for post-wildfire discharge simulation.

4 Conclusions

This part is Conclusions. This study aims to understand how the wildfires can alter the design flood in the target basins. As a first step of the afore-mentioned objective, this study examines how extensive wildfires can change watershed characteristics, which can then be used to examine the possible significant change in pre- and post-fire runoff. This study found that curve number (CN), was among the top 3 sensitive parameters for pre-and post-wildfire discharge simulations on daily and monthly temporal scales. Overall, this study can provide important insights on how the wildfires can alter the basin characteristics, consequently, flood risk downstream. Further studies are needed to identify probable flood scenarios even in the context of post-fire low precipitation levels and to enhance simulation outcomes under various parameter modifications.

Reference

[1] Liu, Y., Stanturf, J. and Goodrick, S. (2010). Trends in global wildfire potential in a changing climate. Forest Ecology and Management, 259(4), pp.685–697.

[2] Beguería, S., Vicente-Serrano, S.M., Reig, F. and Latorre, B. (2013). Standardized precipitation evapotranspiration index (SPEI) revisited: parameter fitting, evapotranspiration models, tools, datasets and drought monitoring. International Journal of Climatology, 34(10), pp.3001–3023.

[3] C L I M A T O L O G Y, C., Touma, D., Stevenson, S., Swain, D., Singh, D., Kalashnikov, D. and Huang, X. (2022). Climate change increases risk of extreme rainfall following wildfire in the western United States. Sci. Adv, [online] 8(0320). Available at: https://par.nsf.gov/servlets/purl/10321481 [Accessed 24 May. 2023].

[4] Blasko, C. (2020). Assessing hydrologic impacts of the 2013 Rim Fire on the Tuolumne River Watershed in Central Valley, California. [online] etd.ohiolink.edu. Available at: https://etd.ohiolink.edu/acprod/odb_etd/etd/r/1501/10?clear =10&p10_accession_num=bgsu1586445449253322 [Accessed 8 June. 2023].

[5]Neary, D., Gottfried, G. and Ffolliott, P. (2016). Post-wildfire watershed flood responses 1B.7 POST-WILDFIRE WATERSHED FLOOD RESPONSES. [online] Available at:https://postfiresw.info/sites/postfiresw.info/files/Neary_2 003.pdf

[6].Hiraga, Y. and Kavvas, M.L. (2021). Hydrological and Meteorological Controls on Large Wildfire Ignition and Burned Area in Northern California during 2017–2020. Fire, 4(4), p.90. doi:https://doi.org/10.3390/fire4040090.

The 11th International Symposium on Water Environment Systems
----- with Perspective of Global Safety (Nov. 16th ~ 17th, 2023)

GP-RSS & SyDE
Tohoku University

Simulation of the training-rainband in the western Tohoku region in 2022

○ Ryotaro TAHATA[1*], So KAZAMA , Yusuke HIRAGA

[1]Department of Civil Engineering and Architecture, Tohoku University, Miyagi 980-8579, Japan.
*E-mail: tahara.ryotaro.q7@dc.tohoku.ac.jp

Abstract

In recent years, climate change effects have led to an increase in rainfall intensity and changes in rainfall patterns throughout Japan. Therefore, advances in numerical forecasting methods for severe rainstorms are important not only for early warming, but also for determining future flood control plans. In this study, the WRF model is applied to the July 2022 heavy rainfall in the western Tohoku region and its accuracy is evaluated. The microphysics scheme was changed in WRF and the results were compared with radar AMeDAS observations. The results showed that the WRF reproduction generally captured the shape and location of the precipitation area compared to the radar AMeDAS observations. It was also found that the shape and location of the precipitation area varied significantly depending on the type of microphysical scheme. Although the locations of the high precipitation area were generally consistent with the observed value, accumulated precipitation for the entire Mogami River catchment was found to be less than observed when some schemes were used.

Keywords: Training-rainband; WRF; Tohoku; Microphysics.

1 Introduction

In recent years, climate change has caused more severe and frequent heavy rainfall disasters, and changes in rainfall patterns have been observed. Against this background, there is the concept of PMP (Probable Maximum Precipitation). A PMP is defined as "theoretical maximum precipitation for a given duration under modern meteorological conditions".[1] PMP is important as input data for the creation of flood hazard maps, construction of levees and dams, and other flood control measures, considering the worst-case scenario. The PMP estimation method currently used in Japan analyzes historical rainfall data for each region by rainfall duration and area.[2] However, because this method bases the PMP on historical rainfall data, it can lead to results that are meteorologically improbable. Therefore, it is necessary to reproduce and forecast rainfall using numerical weather forecast models based on the physical laws used in meteorology. In previous studies, Kita et al. (2016) reproduced 2014 Hiroshima heavy rainfall using WRF model, and Mitsui et al. (2018) reproduced training-rainband observed in the western part of the Chubu region, as a preliminary step in PMP estimation.[3][4] However, there are no examples of such a numerical weather forecast model being applied to the heavy rainfall in the Tohoku region. Therefore, the objective of this study was to apply the WRF model to the August 2022 heavy rainfall in the western Tohoku region of Japan and evaluate its accuracy. Especially, this study evaluates the difference in reproducibility due to the different microphysics schemes selected within the WRF .

2 Materials and methods

(1) Numerical model and calculation condition

Weather Research and Forecasting (WRF) Model is a state-of-the-art mesoscale numerical weather forecast model. In this study, WRF-4.1.2 was used. Three calculation domains were set up to perform calculations over a wide to narrow area by nesting (Figure 1). Nesting enables high-resolution numerical simulations in the area surrounding the target Tohoku region while reducing the computational load in the area encompassing the whole of Japan. The first area was set at 12 km resolution, the second area at 4 km resolution, and the third area at 1.3 km resolution.

In this study, 2-way nesting was employed, in which the results of calculations in the outer region are reflected in the inner region and the results of calculations in the inner region are feedback to the outer region.

Table 1 Calculation condition.

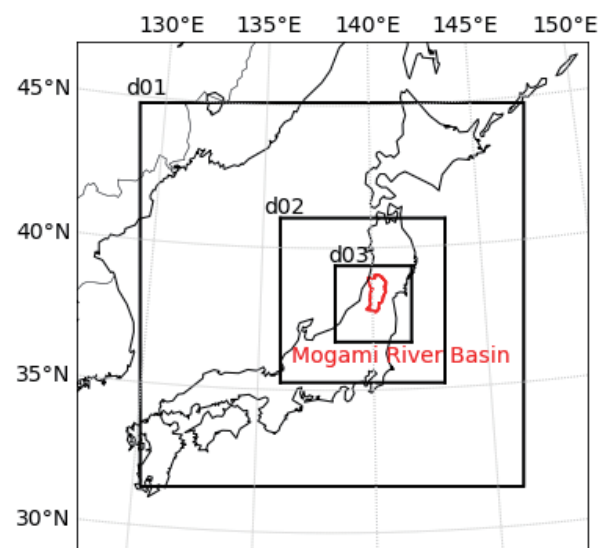|	d01	d02	d03
number of grids (WE×NS×V)	101×103×45	115×121×45	178×196×45
resolution (km)	12	4	1.3
time step (sec)	100	33	33
microphysics	Eta (Ferrier) Scheme		
	Goddard Scheme		
	WRF Single-Moment 6-class Scheme (WSM6)		
cumulus physics	Kain-Fritsch Scheme		
Planetary Boundary Layer physics	Yonsei University Scheme (YSU)		

Fig. 1. Calculation domain.

The 11th International Symposium on Water Environment Systems
----- with Perspective of Global Safety   (Nov. 16th ~ 17th , 2023)
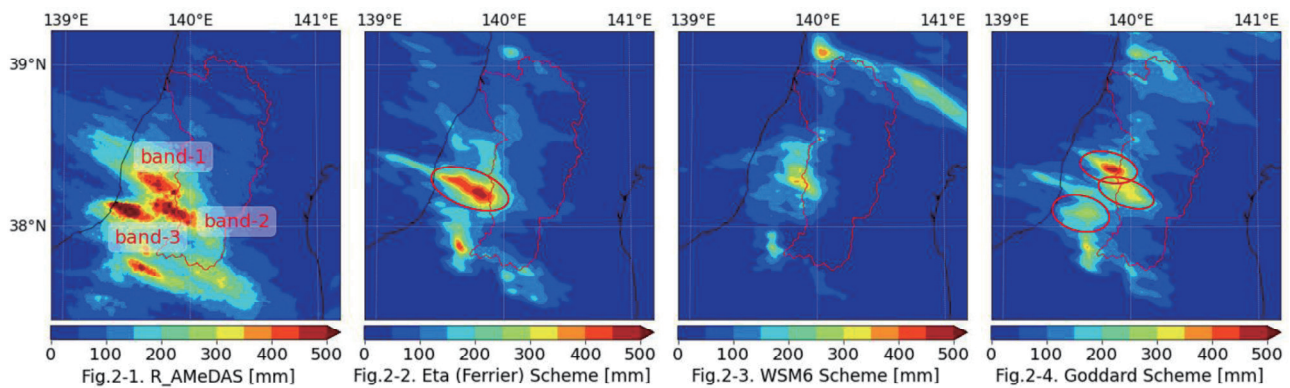
GP-RSS & SyDE
Tohoku University

Fig. 2. Accumulated precipitation distribution from 0:00 on August 3 to 0:00 on August 4.

For the data used, NCEP Final Analysis was used for the initial and boundary conditions (spatial resolution: 0.25 degrees, temporal resolution: 6 hours). The USGS Global Multi-resolution terrain Elevation Data 2010 (spatial resolution: 30 arcsec) was used for topographic data. Also radar AMeDAS observations were used for comparison with WRF calculations.

The physical model used is shown in Table-1. In this study, the microphysics schemes were changed to the three listed in Table 1 for calibration purposes.

(2) Target event

Figure 2-1 shows the rainfall distribution by radar AMeDAS from 0:00 on August 3 to 0:00 on August 4, 2022. The area surrounded by the red line indicates the Mogami River catchment. A training-rainband was occurred by a frontal system and a low-pressure system from August 3 to 4, resulting in very heavy rainfall mainly over Yamagata Prefecture. The Yonezawa and Tsubaki rainfall stations recorded the highest 24-hour rainfalls in observation history at 262 mm and 472 mm, respectively.

3 Results and discussion

Figures 2-2 to 2-4 show the rainfall distribution from 0:00 on August 3 to 0:00 on August 4, 2022, for each scheme. In the radar AMeDAS rainfall distribution, three bands of particularly high precipitation occur on the west side of the upstream of the Mogami River basin (band-1, band-2, and band-3 as shown in Figure 2-1). On the other hand, the results of WRF simulations using the Eta (Ferrier) Scheme reproduce band-1 in terms of both position and precipitation, but not band-2 and band-3 (Figure 2-2). The results using the Goddard Scheme reproduce all bands, but underestimate the amount and extent of precipitation compared to the radar AMeDAS results (Figure 2-4). None of the bands were reproduced using the WSM6 scheme (Figure 2-3).

Figure 3 shows a time series of accumulated precipitation from 0:00 on August 1 to 0:00 on August 7. Accumulated precipitation is the area average of the total precipitation that fell in the Mogami River basin. Figure 3 shows that the accumulated precipitation trend using the Goddard Scheme is almost consistent with the radar AMeDAS values. On the other hand, the results using the Eta (Ferrier) Scheme and WSM6 scheme show a sharp increase in precipitation at about the same time as the radar AMeDAS. However, they underestimate the final accumulated precipitation.
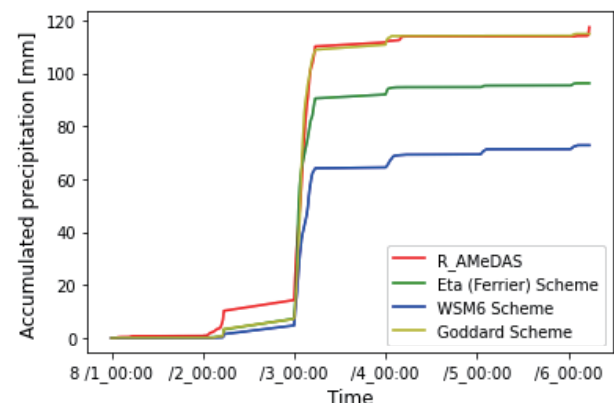

Fig. 3 Accumulated precipitation (basin area average).

4 Conclusions

In this study, WRF was applied to the August 2022 heavy rainfall in the western Tohoku region of Japan to evaluate the accuracy of different microphysics schemes used in the model. The results showed that the reproduced results varied greatly depending on the microphysics scheme. In the future, we would like to improve the accuracy of the reproduction by modifying the data of cumulus physics schemes, planetary boundary layer physics schemes, and topographic data we used. In addition, to estimate the PMP, we would like to examine whether similar training-rainbands will occur under a warming environment and, if so, how their scale and location will change, using the future climate after warming as the initial and boundary conditions.

Reference

[1] WMO, Manual on Estimation of Probable Maximum Precipitation (PMP), 2009.
[2] Ministry on Land, Infrastructure, Transport and Tourism, Methodology for setting the assumed maximum external force for the preparation of inundation assumptions (flood from rivers and inland waters), 2015.
[3] Kita et al., High-resolution downscaled simulation of heavy rainfall in Hiroshima in August 2014 using WRF, Journal of Japan Society of Civil Engineers, Vol. 72, No. 4, pp. I_211-I_216, 2016.
[4] Mitsui et al., Analysis on the training-rainband that stagnated in the western part of the Chugoku region in July 2017, Journal of Japan Society of Civil Engineers, Vol. 74, No. 4, pp. I_289-I_294, 2018.

The 11th International Symposium on Water Environment Systems
----- with Perspective of Global Safety   (Nov. 16th ~ 17th , 2023)

GP-RSS & SyDE
Tohoku University

Land Subsidence in Bangkok Vicinity: Causes and Long-term Trend Analysis Using InSAR and Random Forest

◯ Sakina AHMED[1*], Yusuke HIRAGA[1] & So KAZAMA[1]

[1]Department of Civil and Environmental Engineering, Tohoku University, Miyagi 980-8579, Japan.
*E-mail: ahmed.sakina.r5@dc.tohoku.ac.jp

Abstract

Land subsidence in Bangkok, a pressing environmental concern, necessitates long-term policy actions. Mitigation efforts have curbed subsidence rates within inner Bangkok, but neighboring provinces face escalating rates. This study aims to provide future predictions for subsidence in the near (2023-2048), mid (2049-2074), and far-future (2075-2100) using the LiCSBAS package, Random Forest algorithm, and combined SSP-RCPs scenarios. The proposed model demonstrated good performance with an R^2 value of 0.80 and showed no signs of overfitting. The 'only-rainfall-change' scenario produced the highest subsidence among all scenarios. Excluding the 'only-urban-LU-change' scenario, the results for all scenarios demonstrated an increasing subsidence trend in the near-future, while the mid and far-future exhibited different tendencies.

Keywords: Subsidence; Bangkok; InSAR; LiCSBAS; Random Forest.

1 Introduction

Land subsidence (LS) has been a persistent problem in Bangkok, Thailand since the late 1960s. The excessive extraction of groundwater was identified as the main cause of LS, leading to the declaration of critical groundwater zones in 1983, which included Bangkok (BK), Samut Prakan (SP), Nonthaburi (NONT), and Pathum Thani (PT). Later, in 1995, it expanded to include Samut Sakhon (SS), Nakhon Pathom (NP), and Ayutthaya (PNSA). Strict mitigation policies have helped reduce LS rates. However, despite the decreasing rates in the inner areas of Bangkok, the subsidized areas expanded into provincial suburbs [1]. Land-based monitoring methods have limited coverage, require continuous maintenance, and exhibit seasonal bias during measurement. Satellite-based techniques like Multi-temporal Interferometric Synthetic Aperture Radar have been particularly valuable in overcoming some of these issues by providing enhanced spatial density, precise deformation monitoring, and wider coverage compared to land-based methods. Due to the complexity of the subsidence process, focusing on one driver in isolation may underestimate the cumulative impact of other drivers, and the sparsity of field data and locality of results may impose limitations. Moreover, future changes in climate, socio-economic factors, and policies impose nonlinear variability. These future changes can be projected using the Shared Socioeconomic Pathways and Representative Concentration Pathways combination (SSP-RCPs), which provides a new integrated framework that considers both societal policies and climate impact in parallel. The Random Forest machine learning algorithm (RF) has been widely used in complex model prediction with large datasets, and due to its robustness and ability to limit overfitting, it has been used in many hydrological and environmental modeling.

The purpose of this study is to construct a regression model using RF based on a set of subsidence predictors (population, rainfall, land use, and soil type) and combined SSP-RCP scenarios (2.45, 3.70, and 4.60) to predict future LS in the near (2023-2048), mid (2049-2074), and far-future (2075-2100).

2 Materials and methods

The study area consists of seven provinces resting atop a clay layer in the lower Chao Phraya River delta (Fig. 1). The climate is classified as tropical monsoon, with a mean annual rainfall of around 1,400 mm. Agricultural land use (LU) is the predominant use of the land; however, it has recently shrunk due to rapid urbanization [2]. The population growth rate over the past decade was approximately 3.9%.
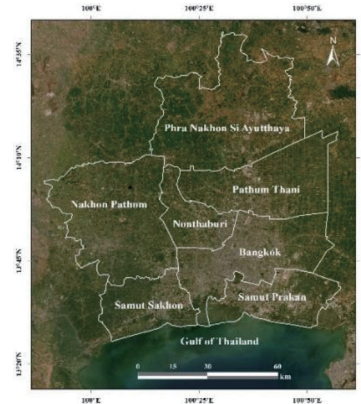

Fig. 1. Location of the study area

Sentinel-1 descending orbit data (9/10/2014 - 27/10/2022) from the COMET-LiCS portal were used as input for the LiCSBAS package to drive displacement velocities and time series. Due to the limited leveling station data with the same overlapping period as our analysis, the output was validated against GPS data from the Nevada Geodetic Laboratory GPS networks. Rainfall, population, LU/LC, and soil type (independent variables) with the highest resolution available were obtained from PERSIANN-CCS-CDR datasets, WorldPop Hub, Esri's Sentinel-2 LU/LC v.30 map, and FAO's digital soil map of the world, respectively. Predictor variables were examined for multicollinearity before applying the random forest algorithm. Then, inputs were divided into two sets (test and train) to be fitted into a regression model. The model was tested for accuracy and overfitting.

The 11th International Symposium on Water Environment Systems
----- with Perspective of Global Safety   (Nov. 16th ~ 17th , 2023)

GP-RSS & SyDE
Tohoku University

For future LS predictions, the Coupled Model Intercomparison Project 6 (CMIP6) rainfall projections from the Copernicus Climate Change Service were acquired for three models (CanESM5, MRI-ESM2-0, and MIROC6), then downscaled and bias-corrected using the CMhyd tool. Downscaled population and urban land extent projections based on SSPs were obtained at a 1-km grid resolution from NASA's Socioeconomic Data and Applications Center (SEDAC) database. Soil types were assumed to undergo no considerable changes and hence remain constant in the future. For consistency, for each projection, future changes in predictors were applied to the original inputs to be inserted back into the regression model to calculate LS future predictions.

3 Results and discussion

The mean Line-of-Sight (LoS) velocity was -45.0 mm/year, with a maximum subsidence rate of -52.9 mm/year recorded in SP (Fig. 2). The average cumulative displacement was -54.7 mm, with a maximum subsidence of -392.6 mm recorded in PNSA. Predominantly, subsidence was concentrated in the outer provinces and parts coinciding with major industrial areas where water demand is the highest. Annual fluctuations between -4 and -20 mm/year were observed (Fig. 2), with higher rates recorded in NP, PNSA, and SS. Moreover, higher LS was observed in areas related to agricultural LU compared to urban areas. For instance, SS and SP shorelines and a few areas in NP exhibited high LS rates (above -15 mm/year), coinciding with shrimp farms, as farmers shifted to it due to its profitability compared to rice production [3].
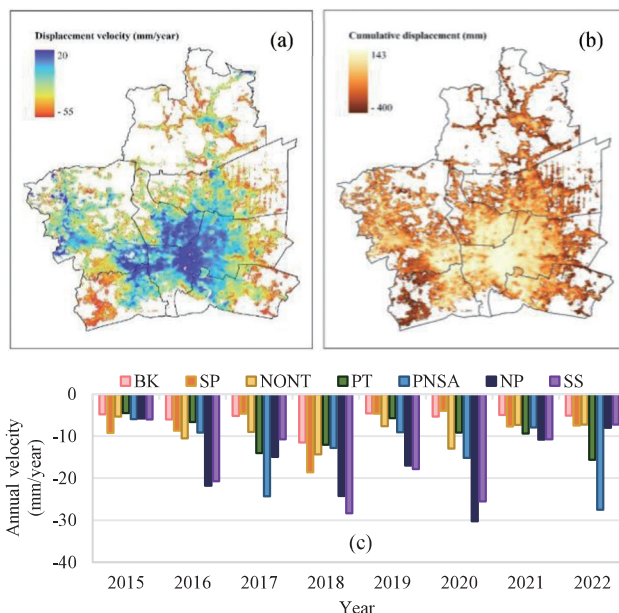

Fig. 2. LoS (a) velocities, (b) cumulative displacements, and (c) annual average LS rates between 2015 and 2022

With over 400,000 points, the regression model yielded relatively good results with R^2 = 0.80, RMSE = 12.82, MAE = 8.11, and no significant difference between train and test set accuracies, ensuring no overfitting. Feature importance showed that LS is significantly affected by population and rainfall compared to LU and soil type. Three basic scenarios were performed by changing each independent variable while

keeping other predictors unchanged. For all scenarios, LS demonstrated an increasing trend in the near-future, except for the 'only-urban-LU-change' scenario, where the trend gradually decreased all the way to the far-future. The 'only-population-change' scenario indicated that for SSP2 and SSP4, LS will decrease in the mid-future; however, it will rise again in the far-future, while subsidence in SSP3 will decrease in the far-future. Relatively higher LS was observed in the 'only-rainfall-change' scenario (Fig. 3), where the average of the three models showed that despite having the highest LS, SSP3.70 will have a tendency for lower subsidence in the far-future, unlike SSP2.45 and SSP4.60.
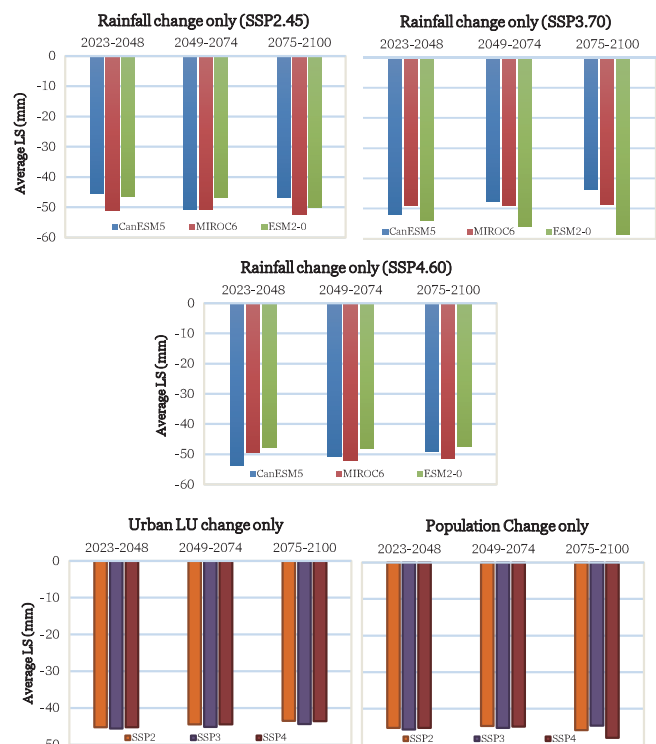

Fig. 3. Future subsidence predictions

4 Conclusions

Subsidence is a critical concern for long-term policies. Our model accurately predicted LS, highlighting population and rainfall as significant factors. In most scenarios, subsidence shows an increasing trend in the near-future. Notably, the 'only-rainfall-change' scenario saw the highest subsidence but projected lower LS for SSP3.70 in the far-future.

Reference

[1] Bremard, T., Monitoring land subsidence: the challenges of producing knowledge and groundwater management indicators in the Bangkok metropolitan region, Thailand, Sustainability, 14 (2022) 10593.

[2] Iamtrakul, P., Padon, A., Klaylee, J., Analysis of urban sprawl and growth pattern using geospatial technologies in megacity, Bangkok, Thailand, In: Bourennane, S., Kubicek, P. (Eds) Geoinformatics and data analysis: Selected proceedings of ICGDA (2022) 109-123.

[3] Flaherty, M., Szuster, B., & Miller, P., Low salinity inland shrimp farming in Thailand, AMBIO: A Journal of the Human Environment, 29, (2000) 174-179.

The 11th International Symposium on Water Environment Systems
----- with Perspective of Global Safety   (Nov. 16th ~ 17th , 2023)

GP-RSS & SyDE
Tohoku University

Classification of Deep-Seated and Shallow Landslides Using Spectral Indices and Amplitude Change Ratio in Response to Rainfall and Earthquake Events

○ Sartsin PHAKDIMEK[1*], Daisuke KOMORI[1,2], Thapthai CHAITHONG[3] & Yuta ABE[4]

[1]Graduate School of Environmental Studies, Tohoku University, Miyagi 980-0845, Japan.
[2]Green Goals Initiative, Tohoku University, Miyagi 980-8579, Japan.
[3]Department of Geography, Faculty of Social Sciences, Kasetsart University, Bangkok, Thailand, 10900.
[4]Graduate School of Civil Engineering, Tohoku University, Miyagi 980-8579, Japan.
*E-mail: sartsin.p@gmail.com, sartsin.phakdimek.q3@dc.tohoku.ac.jp

Abstract

This study aims to classify landslide types using spectral indices by Sentinel-2 (Optical images) and amplitude change ratio by Sentinel-1 (SAR images). This study presents a comprehensive analysis of landslide events in three distinct regions Ehime, Kumamoto, and Hokkaido each characterized by unique environmental conditions. The primary objective is to classify landslide types, particularly focusing on high-mobility landslides, both deep-seated landslides and shallow landslides, as they result in prominent alterations to the land surface following triggering events like rainfall and earthquakes. Successful classification using the deep-seated landslide threshold was achieved for Ehime and Kumamoto events triggered by rainfall. However, the proposed model faced challenges in classifying Hokkaido events triggered by both rainfall and earthquakes. The seismic activity induced rapid and extensive alterations to the ground surface, including liquefaction phenomena, and substantial damage to vegetated areas, potentially influencing radar reflectance and backscattering distribution.

Keywords: Spectral indices; Amplitude change ratio; Landslide types; Rainfall; Earthquakes.

1 Introduction

A landslide is characterized as the downward movement of earth material along a slope, often triggered by heavy rainfall and earthquakes. These events result in considerable damage to human lives, property, and economies. Timing of landslide detection is of paramount importance for generating landslide inventories in the weeks and months following a triggering event. These inventories serve as invaluable tools for mitigating landslide risks by identifying and mapping areas susceptible to landslides and regions that have experienced landslides in the past.

For landslide detection, remote sensing techniques are typically used to construct landslide inventories over areas that have experienced catastrophic events. Several studies have used satellite-based optical images, such as those provided by Landsat-8 and Sentinel-2, and satellite-based synthetic aperture radar (SAR) images such as Sentinel-1 and ALOS/PALSAR. The optical images are limited in terms of quick response because optical image requires sunlight and cloud and shadow-free condition to identify landslide accurately. SAR images can minimize these limitations of optical imagery that can penetrate clouds and acquire data day and night. That can be beneficial for rapid mapping of event landslides triggered by intense or prolonged rainfall, but its limitation is geometric shading and distortion.

In mountainous regions, which are particularly vulnerable to landslides, two primary types of landslides are prevalent: shallow and deep-seated landslides. According to the field investigation, the shallow and deep-seated landslides differed in size, geomaterial, and movement mechanism [1]. Shallow landslides, characterized by the movement of the surface soil mantle, typically is smaller in area and volume than deep-seated landslides, which involve the movement of the surface mantle and underlying weathered bedrock. These events pose

a significant threat to human life, property, and infrastructure, given the substantial mass and energy involved in these movements. Effectively mitigating the risks associated with landslide hazards necessitates the identification of potential landslide-prone areas and an understanding of landslide sizes and types, all of which present challenges in disaster management.

The main objective of this study was to investigate how a combination of multitemporal SAR and optical images can be used to classify landslide types under different trigger conditions. This study explored change detection approaches with a minimum threshold of amplitude ratio change (A_{ratio}), using Sentinel−1 images and the relative difference in the normalized difference vegetation index (rdNDVI), differential bare soil index (dBSI), and differential brightness index (dBI) was obtained using Sentinel−2 images for landslide types classification.

2 Materials and methods

This study consists of case studies of landslide events in three distinct regions: Ehime, Kumamoto, and Hokkaido. The selected study areas exhibited different environmental conditions, including slope exposition, land use, landslide size and type, and triggering factors, with the aim to classify landslide types. The types of landslides considered were high-mobility landslides (deep-seated landslide and shallow landslide), because they result in clear changes to the land surface after the triggering event (typhoons and earthquakes). The selected cases represent different triggers: heavy rainfall induced landslides in the cases of Ehime and Kumamoto, while the Hokkaido case involves landslides triggered by earthquakes.

Potential landslides are predicted by examining the change in amplitude by Sentinel-1 SAR image, A_{ratio}, which is defined as the pre-landslide event stack subtracted by the

The 11th International Symposium on Water Environment Systems
----- with Perspective of Global Safety   (Nov. 16th ~ 17th , 2023)

GP-RSS & SyDE
Tohoku University

post-landslide event stack, $A_{pre} - A_{post}$. $A_{pre} - A_{post}$ is equivalent to the standard amplitude ratio approach according to Eq. (1).

$$A_{ratio} = log_{10} \frac{A_{pre}}{A_{post}} \qquad (1)$$

where A_{pre} is amplitude of pre-event and A_{post} is amplitude of post event. A_{ratio} can be either positive or negative, with positive values corresponding to a decrease in SAR amplitude after a landslide event. The SAR amplitude changes following landslide events because landslides cause major changes in ground surface properties that alter the radar reflectance, hillslope geometry, roughness, and dielectric properties.

 Landslide identification was carried out based on the loss of vegetation cover and change in land cover, using the differential normalized spectral indices. These indices have been applied to identify landslides in the target area with minimum thresholds. To detect a landslide by its spectral indices, the normalized difference vegetation index (NDVI), bare soil index (BSI), and brightness index (BI) are calculated using Eq. (2) to (4).

$$NDVI = \frac{(NIR - RED)}{(NIR + RED)} \qquad (2)$$

$$BSI = \frac{(SWIR + RED) - (NIR + BLUE)}{(SWIR + RED) + (NIR + BLUE)} \qquad (3)$$

$$BI = \sqrt{BLUE^2 + GREEN^2 + RED^2} \qquad (4)$$

where BLUE (band 2) is the visible blue response, GREEN (band 3) is the visible green response, RED (band 4) is the visible red response, SWIR (band 11) is the short-wave infrared response, and NIR (band 8) is the near-infrared response. In this study, the types of landslides (shallow and deep-seated landslides) were classified using combination of optical- and SAR-based classification by framework of landslide detection model [2]. The analysis was based on the relationship between the differential spectral indices and amplitude ratio changes. In addition, the classification was based on changes to the ground surface, roughness, and source material in post-landslide areas because these factors substantially affect spectral reflectance, radar reflectance, and scattering.

3 Results and discussion

 The classification of landslides (deep-seated and shallow landslides) was analyzed by considering the relationship between the differential spectral indices and amplitude ratio changes. Fig. 1 shows the relationship between the differential spectral indices and amplitude ratio changes in the Ehime and Kumamoto events, which were two types of landslides triggered by rainfall. The differential spectral indices and amplitude ratio changes of the deep-seated landslide were greater than those of the shallow landslide because the deep-seated landslide caused considerable damage on the ground surface, exhibited different soil texture and mineral composition, and changed the depth of the ground surface of the post-landslide body. However, the relationship between the differential spectral indices and amplitude ratio changes of deep-seated and shallow landslides in Hokkaido differed from those in Ehime and Kumamoto. The distribution of differential spectral indices and changes in the amplitude ratio was the same for both deep-seated and shallow landslides because an earthquake

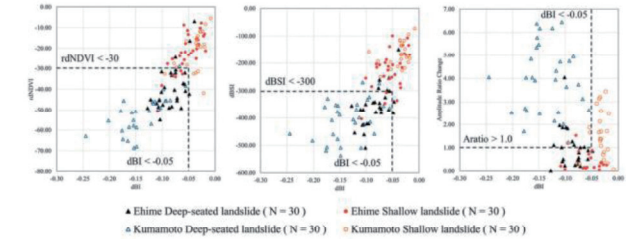was the trigger and caused liquefaction phenomena by lithology condition (Fig. 2) [3].

Fig. 1. Relation between spectral indices and Amplitude ratio change for landslide types classification in case of Ehime and Kumamoto events.
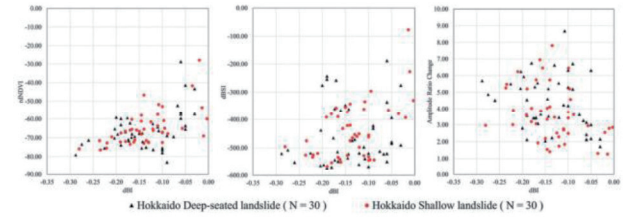

Fig. 2. Relation between spectral indices and Amplitude ratio change for landslide types classification in case of Hokkaido events.

4 Conclusions

 Landslides were classified into two types (deep-seated and shallow landslides) using the thresholds of the differential spectral indices (rdNDVI, dBSI, and dBI). The differential spectral indices of the deep-seated landslide were greater than those of the shallow landslide because of the greater changes to the ground surface and texture of the material after the landslide event. These indices detected the different textures of the soil and weathered rock material in the post-landslide body, which affected radar reflectance and change detection. Classification of landslides using the deep-seated landslide threshold was successful for the Ehime and Kumamoto events, which were triggered by rainfall. However, the model could not perform a classification for the Hokkaido events, which were triggered by rainfall and an earthquake. The earthquake caused rapid and extensive changes to the ground surface by liquefaction phenomena as well as substantial damage to the vegetated area, which may have affected the radar reflectance and backscattering distribution.

Reference

[1] Dou, J., U. Paudel, T. Oguchi, S. Uchiyama, and Y. S. Hayakawa. (2015). Shallow and Deep-Seated Landslide Differentiation Using Support Vector Machines: A Case Study of the Chuetsu Area, Japan. Terrestrial Atmospheric and Oceanic Sciences, 26 (2–2): 227–239. https://doi.org/10.3319/ TAO.2014.12.02.07(EOSI).

[2] Phakdimek, S., Komori, D., and Chaithong, T. (2023). Combination of optical images and SAR images for detecting landslide scars, using a classification and regression tree. International Journal of Remote Sensing, 44:11, 3572-3606. https://doi.org/10.1080/01431161.2023.2224096.

[3] Li, R., Wang, F. & Zhang, S. (2020). Controlling role of Ta-d pumice on the coseismic landslides triggered by 2018 Hokkaido Eastern Iburi Earthquake. Landslides 17, 1233–1250. https://doi.org/10.1007/s10346-020-01349-y.

The 11th International Symposium on Water Environment Systems
----- with Perspective of Global Safety   (Nov. 16th ~ 17th , 2023)
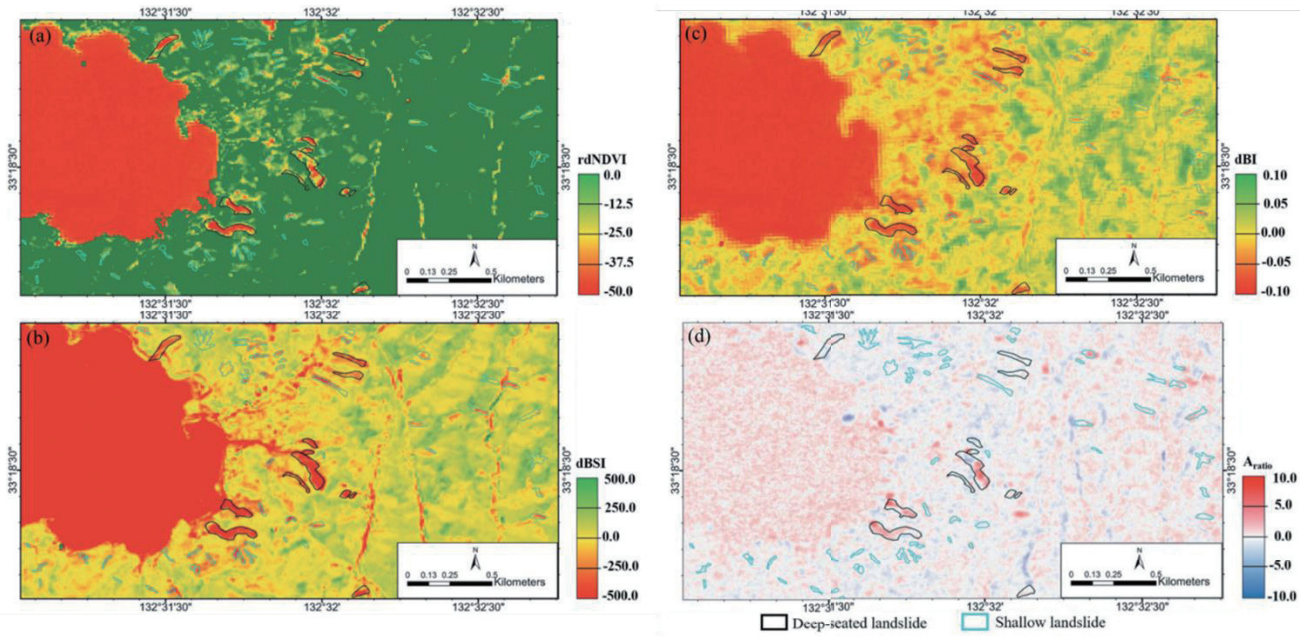
GP-RSS & SyDE
Tohoku University

Appendix

Figure S1 *Differentiate deep-seated and shallow landslides based on satellite images indices in the case of Ehime events. (a) rdNDVI (b) dBSI (c) dBI and (d) Amplitude ratio change*
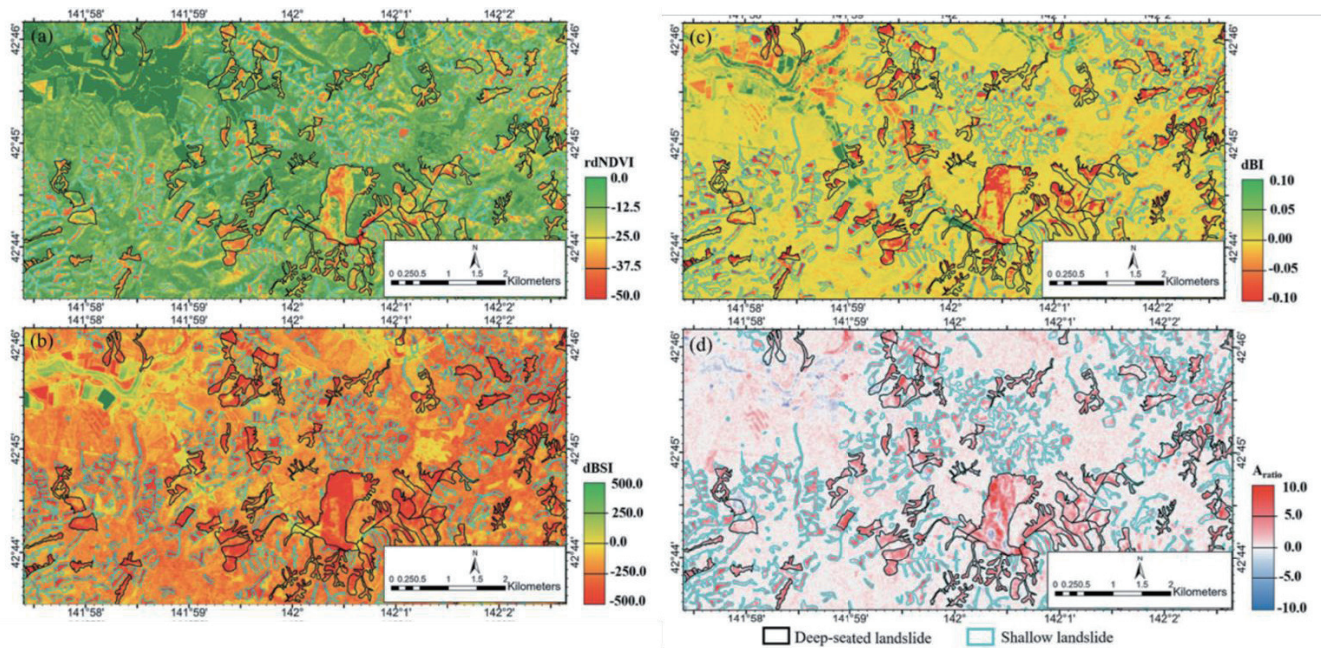

Figure S2 *Differentiate deep-seated and shallow landslides based on satellite images indices in the case of Hokkaido events. (a) rdNDVI (b) dBSI (c) dBI and (d) Amplitude ratio change*

The 11th International Symposium on Water Environment Systems
----- with Perspective of Global Safety   (Nov. 16th ~ 17th , 2023)

GP-RSS & SyDE
Tohoku University

Designing a prototype for disaster education using 3D city models and video games

○ Keitaro SUSUKIDA[1*], Keisuke ONO[1], Shota OKADA[2], Masanori SUZUKI[2],

Yasutaka KOUSAKA[2]

[1]Department of Civil Engineering and Management, Tohoku Institute of Technology,
Miyagi 982-8577, Japan.
[2]CTI Engineering Co., Ltd., Miyagi 980-0811, Japan.
*E-mail: s2014130@st.tohtech.ac.jp

Abstract

Education is key for reducing children's risks to disasters. This study developed a 1/1-scale inland flood hazard map in Sendai in the popular game Minecraft, deriving the 3D data of city from Project PLATEAU by MLIT. The developed world with a finer spatial resolution was successfully represented actual topography, shape and color of buildings and roads, and inland flood inundation area in the watershed. Finally, questionnaire survey was conducted to assess the applicability of the developed content in a research presentation event. The comparison of preferences among students between the paper map format and the Minecraft format showed that 80 out of 94 students preferred Minecraft format, indicating its potential to catch students' attraction in the topic and its potential to enable student to spatially understand the hazard of natural disasters.

Keywords: Minecraft; disaster education; hazard map; questionnaire survey

1 Introduction

Floods are becoming more frequent throughout the world in a changing climate. In Japan, serious floods are causing inundation damage almost every year. As a non-structural countermeasure against floods, Japanese river administrators, such as the Ministry of Land, Infrastructure, Transport and Tourism (MLIT), and prefectural governments, designate potential areas of flood inundation as "flood inundation areas", covering 99% of major river streams in the country. Based on the inundation areas designated, municipalities prepare and disseminate flood hazard maps to the residents. Many reports indicate that the hazard map demonstrated a high reliability in several historical floods in the country.

Regarding the use of flood hazard maps by citizens, municipalities disseminate the maps in a paper format, make them available in their city websites, and conduct disaster drills based on the maps. These activities have improved the understanding of flood risk among citizens who have a high degree of disaster awareness and who are capable to access to related disaster information. On the other hand, youth citizen in compulsory education, such as elementary or junior high school students, sometimes have a less awareness or less access to disaster information. Given the basic idea of disaster prevention and mitigation in Japan is based on a self-help and mutual-help, it is important to provide disaster information in an improved format for the youth, so that they can understand the flood hazard in their community and make appropriate decision by themselves in a moment of floods.

Past studies reported the usefulness of gamification for disaster education. Nemoto et al. defined gamification as the use of game thinking and game mechanics in a non-game context [1]. One of the advantages of applying gamification for disaster education is its potential to catch students' attraction in the topic. Another advantage is its potential to enable student to spatially understand the hazard of natural disasters. Applying gamification for disaster education in 3D makes it easier for students to visualize the hazard situation.

Ono proposed a case study of gamification of flood inundation in Fukushima, Japan, using Minecraft as a tool for disaster education [2]. In the case study, the developed world successfully represented actual topography, shape of buildings and roads, and flood inundation area in the watershed, where game players can manipulate their avatar and experience the flood hazard in the reproduced virtual 3D world. This result indicated that the flood hazard map in Minecraft can be a potential tool for disaster education. However, the case study only focused the building data of LOD1 (LOD: Level of Detail), modelling buildings in a coarse spatial resolution. Moreover, assessment of applicability of the developed content in an actual classroom is needed to disseminate the study to the public.

This study developed a hazard map in Sendai, Miyagi, in the game Minecraft, modelling buildings in a finer spatial resolution (LOD2). This study also conducted a questionnaire survey to assess the applicability of the content in disaster education through a research presentation event for the public held at the university.

2 Materials and methods

(1) Dataset

The 3D data of terrain, building shape, road shape, and water body (e.g., rivers and lakes), were downloaded from the website of Association for Promotion of Infrastructure Geospatial Information Distribution. In the website, "Project PLATEAU", a leading program of 3D city data by MLIT, disseminate the data for free of charge [3]. The data format is CityGML for terrain, building shape, and road shape, and Geodatabase for water body. The data of inland flood inundation in Sendai was provided by Sendai City in ESRI shape format.

The 11th International Symposium on Water Environment Systems
----- with Perspective of Global Safety   (Nov. 16th ~ 17th , 2023)

GP-RSS & SyDE
Tohoku University

(2) Data transformation

Development of virtual world in Minecraft needs a data transformation from CityGML and Geodatabase to a format which Minecraft can import. The data transformation was conducted by FME Desktop software developed by Safe Software Inc. This software is the data integration platform that allows users to connect and transform data between hundreds of systems, with the best support for spatial data. In the transformation, all of the 3D data were converted to a format of Minecraft with a scale of 1/1, where one block represent an object of $1m^3$ (1 m x 1 m x 1 m) in the actual world.

(3) Questionnaire survey

Questionnaire survey was conducted to assess the applicability of the developed content in an actual classroom in the Science Day at Tohoku university on July 16, 2023. This is a research presentation event for the public to share academic knowledge, especially for younger ages. Our research team exhibited the developed Minecraft world and provided the participants short lecture where they can study the inland flood hazard in downtown Sendai on laptop computer. After the lecture, questionnaire survey was conducted to students and their parents.

3 Results and discussion

The figure 1 shows an overview of flood hazard map in 3D format in Minecraft. The world successfully reproduces the terrain and buildings in Minecraft. With LOD1, the buildings are mono-colored and shape of them are simplified. With LOD2, the buildings have multiple colors and shape of them are detailed compared with that of LOD1. This result indicates that the developed world with LOD2 provides a visually finer content and rich game experience to players.

The figure 2 shows the age distribution of the respondents from the questionnaire survey. Since the research event was mainly for younger ages, elementary school students were dominant (71 out of 95). It was worth noting that even students in preschool took the lecture and operated the game without any trouble, suggesting the content was even applicable to young children. Figure 3 displays the comparison of preferences among students between the paper map format and the Minecraft format. The result shows that 80 out of 94 students preferred Minecraft format, suggesting its potential to catch students' attraction in the topic and its potential to enable student to spatially understand the hazard of natural disasters.

Fig. 1. Comparison of developed map with different spatial resolution
(Left: LOD1, Right: LOD2)

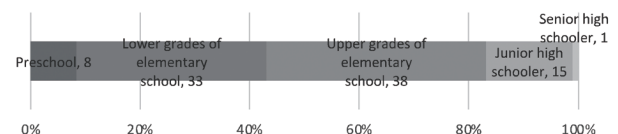**Photo 1. Classroom in the Science Day at Tohoku university on July 16, 2023**

Fig. 2. Age distribution of the respondents from the questionnaire survey (Respondent=95 students)
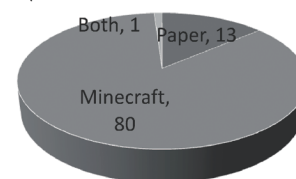

Fig. 2. comparison of preferences among students between the paper map format and the Minecraft format (Respondent=94 students)

4 Conclusions

This study developed a 1/1-scale inland flood hazard map in Sendai in the popular game Minecraft, deriving the 3D data of city from Project PLATEAU by MLIT. The developed world with a finer spatial resolution (LOD2) was successfully represented actual topography, shape and color of buildings and roads, and inland flood inundation area in the watershed. Finally, questionnaire survey was conducted to assess the applicability of the developed content in a research presentation event, indicating its potential to catch students' attraction in the topic and its potential to enable student to spatially understand the hazard of natural disasters.

Reference

[1] Nemoto, K. et al. (2014), Gamification platform for supporting self-motivated and sustained actions, IPSJ Journal, 55(6), pp. 1600-1613.
[2] Ono, K. (2022), Minecraft as a tool for disaster education: A case study of flood inundation in Fukushima, Japan, The 10th International Symposium on Water Environment Systems, pp. 40-41
[3] Ministry of Land, Infrastructure, Transport and Tourism, Project PLATEAU, https://www.mlit.go.jp/plateau

The 11th International Symposium on Water Environment Systems
----- with Perspective of Global Safety   (Nov. 16th ~ 17th , 2023)

GP-RSS & SyDE
Tohoku University

Initial analysis on the characteristics of Atmospheric Rivers inducing heavy precipitation in Japan

○ Sohta TADAKI[1]*, Yusuke HIRAGA[1] & So KAZAMA[1]

[1]Hydro-Environment System Laboratory, Department of Civil Engineering,
Tohoku University, Miyagi 980-8579, Japan.
*E-mail: sota.tadaki.r5@dc.tohoku.ac.jp

Abstract

Atmospheric Rivers (ARs) are a flow of strong water vapor transport, that have been causing extreme rainfalls mainly on West Coast of mid-latitude land area. But because of the climate change, they have been affecting the Eastern Asia area recently. In order to predict and prepare for the heavy precipitation, the need to understand the connection between ARs and heavy precipitation in this area is increasing. In this research, we used the AR Detection Algorithm created by Kennet (2021) to detect ARs forming near Japan and compared it with precipitation data. We found large, intense ARs on both of the target heavy precipitation event and see how the water vapor was going through the target area when the rain happened. But there were some uncertain relations between the ARs and the precipitation, so we need to create a algorithm that is able to take account in more climatological element, like sea-level pressure.

Keywords: Atmospheric River, Heavy precipitation, Water vapor.

1 Introduction

Recently, there have been a number of heavy precipitations happening in Eastern Asia. In numerous past research, they are shown to have connection to a large amount of water vapor flowing through. These flow of water vapor transport through the air are called Atmospheric Rivers (ARs), which have been causing extreme rainfalls mainly on west coast of America, and west coast of northern Europe. Most of the Ars have been analyzed in those areas, but since they have started to influence Eastern Asia like Japan, we need to understand the connection between ARs, and the heavy precipitation caused by them.

There have already been several research about the ARs happening near Japan. Kamae et al [1]. analyzed them from climatology perspective, but how ARs cause the heavy precipitation varies by the landscapes, and the state of the atmosphere. So in order to understand them, we need a more quantitative approach, especially in Eastern Asia region.

Also, a linear precipitation belt, which is a row of Cumulonimbus cloud, are forming around Japan and causing a devastating rainfall recently. The cause of them being formed are still unknown, but ARs are thought to have some relation to them [2]. But since one of the first event caused by the linear precipitation belt happened on 2022, we don't have much past research about them. We believe that by analyzing the connection between ARs and the heavy precipitation, we might also be able to see connection to the linear precipitation belts.

The goal of this study is to see the characteristics of the ARs that induces heavy precipitation and understand their connection. We focused on Mogami river basin and analyzed the duration and the intensity of the water vapor transport in the ARs that caused a heavy rainfall in 2020 and 2022.

2 Materials and methods

In this study, we chose the heavy precipitation happened in 2020 and 2022, in Mogami river basin. This is where the first extreme rainfall caused by a linear precipitation belt happened.

For the AR detection, we used the AR Detection Algorithm created by Kennet (2021) [3]to see when and where they are being formed, its duration, and intensity of water vapor transport.

In order to calculate the Integrated Water Vapor Transport (IVT), we used ERA-5 reanalysis data. ERA-5 reanalysis data is a grid data with a resolution of 0.25°, and we used 6-hourly data to match the Kennet algorithm. IVT is calculated by the equation below. This is mainly used to track the ARs in the past research.

$$\text{IVT}=\sqrt{\left(\frac{1}{g}\int_{1000}^{300} qu\, dp\right)^2 + \left(\frac{1}{g}\int_{1000}^{300} qv\, dp\right)^2}$$

g : gravitational accelaration (m・s^{-2})
q : relative humidity (kg・kg^{-1})
u, v : East-West, and North-South wind (m・s^{-1})
p : pressure (hPa)

To identify regions of enhanced IVT, the IVT magnitude is checked against a threshold value; defined for each month as the 85th percentile IVT for the 5-month period centered on that month. A fixed lower limit of 150 kg/m/s is also imposed. To be identified as an AR, length, narrowness, mean meridional IVT, Coherence in IVT direction, and consistency between IVT direction and object were checked.

Then we compared it to the precipitation of the Mogami river basin. For the precipitation data, we used the Rader AMEDAS.

3 Results and discussion

In Figure 1, we show the precipitation graph in the Mogami river basin from 7/1 to 8/31, on each 2020 and 2022. You can see the spike in the graph when the extreme rainfall event happened, caused by the linear precipitation belt. We also detected ARs around the time of the extreme rainfall.
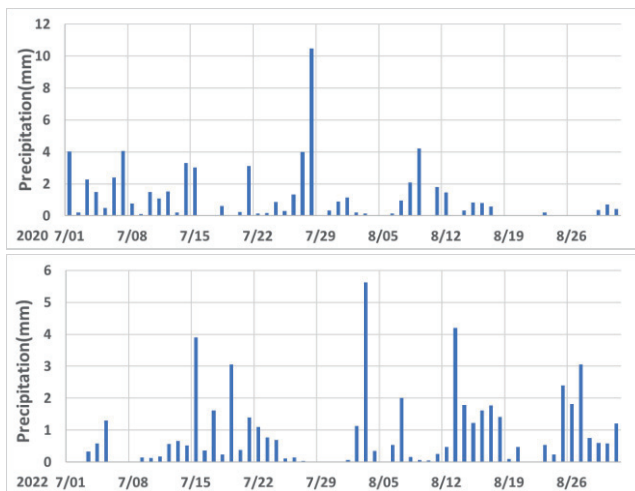
The 11ᵗʰ International Symposium on Water Environment Systems
----- with Perspective of Global Safety   (Nov. 16ᵗʰ ~ 17ᵗʰ, 2023)

GP-RSS & SyDE
Tohoku University

Figure 1 (a)(b): Rader AMEDAS 6-hourly precipitation from 7/1 to 8/30 in **(a)** 2020, **(b)** 2022

First, on 2020/7/25 18:00, we found a large flow of water vapor over Japan. The extreme rainfall happened around 2020/7/28 00:00, so there is a little lag between them. Also, even though we found a rather large AR, Mogami river is located in the Tohoku region, which is the northern area of Japan. And AR is not directly going through the target area, so we still don't know how much they are connected.

Second, on 2022/8/1 18:00, we found another AR with more intense maximum IVT. This one on the other hand is directly hitting the target area and seems to be causing the heavy rain on 8/3. On 2022/8/2 06:00, we noticed that the AR that we saw on 2022/8/1 18:00 isn't detected as an AR anymore when it is closer to the rainfall. This might have been caused by the fact that after reaching the land, the wind got weaker. Since we are using the criteria for the ARs from the past research, we might need to change them in order to match the Japan environment.

After comparing the two events, even though the IVT on the 2022 is stronger, the precipitation caused by the AR is lower. There are still a lot of unknown elements that have an influence on these events, so we need to take account in every possible element in order to accurately replicate the ARs and predict the heavy precipitation.

4 Conclusions

In this research, we tried to understand the characteristics of the ARs that causes the heavy precipitation in Japan. We focused on Mogami river basin in 2020 and 2022, which is when the extreme rainfall event happened caused by the linear precipitation belt. We were able to detect the ARs using AR Detection Algorithm and IVT, calculated from ERA-5 reanalysis data. We found some connection between the precipitation and the ARs, but also realized that there are definitely more elements responsible for the heavy rainfall. For example, we need to consider not just the horizontal movement of the water vapor, but also the vertical movement, like sea-level pressure.

Reference

[1] Y. Kamae, Y. Imada, H. Kawase, and W. Mei, Atmospheric Rivers Bring More Frequent and Intense
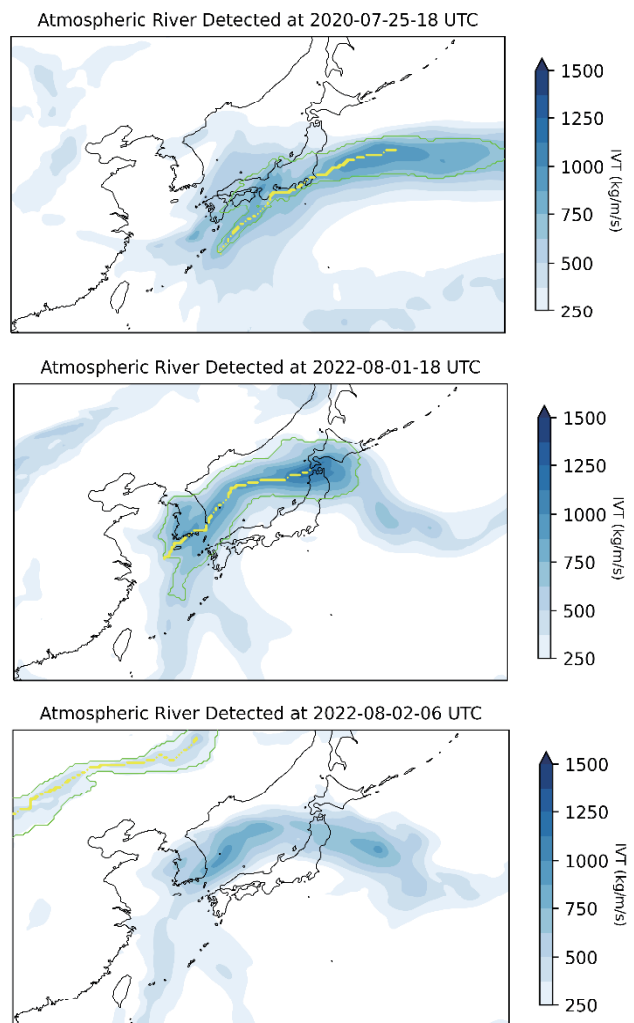
Figure 2 (a)(b)(c): ARs detected using the algorithm, on **(a)** 2020/7/25 18:00, **(b)** 2022/8/1 18:00, **(c)** 2022/8/2 06:00

Extreme Rainfall Events Over East Asia Under Global Warming, Geophysical Research Letters, 2021, 48(24)

[2] Kamae, Y., Mei, W., & Xie, S.-P. (2017). Climatological relationship between warm season atmospheric rivers and heavy rainfall over East Asia. Journal of the Meteorological Society of Japan, 95(6), 411–431.

[3] Bin Guan and Duane E. Waliser, Detection of atmospheric rivers: Evaluation and application of an algorithm for global studies, Journal of Geophysical Research: Atmosphere, 2015, 120, 12,514–12,535

The 11ᵗʰ International Symposium on Water Environment Systems
----- with Perspective of Global Safety (Nov. 16ᵗʰ ~ 17ᵗʰ , 2023)

GP-RSS & SyDE
Tohoku University

Potential of machine learning technique for prediction of 1-dimensional riverbed deformation along the Mogami river

○ Tao YAMAMOTO[1]*& So KAZAMA[1]

[1]Department of Civil and Environmental Engineering, Graduate School of Engineering, Tohoku University, Miyagi 980-8579, Japan.
*E-mail: yamamoto.tao.t8@dc.tohoku.ac.jp

Abstract

In order to maintain the river environment, there is a need to predict the change of riverbed morphology. Physicsbased computational models are widely used for prediction. Yet, the more precise model has heavier computational cost, so we tried to develop a model that can predict long-term riverbed deformation with low computational load by applying machine learning. In this work, as a first step, we began developing a model to predict the 1D deformation of riverbed. We built a simple artificial neural network, where the riverbed elevation change was used as objective variable, and the spectrum of river discharge and riverbed slope as explanatory variables. The prediction accuracy was 0.42 m~ 0.83 m in RMSE, but the model was unable to represent detailed trends in riverbed elevation change. It was implied that we need some variables to describe geometric information specific to each cross section.

Keywords: Artificial Neural Networks; Fast Fourier Transform; riverbed morphology; sediment transportation; long-term prediction.

1 Introduction

In river channel management, it is important for river administrators to grasp and predict the river morphology change. Especially, the riverbed deformation is critical issue to maintain river channels and hydraulic structures. To predict these change of river conditions, physical-based computational models have been developed to calculate the change in riverbed elevation for a long time. Most models solve the continuity and the Navier-Stokes equations, along with the sediment mass balance equation. It is not easy to determine boundary and initial conditions reasonably well. In addition, it takes heavy computation cost to compute the fluid flow and sediment transport for long distance and period. Therefore, it is required to develop a model that can reduce the computational load and be dealt with easily.

Recently, machine learning techniques have been used to clear similar hydrology problems. Some papers that try to predict riverbed changes also exist. Rahman and Chakrabarty(2020) [1] predicted the 1D riverbed elevation change for the 8 km section of the Nittany River. Discharge, sediment gradation, and dam gate opening height were input to the Artificial Neural Networks, and the change of the riverbed was obtained. Hoang et. al, (2018) [2] estimated the local scour depth around complex piers with the support vector regression. However, there is no research for long-term and long-distance prediction. Therefore, this study focusses on the prediction of riverbed deformation for the long-term and distance along the Mogami river with a machine learning technique and consider the future work to proceed this methodology.

2 Materials and methods

(1) Machine learning model description

A simple artificial neural network (ANN) was constructed as a machine learning algorithm. This ANN has 4 layers ; the input layer consists of the neurons of which number of explain variables, the two intermediate layers consist of 25 and 4 neurons, respectively, and the output layer consists of one neuron. ReLU was used as the activation function, and the data was standardized with the mean set to 0 and the variance set to 1. The learning method is backpropagation with mean squared error (MSE) as the loss function. The parameters (weights) were optimized using stochastic gradient descent (SGD). Since there was not a large amount of training data, online training and five-fold cross-validation were conducted. The neural network was tested by randomly allocating 20% of the total data.

(2) Datasets

The target river channel is the mainstream of the Mogami River, which runs through Yamagata prefecture. The study area covers a section of the Mogami River from Oyodo to 117 km upstream of the Kawanishi-Nanyo section. This section is divided into five sections, Oyodo, Murayama, Asahi, Nagai, and Kawanishi-Nanyo, and regular bathymetry surveys were conducted in each section approximately every 5 to 10 years at 200 m intervals.

The daily average river discharge dataset was obtained from the Water Information System provided by MLIT [3]. The observe station is Inakudashi, which is located 105.7km from the river mouth.

(3) Preparing learning datasets

For each cross-section, the combinations of the two survey results were created. The daily discharge data for these periods were then obtained and discrete Fourier transformed by Fast Fourier Transform.

3 Results and discussion

At first, the object variable was set to the change of riverbed elevation, and the explanatory variables were set to the amplitude of maximum daily discharge spectrum and the frequency at that time. The **Fig.1** shows the comparison between the observed riverbed elevation change and the predicted riverbed elevation change. The proportional line shows the best fit line. The RMSE value was 0.83 (m) and R^2 score was -4.6. The many plots in **Fig.1** are located under the

The 11th International Symposium on Water Environment Systems
----- with Perspective of Global Safety   (Nov. 16th ~ 17th , 2023)

GP-RSS & SyDE
Tohoku University

proportional line. This means that this model has trend to underestimated. It implies that the maximum spectrum of the daily discharge is not enough to describe sediment transport.

Next, the objective variable was set to the change of riverbed elevation, and the explanatory variables were set to the amplitude of every 10-percentile daily discharge spectrum and the frequency at that time. In other words, the amount of the daily discharge information increased. The **Fig.2** shows the comparison between the observed riverbed elevation change and the predicted riverbed elevation change. The RMSE value was 0.42 (m) and R^2 score was -0.41. These plots didn't fit the proportional line. However, the trend of underestimate was eased. Adding some variables related to the daily discharge played role to revise the underestimate trend.

Finally, the slope of riverbed at each cross section was added as explanatory variables. We should add some variables specific to each cross-section because the spectrum of daily discharge is only related to the duration of the bathymetry surveys. The slope of riverbed is deeply related to flow velocity, and of course, sediment transport capacity. **Fig.3** shows the comparison between the observed riverbed elevation change and the predicted riverbed elevation change. The RMSE value was 0.52 (m) and R^2 score was -1.2. Adding the slope to the explanatory variables increased the RMSE value, but the range of predicted elevation change became similar to the range of measured elevation change.

The discharge we utilized was the one-point data, so we need more variables specific to each section. For instance, the shape of river cross section and the material of riverbed are desirable. Also, the hyperparameters influence prediction result. Optimization of hyperparameters is necessary for considering which parameter heavily affect to the prediction.

4 Conclusions

This study tried to predict 1-D riverbed change using a ANN. Some factors which are considered to be related sediment transport were selected as the explanatory variables. The spectrum of river discharge at one observation station was important because it affects bed-load transport rate very well. However, when we set it to the explanatory variable, the ANN model could not predict riverbed deformation with accuracy. Even though the slope of each cross section was set to the explanatory variable, the accuracy of the prediction was not enough. It was implied that we need some variables to describe geometric information specific to each cross section.

Reference

[1] Rahman, S. A., & Chakrabarty, D., Sediment transport modelling in an alluvial river with artificial neural network, J. Hydrol., 588 (2020) 125056.
[2] Hoang, ND., Liao, KW. & Tran, XL., Estimation of scour depth at bridges with complex pier foundations using support vector regression integrated with feature selection, J Civil Struct Health Monit, 8 (2018) 431–442.
[3] Ministry of Land, Infrastructure, Transport and Tourism, Water Information System, http://www1.river.go.jp/ (Accessed at 14th July 2023)
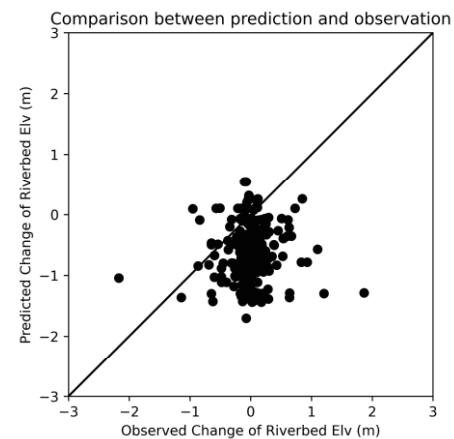

Fig.1 The result using the amplitude of maximum daily discharge spectrum and the frequency at that time as the explanatory variables.
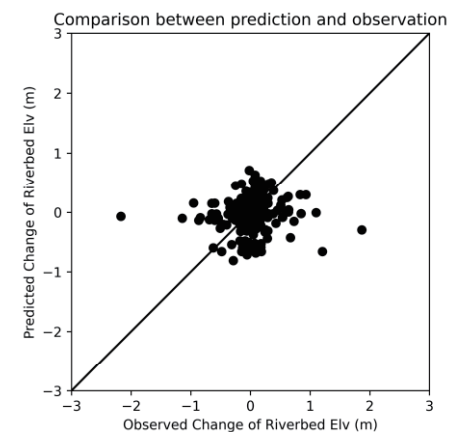

Fig.2 The result using the amplitude of every 10-percentile daily discharge spectrum and the frequency at that time as the explanatory variables.
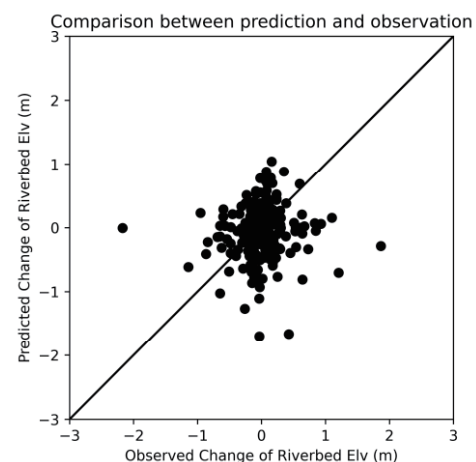

Fig.3 The result using the amplitude of every 10-percentile daily discharge spectrum, the frequency at that time and riverbed slope as the explanatory variables.